DIFFERENTIAL GAM BARRIERS AND THEIR APPLICATION IN AIR-TO-AIR COMBAT

Urban H. D. Lynch

Air Force Institute of Technology

Prepared for:

Air Force Flight Dynamics Laboratory

March 1973

AD 766890

DIFFERENTIAL GAME BARRIERS AND THEIR APPLICATION IN AIR-TO-AIR COMBAT

DISSERTATION

DS/MC/73-1 URBAN H.D. LYNCH
MAJOR USAF

Security Classification

DOCUMENT CONTROL DATA - R & D

(Security classification of title, body of abstract and indexing annotation must be entered when the overall report is classified)

1. ORIGINATING ACTIVITY (Corporate author)	2a. REPORT SECURITY CLASSIFICATION
Air Force Institute of Technology (AFITSE) Wright-Patterson AFB, Ohio 45433	Unclassified
	2b. GROUP

3. REPORT TITLE

DIFFERENTIAL GAME BARRIERS AND THEIR APPLICATION IN AIR-TO-AIR COMBAT

4. DESCRIPTIVE NOTES (Type of report and inclusive dates)

AFIT Dissertation

5. AUTHOR(S) (First name, middle initial, last name)

Urban H.D. Lynch
Major USAF

6. REPORT DATE	7a. TOTAL NO. OF PAGES	7b. NO. OF REFS
March 1973	~~237~~ 251	15

8a. CONTRACT OR GRANT NO	9a. ORIGINATOR'S REPORT NUMBER(S)
b. PROJECT NO	DS/MC/73-1
c.	9b. OTHER REPORT NO(S) (Any other numbers that may be assigned this report)
d.	

10. DISTRIBUTION STATEMENT

This document has been approved for public release and sale; its distribution is unlimited.

11. SUPPLEMENTARY NOTES	12. SPONSORING MILITARY ACTIVITY
Approved for public release; IAW AFR 190-17 JERRY C. HIX, Captain, USAF Director of Information	Air Force Flight Dynamics Laboratory Wright-Patterson AFB, Ohio 45433

13. ABSTRACT

The mathematical theory of perfect information, zero-sum, differential games is used as an analytical tool to learn as much as possible about the one-on-one, air-to-air combat problem and the problem parameters which have major effect on its outcome. The primary emphasis is on differential game Barrier theory and the application of the Barrier as an analytical tool for air-to-air combat analysis. A series of progressively more complex air-to-air combat models is developed and solved in such a way that the solution results of a given model have direct input to the more complex model that follows and learning from one model to the next is accumulative. The importance of the Barrier, its shape and its sensitivity to aircraft design parameters is discussed and demonstrated.

Barrier sensitivity analysis of the models shows that given the opportunity to increase a fighter aircraft's air-to-air combat capability with either improved turning gs, weapons system, or thrust to weight ratio, increased thrust to weight ratio yields the greatest improvement in this capability. Barrier results of the model are designed into a workable computational technique to relatively evaluate the air-to-air combat capability of a series of fighter aircraft. This is the first known practical application of differential game theory to an air-to-air combat problem of real importance to the Air Force. A general zero-sum payoff function is also developed which allows the roles of the players to be an inherent decision in the model itself based on terminal state.

DD FORM 1 NOV 68 1473

Security Classification

Security Classification

14 KEY WORDS	LINK A		LINK B		LINK C	
	ROLE	WT	ROLE	WT	ROLE	WT
Differential Gases						
Barrier						
Air to Air Combat						
Capture Zone						
Escape Zone						

Security Classification

DIFFERENTIAL GAME BARRIERS AND THEIR APPLICATION IN AIR-TO-AIR COMBAT

DISSERTATION

Presented to the Faculty of the School of Engineering
of the Air Force Institute of Technology

Air University

in Partial Fulfillment of the Requirements for
the Degree of Doctor of Philosophy in
Aerospace Engineering

by

Urban H.D. Lynch, M.S.
Major USAF

March 1973

10

DIFFERENTIAL GAME BARRIERS AND
THEIR APPLICATION IN
AIR-TO-AIR COMBAT

by

Urban H.D. Lynch, M.S.
Major USAF

Approved:

Gerald M Anderson
Chairman
Dick H. de Does
Russell A Kemmer
Lynn E. Wolaver

Accepted.

J S Przemieniecki
Dean, School of Engineering

ict

Preface

This dissertation is the result of my effort to use the mathematical theory of zero-sum differential games as an analytical tool to learn as much as possible about the one-on-one air-to-air combat problem and the problem parameters which have major effect on its outcome. My thanks are given to the faculty of the Air Force Institute of Technology and especially to Professor Gerald M. Anderson for his interest and guidance. I am indebted to the Air Force Flight Dynamics Laboratory for not only willingly providing time, but encouragement to do this research. In this respect I wish to recognize William L. Othling Jr. and Anthony L. Leatham whose research efforts created the original interest in the laboratory for differential games research.

I am especially grateful to my wife, Janet, for her encouragement and support throughout this course of study, and to my sons Andrew and Matthew who gave up their father many an evening.

Contents

List of Figures

List of Symbols and Abbreviations

$(\_),[\,]$	Column vector symbol
$(\_)^T$	Vector transpose
$(\dot{})$	Time Derivative
$\partial(\,)/\partial(\,)$	Partial derivative
$(\_)\times(\_)$	Vector cross product
$\dot{(\_)}\big\vert$	Vector time derivative relative to a coordinate system
$\nabla(\,),(\,)_x$	Gradient row vector
$\vert\,\vert$	Absolute scalar value, vector length, determinant
$\epsilon, \subset$	"contained in"
$\exists$	"there exists"
$\ni$	"such that"
$\forall$	"for all"
$\Rightarrow$	"implies"
$\equiv$	"identically equals" or "defined as"
$\simeq$	"approximately equals"
$\sim$	set subtraction
$\cup$	set union
$\mathrm{sgn}(\,)$	sign function
$h(\,)$	Heavyside function
P	Pursuer
E	Evader
$\underline{x}$	State vector
$\underline{f}$	Vector state equation

List of Symbols and Abbreviations (cont'd)

$\underline{u}, \underline{v}$	Control vectors
$\mathcal{C}$	Terminal surface
$\mathcal{E}$	State space
$\underline{s}$	Parameter vector for $\mathcal{C}$
s_j	component of $\underline{s}$
J	Payoff functional
H	Hamiltonian function
$()^*$	Indicates optimal value
$\underline{\lambda}$	Costate vector
λ_i	Component of $\underline{\lambda}$
$\underline{\nu}$	Barrier costate vector
ν_i	component of $\underline{\nu}$
$\tilde{\underline{u}}, \tilde{\underline{v}}$	Barrier controls
UP	Useable part of $\mathcal{C}$
NUP	Non-useable part of $\mathcal{C}$
BUP	Boundary of the useable part of $\mathcal{C}$
t	time
t_f	Final time
τ	Backward time
P_s	Specific power
π	3.141592
SPS	Semipermeable Surface

Abstract

The mathematical theory of perfect information, zero-sum, differential games is used as an analytical tool to learn as much as possible about the one-on-one, air-to-air combat problem and the problem parameters which have major effect on its outcome. The primary emphasis is on differential game Barrier theory and the application of the Barrier as an analytical tool for air-to-air combat analysis. A series of progressively more complex air-to-air combat models is developed and solved in such a way that the solution results of a given model have direct input to the more complex model that follows and learning from one model to the next is accumulative. The importance of the Barrier, its shape and its sensitivity to aircraft design parameters is discussed and demonstrated.

Barrier sensitivity analysis of the models shows that given the opportunity to increase a fighter aircraft's air-to-air combat capability with either improved turning gs, weapons system, or thrust to weight ratio, increased thrust to weight ratio yields the greatest improvement in this capability. Barrier results of the models are designed into a workable computational technique to relatively evaluate the air-to-air combat capability of a series of fighter aircraft. A general zero-sum payoff function is also developed which allows the roles of the players to be an inherent decision in the model itself based on terminal state.

I. Introduction

Background

Limited war and its associated use of conventional airpower, has in recent years led many researchers to study the air-to-air combat problem. To appropriately model this problem, many factors must be considered. The following list suggest a few of the major factors involved:

1) How many combatants are involved?

2) What is each combatant trying to do?

3) What roles (i.e. pursuer or evader) do the combatants assume? Do the roles change?

4) How much information does each combatant have?

5) Based on the information, what strategy (control logic) should each combatant employ?

6) For a given initial encounter, what is the outcome of the combat?

7) If a particular combatant does not like the outcome, how can he change the system parameters under his control to best influence the outcome in his favor?

An ideal model of the air-to-air combat problem would have an analytical structure which would couple these seven factors together. Such a model could be used to define the air superiority aircraft and its associated tactics.

Many air-to-air combat models exist which attempt to simulate several of the factors involved; however, their usual disadvantage is that the control logic for one or more of the combatants is assumed and not derived. As such, the outcome of the combat or the effect of a particular system parameter change is subject to the question: "What if?" or "Is there a better way?", etc.

The mathematical theory of zero-sum differential games, as developed by Isaacs [7] in 1954, is an analytical tool which models systems with conflicting objectives. It can be likened to an optimal control problem with two players - one choosing controls to maximize a payoff and the other choosing controls to minimize the payoff. As such, the control logics of the game are derived to optimize the outcome and are not an input variable when assessing the effects of system parameter changes. Therefore, the mathematical theory of zero-sum differential games, as introduced by Isaacs, does possess an inherent mathematical structure that couples factors 2, 5, 6 and 7 for two combatants. In actuality, there is a broader theory of differential games called nonzero-sum differential games (see Starr [14] and Leatham [8]) which involves factor 1 (i.e. more than two players) and stochastic differential game theory which involves factor 4 (i.e. games with incomplete information). Chapter IX of this dissertation examines factor 3, i.e. role. Thus, the math theory of differential games is capable of coupling the major factors involved in the air-to-air combat problem.

Even though the math theory of differential games does possess the desired analytical structure and great promise for problems with systems in conflict, the facts are, however, that it is little used today as a practical analysis tool for such problems. What then are the reasons for the apparent failure of such a powerful analysis tool? Isaacs [7:2] suggest two reasons. One is the increased difficulty of the problem when an opposing player is added. The second

reason is that the theory abounds with general theorems usually of the highest calibre mathematics, but of very little use in obtaining answers to practical problems. Since Isaacs's book, much work has been done in practical techniques to solve the differential game, e.g. Roberts [13]. But even these techniques have not been brought to the point of real practical application.

Dissertation Purpose

The researches of this author have led him to add a third reason to Isaac's list. Of the problems that can be solved, however simplified, and of the techniques and concepts that exist, little or nothing has been done to show how and where they can be practically applied. To this end the purpose of this dissertation is devoted.

This dissertation concerns itself with one-on-one, air-to-air combat models employing zero-sum payoff and perfect information. The technique of "dynamic modelling" employed by Othling [11] and inherently suggested by Isaacs [7] is used to progressively complex the air-to-air combat model and to learn the influence of the added realism on the solution. As will be shown, the models are developed in such a way that the solution results of a given model have direct input into the more complex models that follow. In this way the models build on one another and learning from one model to the next is accumulative.

Dissertation Contributions

The original contributions of this dissertation are: 1) The Barrier results of a three-dimensional model are used in a new technique to realistically and numerically rank fighter aircraft in terminal combat throughout the flight envelope. The technique was used by AFFDL in the recent Light-Weight-Fighter proposal evaluation. This is the first known practical application of differential games to the air-to-air combat problem. 2) The concept of a differential game Barrier, as developed by Isaacs [7], is brought to usefulness by recognizing the importance of its existence, shape, and sensitivity to aircraft parameters. This research is vitally important in recognizing those parameters which have major effect on combat outcome, and therefore help to define the air superiority aircraft. 3) The field of optimal control, in general, receives much criticism because the results of the method are often obtained by the use of very basic payoff forms such as minimum time, minimum fuel, etc. The same problem exists in differential games i.e. what payoff form really models the air-to-air combat problem? In this dissertation, a realistic general purpose zero-sum payoff is developed for the first time that allows different roles to be assumed by each of the players. This is done by simply selecting constants in the payoff function. The importance of this payoff is demonstrated by its use in air-to-air combat role decision-a problem of air-to-air combat yet to be solved by any technique. Its use in the combat role decision

logic of a simple air-to-air combat model is demonstrated.

Guide to Chapters

Chapter II presents a summary of the mathematical theory of zero-sum differential games, the "Isaac's approach" to differential games, and the Isaac's Barrier theory. In this chapter the nature and importance of the Barrier is discussed which is the basic motivation of the dissertation.

A major portion of the dissertation (Chapters III, IV, VI, VIII) concerns itself with the application of the theory in Chapter II to a series of progressively more complex air-to-air combat models - i.e. "dynamic modelling". In each model chapter, the following approach is used:

1) Set up the problem
2) Apply the necessary conditions of Chapter II
3) Solve the problem backward from the terminal surface and identify the control singular surfaces
4) Apply the necessary conditions for the Barrier and solve for the Barrier
5) Examine the model parameter relationships that cause interesting cases of Barrier closure
6) Examine the sensitivity of the closure conditions
7) Draw conclusions from 1-6

Chapters III, IV, and VI are model chapters that follow the above plan. Chapter VIII is also a model chapter, however, its main purpose is to evaluate the first order effects of variable velocity magnitude on the problem.

Interspersed in the model chapters are Chapters V and VII which apply the model results to a real Air Force problem - the relative evaluation of fighter aircraft.

In the process of solving the models in Chapters III, IV, VI and VIII, certain deficiencies were noticed in the fixed roles that were assigned to the combatants. This deficiency led to the development of a general purpose payoff and its use in the role decision logic of a given model. This work is presented in Chapter IX. As will be seen, the Barrier plays an important function in the role decision logic of a model.

Chapter X summarizes conclusions of the dissertation and makes recommendations for further work.

II. Differential Game/Barrier Theory

The air-to-air combat models treated in this dissertation are modeled as zero-sum, perfect information differential games. The purpose of this chapter is to mathematically define this class of differential games, to summarize what this author calls the "Isaacs approach", and to define the Barrier mathematically with its associated implications. The mathematical conditions summarized in this chapter can be found in References [1], [2], [4], and [7]. Throughout this chapter classical control theory terminology is used, often followed by a parenthetical expression showing Isaac's terminology.

Zero-Sum, Perfect Information Differential Games

1. Problem Formulation:

The state equations (kinematic equations) defining the dynamic systems of the combatants are

$$\dot{\underline{x}} = \underline{f}(\underline{x}, \underline{u}, \underline{v}, t) \quad ; \quad \underline{x}(t_o) = \underline{x}_o \tag{2.1}$$

where $\underline{x}$ is an n-vector of states, $\underline{u}$ is an m-vector of player 1 (P) controls, $\underline{v}$ is a p-vector of player 2 (E) controls and t is the scalar time. The initial conditions are $\underline{x}_o$ at t_o. The control vectors may be subject to inequality constraints of the form

$$\underline{R}(\underline{u}, \underline{v}) \geq \underline{0} \tag{2.2}$$

where $\underline{f}$ is an r-vector. The goal of the players is to find the controls $\underline{u}^*$ and $\underline{v}^*$ that satisfy Eq (2.2) and produce a final state $\underline{x}(t_f)$ so that a k-vector of terminal conditions, $\underline{\Psi}$, (terminal surface, $\underline{\zeta}$) is satisfied

$$\underline{\Psi}[\underline{x}(t_f)] = \underline{0} \tag{2.3}$$

and such that the scalar payoff

$$J = \phi[\underline{x}(t_f), t_f] + \int_{t_o}^{t_f} L(\underline{x}, \underline{u}, \underline{v}, t)\, dt \tag{2.4}$$

satisfies

$$J(\underline{u}^*, \underline{v}) \leq J(\underline{u}^*, \underline{v}^*) \leq J(\underline{u}, \underline{v}^*) \quad . \tag{2.5}$$

ϕ is a smooth scalar function defined on $\underline{\zeta}$.

$\underline{f}$ and L are assumed to have all partial derivatives.

If $\underline{u}^*$ and $\underline{v}^*$ can be found, the pair of controls is called a saddle point of the game, for obvious geometric reasons in Eq (2.5), and $J(\underline{u}^*, \underline{v}^*)$ is called the value of the game. As defined in Eq (2.5), P (the pursuer) is minimizing J and E (the evader) is maximizing J. It is the nature of Eq (2.5) that if E does not play the saddle point strategy $\underline{v}^*$, P will be able to reduce J below $J(\underline{u}^*, \underline{v}^*)$ and gain an advantage never to be recovered by E. Likewise E can increase J above $J(\underline{u}^*, \underline{v}^*)$ if P does not play $\underline{u}^*$. The loss in J of the non-optimal player becomes the gain of J to the optimal player, hence the name zero-sum payoff. Perfect information comes from the fact that each

player knows the exact state of the game and the goal, capability, and limitations of the other player.

2. Necessary Conditions:

In the necessary conditions that follow, the existence of a J saddle point solution is assumed. If U is the class of $\underline{u}$ controls satisfying Eq (2.2) and V is the class of $\underline{v}$ controls satisfying Eq (2.2), i.e. they are admissible controls, then a necessary condition for the existence of the J saddle point is

$$\min_{\underline{u}\in U}\max_{\underline{v}\in V} J(\underline{u},\underline{v}) = \max_{\underline{v}\in V}\min_{\underline{u}\in U} J(\underline{u},\underline{v}) \quad . \tag{2.6}$$

A necessary condition for a saddle point of J is that the Hamiltonian defined by

$$H(\underline{x},\underline{u},\underline{v},\underline{\lambda},t) = \underline{\lambda}^T\underline{f} + L \tag{2.7}$$

be minimized over U and maximized over V i.e.

$$H^* = \min_{\underline{u}\in U}\max_{\underline{v}\in V} H = \max_{\underline{v}\in V}\min_{\underline{u}\in U} H \quad . \tag{2.8}$$

$\underline{\lambda}$ is an n-vector of costates that satisfies the costate differential equation

$$\dot{\underline{\lambda}}^T = -\nabla H \quad . \tag{2.9}$$

The transversality conditions at t_f are given by

$$H(t_f) = -\partial\Phi/\partial t_f \tag{2.10}$$

$$\underline{\lambda}^T(t_f) = \nabla\Phi\Big|_{t_f} \tag{2.11}$$

where

$$\Phi = \phi + \underline{e}^T\underline{\Psi} \tag{2.12}$$

and $\underline{e}$ is a constant k-vector to be determined. It can further be shown that

$$\dot{H}^* = \partial H/\partial t \tag{2.13}$$

so if H does not envolve t explicity, then

$$H^*(t) = \text{constant} = H(t_f) = -\partial\Phi/\partial t_f \tag{2.14}$$

Eq (2.8) requires that the minimization and maximization operations commute which in general is not true. It can be shown, however, that if the H function can be separated into a function H_P not involving $\underline{v}$ and a function H_E not involving $\underline{u}$, i.e.

$$H(\underline{x},\underline{u},\underline{v},\underline{\lambda},t) = H_P(\underline{x},\underline{u},\underline{\lambda},t) + H_E(\underline{x},\underline{v},\underline{\lambda},t) + H_0(\underline{x},\underline{\lambda},t) \tag{2.15}$$

then Eq (2.8) is satisfied and a saddle point of H does exists. Unfortunately, the existence of a saddle point of H does not necessarily imply a saddle point of J. Other procedures must be used to insure that a candidate solution of Eq (2.8) does indeed satisfy Eq (2.5).

In many cases, and very often in simplified models, a control variable C will appear linearly in H. If the function $\partial H/\partial c$ happens to be zero for a finite time, then in effect H is independent of C and it is not possible with conventional extremum techniques to determine the C that extremizes H. Extremal solutions that have a control component such that $\frac{\partial H}{\partial c} \equiv 0$ along the solution are called singular solutions. Anderson [1] presents necessary conditions for singular solutions in two-player, zero-sum differential games. If H_c is defined as $H_c \equiv \frac{\partial H}{\partial c}$, then necessary conditions for the existence of a singular solution require that H_c and all of its time derivatives vanish. Successive differentiation of H_c, with appropriate substitution of the state and costate equations, yields auxiliary necessary conditions such as $H_c(\underline{x}, \underline{\lambda}, t) = 0$, $\dot{H}_c(\underline{x}, \underline{\lambda}, t) = 0$, etc., which must be satisfied all along the singular arc. Continued differentiation of H_c often leads to an expression involving C explicitly which can be solved for the singular control C_s. A necessary condition for the control to be singular is

$$(-1)^q \frac{\partial}{\partial c}\left[\frac{d^{2q} H_c}{dt^{2q}}\right] \gtrless 0 \quad . \tag{2.16}$$

The number $2q$ is the order of the H_c derivative in which C first appears explicitly. The upper inequality applies if C belongs to P's controls and the lower inequality if C belongs to E's controls.

3. Problem Solution:

As can be seen by the basic necessary conditions (i.e. Eqs (2.1), (2.3), (2.8), (2.9), (2.10), (2.11), (2.12)) the solution of the posed differential game requires the solution of a two point boundary value problem (TPBVP). This is usually done on a high speed digital computer using sophisticated numerical techniques. The form of these computer solutions is such that for a given initial state $\underline{x}_o$, the control vectors will take the form

$$\underline{u}^* = \underline{u}(\underline{x}_o, t)$$
$$\underline{v}^* = \underline{v}(\underline{x}_o, t) \qquad (2.17)$$

Eqs (2.17) are referred to as open-loop controls and are optimal only for the starting position $\underline{x}_o$ and assuming that both players continue to play optimally. In order to know the solution for another $\underline{x}_o$ or to take advantage of the inequalities in Eq (2.5), when either player plays non-optimally, the control vectors must have the form

$$\underline{u}^* = \underline{u}(\underline{x}, t)$$
$$\underline{v}^* = \underline{v}(\underline{x}, t) \qquad (2.18)$$

Eqs (2.18) are referred to as closed-loop controls. In order for differential games to have real time application in an actual air-to-air engagement, the optimal controls or approximate optimal controls must have the closed-loop form. It should be noted that finding the open-loop solution for all initial states of interest is equivalent to closed-loop control.

The Isaac's Approach

Several major concepts and an underlying theme pervade Isaac's book which this author chooses to call the "Isaac's approach".

1. Isaac's Problem Formulation:

Isaacs begins in Chapter I by developing the concept of an n-dimensional state vector $\underline{x}$ which is an element of a playing space, ξ . ξ is defined as some subregion of Euclidean n-space. The $\underline{x}$ vector is known by both players so complete information is assumed. He envisions the game terminating on a smooth n-1 dimensional surface, γ , which is taken as part of the boundary of ξ . In terms of the previous section, k has the value one (1). He justifies this single scalar terminal constraint from two points of view. The first is that termination on a physical surface surrounding P makes sense in terms of relative position. A locus of positions surrounding P is described by one scalar equation. The second is practically; i.e., it is easy to solve this differential game backwards since all the states and costates will be known on γ .

Isaacs then discusses the problem of controliability in his own unique way. He distinguishes between the "game of kind" which addresses the question: can termination be achieved at all? and the "game of degree" where there are a continuum of outcomes and we are interested in terminating in some "best" way. It is the game of kind that later leads to the concept of a differential game Barrier.

In Chapter II he presents the concept of a "reduced" playing space ξ . This is a space where the states are measured relative to P and results in a playing space of lower dimension which is easier to visualize. As will be shown, it also has more meaning for the players actually involved.

Instead of characterizing ξ with a single scalar equation, he chooses to describe this n-1 dimensional surface in ξ with n equations involving n-1 parameters s_i i.e.

$$\begin{aligned} x_1 &= h_1(s_1, s_2, \cdots, s_{n-1}) \equiv h_1(\underline{s}) \\ &\vdots \\ x_i &= h_i(s_1, s_2, \cdots, s_{n-1}) \equiv h_i(\underline{s}) \\ &\vdots \\ x_n &= h_n(s_1, s_2, \cdots, s_{n-1}) \equiv h_n(\underline{s}) \end{aligned} \quad . \tag{2.19}$$

In his development, Isaacs never lets t appear explicitly. If t is involved explicitly, he adds one more state equation

$$\dot{x}_{n+1} = 1 \qquad x_{n+1}(t_o) = o \tag{2.20}$$

and increases the dimensionality of ξ by one (1). As such, Isaac's payoff takes the form

$$J = \Phi(\underline{s}) + \int_{t_o}^{t_f} L(\underline{x}, \underline{u}, \underline{v})\, dt \quad . \tag{2.21}$$

For each initial condition, $\underline{x}_o$, there is an associated value of the game $J(\underline{x}_o)$. J can be looked upon as a function of the state $\underline{x}$ i.e. if the game were to be played optimally from $\underline{x}$, $J(\underline{x})$ would be the value of the game.

2. Isaac's Necessary Conditions:

In the development of the necessary conditions, Isaacs defines

$$J_{\underline{x}} \equiv \nabla J(\underline{x}) \tag{2.22}$$

and "main equation 1" (ME1) is derived as

$$\min_{\underline{u}} \max_{\underline{v}} \left[J_{\underline{x}} \underline{f}(\underline{x}, \underline{u}, \underline{v}) + L(\underline{x}, \underline{u}, \underline{v}) \right] = 0 \tag{2.23}$$

where the $\min_{\underline{u}}$ and $\max_{\underline{v}}$ are done subject to the constraints on $\underline{u}$ and $\underline{v}$. Eq (2.23) is the same as Eqs (2.7) and (2.8). He then substitutes the optimal controls $\underline{u}^*$ and $\underline{v}^*$ into Eq (2.23) which yields

$$J_{\underline{x}} \underline{f}(\underline{x}, \underline{u}^*, \underline{v}^*) + L(\underline{x}, \underline{u}^*, \underline{v}^*) = 0 \quad . \tag{2.24}$$

Eq (2.24) is the same as Eq (2.14) and is called 'main equation 2" (ME2). He further develops

$$\dot{J}_{\underline{x}} = - \nabla \left[J_{\underline{x}} \underline{f} + L \right] \quad . \tag{2.25}$$

Eq (2.25) is the same as Eq (2.9) (note the row vector $J_{\underline{x}} \equiv \underline{\lambda}^T$).

For the terminal conditions he points out that J evaluated on ζ is

$$J|_{\zeta} = \phi(\underline{s}) \quad . \tag{2.26}$$

Therefore on ζ

$$\frac{\partial \phi(\underline{s})}{\partial s_k} = \sum_{i=1}^{n} J_{x_i} \frac{\partial h_i(\underline{s})}{\partial s_k} \quad , \quad k = 1, \cdots, n-1 \quad . \tag{2.27}$$

Eq (2.27) can be shown equivalent to the transversality conditions of Eq (2.11). Eq (2.27) contains n-1 scalar equations and together with ME2 evaluated on ζ completely determines $J_{\underline{x}}|_{\zeta}$.

3. Isaac's Problem Solution:

Since for a given $\underline{x} \in \zeta$, $J_{\underline{x}}|_{\zeta}$ is known, Isaacs solves the problem backward for all $\underline{x} \in \zeta$ thereby converting the TPBVP into a final value problem. This he calls the "retrogression principle". Note, this is only possible because ζ has n-1 dimensions. This backward solution from ζ , not involving the definition of unusual singular surfaces, Is acs refers to as the "solution in the small". The complete solution of a differential game requires the identification of unusual singular surfaces such as the Universal surface (same as the singular control discussed on pg 11), Barrier surface, Dispersal surface, Equivocal surface (see Isaacs for the other surfaces) etc. Isaacs refers to the complete solution as the "solution in the large".

Isaac's Barrier Theory/The Game of Kind

Isaac's Barrier theory begins with the assumption that P's goal is to force game termination (i.e. force E to cross ζ) and E's goal

is to prevent game termination.

1. The Game of Kind Near ζ :

Let $\underline{v}$ be a vector originating on ζ , normal to ζ , and extending into ξ . Then $\underline{v}^T \underline{f}(\underline{x}, \underline{u}, \underline{v})$ represents the rate of change of state normal to and away from ζ . If $\underline{x}$ is on or infinitesimally close to ζ and if $\underline{v}^T \underline{f} > 0$, then ζ will not be penetrated. If $\underline{v}^T \underline{f} < 0$ then penetration of ζ will occur and game termination. Therefore, in light of the goals of P and E, P wants $\underline{v}^T \underline{f}\big|_{\zeta} < 0$ and E wants $\underline{v}^T \underline{f}\big|_{\zeta} > 0$. Since $\underline{v}^T \underline{f}$ may involve the controls $\underline{u}$ and $\underline{v}$, P should do his best to make $\underline{v}^T \underline{f}$ as negative as possible to insure termination and E should do his best to prevent this i.e.

$$\min_{\underline{u}} \max_{\underline{v}} \underline{v}^T \underline{f}(\underline{x}, \underline{u}, \underline{v})\Big|_{\zeta} \quad . \tag{2.28}$$

The sign of expression (2.28) depends solely on the $\underline{x}$ on ζ . The region of ζ where (2.28) is positive represents a region where E can prevent termination regardless of P's best attempts. Isaacs calls this region the "non-useable part" (NUP) of ζ . The region of ζ where (2.28) is negative represents a region where P can force termination regardless of E's best attempts to get away. Isaacs calls this region the "useable part" (UP) of ζ . The states on ζ for which (2.28) is identically zero form a curve on ζ which separates the UP from the NUP. Isaacs calls this curve the "boundary of the useable part" (BUP). Its significance is in that it

divides ξ into regions where P can force capture and where E can prevent capture. As will be seen, it has major importance in the game of kind and construction of the Barrier.

2. Necessary Conditions for a Semipermeable Surface:

Consider the small portion of a surface S (n-1 dimensions) in ξ shown in Fig. 1. Isaacs assumes that the surface separates the neighboring space. The two sides of the surface are labeled by P and E.

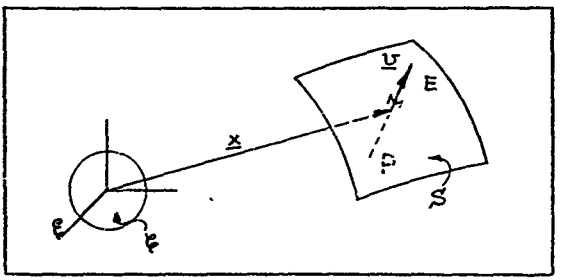

Figure 1: Semipermeable Surface (SPS)

Definition: The surface S is semipermeable at $\underline{x} \in S \subset \xi$ if $\exists$ a $\tilde{\underline{u}} \in U \ni$ if $\underline{u} = \tilde{\underline{u}}$ then $\exists$ no $\underline{v} \in V$ that causes penetration to the P side. Similarly $\exists$ a $\tilde{\underline{v}} \in V \ni \exists$ no $\underline{u} \in U$ that causes penetration to the E side.

Definition: If the surface S is semipermeable $\forall \underline{x} \in S$, then S is said to be semipermeable.

Let $S \subset \xi$ be a smooth, semipermeable surface and let $\underline{n}$ be its normal pointing to the E side. Then by definition of S semipermeable

$$\min_{\underline{u} \in U} \max_{\underline{v} \in V} \underline{n}^T \underline{f}(\underline{x}, \underline{u}, \underline{v}) = 0 \quad . \tag{2.29}$$

Isaacs refers to Eq (2.29) as "pseudo" ME1. Substituting the semipermeable controls $\tilde{\underline{U}}$ and $\tilde{\underline{V}}$ into Eq (2.29) yields "pseudo' ME2.

$$\underline{v}^T \underline{f}(\underline{x}, \tilde{\underline{U}}, \tilde{\underline{V}}) = 0 \quad . \tag{2.30}$$

On the assumption that S can be imbedded in a family of semipermeable surfaces which fill a neighborhood of S, Isaacs derives the following differential equation for $\underline{v}$.

$$\dot{\underline{v}}^T = -\nabla(\underline{v}^T \underline{f}) \tag{2.31}$$

Now consider a curve $\mathcal{D}$ in ξ (i.e. n-2 dimensional surface in ξ) characterized by

$$\mathcal{D}: \quad \begin{aligned} x_1 &= h_1(s_1, \cdots, s_{n-2}) \\ &\vdots \\ x_i &= h_i(s_1, \cdots, s_{n-2}) \\ &\vdots \\ x_n &= h_n(s_1, \cdots, s_{n-2}) \end{aligned} \tag{2.32}$$

and the problem of passing a unique semipermeable surface through $\mathcal{D}$. Since $\mathcal{D} \in S$, normality of $\underline{v}$ on $\mathcal{D}$ requires that

$$\sum_{i=1}^{n} v_i \frac{\partial h_i}{\partial s_j} = 0 \quad , \quad j = 1, \cdots, n-2 \tag{2.33}$$

and since the length of $\underline{v}$ is arbitrary, $\underline{v}$ is made a unit vector by requiring

$$\underline{v}^T\underline{v}\Big|_{\mathcal{D}} = 1 \qquad . \qquad (2.34)$$

Eqs (2.30), (2.33), and (2.34) provide n scalar equations which define $\underline{v}$ on $\mathcal{D}$. Isaacs then proves the following theorem.

Theorem: Let $\tilde{\underline{U}}$ and $\tilde{\underline{V}}$ denote functions of $\underline{x}$ and $\underline{v}$ as obtained from Eq (2.29). For a given curve $\mathcal{D}$, let $\underline{v} \neq 0$ on $\mathcal{D}$ be defined as by Eqs (2.30), (2.33), and (2.34). Let $\underline{x}(\tau, s_1, \cdots, s_{n-2})$ and $\underline{v}(\tau, s_1, \cdots, s_{n-2})$ be integrals of the differential equations (2.31) and the state equation, then $\underline{x}(\tau, s_1, \cdots, s_{n-2})$ is the parametric representation of a unique semipermeable surface which contains $\mathcal{D}$.

3. Barrier Construction:

As defined, the BUP on ζ has zero closing rate and can be though of as a neutral outcome where the trajectory just grazes ζ . To either side of the BUP, E either gets captured or E escapes. Since the BUP is an n-2 dim curve on $\zeta \subset \xi$, Isaacs constructs a SPS backward from ζ starting at the BUP. He calls this SPS the Barrier.

4. Barrier Importance and Physical Interpretation:

The importance of the Barrier can be seen by the implications of the following observations:

1) The Barrier is a surface of state positions in ξ that leads to a neutral outcome for optimal Barrier play (i.e. the Barrier is a family of optimal escape trajectories where termination is just prevented).

2) Because the Barrier is an SPS, it is never crossed provided both players know its existence and play optimally.

3) If the Barrier forms a completely closed surface in ξ, it will divide ξ into two parts. The region between ζ and the Barrier represents a capture region; the region of ξ outside the Barrier represents a region of escape.

4) If play starts with E outside the completely closed Barrier, E can play nc· uniquely until the Barrier is reached at which time $\tilde{v}$ provides an escape strategy for E regardless of what P does.

5) Even if the Barrier is not completely closed, its controls, size, shape and sensitivity to system parameter changes, are important to know.

It is instructive to note that the method of Isaac's Barrier development finds its counterpart in control theory. Since every optimal control problem can be converted to one with a terminal payoff (i.e. a Mayer problem), the terminal surface can be mapped with lines of constant J payoff whose backward optimal trajectories form surfaces of constant payoff (see isocost surfaces in Leitman [9]). The costate vectors are normal to these surfaces. These isocost surfaces parallel Isaac's SPS in that the isocost surface is not penetrated provided the single player plays optimally. In the event play is not optimal, the trajectory moves off to another isocost surface of higher J (in the case of a minimum problem) where the trajectory will remain provided play remains optimal from there on.

Simplifying the necessary conditions of the differential game (i.e. Eqs (2.14), (2.9), (2.11), (2.12)) to the case where $L = 0$ yields.

$$\min_{u \in U} \max_{v \in V} \left[\lambda^T f(x, u, v) \right] = -\partial \Phi / \partial t_f \tag{2.35}$$

$$\dot{\lambda}^T = -\nabla \left[\lambda^T f(x, u, v) \right] \tag{2.36}$$

$$\lambda^T(t_f) = \nabla \Phi \Big|_{t_f} \tag{2.37}$$

$$\Phi = \phi + \xi^T \psi \quad . \tag{2.38}$$

Assume now that ϕ is some terminal payoff with no terminal constraint. Then Eqs (2.35), (2.36), and (2.37) become

$$\lambda^T f(x, u^*, v^*) = 0 \tag{2.39}$$

$$\dot{\lambda}^T = -\nabla \left[\lambda^T f(x, u^*, v^*) \right] \tag{2.40}$$

$$\lambda^T(t_f) = \nabla \phi \Big|_{t_f} \quad . \tag{2.41}$$

Now consider the ϕ isocost surface associated with a particular minimax value. Note that Eq (2.41) implies that $\lambda(t_f)$ is normal to this isocost surface and that Eq (2.39) at t_f implies the trajectory just grazes this surface. If ϕ is specialized to be the physical distance from P to the terminal surface ζ, then Eqs (2.39) and (2.40) are the same as Isaac's Eqs (2.30) and (2.31) for the Barrier. This shows that the Barrier, often solved for by Isaacs, is a family of minimax distance trajectories - in particular the distance associated with the terminal surface ζ. This particular Barrier separates those trajectories that can be drawn into ζ from those which can not.

III. The Simplest Model

This chapter applies the necessary conditions of Chapter II to the simplest of air-to-air combat models. It is instructive in that it illustrates the Isaac's approach which will be applied to all models in this dissertation. The model assumes that the players move with constant velocity magnitude, their controls (simple motion model) being the angular orientation of their velocity vectors. In essence, the model assumes that each combatant is highly maneuverable. The model is first examined in two dimensions. A three dimensional model is briefly discussed as an extension of the two dimensional model.

2D Constant Velocity

1. Problem Setup:

The coordinate system used for this model is shown in Figure 2. The roles of the players are fixed with F pursuing and E evading. At this point, this selection of role is very much intuitive and subjective. Chapter 9 addresses the role decision problem later.

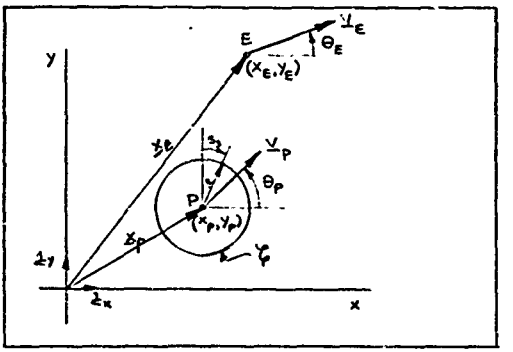

Figure 2: 2D Coordinate System

To make P pursue and E evade, the payoff is taken as the time for P to force E to the terminal surface $\mathcal{C}$, i.e. $L = 1$. P is minimizing and E is maximizing. Note again that the selection of time as the payoff is somewhat arbitrary. For the moment, it is simply a payoff that makes P and E assume the desired roles. There is nothing to say that this is the best payoff to use to simulate pursuit-evasion in a real combat situation.

The terminal surface, $\mathcal{C}$, is assumed to be a circle about P at a radius ℓ taken to be the effective gun radius of P. Its usual description with Eq (2.3) is

$$\underline{\Psi}[\underline{x}(t_f)] = (x_E - x_P)^2 + (y_E - y_P)^2 - \ell^2 = 0 \qquad (3.1)$$

$\mathcal{C}$ can also be described with Eq (2.19) as

$$\begin{aligned} x_P(t_f) &= s_1 &&= h_1(\underline{s}) \\ y_P(t_f) &= s_2 &&= h_2(\underline{s}) \\ x_E(t_f) &= s_1 + \ell \sin s_3 &&= h_3(\underline{s}) \\ y_E(t_f) &= s_2 + \ell \cos s_3 &&= h_4(\underline{s}) \end{aligned} \qquad (3.2)$$

where

$$\underline{s} = \begin{bmatrix} s_1 \\ s_2 \\ s_3 \end{bmatrix} \qquad (3.3)$$

The state vector of the game is

$$\underline{x} = \begin{bmatrix} \underline{x}_P \\ \underline{x}_E \end{bmatrix} = \begin{bmatrix} x_P \\ y_P \\ x_E \\ y_E \end{bmatrix} \tag{3.4}$$

and the state equations are

$$\dot{\underline{x}} = \underline{f}(\underline{x}, \underline{u}, \underline{v}) = \begin{bmatrix} \dot{x}_P \\ \dot{y}_P \\ \dot{x}_E \\ \dot{y}_E \end{bmatrix} = \begin{bmatrix} V_P \cos\theta_P \\ V_P \sin\theta_P \\ V_E \cos\theta_E \\ V_E \sin\theta_E \end{bmatrix} \tag{3.5}$$

where

$$\begin{aligned} \underline{u} &= \theta_P \\ \underline{v} &= \theta_E \end{aligned} \tag{3.6}$$

The costate vector $\underline{\lambda}$ is

$$\underline{\lambda} = \begin{bmatrix} \lambda_{x_P} \\ \lambda_{y_P} \\ \lambda_{x_E} \\ \lambda_{y_E} \end{bmatrix} \tag{3.7}$$

2. Application of Necessary Conditions:

MEl is

$$0 = \min_{\theta_P} \max_{\theta_E} \left[\lambda_{x_P} V_P \cos\theta_P + \lambda_{y_P} V_P \sin\theta_P + \lambda_{x_E} V_E \cos\theta_E + \lambda_{y_E} V_E \sin\theta_E + 1 \right] \equiv$$

$$\equiv \min_{\theta_P} V_P \left[\lambda_{x_P} \cos\theta_P + \lambda_{y_P} \sin\theta_P \right] + \max_{\theta_E} V_E \left[\lambda_{x_E} \cos\theta_E + \lambda_{y_E} \sin\theta_E \right] + 1 \equiv$$

$$\equiv \min_{\theta_P} H_P + \max_{\theta_E} H_E + 1 \tag{3.8}$$

where

$$H_P = V_P\left[\lambda_{x_P}\cos\theta_P + \lambda_{y_P}\sin\theta_P\right]$$
$$H_E = V_E\left[\lambda_{x_E}\cos\theta_E + \lambda_{y_E}\sin\theta_E\right] \quad . \tag{3.9}$$

The $\min_{\theta_P} H_P$ conditions are

$$\frac{\partial H_P}{\partial \theta_P} = 0 \Rightarrow \quad \tan\theta_P^* = \lambda_{y_P}/\lambda_{x_P} \tag{3.10}$$

$$\frac{\partial^2 H_P}{\partial \theta_P^2} \geq 0 \Rightarrow \quad \sin\theta_P^* = \frac{-\lambda_{y_P}}{\sqrt{\lambda_{x_P}^2 + \lambda_{y_P}^2}} \quad , \quad \cos\theta_P^* = \frac{-\lambda_{x_P}}{\sqrt{\lambda_{x_P}^2 + \lambda_{y_P}^2}} \quad . \tag{3.11}$$

The $\max_{\theta_E} H_E$ conditions are

$$\frac{\partial H_E}{\partial \theta_E} = 0 \quad \Rightarrow \quad \tan\theta_E^* = \lambda_{y_E}/\lambda_{x_E} \tag{3.12}$$

$$\frac{\partial^2 H_E}{\partial \theta_E^2} \leq 0 \quad \Rightarrow \quad \sin\theta_E^* = \frac{+\lambda_{y_E}}{\sqrt{\lambda_{x_E}^2 + \lambda_{y_E}^2}} \quad , \quad \cos\theta_E^* = \frac{+\lambda_{x_E}}{\sqrt{\lambda_{x_E}^2 + \lambda_{y_E}^2}} \quad . \tag{3.13}$$

The costate equations are

$$\dot{\underline{\lambda}} = -\left[H_P + H_E\right]_{\underline{x}}^T = -\begin{bmatrix}0\\0\\0\\0\end{bmatrix} = \underline{0} \tag{3.14}$$

implying that

$$\underline{\lambda}(t) = \text{constant vector} = \underline{\lambda}(t_f) \quad . \tag{3.15}$$

The transversality conditions are

$$\sum_{i=1}^{4} \lambda_i \frac{\partial h_i(\underline{z})}{\partial s_k} = \frac{\partial \phi(\underline{z})}{\partial s_k} \equiv 0 \quad , \quad k = 1,2,3$$

$$k = 1 \Rightarrow \quad \lambda_{x_p}(t_f) + \lambda_{x_E}(t_f) = 0 \tag{3.16}$$

$$k = 2 \Rightarrow \quad \lambda_{y_p}(t_f) + \lambda_{y_E}(t_f) = 0 \tag{3.17}$$

$$k = 3 \Rightarrow \quad \lambda_{x_E}(t_f)\, \ell \cos s_3 - \lambda_{y_E}(t_f)\, \ell \sin s_3 = 0 \quad . \tag{3.18}$$

3. Problem Solution:

Eqs (3.12) and (3.18) show that on $\mathcal{C}$

$$\tan \theta_E^* \Big|_{t_f} = \frac{\lambda_{y_E}}{\lambda_{x_E}} \Bigg|_{t_f} = \cot s_3 \equiv \tan(90^\circ - s_3) \tag{3.19}$$

or

$$\theta_E^*(t_f) = 90^\circ - s_3 \equiv \theta_{t_f} \quad . \tag{3.20}$$

Also, Eqs (3.16), (3.17), and (3.10) show

$$\tan \theta_p^* \Big|_{t_f} = \frac{\lambda_{y_p}}{\lambda_{x_p}} \Bigg|_{t_f} = \frac{\lambda_{y_E}}{\lambda_{x_E}} \Bigg|_{t_f} = \tan \theta_E^* \Big|_{t_f} \tag{3.21}$$

and because $\underline{\lambda}(t) = \underline{\lambda}(t_f)$ then

$$\theta_p^*(t) = \theta_E^*(t) = \theta_{t_f} \quad . \tag{3.22}$$

Even without integrating the state equations, the closed form control laws are obvious, i.e. $\Theta_p(t) = \Theta_\varepsilon(t)$ is the instantaneous line of sight angle as viewed by P. The optimal minimax t trajectories are straight, co-linear lines.

4. Barrier Solution:

To examine the game of kind and the Barrier, we first examine $\mathcal{C}$ and find the UP, NUP, and BUP. Define $\underline{v}|_{\mathcal{C}}$ as

$$\underline{v}|_{\mathcal{C}} = \begin{bmatrix} v_{x_p} \\ v_{y_p} \\ v_{x_\varepsilon} \\ v_{y_\varepsilon} \end{bmatrix} \equiv \begin{bmatrix} v_1 \\ v_2 \\ v_3 \\ v_4 \end{bmatrix} \qquad (3.23)$$

The normality condition of $\underline{v}$ on $\mathcal{C}$, $\sum_{i=1}^{4} v_i \frac{\partial h_i(\underline{s})}{\partial s_j} = 0$, $j = 1,2,3$ yields

$$j=1 \Rightarrow \quad v_1(t_f) + v_3(t_f) = 0 \qquad (3.24)$$

$$j=2 \Rightarrow \quad v_2(t_f) + v_4(t_f) = 0 \qquad (3.25)$$

$$j=3 \Rightarrow \quad v_3(t_f)\, \ell \cos s_3 - v_4(t_f)\, \ell \sin s_3 = 0 \qquad (3.26)$$

The unit vector condition implies

$$\left(v_1^2 + v_2^2 + v_3^2 + v_4^2 \right)\Big|_{t_f} = 1 \qquad (3.27)$$

Eqs (3.24) to (3.27) simultaneously yield

$$\underline{v}\Big|_{\zeta} = \begin{bmatrix} -\frac{\sin S_3}{\sqrt{2}} \\ -\frac{\cos S_3}{\sqrt{2}} \\ \frac{\sin S_3}{\sqrt{2}} \\ \frac{\cos S_3}{\sqrt{2}} \end{bmatrix} \quad . \tag{3.28}$$

Expression (2.28) becomes

$$\min_{\underline{u}} \max_{\underline{v}} \underline{v}^T \underline{f}\Big|_{\zeta} = \min_{\theta_P} \max_{\theta_E} \left[-\frac{\sin S_3}{\sqrt{2}} V_P \cos\theta_P + \right. \tag{3.29}$$

$$\left. -\frac{\cos S_3}{\sqrt{2}} V_P \sin\theta_P + \frac{\sin S_3}{\sqrt{2}} V_E \cos\theta_E + \frac{\cos S_3}{\sqrt{2}} V_E \sin\theta_E \right] .$$

The minimax operation in Eq (3.29) is similar in form to the minimax operation in Eq (3.8) implying

$$\sin\tilde{\theta}_P = \cos S_3 \quad , \quad \cos\tilde{\theta}_P = \sin S_3 \tag{3.30}$$

and

$$\sin\tilde{\theta}_E = \cos S_3 \quad , \quad \cos\tilde{\theta}_E = \sin S_3 \quad .$$

Eq (3.29) now becomes

$$\min_{\theta_P} \max_{\theta_E} \underline{v}^T \underline{f}\Big|_{\zeta} = \frac{-V_P + V_E}{\sqrt{2}} \quad . \tag{3.31}$$

Eq (3.31) implies that if

1) $V_P > V_E$ then all of ζ is the UP.

2) $V_P = V_E$ then all of ζ is the BUP.

3) $V_P < V_E$ then all of ζ is the NUP.

In case 1, all of ζ is useable for termination and no Barrier exists. In this case all of ξ is a capture region; E can not avoid capture so long as P uses the line of sight control logic. Similarly, in case 3 none of ζ is useable for termination and all of ξ is an escape region for E provided line of sight evasion is used by E. A BUP exists on ζ only for the special case 2 where $V_P = V_E$ in which case all of ζ is the BUP. The backward trajectories from the BUP become the Barrier which in this case is simply ζ itself. Note that the Barrier in this case is a closed surface and in a trivial way separates ξ. The Barrier, ζ, represents the initial states for which the outcome of the combat is neutral. Outside the closed Barrier is the escape region where E can play non-optimally until the Barrier is approached.

5. Model and Barrier Conclusions:

Several things can be learned even from this simplest of models involving highly maneuverable players:

1) In this pursuit-evasion model, the highly maneuverable combatants want to align their velocity vectors along the line of sight P-E.

2) The Barrier and the outcome of the combat is critically linked to the ratio of the combat velocities $\frac{V_E}{V_P}$.

3) In an attempt to improve the combat capabilities of either player, the Barrier results indicate that the players should increase their velocity advantage.

3D Constant Velocity

This model is a trivial extension of the 2D model. The terminal surface, $\mathcal{C}$, is a sphere of radius, ℓ , about P. The closed form control logic is again line of sight from P to E. The optimal trajectories are straight, co-linear lines in 3D space. The same general conclusions made in the 2D model apply in the 3D model.

IV. Limited Pursuer Model

The dynamics of the pursuer model is made more realistic by constraining him to maneuver his constant magnitude velocity vector within a bounded turning rate, $\dot{\Theta}_P$.

For a real aircraft

$$\dot{\Theta}_P = \frac{\text{acceleration } \perp \text{ to } \underline{V}_P}{|V_P|} .$$

Therefore, the added realism of the bounded turning rate model in actuality is recognizing the maneuvering g limits of a real aircraft imposed by either a structural or human limit. The evader has the dynamics of Chapter III so he can be thought of as highly maneuverable. The model is examined in both two and three dimensions.

2D Limited Pursuer

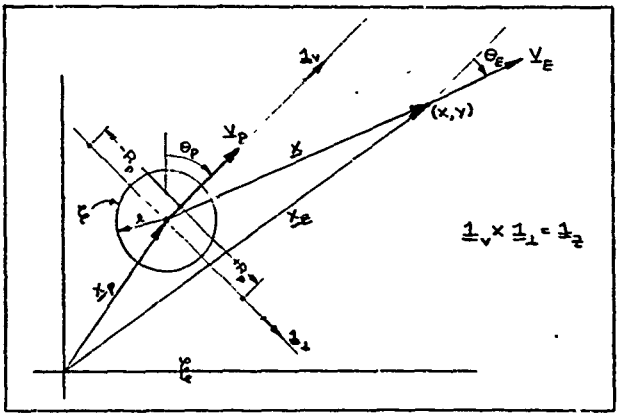

Figure 3: Reduced ξ Coordinate System

Isaacs [7] solves this problem but does not interpret or apply the model or Barrier results.

1. State Equation Formulation:

The model dynamics in Chapter III was formulated in an inertial coordinate system (realistic ξ). The model dynamics here will be formulated in the reduced ξ .

The reduced ξ is the set of orthogonal unit vectors $\underline{1}_v$ and $\underline{1}_\perp$ fixed to P's position and rotating such that $\underline{1}_v$ is always aligned with $\underline{V}_p$. The details of the state equation formulation can be found in Appendix A. The state equations are

$$\begin{bmatrix} \dot{x} \\ \dot{y} \end{bmatrix} = \begin{bmatrix} V_E \sin\theta_E - y\frac{V_p}{R_p}\alpha \\ V_E\cos\theta_E - V_p + x\frac{V_p}{R_p}\alpha \end{bmatrix} \qquad (4.1)$$

Note that

x - distance from P to E along $\underline{V}_p$

y - distance from P to E perpendicular to $\underline{V}_p$

θ_E - E's control; the angle between $\underline{V}_p$ and $\underline{V}_E$

α - P's control; $\alpha = +1\ (-1)$ is a hard right(left) turn

2. Problem Setup:

The terminal surface, $\mathcal{C}$, is again assumed to be a circle about P of radius ℓ . Its usual description with Eq (2.3) is

$$\psi[\underline{x}(t_f)] = x^2(t_f) + y^2(t_f) - \ell^2 = 0 \quad . \tag{4.2}$$

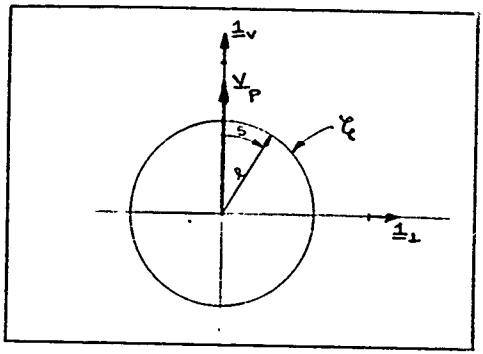

Figure 4: Terminal Surface .

$\mathcal{C}$ can also be described with Eq (2.19) as

$$\begin{aligned} x(t_f) &= h_1(\underline{s}) = \ell \sin s \\ y(t_f) &= h_2(\underline{s}) = \ell \cos s \end{aligned} \tag{4.3}$$

where

$$\underline{s} = [s] \quad . \tag{4.4}$$

The controls for the players are

$$\begin{aligned} \underline{u} &= [\alpha] \\ \underline{v} &= [\theta_E] \end{aligned} \quad . \tag{4.5}$$

and the costate vector $\underline{\lambda}$ is

$$\underline{\lambda} = \begin{bmatrix} \lambda_x \\ \lambda_y \end{bmatrix} \quad . \tag{4.6}$$

As in Chapter III, the roles of the players are preselected by choosing $\phi=0, L=1$ with P minimizing and E maximizing.

3. Application of Necessary Conditions:

ME1 becomes

$$0 = \min_{\alpha} \max_{\theta_E} \left[\lambda_x (V_E \sin\theta_E - y\frac{V_P}{R_P}\alpha) + \lambda_y (V_E \cos\theta_E - V_P + x\frac{V_P}{R_P}\alpha) + 1 \right] \equiv$$

$$\equiv \frac{V_P}{R_P} \min_{\alpha} (x\lambda_y - y\lambda_x) + V_E \max_{\theta_E} (\lambda_x \sin\theta_E + \lambda_y \cos\theta_E) - V_P\lambda_y + 1 \tag{4.7}$$

$$\equiv \frac{V_P}{R_P} \min_{\alpha} H_P + V_E \max_{\theta_E} H_E + H_O$$

where

$$H_P = (x\lambda_y - y\lambda_x)\alpha$$

$$H_E = \lambda_x \sin\theta_E + \lambda_y \cos\theta_E \tag{4.8}$$

$$H_O = -V_P\lambda_y + 1$$

The $\min_{\alpha} H_P$ conditions are

$$\alpha^* = -\text{sgn}(x\lambda_y - y\lambda_x) \equiv -\text{sgn } A \tag{4.9}$$

provided $A \equiv x\lambda_y - y\lambda_x \neq 0$ for a finite time. Since α appears linearly in H_P, there exists the possibility of a singular control in α if $A \equiv 0$ for a finite time. A summary from Appendix A of the α singular

control necessary conditions shows

$$A = x\lambda_y - y\lambda_x = 0 \tag{4.10}$$

$$\dot{A} = V_p\lambda_x = 0 \tag{4.11}$$

$$\ddot{A} = -\frac{V_p^2}{R_p}\lambda_y\alpha = 0 \tag{4.12}$$

$$\lambda_y \geq 0 \quad . \tag{4.13}$$

Therefore, along a singular arc the following conditions hold

$$\alpha = \lambda_x = x = s = 0 \quad . \tag{4.14}$$

The $\max_{\theta_E} H_E$ conditions are

$$\frac{\partial H_E}{\partial \theta_E} = 0 \Rightarrow \tan\theta_E^* = \frac{\lambda_x}{\lambda_y} \tag{4.15}$$

$$\frac{\partial^2 H_E}{\partial \theta_E^2} \leq 0 \Rightarrow \sin\theta_E^* = \frac{\lambda_x}{\sqrt{\lambda_x^2 + \lambda_y^2}} \quad \cos\theta_E^* = \frac{\lambda_y}{\sqrt{\lambda_x^2 + \lambda_y^2}} \tag{4.16}$$

ME2 becomes

$$-\frac{V_p}{R_p}|A| + V_E\sqrt{\lambda_x^2 + \lambda_y^2} - V_p\lambda_y + 1 = 0 \quad . \tag{4.17}$$

The costate equations are

$$\dot{\underline{\lambda}} = -\nabla H^T = -\begin{bmatrix}\frac{\partial H}{\partial x}\\ \frac{\partial H}{\partial y}\end{bmatrix} = -\begin{bmatrix}\frac{V_p}{R_p}\lambda_y\alpha\\ -\frac{V_p}{R_p}\lambda_x\alpha\end{bmatrix} \tag{4.18}$$

The transversality conditions are $\sum_{i=1}^{2} \lambda_i \frac{\partial h_i(s)}{\partial s_j} = \frac{\partial \phi(s)}{\partial s_j} \equiv 0, \; j = 1$

$$j=1 \Rightarrow \lambda_x(t_f)\ell\cos s - \lambda_y(t_f)\ell \sin s = 0 \quad . \tag{4.19}$$

4. Problem Backward Solution From $\mathcal{C}_\epsilon$:

As indicated on pg 12, a closed form control is needed for a real time application of differential games. In the case of the Barrier, closed form control on either side of the Barrier is needed to insure that the Barrier is not inadvertenly crossed. The backward solution from the UP of $\mathcal{C}_\epsilon$ is analyzed to provide the closed form control on the pursuer side of the Barrier. The details of the analysis are presented in Appendix A of which the following is a summary.

The controls on the UP of $\mathcal{C}_\epsilon$ are

$$\theta_\epsilon^*(t_f) = s \tag{4.20}$$

$$\alpha^*(t_f) = \text{sgn}(\sin s) \quad . \tag{4.21}$$

A singular control in α occurs at $\mathcal{C}_\epsilon$ for $S=0$ and has the following necessary state and control conditions.

$$\begin{aligned} \dot{x} &= 0 \\ \alpha &= 0 \\ \theta_\epsilon &= 0 \end{aligned} \tag{4.22}$$

The singular surface in the reduced ξ is simply the y-axis and represents a non-turning direct tail chase.

The trajectories and controls backward from the UP of ξ for $s>0$ (note $s<0$ is symmetric about the y-axis) are

$$\theta_E^*(\tau) = s + \frac{V_p}{R_p}\tau \tag{4.23}$$

$$\alpha^*(\tau) = \text{sgn}\left[\cos s - \cos\left(s+\frac{V_p}{R_p}\tau\right)\right] \quad . \tag{4.24}$$

α^* switching occurs when

$$\frac{V_p}{R_p}\tau = 2(\pi - s) \quad . \tag{4.25}$$

Prior to α^* switching the state trajectories are

$$x(\tau) = (\ell - V_E\tau)\sin\left(s+\frac{V_p}{R_p}\tau\right) + R_p\left(1-\cos\frac{V_p}{R_p}\tau\right) \tag{4.26}$$

$$y(\tau) = (\ell - V_E\tau)\cos\left(s+\frac{V_p}{R_p}\tau\right) + R_p\sin\frac{V_p}{R_p}\tau \quad . \tag{4.27}$$

As will be seen later, the Barrier is completely closed for realistic system parameters and the above trajectories intersect the Barrier and terminate prior to α^* switching.

Fig 5 shows some of the basic backward trajectories and controls (neglecting the Barrier) in both the reduced and realistic ξ.

For most of the initial states, E orients

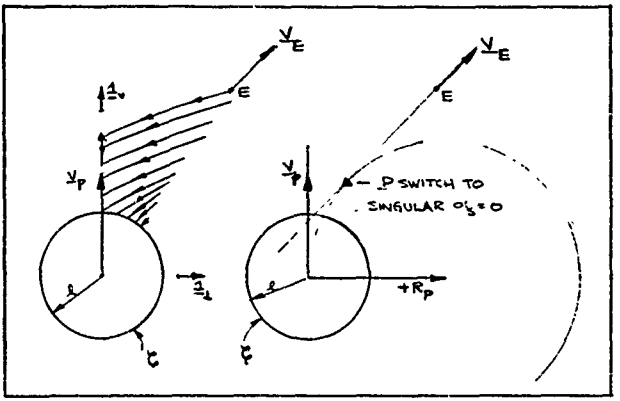

Figure 5: 2D Limited Pursuer Trajectories & Controls

V_E tangent to P's circular path which is a fixed angle in the realistic $\mathcal{C}_\xi$ and travels in a straight line. P does a hard right turn until E is directly down the line of sight along $\underline{V}_P$ at which time P switches to the singular control $\alpha=0$ and the remainder of the trajectory is a direct tail chase. Now we examine the Barrier and its influence on the solution of the game.

5. Barrier Backward Solution From $\mathcal{C}_\xi$:

As in Chapter III we first examine $\mathcal{C}_\xi$ and find the UP, NUP, and BUP.

Define $\underline{v}|_{\xi}$ as

$$\underline{v}|_{\xi} = \begin{bmatrix} v_x \\ v_y \end{bmatrix} \equiv \begin{bmatrix} v_1 \\ v_2 \end{bmatrix} \quad . \tag{4.28}$$

The normality condition of $\underline{v}$ on ξ, $\sum_{i=1}^{2} v_i \frac{\partial h_i(s)}{\partial s_j} = 0$, $j = 1$

yields

$$v_x(t_f)\ell \cos s - v_y(t_f)\ell \sin s = 0 \quad . \tag{4.29}$$

The unit vector condition implies

$$(v_x^2 + v_y^2)\Big|_{t_f} = 1 \quad . \tag{4.30}$$

Eq (4.29) and (4.30) yield

$$\underline{v}|_{\xi} = \begin{bmatrix} \sin s \\ \cos s \end{bmatrix} \quad . \tag{4.31}$$

Expression (2.28) becomes

$$\min_{\underline{u}} \max_{\underline{v}} \underline{v}^T \underline{f}\Big|_{\xi} = \min_{\alpha} \max_{\theta_E} \left[v_x \left(V_E \sin\theta_E - \frac{V_P}{R_P} y\alpha \right) + \right.$$

$$\left. + v_y \left(V_E \cos\theta_E - V_P + \frac{V_P}{R_P} x\alpha \right) \right] = \tag{4.32}$$

$$= \frac{V_P}{R_P} \min_{\alpha} (x v_y - y v_x)\alpha + V_E \max_{\theta_E} (v_x \sin\theta_E + v_y \cos\theta_E) - V_P v_y \quad .$$

The similarity of Eqs (4.32) and (4.7) show that

$$\tilde{\alpha} = -\operatorname{sgn}(x v_y - y v_x) \tag{4.33}$$

$$\sin\tilde{\theta}_E = \frac{v_x}{\sqrt{v_x^2 + v_y^2}} \quad , \quad \cos\tilde{\theta}_E = \frac{v_y}{\sqrt{v_x^2 + v_y^2}} \quad .$$

Substituting Eq (4.33) into Eq (4.32) yields

$$\min_{\underline{U}} \max_{\underline{V}} \underline{v}^T \underline{f}\Big|_{t_f} = -\frac{V_p}{R_p} |x v_y - y v_x| + \sqrt{v_x^2 + v_y^2} - V_p v_y. \tag{4.34}$$

Substituting Eqs (4.3) and (4.31) into Eq (4.34) yields

$$\min_{\underline{U}} \max_{\underline{V}} \underline{v}^T \underline{f}\Big|_{t_f} = V_E - V_p \cos S \ . \tag{4.35}$$

Eq (4.35) and the definition of the UP, NUP and BUP implies that if

1) $\cos S < \frac{V_E}{V_p} \Rightarrow S \in UP$

2) $\cos S = \frac{V_E}{V_p} \Rightarrow S \in BUP$

3) $\cos S > \frac{V_E}{V_p} \Rightarrow S \in NUP$.

If we define $S_o = \cos^{-1} \frac{V_E}{V_p}$ then

1) $-S_o < S < S_o \Rightarrow UP$

2) $S = \pm S_o \Rightarrow BUP$

3) $|S| > S_o \Rightarrow NUP$.

If Eq (4.32) is equated to zero it becomes pseudo ME1. Eqs (4.33) are the Barrier controls and Eq (4.34) equated to zero is pseudo ME2. The costate Eq (2.31) for the Barrier takes the same form as Eq (4.18) except that $\underline{\lambda}$ is replaced by $\underline{v}$ i.e.

$$\dot{\underline{v}} = -\begin{bmatrix} \frac{V_p}{R_p} v_y \alpha \\ -\frac{V_p}{R_p} v_x \alpha \end{bmatrix} \tag{4.36}$$

The state equations and Eq (4.36) are now integrated backward from the BUP on $\mathcal{C}_E$ to get the Barrier. In doing this it is instructive to note that the state, costate and control equations (i.e. Eqs (4.1), (4.18), (4.9), (4.11)) for the UP of $\mathcal{C}_E$ have the same form as the state, costate and control equation (i.e. Eqs (4.1), (4.36), (4.33)) of the Barrier. The state boundary conditions, Eq (4.3), have the same form except in the case of the Barrier, S is specialized to S_o. The costate boundary condition Eqs (A.17) and (4.31) are similar except in the latter case $V_p \cos S - V_E$ does not appear and S is specialized to S_o. Even though the backward trajectories of Eqs (4.26) and (4.27) are quite different from the Barrier, the backward solution of the Barrier equations take the same general form as Eqs (A.32), (4.23), (A.36), (4.26), (4.27), i.e.

$$v_x(T) = \sin\left(S_o + \frac{V_p}{R_p} T\right) \tag{4.37}$$

$$v_y(T) = \cos\left(S_o + \frac{V_p}{R_p} T\right) \tag{4.38}$$

$$\Theta_E(T) = S_o + \frac{V_p}{R_p} T \tag{4.39}$$

$$A(T) = x v_y - y v_x = -R_p\left[\cos S_o - \cos\left(S_o + \frac{V_p}{R_p} T\right)\right] \tag{4.40}$$

$$x(T) = (\ell - V_E T)\sin\left(S_o + \frac{V_p}{R_p} T\right) + R_p\left(1 - \cos\frac{V_p}{R_p} T\right) \tag{4.41}$$

$$y(T) = (\ell - V_E T)\cos\left(S_o + \frac{V_p}{R_p} T\right) + R_p \sin\frac{V_p}{R_p} T \tag{4.42}$$

Isaacs [7,236] gives a very instructive construction aid for visualizing the shape of one side of the Barrier which is shown in Figure 6. A circle C_1 of radius $V_E/V_P R_P$ is constructed at position R_P on the x axis. The terminal surface ζ_e is constructed at the origin. A line is drawn from the origin tangent to the upper part of C_1. This line cuts ζ_e at the BUP. A taught string can be visualized as wound around C_1 and coming off of C_1 to initially lie on the above line thru the origin. The point on the string over the BUP is marked. As the string is unwound in a taught fashion, the point on the string which was initially over the BUP traces the Barrier, i.e. physically behaves as Eq (4.41) and (4.42). The angle $\frac{V_P}{R_P}\tau$ is the angle between the initial tangent point of the string on C_1 and the instantaneous tangent point of the string on C_1.

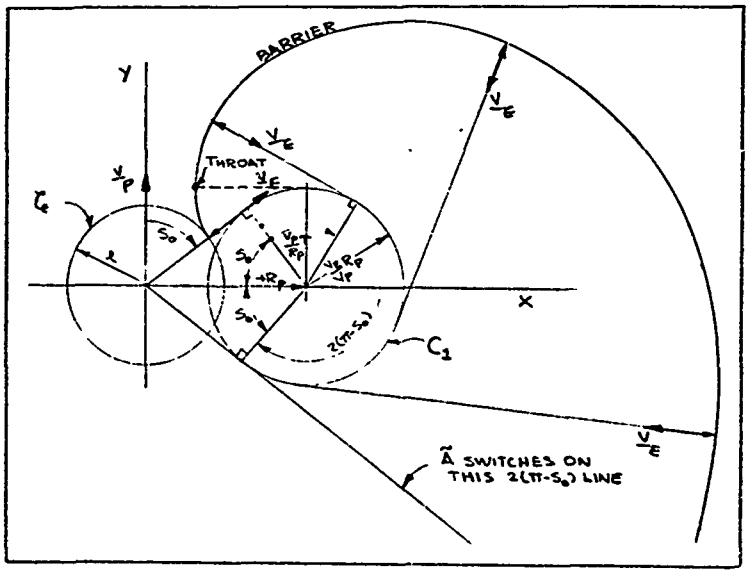

Figure 6: Isaac's Barrier Construction

6. Barrier Interpretation:

Note from Fig 6 that the Barrier throat always occurs when

$$S_o + \frac{V_p}{R_p} T = \pi/2 \quad . \tag{4.43}$$

This is easily seen in Fig 6, but can also be obtained from Eq (4.41) as a condition to make $\dot{x} = 0$. Substituting Eq (4.43) into Eq (4.42) yields

$$Y_{throat} = R_p \sin(\pi/2 - S_o) = R_p \cos S_o = R_p \frac{V_E}{V_p} \quad . \tag{4.44}$$

Since the left half of the barrier is symmetric about the Y-axis, the condition for complete Barrier closure is for any portion of the right Barrier to have negative X i.e.

$$R_p \sin S_o - \ell + (\pi/2 - S_o) \frac{V_E}{V_p} R_p > R_p \quad . \tag{4.45}$$

Since $\cos S_o = V_E / V_p$ then

$$\sin S_o = \sqrt{1 - (V_E/V_p)^2} \tag{4.46}$$

and

$$\sin(\pi/2 - S_o) = \cos S_o = V_E/V_p \tag{4.47}$$

implying

$$\pi/2 - S_o = \sin^{-1} V_E/V_p \quad . \tag{4.48}$$

Rearranging Eq (4.45) and dividing by R_p yields

$$\ell/R_p \leq \sqrt{1 - (V_E/V_p)^2} + \frac{V_E}{V_p} \sin^{-1}\left(\frac{V_E}{V_p}\right) - 1 \quad . \tag{4.49}$$

Defining $f\left(\frac{V_E}{V_P}\right)$ as

$$f\left(\frac{V_E}{V_P}\right) = 1-\left(\frac{V_E}{V_P}\right)^2 + \frac{V_E}{V_P}\sin^{-1}\left(\frac{V_E}{V_P}\right) - 1 \qquad (4.50)$$

Eq (4.49) becomes

$$\frac{\ell}{R_P} \leq f\left(\frac{V_E}{V_P}\right) \quad . \qquad (4.51)$$

The equality in Eq (4.51) corresponds to the case where the Barrier is tangent to and just touches the Y-axis. For $\frac{\ell}{R_P} < f\left(\frac{V_E}{V_P}\right)$, closure of the Barrier at the Y-axis is not grazing and occurs for $S_o + \frac{V_P}{R_P}\tau < \pi/2$.

If we assume $\frac{\ell}{R_P} < f\left(\frac{V_E}{V_P}\right)$ and define Θ_c as that value of $\frac{V_E}{R_P}\tau$ for which X = 0, then the time of closure τ_c is

$$\tau_c = \Theta_c \frac{R_P}{V_P} \quad . \qquad (4.52)$$

Substituting Eq (4.52) into Eq (4.41) with X = 0 yields

$$0 = \left(\ell - \frac{V_E}{V_P}R_P\Theta_c\right)\sin(S_o+\Theta_c) + R_P(1-\cos\Theta_c) \, . \qquad (4.53)$$

Dividing Eq (4.53) by R_P and rearranging yields the closure condition when $\Theta_c \leq \pi/2 - S_o$, i.e.

$$\frac{\ell}{R_P} = \frac{V_E}{V_P}\Theta_c - \frac{1-\cos\Theta_c}{\sin(S_o+\Theta_c)} \quad . \qquad (4.54)$$

Substituting the definition of Θ_c into "pseudo" ME2, Eq (4.34), and using Eqs (4.37) and (4.38) yields

$$-\frac{V_P}{R_P}\left|-\gamma_c\sin(S_o+\Theta_c)\right| + V_E - V_P\cos(S_o+\Theta_c) = 0 \, . \qquad (4.55)$$

Since $Y_c > 0$ and $\sin(\delta_o + \theta_c) > 0$, rearranging Eq (4.55) yields

$$\frac{Y_c}{R_p} = \left[\frac{V_E}{V_p} - \cos(\delta_o + \theta_c)\right] \Big/ \sin(\delta_o + \theta_c) \qquad (4.56)$$

which can be used to get $\frac{Y_c}{R_p}$ for given θ_c. Figure 7 is a plot of Eq (4.54) for lines of constant $\delta_o + \theta_c \leq 90^\circ$. Superimposed on these lines are lines of constant $\frac{Y_c}{R_p}$.

We now use the Barrier and its closing conditions in Fig 7 to learn as much as possible about the air-to-air combat problem and the problem parameters which have major affect on its outcome. Consider a combat engagement where P is at Mach # = .8 at 30000 ft. altitude (i.e. V_p = 800 ft/sec). We assume that P maneuvers with a maximum load factor of 5 gs. The 800 ft/sec velocity and 5 g load factor together yield a turning radius R_p = 4000 ft. We further assume that under these conditions, P's guns can effect a kill at a radius ℓ = 1000 ft. Since $\frac{\ell}{R_p}$ = .25, Fig 7 shows that in order for P to insure that the Barrier is not closed, he must have sufficient velocity advantage so that $\frac{V_E}{V_p} \leq .69$. This is quite a large advantage to assume P to have. In a more realistic situation we might expect P to have a velocity advantage $\frac{V_E}{V_p} \simeq .85 - .95$ which implies that the Barrier is closed. Note how the added realism of P's model has limited his capability as compared to the simplest model in Chapter III where the only requirement for capture was $\frac{V_E}{V_p} < 1$. We therefore see that for a combat engagement with realistic parameters (against a highly maneuverable evader), the Barrier is completely closed.

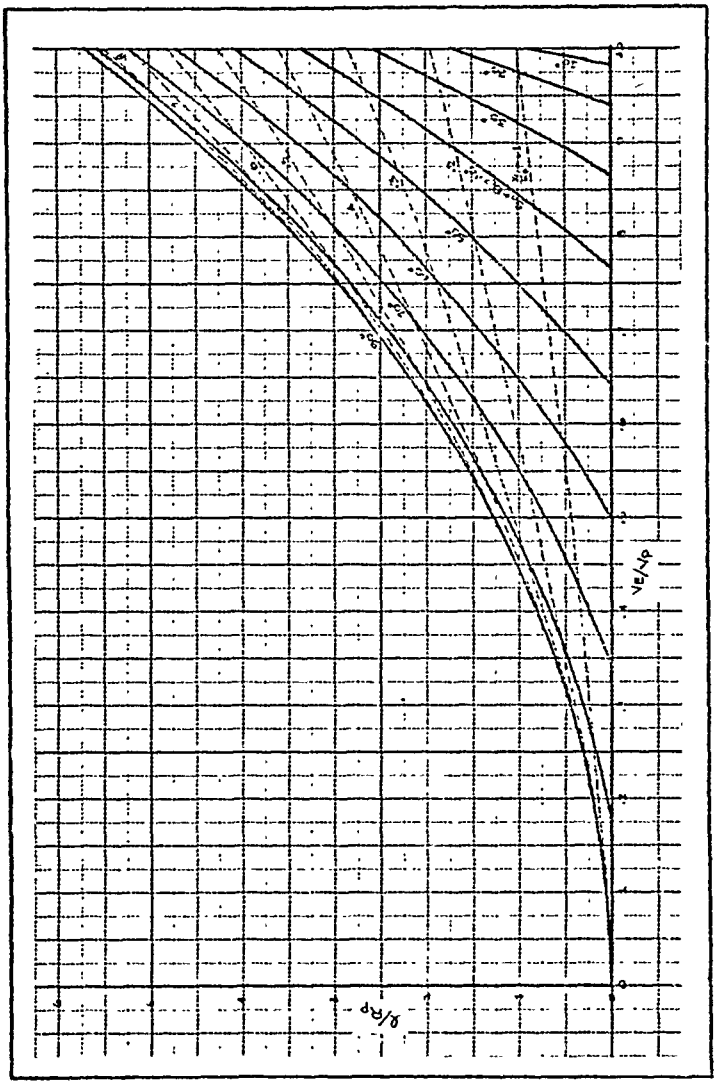

Figure 7: Barrier Closing Conditions

Faced with P's limited capability and a closed Barrier, we are interested in the best way to improve P's air-to-air combat capability. Any of the following three improvements should increase P's combat capability: 1) increase V_p , 2) increase ℓ (i.e. weapons system capability), 3) decrease the turning radius R_p (i.e. higher gs). To make this decision, we assume that the area of the capture region is a good measure of P's air-to-air combat capability. A closed Barrier is shown in Fig 8.

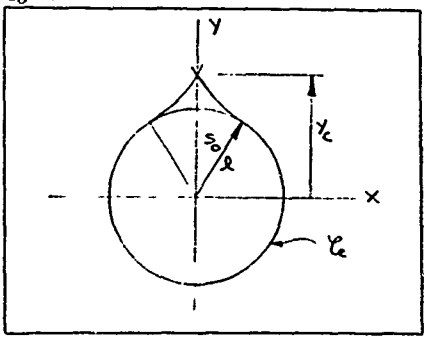

Figure 8: Closed Barrier

The area of the capture region, A_c , is approximated by

$$A_c = y_c \ell \sin s_o = R_p \frac{y_c}{R_p}\left(\frac{\ell}{R_p}, \frac{V_E}{V_p}\right) \ell \sqrt{1 - \left(\frac{V_E}{V_p}\right)^2} \qquad (4.57)$$

where the $\frac{y_c}{R_p}\left(\frac{\ell}{R_p}, \frac{V_E}{V_p}\right)$ relationship is given in Fig 7. The nominal condition $\frac{\ell}{R_p} = .25$, $\frac{V_E}{V_p} = .9$, $\ell = 1000$ ft and $V_p =$ 800 ft/sec is assumed and the gradient of A_c is given in Eq (4.58).

$$\nabla A_c = \begin{bmatrix} \frac{\partial A_c}{\partial R_p} \\ \frac{\partial A_c}{\partial \ell} \\ \frac{\partial A_c}{\partial V_p} \end{bmatrix} = \begin{bmatrix} \frac{Y_c}{R_p}\ell \sin s_o + R_p \ell \sin s_o \frac{\partial\left(\frac{Y_c}{R_p}\right)}{\partial\left(\frac{\ell}{R_p}\right)} \frac{\partial\left(\frac{\ell}{R_p}\right)}{\partial R_p} \\ Y_c \sin s_o + R_p \ell \sin s_o \frac{\partial\left(\frac{Y_c}{R_p}\right)}{\partial\left(\frac{\ell}{R_p}\right)} \frac{\partial\left(\frac{\ell}{R_p}\right)}{\partial \ell} \\ \left(R_p \ell \sin s_o \frac{\partial\left(\frac{Y_c}{R_p}\right)}{\partial\left(\frac{V_E}{V_p}\right)} - \frac{R_p \frac{Y_c}{R_p} \ell \frac{V_E}{V_p}}{\sin s_o}\right) \frac{\partial\left(\frac{V_E}{V_p}\right)}{\partial V_p} \end{bmatrix} \quad (4.58)$$

Since

$$\frac{\partial\left(\frac{\ell}{R_p}\right)}{\partial R_p} = -\frac{\ell}{R_p^2} \quad , \quad \frac{\partial\left(\frac{\ell}{R_p}\right)}{\partial \ell} = \frac{1}{R_p} \quad , \quad \frac{\partial\left(\frac{V_E}{V_p}\right)}{\partial V_p} = -\frac{V_E}{V_p{}^2}$$

then Eq (4.58) becomes

$$\nabla A_c = \begin{bmatrix} \ell \sin s_o \left[\frac{Y_c}{R_p} - \frac{\ell}{R_p} \frac{\partial\left(\frac{Y_c}{R_p}\right)}{\partial\left(\frac{\ell}{R_p}\right)}\right] \\ R_p \sin s_o \left[\frac{Y_c}{R_p} + \frac{\ell}{R_p} \frac{\partial\left(\frac{Y_c}{R_p}\right)}{\partial\left(\frac{\ell}{R_p}\right)}\right] \\ \frac{R_p}{V_p} \frac{V_E}{V_p} \ell \left[\frac{Y_c}{R_p} \frac{V_E}{V_p} / \sin s_o - \sin s_o \frac{\partial\left(\frac{Y_c}{R_p}\right)}{\partial\left(\frac{V_E}{V_p}\right)}\right] \end{bmatrix} \quad (4.59)$$

From Figure 7 we get $\frac{Y_c}{R_p} = .313$, $\frac{\partial\left(\frac{Y_c}{R_p}\right)}{\partial\left(\frac{\ell}{R_p}\right)} = 1.51$, and $\frac{\partial\left(\frac{Y_c}{R_p}\right)}{\partial\left(\frac{V_E}{V_p}\right)} =$ -.60. Therefore Eq (4.59) becomes

$$\nabla A_c = \begin{bmatrix} \frac{\partial A_c}{\partial R_p} \\ \frac{\partial A_c}{\partial \ell} \\ \frac{\partial A_c}{\partial V_p} \end{bmatrix} = \begin{bmatrix} -28 \text{ ft}^2/\text{ft} \\ 1200 \text{ ft}^2/\text{ft} \\ 4080 \text{ ft}^2/\text{ft/sec} \end{bmatrix} \quad (4.60)$$

Eq (4.60) shows the overriding influence of V_P (i.e. $\frac{V_E}{V_P}$) on P's combat capability. This result suggests that an increase of V_P inhances P's combat capability more than corresponding improvements in the weapons system or turn radius. It should be noticed that the tip of the Barrier is located at $Y_c = .313 \times 4000 = 1250$ ft in front of P and E's velocity angle off at the tip to effect the escape is $\Theta_E = S_o + \Theta_c = 47°$. Inside the Barrier, E's optimal velocity angle off is much smaller (i.e. less than 10°) and indicative of a tail chase maneuver. This discontinuity of E's control across the Barrier is a characteristic of the Barrier.

7. Model and Barrier Conclusions:

1) The simplest model showed that for P to guarantee capture, all that was needed was for $V_E/V_P < 1$. P's dynamics was made more realistic in the present model, in that P was limited in turn capability. For realistic P model parameters, and $\frac{V_E}{V_P} < 1$, the Barrier closes within P's visibility range and much of the state space, ξ_c, is outside the Barrier and unavailable for capture of E by P. The main observation to be made here, is that the effect of P's limited turn rate on his combat capability (note one would expect this to decrease his capability) is reflected in the Barrier capture area as a numerically measurable decrease.

2) In this pursuit-evasion model, the combatants are still attempting to align their velocity vectors along the line of sight P-E; however, the optimal control laws to do this have been refined by the added parameters in the problem.

3) Sensitivity analysis of the Barrier continues to show that $\frac{V_E}{V_P}$ is the most important parameter. The weapons capability ℓ is next, followed by the turn radius R_p.

3D Limited Pursuer

This model development is original work. The intent in studying this model is to begin to reveal what the out-of-plane optimal maneuvers are and how they affect air-to-air combat.

1. State Equation Formulation:

The coordinate system for this model is shown in Fig. 9. P maneuvers by selecting the magnitude, α, of his transverse

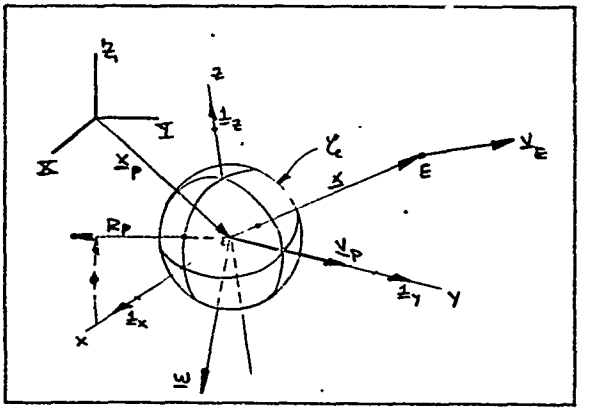

Figure 9: 3D Coordinate System

acceleration and its clock angle orientation, ϕ . The added complexity of this model is that P must not only select the magnitude of his transverse acceleration but also the bank angle. E continues to maneuver by selecting the orientation of $\underline{V}_E$ through the direction cosines ($\bar{l}, \bar{m}, \bar{n}$) which are relative to the x, y, z axes system. The model dynamics is formulated in the reduced ξ i.e. (x, y, z). The details of the state equation formulation can be found in Appendix A. The state equations are

$$\begin{bmatrix} \dot{x} \\ \dot{y} \\ \dot{z} \end{bmatrix} = \begin{bmatrix} V_E \bar{l} - \frac{V_P}{R_P} \alpha y \cos\phi \\ V_E \bar{m} - V_P + \frac{V_P}{R_P} \alpha (x \cos\phi + z \sin\phi) \\ V_E \bar{n} - \frac{V_P}{R_P} \alpha y \sin\phi \end{bmatrix} \tag{4.61}$$

where

$$0 \le \phi \le 2\pi \quad , \quad 0 \le \alpha \le 1 \tag{4.62}$$

$$\bar{l}^2 + \bar{m}^2 + \bar{n}^2 = 1 \quad . \tag{4.63}$$

2. Problem Setup:

The terminal surface, ζ , is assumed to be a sphere about P of radius ℓ . Its usual description with Eq (2.3) is

$$\psi[\underline{x}(t_f)] = x^2(t_f) + y^2(t_f) + z^2(t_f) - \ell^2 = 0 \quad . \tag{4.64}$$

ζ can also be described with Eq (2.19) as

$$\begin{aligned} x(t_f) &= h_1(\underline{s}) = \ell \cos s_2 \sin s_1 \\ y(t_f) &= h_2(\underline{s}) = \ell \cos s_2 \cos s_1 \\ z(t_f) &= h_3(\underline{s}) = \ell \sin s_2 \end{aligned} \tag{4.65}$$

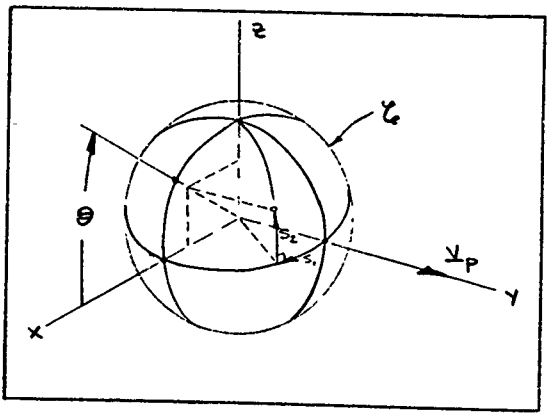

Figure 10: 3D Terminal Surface

where

$$\underline{s} = \begin{bmatrix} s_1 \\ s_2 \end{bmatrix} \tag{4.66}$$

The controls for the players are

$$\underline{u} = \begin{bmatrix} \alpha \\ \phi \end{bmatrix}$$

$$\underline{v} = \begin{bmatrix} \bar{\ell} \\ \bar{m} \\ \bar{n} \end{bmatrix} \tag{4.67}$$

and the costate vector $\underline{\lambda}$ is

$$\underline{\lambda} = \begin{bmatrix} \lambda_x \\ \lambda_y \\ \lambda_z \end{bmatrix} \tag{4.68}$$

As with the other models, the roles of the players are preselected by choosing $\phi = 0$, L = 1 with P minimizing and E maximizing.

3. Application of Necessary Conditions:

NE 1 becomes

$$0 = \min_{(\alpha,\phi)} \max_{(\bar{\ell},\bar{m},\bar{n})} \left\{ \lambda_x \left[V_E \bar{\ell} - \frac{V_P}{R_P} y \alpha \cos\phi \right] + \lambda_y \left[V_E \bar{m} - V_P + \right.\right.$$

$$\left.\left. + \frac{V_P}{R_P} \alpha (x\cos\phi + z\sin\phi) \right] + \lambda_z \left[V_E \bar{n} - \frac{V_P}{R_P} \alpha y \sin\phi \right] + 1 \right\} =$$

$$= \min_{(\alpha,\phi)} \frac{V_P}{R_P} \alpha \left[(x\lambda_y - y\lambda_x)\cos\phi + (z\lambda_y - y\lambda_z)\sin\phi \right] +$$

$$+ \max_{(\bar{\ell},\bar{m},\bar{n})} V_E \left[\bar{\ell}\lambda_x + \bar{m}\lambda_y + \bar{n}\lambda_z \right] - V_P \lambda_y + 1 =$$

$$= \frac{V_P}{R_P} \min_{(\alpha,\phi)} H_P + V_E \max_{(\bar{\ell},\bar{m},\bar{n})} H_E + H_o \qquad (4.69)$$

where

$$H_P = \alpha \left[(x\lambda_y - y\lambda_x)\cos\phi + (z\lambda_y - y\lambda_z)\sin\phi \right]$$

$$H_E = \bar{\ell}\lambda_x + \bar{m}\lambda_y + \bar{n}\lambda_z \qquad (4.70)$$

$$H_o = -V_P\lambda_y + 1 \quad .$$

The min H_P conditions are

$$\frac{\partial H_P}{\partial \phi} = 0 \overset{\alpha \neq 0}{\Longrightarrow} \quad \tan\phi^* = \frac{B}{A}$$

$$\frac{\partial^2 H_P}{\partial \phi^2} \geq 0 \overset{\alpha \neq 0}{\Longrightarrow} \quad \sin\phi^* = \frac{-B}{\sqrt{A^2+B^2}} \;,\; \cos\phi^* = \frac{-A}{\sqrt{A^2+B^2}}$$

$$\alpha^* = 1 \qquad (4.71)$$

where

$$A = x\lambda_y - y\lambda_x$$

$$B = z\lambda_y - y\lambda_z \qquad (4.72)$$

The max H_E conditions subject to the constraint Eq (A.47) are

$$\bar{\ell}^* = \frac{\lambda_x}{\sqrt{\lambda_x^2+\lambda_y^2+\lambda_z^2}}$$

$$\bar{m}^* = \frac{\lambda_y}{\sqrt{\lambda_x^2+\lambda_y^2+\lambda_z^2}} \qquad (4.73)$$

$$\bar{n}^* = \frac{\lambda_z}{\sqrt{\lambda_x^2+\lambda_y^2+\lambda_z^2}}$$

ME 2 becomes

$$0 = -\frac{V_p}{R_p}\sqrt{A^2+B^2} + V_E\sqrt{\lambda_x^2+\lambda_y^2+\lambda_z^2} - \lambda_y V_p + 1 \qquad (4.74)$$

The costate equations are

$$\dot{\underline{\lambda}} = -\nabla H^T = -\begin{bmatrix}\frac{\partial H}{\partial x}\\ \frac{\partial H}{\partial y}\\ \frac{\partial H}{\partial z}\end{bmatrix} = -\begin{bmatrix}\frac{V_p}{R_p}\alpha\lambda_y\cos\phi\\ -\frac{V_p}{R_p}\alpha(\lambda_x\cos\phi+\lambda_z\sin\phi)\\ \frac{V_p}{R_p}\alpha\lambda_y\sin\phi\end{bmatrix} \qquad (4.75)$$

The transversality conditions $\sum_{i=1}^{3}\lambda_i\frac{\partial h_i(\underline{s})}{\partial s_j} = \frac{\partial\phi(\underline{s})}{\partial s_j} \equiv 0$,

$j = 1,2$ are

$$j=1 \Rightarrow (\lambda_x\cos s_1 - \lambda_y\sin s_1)\Big|_{\ell}\, \ell\cos s_2 = 0 \qquad (4.76)$$

$$j=2 \Rightarrow (-\lambda_x\sin s_1\sin s_2 - \lambda_y\sin s_2\cos s_1 + \lambda_z\cos s_2)\Big|_{\ell}\, \ell = 0 \qquad (4.77)$$

4. Problem Backward Solution From ζ :

Ordinarily, the following analysis of the backward solution from ζ would appear in an appendix; however, it is essential to the proof of a proposition that P's motion is planar. We begin by determining the controls on ζ , then the proposition follows.

Subsituting Eq (4.76) into Eq (4.77) yields

$$\lambda_z\Big|_{\zeta} = \lambda_y\Big|_{\zeta} \tan s_2 / \cos s_1 \quad . \tag{4.78}$$

Noting that

$$A\Big|_{\zeta} = (x\lambda_y - y\lambda_x)\Big|_{\zeta} = \ell \cos s_2 \sin s_1 \lambda_y\Big|_{\zeta} - \ell \cos s_2 \sin s_1 \lambda_y\Big|_{\zeta} \equiv 0 \tag{4.79}$$

$$B\Big|_{\zeta} = (z\lambda_y - y\lambda_z)\Big|_{\zeta} = \ell \sin s_2 \lambda_y\Big|_{\zeta} - \ell \sin s_2 \lambda_y\Big|_{\zeta} \equiv 0 \tag{4.80}$$

and substituting Eq (4.76) and (4.78) into Eq (4.74) yields for ME 2 on ζ

$$0 = V_E \sqrt{\tan^2 s_1 \lambda_y\Big|_{\zeta}^2 + \lambda_y^2\Big|_{\zeta} + \frac{\tan^2 s_2}{\cos^2 s_1} \lambda_y^2\Big|_{\zeta}} - V_p \lambda_y\Big|_{\zeta} + 1 \quad . \tag{4.81}$$

Simplying Eq (4.81) yields

$$V_E \left| \frac{\lambda_y|_{\zeta}}{\cos s_2 \cos s_1} \right| - V_p \lambda_y\Big|_{\zeta} + 1 = 0 \quad . \tag{4.82}$$

Since $\lambda_y > 0$ Eq (4.32) yields,

$$\lambda_y\Big|_{\ell_e} = \frac{\cos S_1 \cos S_2}{V_p \cos S_1 \cos S_2 - V_E} \quad . \tag{4.83}$$

Substituting Eq (4.83) into Eqs (4.76) and (4.78) yields

$$\lambda_x\Big|_{\ell_e} = \frac{\sin S_1 \cos S_2}{V_p \cos S_1 \cos S_2 - V_E} \tag{4.84}$$

$$\lambda_z\Big|_{\ell_e} = \frac{\sin S_2}{V_p \cos S_1 \cos S_2 - V_E} \quad .$$

Noting that

$$\sqrt{\lambda_x^2 + \lambda_y^2 + \lambda_z^2}\,\Big|_{\ell_e} = \frac{1}{V_p \cos S_1 \cos S_2 - V_E} \tag{4.85}$$

we see that

$$\begin{aligned} \bar{\ell}^*\Big|_{\ell_e} &= \sin S_1 \cos S_2 \\ \bar{m}^*\Big|_{\ell_e} &= \cos S_1 \cos S_2 \\ \bar{n}^*\Big|_{\ell_e} &= \sin S_2 \end{aligned} \tag{4.86}$$

which shows that $\underline{V}_E\Big|_{\ell_e}$ is perpendicular to ℓ_e . Since $\tan\Phi^*\Big|_{\ell_e} = \frac{B}{A}\Big|_{\ell_e} = \frac{0}{0}$, we use l'Hopital's rule to evaluate $\Phi^*\Big|_{\ell_e}$, i.e.

$$\tan\phi^*\Big|_{\ell_e} = \frac{\lim_{\tau \to 0} \frac{dB}{d\tau}}{\lim_{\tau \to 0} \frac{dA}{d\tau}} \quad . \tag{4.87}$$

Now

$$\frac{dA}{dt} = -\frac{dA}{d\tau} = \dot{x}\lambda_y + x\dot{\lambda}_y - \dot{y}\lambda_x - y\dot{\lambda}_x = V_p\lambda_x + \frac{V_p}{R_p}\alpha \sin\phi (x\lambda_z - z\lambda_x) \quad (4.88)$$

which is obtained by substituting the state and costate equations and E's optimal controls. Likewise

$$\frac{dB}{dt} = -\frac{dB}{d\tau} = \dot{z}\lambda_y + z\dot{\lambda}_y - \dot{y}\lambda_z - y\dot{\lambda}_z = V_p\lambda_z + \frac{V_p}{R_p}\alpha \cos\phi (z\lambda_x - x\lambda_z) \quad (4.89)$$

Since

$$(x\lambda_z - z\lambda_x)\Big|_{\mathcal{C}_E} = \frac{\ell \cos S_2 \sin S_1 \sin S_2 - \ell \sin S_2 \sin S_1 \cos S_2}{V_p \cos S_1 \cos S_2 - V_E} \equiv 0 \quad (4.90)$$

then substituting eqs (4.90) into Eqs (4.88) and (4.89), Eq (4.87) becomes

$$\tan\phi^*\Big|_{\mathcal{C}_E} = \frac{\lambda_z}{\lambda_x}\Big|_{\mathcal{C}_E} = \tan S_2 / \sin S_1 \quad . \quad (4.91)$$

From Fig 10 we see that

$$\tan\Theta = \frac{\sin S_2}{\cos S_2 \sin S_1} = \tan\phi^*\Big|_{\mathcal{C}_E} \quad . \quad (4.92)$$

Therefore on $\mathcal{C}_E$ P's optimal acceleration vector, the relative position vector, and $\underline{V}_E$ all lie in the same plane.

Proposition: For the 3D Limited Pursuer model, P's motion under optimal play is planar (i.e. $\dot{\phi}^* \equiv 0$).

Proof: From Eq (4.71)

$$\frac{d}{dt}(\tan\phi^*) = \frac{A\frac{dB}{dt} - B\frac{dA}{dt}}{A^2} \qquad (4.93)$$

By substituting Eqs (4.88) and (4.89) into Eq (4.93), the numerator N, of Eq (4.93) can be shown to be

$$N = A\frac{dB}{dt} - B\frac{dA}{dt} = (x\lambda_z - z\lambda_x)\left[V_p\lambda_y + \frac{V_p}{R_p}\sqrt{A^2+B^2}\right] \qquad (4.94)$$

Substituting Eq (4.74) into Eq (4.94) yields

$$N = (x\lambda_z - z\lambda_x)\left[1 + V_E\sqrt{\lambda_x^2 + \lambda_y^2 + \lambda_z^2}\right] \qquad (4.95)$$

From Eq (4.90) we see that $N|_{t_c} \equiv 0$

Now

$$\frac{d}{dt}(x\lambda_z - z\lambda_x) = \dot{x}\lambda_z + x\dot{\lambda}_z - \dot{z}\lambda_x - z\dot{\lambda}_x \qquad (4.96)$$

Substitution of the state and costate equations into Eq (4.96) yields

$$\frac{d}{dt}(x\lambda_z - z\lambda_x) = V_E(\bar{l}\lambda_z - \bar{n}\lambda_x) + \frac{V_p}{R_p}\cos\phi\, B - \frac{V_p}{R_p}\sin\phi\, A \qquad (4.97)$$

Substitution of the optimal control Eqs (4.71) and (4.73) into Eq (4.97) yields

$$\frac{d}{dt}(x\lambda_z - z\lambda_x) = V_E\left[\frac{\lambda_x\lambda_z - \lambda_z\lambda_x}{\sqrt{\lambda_x^2+\lambda_y^2+\lambda_z^2}}\right] + \frac{V_p}{R_p}\left[\frac{-AB+AB}{\sqrt{A^2+B^2}}\right] \equiv 0 \qquad (4.98)$$

Since $(x\lambda_z - z\lambda_x)\big|_{\xi} = 0$ we see that for all time

$$x\lambda_z - z\lambda_x \equiv 0 \quad . \tag{4.99}$$

Eq (4.95) for all time is therefore

$$N \equiv 0 \quad . \tag{4.100}$$

Since

$$\frac{d}{dt}(\tan\phi^*) = \frac{\dot{\phi}^*}{\cos^2\phi^*} = \frac{N}{A^2} \tag{4.101}$$

we see that

$$\dot{\phi}^* = \frac{N\cos^2\phi^*}{A^2} = \frac{N}{\sqrt{A^2+B^2}} \equiv 0 \tag{4.102}$$

Eqs (4.102) and (4.92) yield

$$\phi(t) = \text{constant} = \phi^*\big|_{\xi} = \Theta \quad . \tag{4.103}$$

Though it is not immediately obvious in the reduced ξ, E's optimal motion is straight line motion. This fact is more easily seen in the real space in which λ_x, λ_y and λ_z are all constants. Since on ξ P's acceleration vector, the relative position vector and $\underline{V}_E$ all lie in the same plane, we see that P and E are in motion in the same fixed plane. This shows that the solution of the 3D Limited Pursuer model is a simple revolution of the 2D Limited Pursuer model about the

Y-axis. All the conclusions made concerning the 2D model apply in the 3D case.

5. Model Conclusion:

The most important added conclusion to be drawn from the 3D model is the 3D closed form control law of P:

1) P banks his aircraft to keep E in P's longitudinal pitch plane.

2) Following this bank schedule, P pulls max g_s until E is directly line of sight out the nose of P's aircraft.

3) P then pursues a direct tail chase.

This maneuver, which is an optimal tactic for this 3D model, has been suggested by tacticians and is called the "slice" maneuver.

V. A Relative Evaluation of Fighter A/C Capability/An Application

This chapter presents the first known practical application of differential game theory to a real fighter aircraft problem. The problem is the following: Given several fighter aircraft, similar in many respects, which is the best fighter aircraft from an air-to-air combat point of view? This is not unlike the real problem faced by the Air Force when it must select the best contractor proposal on a new fighter aircraft system. Though many factors influence that final decision, a numerical ranking of the proposed aircraft as to their air-to-air combat capability is vital to that decision process. The technique presented here was recently used by the Air Force Flight Dynamics Laboratory as part of its evaluation of the recent Li· ıt Weight Fighter proposals.

Model for Comparing Fighter Aircraft Capabilities

The model is the 3D Limited Pursuer. In this model the pursuer maneuvers by selecting the bank angle and load factor within his capability. Important parameters in this model are maximum load factor, turn radius, weapons envelope and closing velocity. In order to have a means of comparing the several aircraft, the standard evading aircraft will be the highly maneuverable Evader in this model.

The results of Chapter IV show that for a realistic combat engagement (i.e. max tracking g's = 5, $M^{\#}$ = .6 - 1.1, gun capture radius $\simeq$ 1400 ft., $V_E/V_P \simeq .9$), the Barrier is closed and very sensitive to the ratio of combat velocities V_E/V_P. Sensitivity results of that Barrier indicate that it is much better to have the

ability to control V_E/V_P (i.e. accelerating capability) than to increase the load factor. The pursuer employs the 3D slice maneuver.

Evaluation of the 3D Limited Pursuer Model as a Comparison Tool

One of the best means of examining aircraft maneuverability throughout the flight envelope is with the "max maneuver corridor" concept developed by Boyd. It is a one-vehicle, energy maneuverability (EM) analysis which draws attention to the more important regions of the altitude - Mach diagram where a given aircraft has good maneuverability and consequently a good chance of winning a combat engagement. It does not indicate how to use that capability or indicate the outcome of a particular engagement. Though it is a powerful tool for defining and comparing aircraft maneuverability, it, like many other air-to-air combat models, does not address many of the model problems mentioned on page 1 . The technique developed here considers many of those problems and is a blend of EM results with differential game Barrier results.

With a gun capture capability of ℓ = 1400 ft., results of Chapter IV show that in the Mach # range .6 - 1.1, that the Barrier closes in front of P in the range 1550 - 2400 ft. This is within pilot visibility range so, as will be applied here, visibility (i.e. part of the complete information problem) is not a problem. If we place E on the furtherest tip of the Barrier (see Figure 11), we are assuming that P has somehow obtained this tactically superior position.

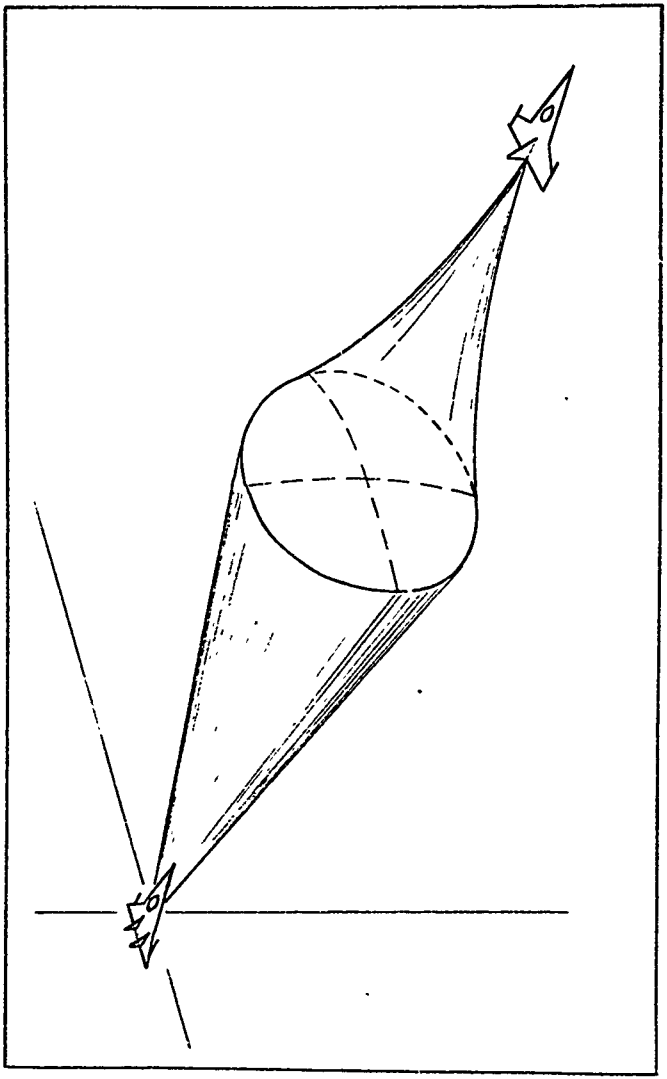

Figure 11: 3D Barrier

This is not an unlikely assumption since many documented kills resulted from a fortunate initial position at engagement. Since the aircraft are close, a one-on-one assumption seems to apply. Since P is tracking for a kill, he will be limited to 5 gs because of pilot limitations. We are assuming that the constant speed model can be applied with small error (see Chapter VIII for justification), that P can effect the slice maneuver, and that the standard evader has the fortunate velocity direction associated with the model's optimal strategy (inside the Barrier the velocity angles off are small and realistic of the not unlikely tail chase maneuver).

Specific Application to Relative Fighter Aircraft Capability

The technique compares each fighter aircraft in the study against a standard evading vehicle. Since the 3D Limited Pursuer model showed that the ability to control $\frac{V_E}{V_P}$ was paramount, the difference in the accelerating capabilities (i.e. specific power, P_s), ΔP_s, of each fighter aircraft against the standard evading vehicle was generated (see Figures 12 - 17). The evader is the superior P_s vehicle in most of the flight regime and is initially placed at the tip of the 3D Barrier (see Figure 11). P is given a closing velocity - here 50 ft/sec. E now employs his ΔP_s advantage in an attempt to improve $\frac{V_E}{V_P}$. As E does this, the Barrier shrinks toward P; however, P is closing at an ever decreasing rate. One of two events will occur; either the Barrier will shrink faster than P is closing and E will escape,

or else E will cross the gun capture radius before he gets outside the Barrier. The specific result depends on the Mach # of P and the altitude of the engagement, i.e. ΔP_s . To make the analysis more meaningful, we define the combat arena to be Mach # .60 to 1.1 and altitude 0 to the aircraft operating limit. This region is representative of the area of the h-mach diagram where visibility is good, turn radius small, and turn rate high. A computer program was built using the numerical Barrier results of Chapter IV and the properties of the aircraft to determine the escape - capture result for each point of the combat arena. The results are shown in Figures 12 - 17.

The area between the heavy black lines in the combat arena is the region where capture of E occurs in spite of his ΔP_s advantage. The area from the dashed lines to the heavy black lines in the combat arena is where E escapes because of the ΔP_s advantage.

Since a standard evading vehicle is used in each case, it is reasonable to assume that the fighter aircraft with the largest capture area in the combat arena is the best aircraft. The percent area of the combat arena associated with capture provides a means of numerically ranking each fighter aircraft. Six aircraft are compared in Figures 12 - 17. A definite numerical ranking results.

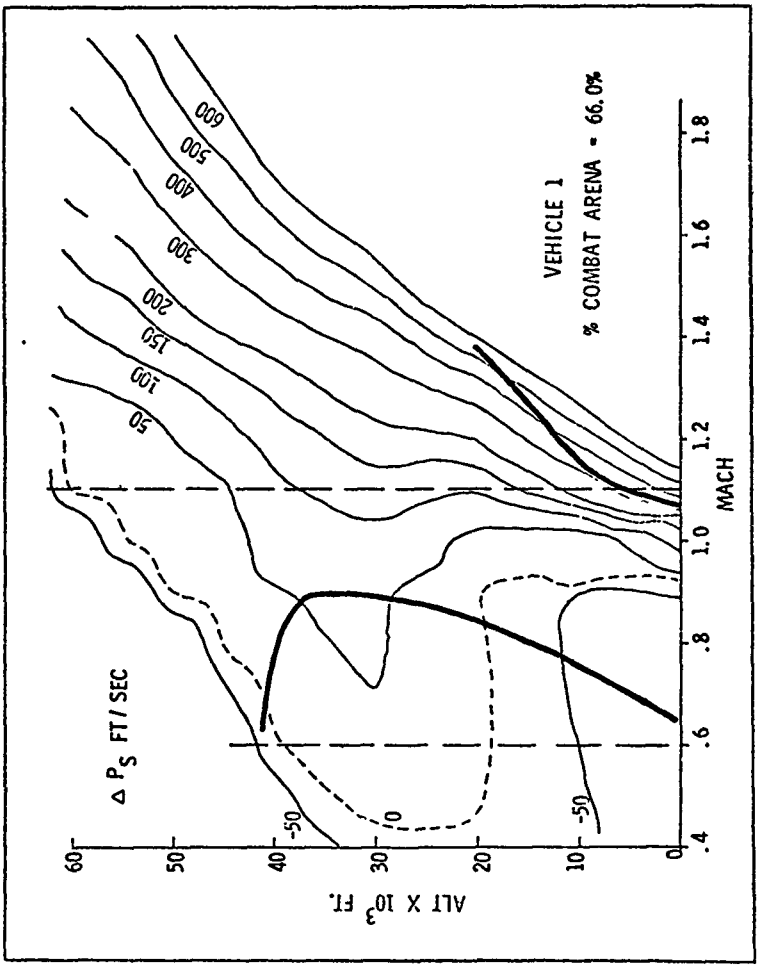

Figure 12: Vehicle 1 Combat Results

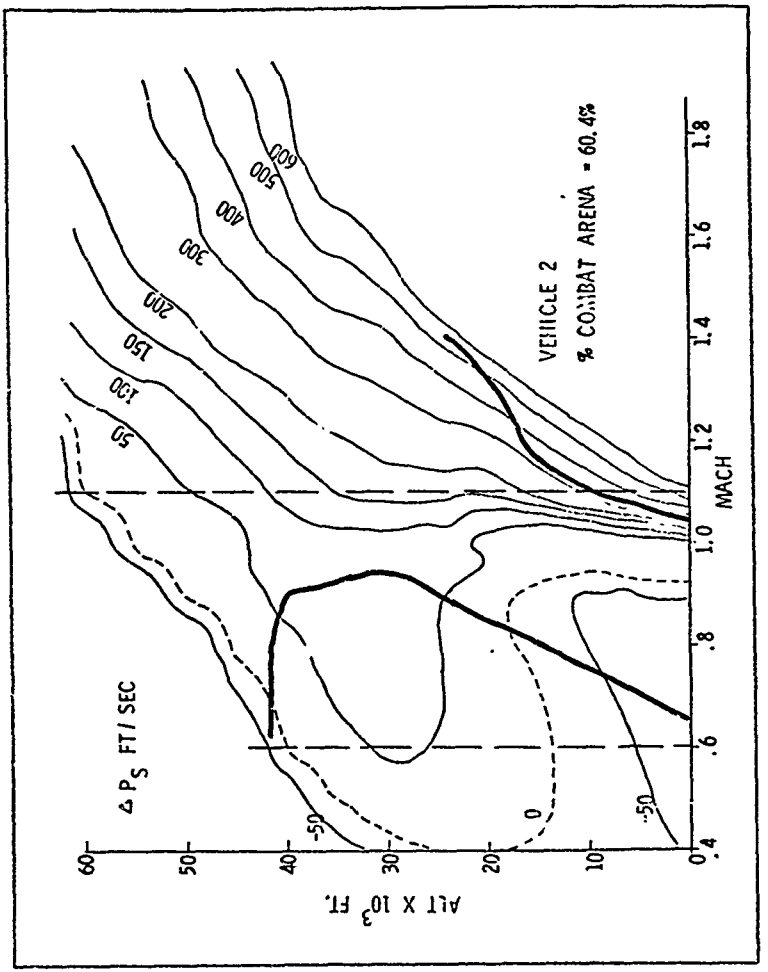

Figure 13: Vehicle 2 Combat Results

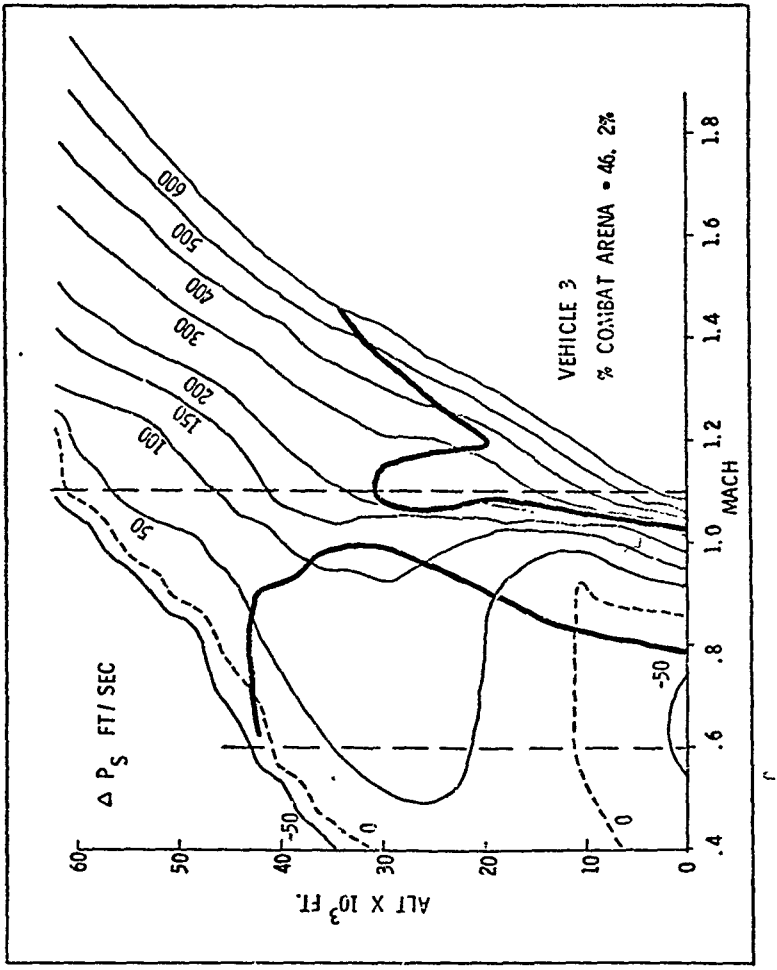

Figure 14: Vehicle 3 Combat Results

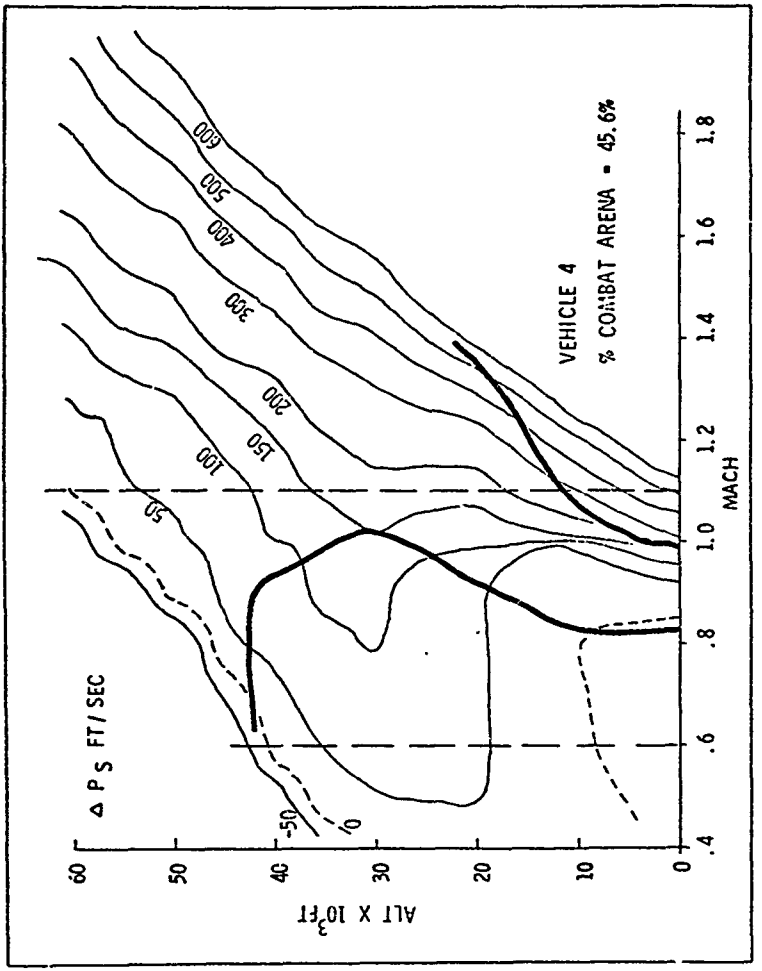

Figure 15: Vehicle 4 Combat Results

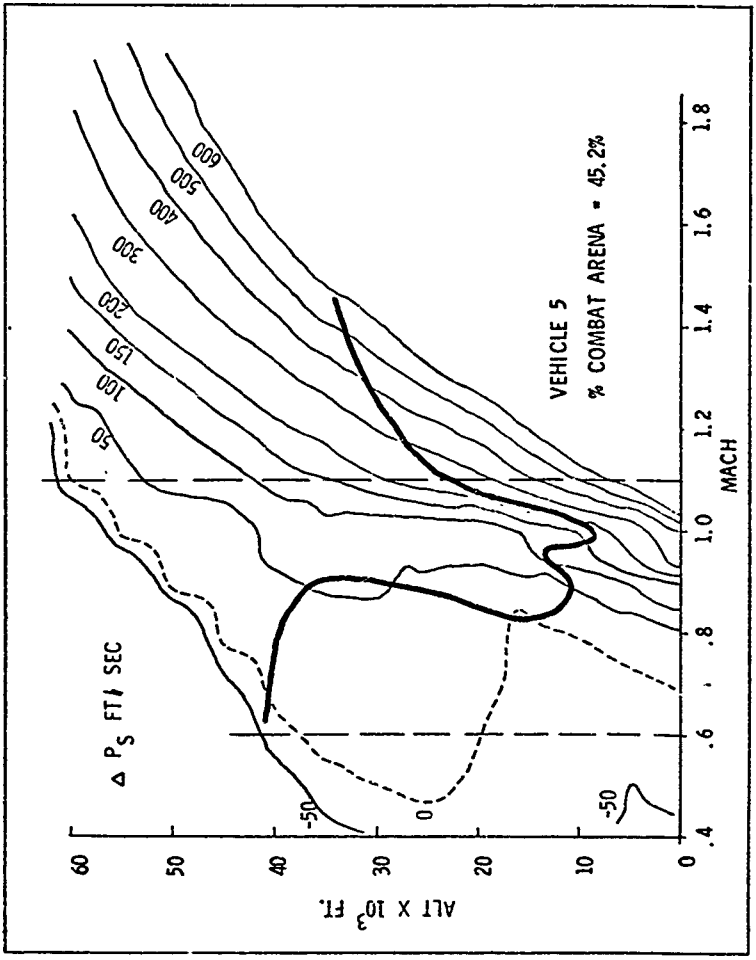

Figure 16: Vehicle 5 Combat Results

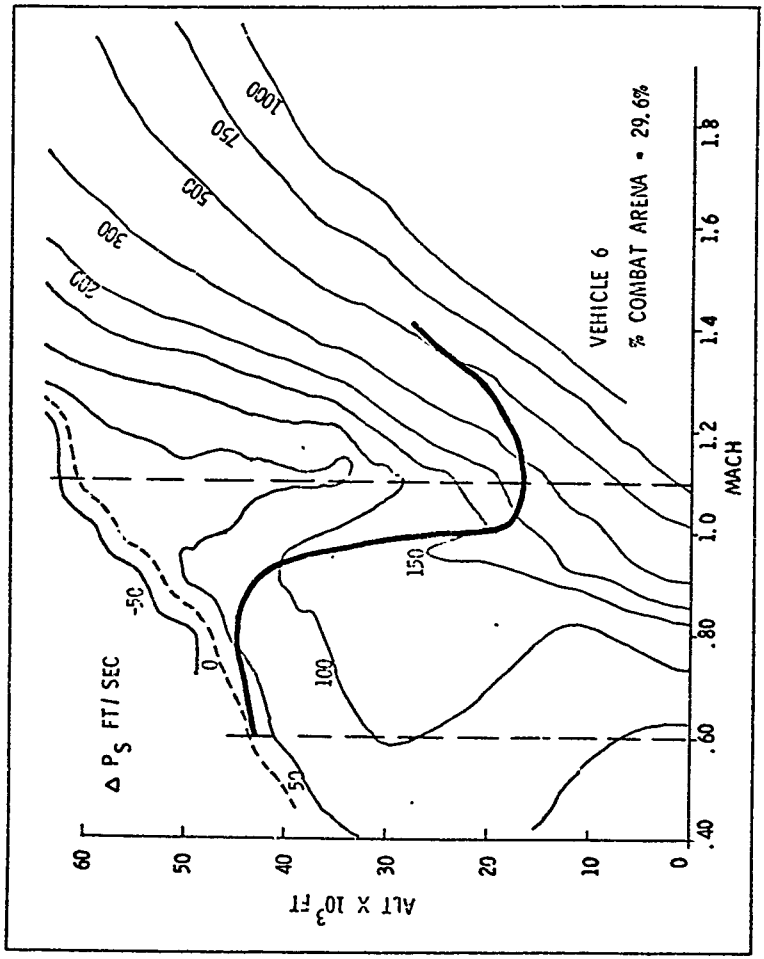

Figure 17: Vehicle 6 Combat Results

VI. Limited Pursuer - Evader Model

The dynamics of the model in this chapter is made more realistic by constraining both the Pursuer and Evader to maneuver their constant speed velocity vectors within bounded turning rates. Neither player is highly maneuverable in the sense that the velocity vector can be oriented instantaneously. The intent in studying this model is to find the effect of the more realistic evader on the solution. The model is examined in both two and three dimensions.

2D Limited Pursuer - Evader

Isaacs [7] partially solves this problem but does not interpret or apply the model or Barrier results. The model dynamics is formulated in the reduced ξ . The coordinate system for the 2D model is shown in Figure 18 (similar to Figure 3).

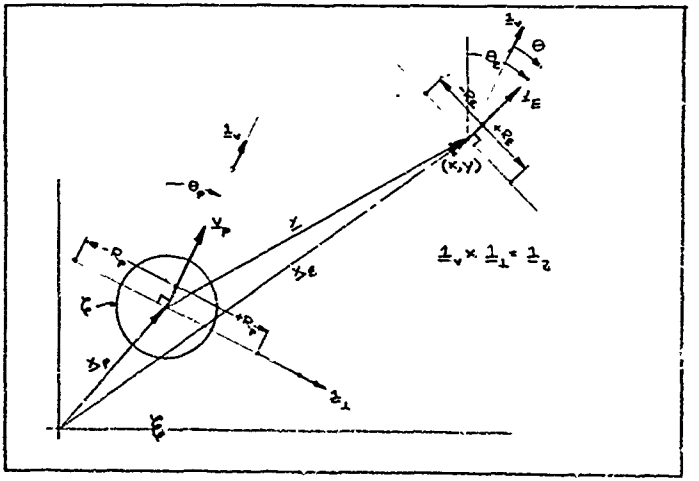

Figure 18: Limited Pursuer-Evader Coordinate System

1. State Equation Formulation:

The reduced $\mathcal{F}_{\varphi}$ is the set of orthogonal unit vectors $\underline{1}_v$ and $\underline{1}_\perp$ fixed to P's position and rotating such that $\underline{1}_v$ is always aligned with $\underline{V}_P$. The details of the state equation formulation can be found in Appendix B. The state equations are

$$\begin{bmatrix} \dot{x} \\ \dot{y} \\ \dot{\theta} \end{bmatrix} = \begin{bmatrix} V_E \sin\theta - y\frac{V_P}{R_P}\alpha \\ V_E \cos\theta - V_P + x\frac{V_P}{R_P}\alpha \\ \frac{V_E}{R_E}\beta - \frac{V_P}{R_P}\alpha \end{bmatrix} \qquad (6.1)$$

where

x - distance from P to E along $\underline{V}_P$

y - distance from P to E perpendicular to $\underline{V}_\perp$.

θ - angle between $\underline{V}_P$ and $\underline{V}_E$

α - P's control; $\alpha = +1(-1)$ is a hard right (left) turn

β - E's control; $\beta = +1(-1)$ is a hard right (left) turn

Note that the state equations here are very similar to the state equation (4.1) for the Limited Pursuer model - the only difference being that θ is no longer a control variable but a state variable whose differential equation is Eq (B.15).

2. Problem Setup:

The terminal surface, $\mathcal{C}_f$, is again assumed to be a circle about P of radius ℓ , however, at any Θ . $\mathcal{C}_f$ is shown in Fig 19 where it is visualized as a cylinder in the reduced $\mathcal{C}_f$. Its usual description with Eq (2.3) is

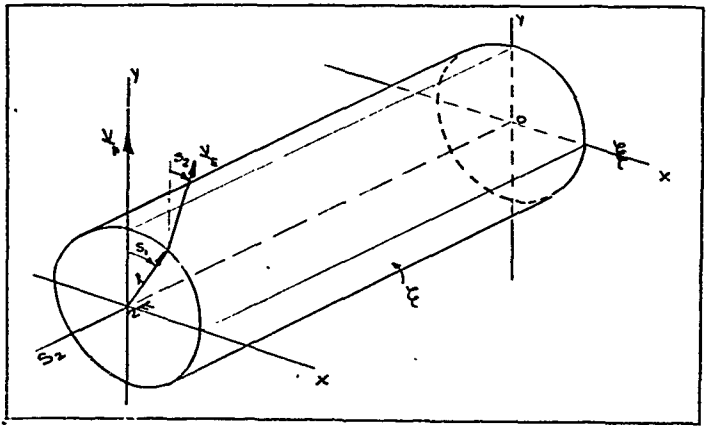

Figure 19: Terminal Surface

$$\psi[\underline{x}(t_f)] = x^2(t_f) + y^2(t_f) - \ell^2 = 0 \qquad (6.2)$$

where $\Theta(t_f)$ is free. $\mathcal{C}_f$ can also be described with Eq (2.19) as

$$\begin{aligned} x(t_f) &= h_1(\underline{s}) = \ell \sin s_1 \\ y(t_f) &= h_2(\underline{s}) = \ell \cos s_1 \\ \Theta(t_f) &= h_3(\underline{s}) = s_2 \end{aligned} \qquad (6.3)$$

where

$$\underline{S} = \begin{bmatrix} S_1 \\ S_2 \end{bmatrix}$$

The controls for the players are

$$\underline{U} = [\alpha]$$
$$\underline{V} = [\beta] \qquad (6.4)$$

and the costate vector $\underline{\lambda}$ is

$$\underline{\lambda} = \begin{bmatrix} \lambda_x \\ \lambda_y \\ \lambda_\theta \end{bmatrix} \qquad (6.5)$$

As done in the previous models, the roles of the players are preselected by choosing $\phi = 0$, $L = 1$ with P minimizing and E maximizing.

3. Application of Necessary Conditions:

ME 1 becomes

$$0 = \min_{\alpha} \max_{\beta} \left[\lambda_x \left(V_E \sin\theta - y \frac{V_p}{R_p} \alpha \right) + \lambda_y \left(V_E \cos\theta - V_p + x \frac{V_p}{R_p} \alpha \right) + \right.$$
$$\left. + \lambda_\theta \left(\frac{V_E}{R_E} \beta - \frac{V_p}{R_p} \alpha \right) + 1 \right] \equiv$$
$$\equiv \frac{V_p}{R_p} \min_{\alpha} \left[x\lambda_y - y\lambda_x - \lambda_\theta \right] \alpha + \frac{V_E}{R_E} \max_{\beta} \left[\lambda_\theta \right] \beta +$$
$$+ V_E \left[\lambda_x \sin\theta + \lambda_y \cos\theta \right] - \lambda_y V_p + 1 \equiv$$
$$\equiv \frac{V_p}{R_p} \min_{\alpha} H_p + \frac{V_E}{R_E} \max_{\beta} H_E + H_o \qquad (6.6)$$

where

$$H_P = [x\lambda_y - y\lambda_x - \lambda_\theta]$$

$$H_E = [\lambda_\theta]\beta$$

$$H_o = V_E[\lambda_x \sin\theta + \lambda_y \cos\theta] - \lambda_y V_p + 1 \quad (6.7)$$

The $\min_\alpha H_P$ condition yields

$$\alpha^* = -\text{sgn}[A_\theta] \quad (6.8)$$

where

$$A_\theta = x\lambda_y - y\lambda_x - \lambda_\theta \quad (6.9)$$

provided $A_\theta \neq o$ for finite time.

The $\max_\beta H_E$ conditions yield

$$\beta^* = \text{sgn}[\lambda_\theta] \quad (6.10)$$

provided $\lambda_\theta \neq o$ for a finite time.

Singular controls in both α and β can occur. A summary of the α singular necessary conditions from Appendix B shows

$$A_\theta = x\lambda_y - y\lambda_x - \lambda_\theta = o \quad (6.11)$$

$$\dot{A}_\theta = V_p\lambda_x = o \quad (6.12)$$

$$\ddot{A}_\theta = -\frac{V_p^2}{R_p}\lambda_y \alpha = o \quad (6.13)$$

$$\lambda_y \geq o \quad (6.14)$$

Therefore, the singular control in α requires the added necessary conditions

$$\alpha = \lambda_x = A_\theta = o \leq \lambda_y \quad (6.15)$$

A summary of the $\mathcal{B}$ singular necessary conditions from Appendix B shows

$$\lambda_\theta = 0 \tag{6.16}$$

$$\dot{\lambda}_\theta = V_E(\lambda_y \sin\theta - \lambda_x \cos\theta) = 0 \tag{6.17}$$

$$\ddot{\lambda}_\theta = \frac{V_E^2}{R_E}\mathcal{B}(\lambda_x \sin\theta + \lambda_y \cos\theta) = 0 \tag{6.18}$$

$$\lambda_x \sin\theta + \lambda_y \cos\theta \geq 0 \quad . \tag{6.19}$$

There it is also shown that Eqs (6.16) to (6.19) imply that

$$\mathcal{B} = \lambda_y \sin\theta - \lambda_x \cos\theta = \lambda_\theta = 0 \leq \lambda_x \sin\theta + \lambda_y \cos\theta \tag{6.20}$$

are the added necessary conditions for a singular $\mathcal{B}$.

Substituting Eqs (6.8) and (6.10) into Eq (6.6) yields ME 2

$$-\frac{V_P}{R_P}|A_\theta| + \frac{V_E}{R_E}|\lambda_\theta| + V_E[\lambda_x \sin\theta + \lambda_y \cos\theta] - \lambda_y V_P + 1 = 0 \quad . \tag{6.21}$$

The costate equations are

$$\dot{\underline{\lambda}} = -\nabla H^T = -\begin{bmatrix} \frac{\partial H}{\partial x} \\ \frac{\partial H}{\partial y} \\ \frac{\partial H}{\partial \theta} \end{bmatrix} = \begin{bmatrix} -\frac{V_P}{R_P}\alpha\lambda_y \\ \frac{V_P}{R_P}\alpha\lambda_x \\ V_E(\lambda_y \sin\theta - \lambda_x \cos\theta) \end{bmatrix} \quad . \tag{6.22}$$

Note that the first two costate equations here, are the same as the costate Eq (4.18) for the Limited Pursuer model. The main influence of the added realism of this model, i.e. the velocity angle off Θ, is thru its effect on λ_θ in the switching functions A_θ and λ_θ which determine the controls.

The transversality conditions are $\sum_{i=1}^{3} \lambda_i \frac{\partial h_i(s)}{\partial s_j} = \frac{\partial \phi(s)}{\partial s_j} \equiv 0$, (6.23)

$j = 1, 2$

$j = 2 \Rightarrow \quad \lambda_\theta(t_f) = 0$

$$j = 1 \Rightarrow 0 = \lambda_x(t_f) l \cos s_1 + \lambda_y(t_f)(-l \sin s_1) + \lambda_\theta(t_f) = -(x\lambda_y - y\lambda_x)\Big|_{t_f} = -A_\theta\Big|_{t_f}. \quad (6.24)$$

4. Problem Backward Solution From $\mathcal{C}$:

As was done in Chapter IV, the backward solution from $\mathcal{C}$ is done to find the control logic on P's side of the Barrier. The details of the analysis can be found in Appendix B of which the following is a summary.

The controls on the terminal surface $\mathcal{C}$ are

$$\beta^*\Big|_{\mathcal{C}} = -\text{sgn}[\sin(s_2 - s_1)] \quad (6.25)$$

$$\alpha^*\Big|_{\mathcal{C}} = \text{sgn}[\sin s_1] \quad . \quad (6.26)$$

There are singular controls for both P and E. The E singular control conditions are characterized by

$$\lambda_\theta = 0$$
$$\beta = 0 \quad . \quad (6.27)$$

Since $\beta = 0$, the E singular control yields a non-turning straight line dash. The P singular control conditions are characterized by

$$A_\theta = x\lambda_y - y\lambda_x - \lambda_\theta = \lambda_x = \alpha = 0 \quad . \quad (6.28)$$

Since $\alpha=0$, P's singular control also yields a non-turning straight line dash. If both P and E are singular together, then $\theta=0$ also and the double singular condition corresponds to a direct tail chase.

Now if E is singular then Appendix B shows $\lambda_\theta=0$, $\beta=0$, $\sin\theta=\frac{\lambda_x}{\sqrt{\lambda_x^2+\lambda_y^2}}$, $\cos\theta=\frac{\lambda_y}{\sqrt{\lambda_x^2+\lambda_y^2}}$, $A_\theta=x\lambda_y-y\lambda_x$. Under these conditions the state equations, Eq(6.1), and the costate equation, Eq (6.22), reduce identically to the state and costate equations for the Limited Pursuer model. From this it can be seen that the E singular case in the present model has the same solution as the Limited Pursuer model. In this singular case, E initially just happens to have the position and Θ angle off associated with the optimal Θ_E freely chosen by the highly maneuverable Evader in the Limited Pursuer model.

The optimal controls, for the majority of ξ , are either hard turns or the singular straight line dashes. Based on the Appendix B discussion of the closed form control logic for E while P is singular, and vice versa, the closed form control logic (see Figure 20) for this model (neglecting other singular surfaces - see pg 16) is: P does a hard turn into E until $\underline{V}_P$ is tangent to E's hard turn circle at which time P switches to the non-turning singular control; E does a hard turn away from P until $\underline{V}_E$ is tangent to P's hard turn circle at which time E switches to the non-turning singular control. With this knowledge about the singular control surfaces, we continue with the backward solution from ξ_f and return to the controls on ξ .

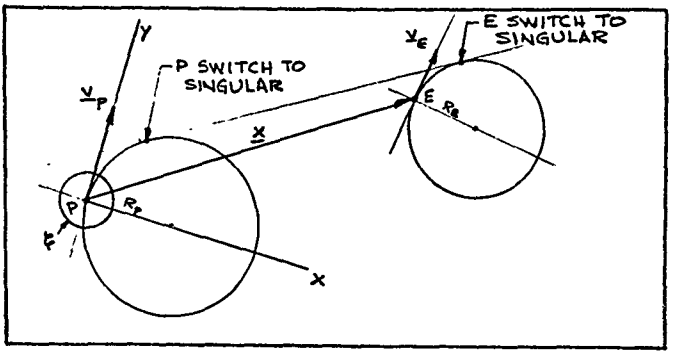

Figure 20: Partial Closed Form Control Logic

Eqs (6.25) to (6.28) are expressions for the controls on ζ as a function of the state on ζ . It was stated, but not shown, that the UP of ζ was characterized by those states on ζ for which

$$V_P \cos S_1 - V_E \cos(S_2 - S_1) > 0 \quad . \tag{6.29}$$

It will be shown (see section on Barrier) that equality in Eq (6.29) defines the BUP.

Figure 21 represents the cylindrical terminal surface, ζ , of Figure 19 cut along the S_2 (i.e. Θ)axis at $S_1 = \pm\pi$ and unrolled on a flat sheet. As in the other models $\frac{V_E}{V_P} < 1$. Eq (6.29) equated to zero defines the BUP and is shown by the curved lines in Figure 21. A pair of curved lines represents the BUP for a given $\frac{V_E}{V_P} < 1$. The area of ζ between the diametrically opposed parts of the BUP is

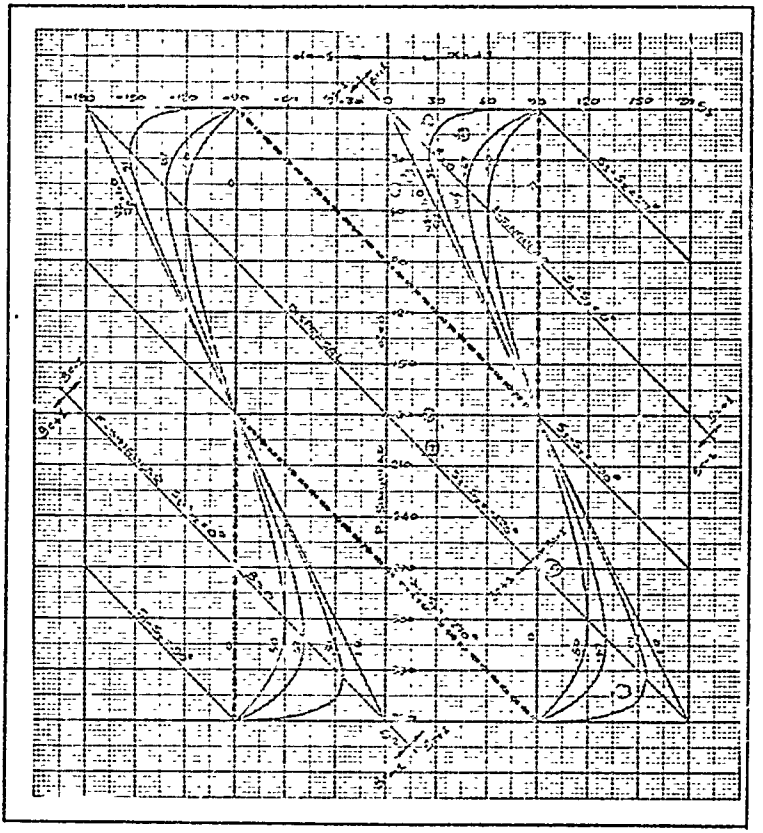

Figure 21: Terminal ζ , BUP and Controls

the UP of $\mathcal{C}$. The remainder of $\mathcal{C}$ is the NUP. Eqs (6.26) and (6.28) show that for the UP of $\mathcal{C}$ and

1) $0 < s_1 < \pi \Rightarrow \alpha|_{\mathcal{C}} = +1$ (i.e. hard right turn)

2) $-\pi < s_1 < 0 \Rightarrow \alpha|_{\mathcal{C}} = -1$ (i.e. hard left turn) (6.30)

3) $s_1 = 0 \Rightarrow \alpha|_{\mathcal{C}} = 0$ (i.e. P singular)

4) $s_1 = \pi \Rightarrow$ Dispersal surface

This shows that at $\mathcal{C}$ termination, P is turning into the position of E. Even though termination on $\mathcal{C}$ does not occur for the NUP, the controls are defined as in Eq (6.30), however, with the signs changed. Eqs (6.25) and (6.27) show that for the UP of $\mathcal{C}$ and

1) $0 < s_2 - s_1 < \pi \Rightarrow \beta|_{\mathcal{C}} = -1$ (i.e. hard left turn)

2) $-\pi < s_2 - s_1 < 0 \Rightarrow \beta|_{\mathcal{C}} = +1$ (i.e. hard right turn) (6.31)

3) $s_2 - s_1 = 0 \Rightarrow \beta|_{\mathcal{C}} = 0$ (i.e. E singular)

4) $s_2 - s_1 = \pi \Rightarrow$ Dispersal surface

This shows that at $\mathcal{C}$ termination, E is turning in the direction of the line of sight i.e. E is trying to lessen the closing rate to prevent termination on $\mathcal{C}$. For the NUP of $\mathcal{C}$ the control signs in Eq (6.31) are reversed.

Figure 22 portrays several kinds of termination on $\mathcal{C}$ by reference to specific points on Figure 21. For points 1, 3, 4, 6 in the UP, P is clearly the attacker and E the evader. Points 7, 8, 9, 10 are also in the UP, however the positions are such that P probably should not

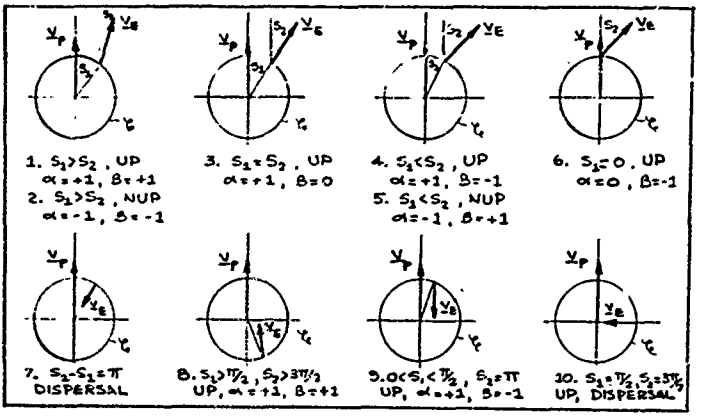

Figure 22: Positions at ζ_c Termination

attack but evade and vice versa with E. The problem here is with the payoff function form and the fixed roles that have been assigned to the players. The problem of choosing a good payoff function was mentioned in Chapter I and again mentioned in Chapter III - 1 in the 2D Constant Velocity model. This payoff problem is addressed later in Chapter IX. The main point to be made here is that the backward solutions from points such as 7, 8, 9, 10 may be interesting to do mathematically (and as it turns out extremely difficult because of the Dispersal surface in this region of ζ_c) but have little use practically since the roles of the players are fixed. This is not to say that the

present model is not good - just limited in some areas of ζ_e for practical application. The area of ζ_e where the present fixed roles have practical application (i.e. when the roles make sense) is around $-\pi/2 < s_1 < \pi/2$ simultaneously with $|s_2 - s_1| < \pi/2$. This area is enclosed by the heavy dashed lines in Figure 21. With the controls on ζ_e and the part of ζ useful for practical application defined, the analytics of the backward solution from this area of ζ is done next. The E singular trajectories are done first.

As was previously discussed, the E singular case is the same as the Limited Pursuer model. The only real distinction to be made here between the models is one of nomenclature i.e. θ_E and θ are similar; A and A_θ are similar; s and s_1 are similar. A summary of the equations for the backward solution in the E singular case follows. These equations come directly from the Limited Pursuer model. Because of the x, θ symmetry in the problem (to be shown later), only the $0 < s_1 < \pi$ that lie in the UP (i.e. $\alpha^* = +1$, $\beta^* = 0$) are examined. The results are

$$s_2 = s_1 \tag{6.32}$$

$$\lambda_\theta(T) = 0 \tag{6.33}$$

$$\lambda_x(T) = \sin\left(s_1 + \frac{V_p}{R_p}T\right) \Big/ \left[V_p \cos s_1 - V_E\right] \tag{6.34}$$

$$\lambda_y(T) = \cos\left(s_1 + \frac{V_p}{R_p}T\right) \Big/ \left[V_p \cos s_1 - V_E\right] \tag{6.35}$$

$$A_\theta(T) = \frac{-R_p}{\left[V_p \cos s_1 - V_E\right]} \left[\cos s_1 - \cos\left(s_1 + \frac{V_p}{R_p}T\right)\right] \tag{6.36}$$

$$\theta(T) = s_1 + \frac{V_P}{R_P} T \qquad (6.37)$$

$$x(T) = (\ell - V_E T)\sin(s_1 + \frac{V_P}{R_P} T) + R_P(1 - \cos\frac{V_P}{R_P} T) \qquad (6.38)$$

$$y(T) = (\ell - V_E T)\cos(s_1 + \frac{V_P}{R_P} T) + R_P \sin\frac{V_P}{R_P} T \quad . \qquad (6.39)$$

As with the Limited Pursuer model, these trajectories will generally intersect the Barrier before switching occurs in Eq (6.36).

The backward solution of the P singular trajectories is straight forward; however, they are not very useful in the analysis of the Barrier. This is because their initial conditions on $\mathcal{C}$ (i.e. s_1) do not intersect the BUP. These P singular solutions are not presented. Next we examine the backward solutions from the UP of $\mathcal{C}$ where $\alpha^* \neq 0$ and $\beta^* \neq 0$. The details of this analysis is done in Appendix B of which the following is a summary.

For the UP of $\mathcal{C}$ the controls are hard turns as shown in Figure 21 with E switching and P switching at T_θ and T_A respectively defined by

$$\frac{V_E}{R_E} T_\theta = 2\pi - 2|s_1 - s_2| \qquad (6.40)$$

$$\frac{V_P}{R_P} T_A = 2\pi - 2|s_1| \quad . \qquad (6.41)$$

For a given s_1, s_2 in the UP of $\mathcal{C}$ and for T smaller than T_θ or T_A the state solutions are

$$\theta(T) = s_2 + \left(\frac{V_P}{R_P}\alpha^* - \frac{V_E}{R_E}\beta^*\right) T \qquad (6.42)$$

$$x(T) = \alpha^* R_P\left(1 - \cos\alpha^* \frac{V_P}{R_P} T\right) + \ell \sin\left(s_1 + \alpha^* \frac{V_P}{R_P} T\right) +$$

$$+ \frac{R_E}{\beta^*}\left[\cos\left(s_2 + \alpha^* \frac{V_P}{R_P} T\right) - \cos\theta(T)\right] \qquad (6.43)$$

$$y(T) = \alpha^* R_p \sin\left(\alpha^* \frac{V_p}{R_p} T\right) + \ell \cos\left(s_1 + \alpha^* \frac{V_p}{R_p} T\right) +$$

$$- \frac{R_E}{\beta^*}\left[\sin\left(s_2 + \alpha^* \frac{V_p}{R_p} T\right) - \sin\theta(T)\right] \quad . \tag{6.44}$$

This completes the solution of those trajectories immediately leaving the UP of ζ_ℓ . These trajectories will be discussed later. To complete the analysis of those trajectories leaving ζ_ℓ , we now examine the Barrier.

5. Barrier Backward Solution From ζ_ℓ :

As was done in Chapters III and IV, we first examine ζ_ℓ and find the UP, NUP and BUP. Define $\underline{\sigma}|_{\zeta_\ell}$ as

$$\underline{\sigma}|_{\zeta_\ell} = \begin{bmatrix} \sigma_x \\ \sigma_y \\ \sigma_\theta \end{bmatrix}_{t_f} \equiv \begin{bmatrix} \sigma_1 \\ \sigma_2 \\ \sigma_3 \end{bmatrix}_{t_f} \tag{6.45}$$

The normality conditions of $\underline{\sigma}$ on ζ_ℓ , $\sum_{i=1}^{3} \sigma_i \frac{\partial h_i(\underline{s})}{\partial s_j} = 0$, yield for

$$j=1 \implies \sigma_x(t_f)\cos s_1 - \sigma_y(t_f)\sin s_1 = 0 \tag{6.46}$$

$$j=2 \implies \sigma_\theta(t_f) = 0 \quad . \tag{6.47}$$

The unit vector condition implies

$$\sigma_x^2(t_f) + \sigma_y^2(t_f) + \sigma_\theta^2(t_f) = 1 \quad . \tag{6.48}$$

Substituting Eq (6.46) for $\sigma_x(t_f)$ and Eq (6.47) for $\sigma_\theta(t_f)$ into Eq (6.48) and solving Eq (6.48) for $\sigma_y(t_f)$ yields

$$\sigma_y(t_f) = \cos s_1 \quad . \tag{6.49}$$

Substituting Eq (6.49) into Eq (6.46) yields

$$v_x(t_f) = \sin s_1 \quad . \tag{6.50}$$

Expression (2.28) becomes

$$\min_{\underline{u}} \max_{\underline{v}} \underline{v}^T \underline{f}\Big|_{t_c} = \min_{\alpha} \max_{\beta} \Big[v_x \Big(V_E \sin\theta - y \frac{V_p}{R_p} \alpha \Big) +$$

$$+ v_y \Big(V_E \cos\theta - V_p + x \frac{V_p}{R_p} \alpha \Big) + v_\theta \Big(\frac{V_E}{R_E} \beta - \frac{V_p}{R_p} \alpha \Big) \Big]\Big|_{t_c} \equiv$$

$$\equiv \frac{V_p}{R_p} \min_{\alpha} \big[x v_y - y v_x - v_\theta \big] \alpha \Big|_{t_c} + \frac{V_E}{R_E} \max_{\beta} [v_\theta] \beta \Big|_{t_c} +$$

$$+ V_E \big[v_x \sin\theta + v_y \cos\theta \big]\Big|_{t_c} - v_y V_p \Big|_{t_c} \quad . \tag{6.51}$$

The $\min_{\alpha}$ operation yields

$$\tilde{\alpha}\Big|_{t_c} = -\operatorname{sgn}\big[\tilde{A}_\theta\big]\Big|_{t_c} \equiv -\operatorname{sgn}\big[x v_y - y v_x - v_\theta\big]\Big|_{t_c} \tag{6.52}$$

provided $\tilde{A}_\theta \neq 0$ for a finite time. The $\max_{\beta}$ operation yields

$$\tilde{\beta}\Big|_{t_c} = \operatorname{sgn}\big[v_\theta\big]\Big|_{t_c} \tag{6.53}$$

provided $v_\theta \neq 0$ for a finite time. Substituting Eqs (6.52) and (6.53) into Eq (6.51) yields

$$\min_{\underline{u}} \max_{\underline{v}} \underline{v}^T \underline{f}\Big|_{t_c} = \Big[-\frac{V_p}{R_p} \big|\tilde{A}_\theta\big| + \frac{V_E}{R_E} |v_\theta| +$$

$$V_E \big(v_x \sin\theta + v_y \cos\theta \big) - v_y V_p \Big]\Big|_{t_c} \quad . \tag{6.54}$$

Substituting Eqs (6.3), (6.49), and (6.50) into Eq (6.54) yields

$$\min_{\underline{u}} \max_{\underline{v}} \underline{v}^T \underline{f}\Big|_{t_c} = V_E \big[\sin s_1 \sin s_2 + \cos s_1 \cos s_2 \big] - V_p \cos s_1 \equiv$$

$$\equiv V_E \cos(s_2 - s_1) - V_p \cos s_1 \quad . \tag{6.55}$$

Eq (6.55) implies that if

1) $V_E\cos(s_2-s_1)-V_p\cos s_1<0$, then $\{s_1,s_2\}\in$ UP of $\mathcal{C}$

2) $V_E\cos(s_2-s_1)-V_p\cos s_1=0$, then $\{s_1,s_2\}\in$ BUP of $\mathcal{C}$

3) $V_E\cos(s_2-s_1)-V_p\cos s_1>0$, then $\{s_1,s_2\}\in$ NUP of $\mathcal{C}$ (6.56)

These equations justify the statements made on pgs 81, 210 and 211 .

Having defined the BUP, the Barrier is constructed backward from the BUP by satisfying the necessary conditions of the Barrier.

The first necessary condition is "pseudo" ME1, Eq (2.29),

$$0=\min_{\underline{U}}\max_{\underline{V}}\underline{\sigma}^T\underline{f}(\underline{x},\underline{U},\underline{V})=\frac{V_p}{R_p}\min_{\alpha}\tilde{H}_p+\frac{V_E}{R_E}\max_{\beta}\tilde{H}_E+$$

$$+V_E(\sigma_x\sin\theta+\sigma_y\cos\theta)-\sigma_y V_p \qquad (6.57)$$

where

$$\tilde{H}_p=[x\sigma_y-y\sigma_x-\sigma_\theta]\alpha\equiv[\tilde{A}_\theta]\alpha \qquad (6.58)$$

$$\tilde{H}_E=[\sigma_\theta]\beta \qquad (6.59)$$

The $\min_{\alpha}\tilde{H}_p$ conditions yield

$$\tilde{\alpha}=-\mathrm{sgn}[\tilde{A}_\theta] \qquad (6.60)$$

provided $\tilde{A}_\theta\neq 0$ for a finite time. The $\max_{\beta}\tilde{H}_E$ conditions yield

$$\tilde{\beta}=\mathrm{sgn}[\sigma_\theta] \qquad (6.61)$$

provided $\sigma_\theta\neq 0$ for a finite time. Note the possibility of singular controls on the Barrier. Substituting Eqs (6.60) and (6.61) into Eq (6.57) yields "pseudo" ME2, Eq (2.30).

$$0=-\frac{V_p}{R_p}|\tilde{A}_\theta|+\frac{V_E}{R_E}|\sigma_\theta|+V_E(\sigma_x\sin\theta+\sigma_y\cos\theta)-\sigma_y V_p \qquad (6.62)$$

The costate equations for the Barrier, Eq (2.31) are

$$\dot{\underline{v}} = -\nabla\left(\underline{v}^T \underline{f}\right) = \begin{bmatrix} -\tilde{\alpha}\frac{V_P}{R_P} v_y \\ \tilde{\alpha}\frac{V_P}{R_P} v_x \\ V_E\left(v_y \sin\theta - v_x \cos\theta\right) \end{bmatrix} \qquad (6.63)$$

As was done in the Limited Pursuer model, the similarity in the form of the necessary conditions for the Barrier and the form of the necessary conditions for trajectories from the UP is pointed out.

UP	BUP(Barriers)
$x(t_f) = \ell \sin s_1$	same form
$y(t_f) = \ell \cos s_1$	except s_1 and s_2
$\theta(t_f) = s_2$	are on BUP.
$\dot{\underline{x}} = \underline{f}(\underline{x}, \underline{u}, \underline{v})$	same state equations
$\dot{\underline{\lambda}} = \begin{bmatrix} -\frac{V_P}{R_P}\alpha\lambda_y \\ \frac{V_P}{R_P}\alpha\lambda_x \\ V_E(\lambda_y \sin\theta - \lambda_x\cos\theta) \end{bmatrix}$	$\dot{\underline{v}} = \begin{bmatrix} -\frac{V_P}{R_P}\tilde{\alpha} v_y \\ \frac{V_P}{R_P}\tilde{\alpha} v_x \\ V_E(v_y \sin\theta - v_x\cos\theta) \end{bmatrix}$
$\lambda_x(t_f) = \frac{\sin s_1}{V_P \cos s_1 - V_E \cos(s_2 - s_1)}$	$v_x(t_f) = \sin s_1$
$\lambda_y(t_f) = \frac{\cos s_1}{V_P \cos s_1 - V_E \cos(s_2 - s_1)}$	$v_y(t_f) = \cos s_1$
$\lambda_\theta(t_f) = 0$	$v_\theta(t_f) = 0$
$\alpha^* = -\text{sgn}[x\lambda_y - y\lambda_x - \lambda_\theta]$	$\tilde{\alpha} = -\text{sgn}[xv_y - yv_x - v_\theta]$
when $A_\theta \neq 0$	when $\tilde{A}_\theta \neq 0$
$\beta^* = \text{sgn}[\lambda_\theta]$	$\tilde{\beta} = \text{sgn}[v_\theta]$
when $\lambda_\theta \neq 0$	when $v_\theta \neq 0$
$\alpha_s^* = 0,\ \beta_s^* = 0$	$\tilde{\alpha}_s^* = 0,\ \tilde{\beta}_s^* = 0$

As can be seen, the BUP (Barrier) equations are similar in form to the equations for the UP - the only difference being the initial values of state and costate variables for the BUP (Barrier). Although the resulting trajectories will be different in shape (because of different boundary conditions) the form of the solutions are the same. Taking advantage of this similarity, the equations for the Barrier are given. The E singular case, for that part of the BUP where $0 < S_1 < \pi$, is done first.

The E singular case requires that $S_2 = S_1$ (see Eq (6.32)). However, since S_1 and S_2 are on the BUP, Eq (6.56) yields

$$\cos S_1 = V_E / V_P \quad . \tag{6.64}$$

The E singular case also requires $\dot{U}_\theta(\tau) = 0$ (see Eq (6.33)

Realizing the Barrier boundary conditions of Eqs (6.49) and (6.50), Eqs (6.34) and (6.35) show that

$$U_x(\tau) = \sin\left(S_1 + \frac{V_P}{R_P}\tau\right) \tag{6.65}$$

$$U_y(\tau) = \cos\left(S_1 + \frac{V_P}{R_P}\tau\right) \quad . \tag{6.66}$$

Likewise, Eq (6.36) shows that

$$\tilde{A}_\theta(\tau) = -R_P\left[\cos S_1 - \cos\left(S_1 + \frac{V_P}{R_P}\tau\right)\right] \tag{6.67}$$

and Eqs (6.37), (6.38) and (6.39) show

$$\theta(\tau) = S_1 + \frac{V_P}{R_P}\tau \tag{6.68}$$

$$x(\tau) = (\ell - V_E\tau)\sin\left(S_1 + \frac{V_P}{R_P}\tau\right) + R_P\left(1 - \cos\frac{V_P}{R_P}\tau\right) \tag{6.69}$$

$$y(\tau) = (\ell - V_E\tau)\cos(S_1 + \frac{V_P}{R_P}\tau) + R_P \sin\frac{V_P}{R_P}\tau \qquad (6.70)$$

where S_1 is defined by Eq (6.64).

Reference to Eqs (4.37) to (4.42) shows that the E singular case on the Barrier of the present model is exactly the same as the Barrier of the Limited Pursuer model. The P singular case is done next.

The P singular case requires $S_1 = 0$. From Figure 21 and Eq (6.56) for the BUP it can be seen that $S_1 \neq 0$ on the BUP. It was for this reason that the P singular trajectories from the UP were not presented. Next we examine the backward Barrier trajectories from that part of the BUP where $\tilde{\beta} \neq 0$.

To be on the BUP, S_1 and S_2 must satisfy Eq (6.56) (see also Figure 21). Eqs (B.46) and (B.47) indicate, realizing the Barrier boundary conditions of Eqs (6.49) and (6.50) that

$$v_x(\tau) = \sin(S_1 + \tilde{\alpha}\frac{V_P}{R_P}\tau) \qquad (6.71)$$

$$v_y(\tau) = \cos(S_1 + \tilde{\alpha}\frac{V_P}{R_P}\tau) \qquad (6.72)$$

Eq (6.42) shows that

$$\theta(\tau) = S_2 + (\frac{V_P}{R_P}\tilde{\alpha} - \frac{V_E}{R_E}\tilde{\beta})\tau \qquad (6.73)$$

Eq (B.50) along with the Barrier boundary conditions of Eqs (6.49) and (6.50) shows that

$$v_\theta(\tau) = \frac{R_E}{\tilde{\beta}}\left[\cos(S_1 - S_2) - \cos(S_1 - S_2 + \frac{V_E}{R_E}\tilde{\beta}\tau)\right] \qquad (6.74)$$

E switching on the Barrier occurs when τ equals

τ_θ defined by (see Eq (6.40))

$$\frac{V_E}{R_E}\tilde{\tau}_\theta = 2\pi - 2|S_1 - S_2| \qquad (6.75)$$

Eq (B.55) shows that

$$\tilde{A}_\theta(\tau) = -\frac{R_p}{\tilde{\alpha}}\left[\cos s_1 - \cos\left(s_1 + \tilde{\alpha}\frac{V_p}{R_p}\tau\right)\right] \qquad (6.76)$$

and switching on the Barrier occurs when τ equals $\tilde{\tau}_A$ defined by (see Eq (6.41))

$$\frac{V_p}{R_p}\tilde{\tau}_A = 2\pi - 2|s_1| \quad . \qquad (6.77)$$

The x and y Barrier solutions are similar to Eqs (6.43) and (6.44) i.e.

$$x(\tau) = \tilde{\alpha} R_p\left(1-\cos\tilde{\alpha}\frac{V_p}{R_p}\tau\right) + \ell \sin\left(s_1 + \tilde{\alpha}\frac{V_p}{R_p}\tau\right) + \\ + \frac{R_E}{\tilde{\beta}}\left[\cos\left(s_2 + \tilde{\alpha}\frac{V_p}{R_p}\tau\right) - \cos\theta(\tau)\right] \qquad (6.78)$$

$$y(\tau) = \tilde{\alpha} R_p \sin\tilde{\alpha}\frac{V_p}{R_p}\tau + \ell\cos\left(s_1 + \tilde{\alpha}\frac{V_p}{R_p}\tau\right) + \\ - \frac{R_E}{\tilde{\beta}}\left[\sin\left(s_2 + \tilde{\alpha}\frac{V_p}{R_p}\tau\right) - \sin\theta(\tau)\right] \quad . \qquad (6.79)$$

This completes the solution of those trajectories immediately leaving the BUP.

6. Barrier Interpretation:

First the x,θ symmetry in the Barrier (as well as the whole problem - was mentioned previously) is shown analytically. Consider a case where $s_1 = s_{10} > 0$ and $s_2 = s_{20}$ where $0 < s_1 - s_2 < \frac{\pi}{2}$.

Then $\tilde{\alpha} = +1$ and $\tilde{\beta} = +1$ and the Barrier trajectory i.e. Eqs (6.73), (6.78) and (6.79) yield

$$\theta^{+}(\tau) = s_{20} + \left(\frac{V_p}{R_p} - \frac{V_E}{R_E}\right)\tau \tag{6.80}$$

$$x^{+}(\tau) = R_p\left(1 - \cos\frac{V_p}{R_p}\tau\right) + \ell \sin\left(s_{10} + \frac{V_p}{R_p}\tau\right) + + R_E\left[\cos\left(s_{20} + \frac{V_p}{R_p}\tau\right) - \cos\theta^{+}(\tau)\right] \tag{6.81}$$

$$y^{+}(\tau) = R_p \sin\frac{V_p}{R_p}\tau + \ell\cos\left(s_{10} + \frac{V_p}{R_p}\tau\right) + - R_E\left[\sin\left(s_{20} + \frac{V_p}{R_p}\tau\right) - \sin\theta^{+}(\tau)\right] . \tag{6.82}$$

Now consider the case where $s_1 = -s_{10}$ and $s_2 = -s_{20}$

Then $s_1 - s_2 = -s_{10} + s_{20} \equiv -(s_{10} - s_{20})$ and since originally $0 < s_{10} - s_{20} < \pi/2$ then in this case $0 > s_1 - s_2 > -\pi/2$.

Therefore in this "mirror image" case, $\tilde{\alpha} = -1$ and $\tilde{\beta} = -1$ and Eqs (6.73), (6.78) and (6.79) yield

$$\theta^{-}(\tau) = -s_{20} - \left(\frac{V_p}{R_p} - \frac{V_E}{R_E}\right)\tau \tag{6.83}$$

$$x^{-}(\tau) = -R_p\left(1 - \cos\frac{V_p}{R_p}\tau\right) - \ell \sin\left(s_{10} + \frac{V_p}{R_p}\tau\right) + - R_E\left[\cos\left(s_{20} + \frac{V_p}{R_p}\tau - \cos\theta^{+}(\tau)\right)\right] \tag{6.84}$$

$$y^{-}(\tau) = R_p \sin\frac{V_p}{R_p}\tau + \ell\cos\left(s_{10} + \frac{V_p}{R_p}\tau\right) + - R_E\left[\sin\left(s_{20} + \frac{V_p}{R_p}\tau\right) - \sin\theta^{+}(\tau)\right] . \tag{6.85}$$

A comparison of equations shows $\theta^{+}(\tau) = -\theta^{-}(\tau)$, $x^{+}(\tau) = -x^{-}(\tau)$ and $y^{+}(\tau) = y^{-}(\tau)$; hence, the x, θ symmetry is shown. With this symmetry in mind, the Barrier shape, possible closing conditions and sensitivities are examined.

As will be demonstrated shortly, by a comparison of the Barriers of the Limited Pursuer model with the present model, the Barrier and its closure properties depend on the particular air-to-air combat model and its system parameters. Except for the simplest of air-to-air

combat models, the Barrier is generally not a completely closed surface in $\mathcal{C}$; however, selected Barrier trajectories or trajectory types can be made to close for judicious choice of the system parameters. As seen in Figure 22, not all of the escape trajectories making up the Barrier are physically interesting for one reason or another - in this particular case, role. However, there are physically important Barrier trajectories on each Barrier. It is the closure of these Barrier trajectories (can be thought of as a partial Barrier closure) and their sensitivities to system parameters that is important to study. This concept will become more clear as we examine specific Barrier trajectory closure in this model.

Figure 23 is a pictorial drawing of the terminal surface, $\mathcal{C}$, and the Barrier leaving the surface. Both the right and left BNP are partially drawn on $\mathcal{C}$. The E singular line on $\mathcal{C}$ is also drawn; it appears as a helix wrapping around $\mathcal{C}$. The origin of the Dispersal Surface on $\mathcal{C}$ is also shown. The A trajectory is the E singular Barrier trajectory in Eqs (6.68), (6.69) and (6.70). The projection of this trajectory onto the X-Y plane (note that $\Theta(T)$ is increasing positive on the right side and is increasing negative on the left side) is identical to the Barrier of the Limited Pursuer model (see Figure 6). If we examine the conditions that allow the E singular projections to just touch the y-axis tangentially (i.e. a grazing Barrier closure for the Limited Pursuer model), Eq (4.43) shows that $\Theta(T) = +\pi/2$ for the

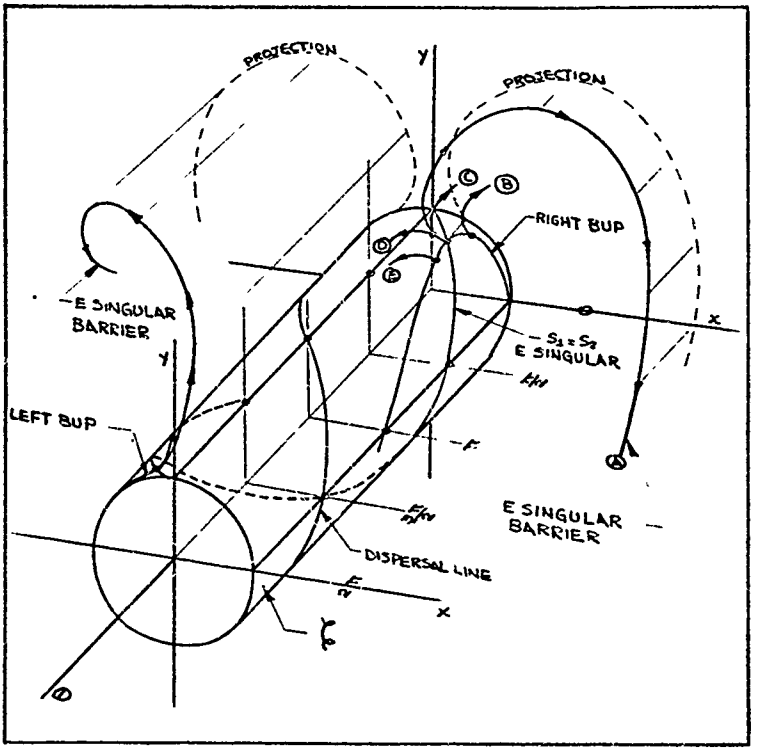

Figure 23: Barrier Trajectories

right projection and $\Theta(T) = -\pi/2$ for the left projection. Therefore, even though the Barrier of the Limited Pursuer model is also a Barrier trajectory in the present model, it can be seen from the above that the completely closed Barrier in the Limited Pursuer model is not a closed Barrier trajectory in the present model. This is not to say that closed Barrier trajectories do not occur in the present model, just that the added realism of the E model has changed the conditions under which closed trajectories occur.

Since P is pursuing E, $\frac{V_E}{V_P} < 1$ was selected earlier to correspond to P's role. Now, the realism added to this model was a limited turning rate for E - previously E was infinitely maneuverable. In order to give E a change at closing the Barrier completely or partially, it seems logical that the turning rate of E should be larger than the turning rate of P i.e. $\frac{\dot{\Theta}_E}{\dot{\Theta}_P} > 1$. In the analysis that follows this is assumed. Therefore, P is faster but can not turn as rapidly as E. We leave the required magnitudes of $\frac{V_E}{V_P}$, $\frac{\dot{\Theta}_E}{\dot{\Theta}_P}$, etc., for closure to the analytics of the Barrier.

The B trajectory in Figure 23 corresponds to the case where $\tilde{\alpha} = +1$ and $\tilde{\beta} = +1$. Eq (6.73) applies here and shows that

$$\Theta(T) = S_2 + (\dot{\Theta}_P - \dot{\Theta}_E)T \qquad . \qquad (6.86)$$

Since $\dot{\Theta}_E > \dot{\Theta}_P$, $\Theta(T)$ is decreasing i.e. the B trajectory is heading toward the X-Y plane of $\Theta = 0$. Likewise, the mirror image of the B trajectory off the left BUP is heading toward the X-Y plane of

$\Theta = 2\pi$ (same as $\Theta = 0$). If both these trajectories meet the respective planes at $X = 0$, the y's of the two trajectories will be identical (because of the symmetry) along with the Θ's being zero (2π). If the parameters of the problem can be found to cause this to occur, the Barrier will be partially closed for these specific trajectories.

The E trajectory in Figure 23 corresponds to the case where $\tilde{\alpha} = +1$ and $\tilde{\beta} = -1$. Eq (6.73) applies here also and shows

$$\Theta(T) = S_2 + (\dot{\Theta}_P + \dot{\Theta}_E)\,T \qquad (6.87)$$

$\Theta(T)$ is increasing rapidly and heading towards the region of the Dispersal surface (defines a surface of unusual encounters which have for each point on the surface two different trajectories leading to the same payoff i.e. escape in the case of the Barrier). The mirror image of the E trajectory off the left BUP is also heading for this region and closure on the Dispersal surface. Note that the Dispersal surface itself is a kind of Barrier trajectory closure. As was mentioned earlier, the encounters on this surface are the head-on-type etc., where the present fixed roles are not justified and have little practical application. As will be shown, this leads to certain anomalies in the Barrier of little practical use.

The C and D trajectories in Figure 23 are trajectories which branch off the E singular trajectory. The D trajectory corresponds to E switching from the singular $\tilde{\beta} = 0$ to $\tilde{\beta} = -1$ which heads the trajectory towards the Dispersal surface region. For the same reasons

just discussed, the D trajectories are not examined. The solution of the C trajectories is done next.

The solution of the C type trajectories (i.e. $\tilde{\alpha} = +1$, $\tilde{\beta} = 0$ followed by $\tilde{\beta} = +1$) satisfies the necessary conditions for the Barrier trajectories, however, subject to the boundary conditions on the E singular trajectory at the point where switching occurs. Let τ_s be the time that E switches controls and define θ_{ps} as

$$\theta_{ps} = \frac{V_P}{R_P}\tau_s \qquad (6.88)$$

Note that θ_{ps} is the angle that P turns thru while E is on the singular Barrier trajectory. Substituting Eq (6.88) into Eqs (6.64) - (6.70) gives the boundary conditions at τ_s i.e.

$$s_1 = \cos^{-1}\left(\frac{V_E}{V_P}\right) \qquad (6.89)$$

$$v_\theta(\tau_s) = 0 \qquad (6.90)$$

$$v_x(\tau_s) = \sin(s_1+\theta_{ps}) \qquad (6.91)$$

$$v_y(\tau_s) = \cos(s_1+\theta_{ps}) \qquad (6.92)$$

$$\breve{A}_\theta(\tau_s) = -R_p[\cos s_1 - \cos(s_1+\theta_{ps})] \qquad (6.93)$$

$$\theta(\tau_s) = s_1+\theta_{ps} \qquad (6.94)$$

$$x(\tau_s) = \left(\ell - \frac{V_E}{V_P}R_p\theta_{ps}\right)\sin(s_1+\theta_{ps}) + R_p(1-\cos\theta_{ps}) \qquad (6.95)$$

$$y(\tau_s) = \left(\ell - \frac{V_E}{V_P}R_p\theta_{ps}\right)\cos(s_1+\theta_{ps}) + R_p\sin\theta_{ps} \qquad (6.96)$$

Note that

$$\theta(\tau_s) = s_1 + \theta_{ps} < 2\pi - |s_1| \tag{6.97}$$

or else switching of $\tilde{\alpha}$ will have occured. The details of the C trajectory analytics can be found in Appendix B of which the following is a summary.

Time after τ_s is defined as

$$\tau' = \tau - \tau_s \tag{6.98}$$

After β switches to +1 the results are

$$\theta(\tau') = s_1 + \theta_{ps} - \dot{\theta}_E\left(1 - \frac{\dot{\theta}_P}{\dot{\theta}_E}\right)\tau' \tag{6.99}$$

The P switching condition remains unchanged i.e.

$$\theta_{ps} + \frac{V_P}{R_P}\tilde{\tau}_{A'} \equiv \frac{V_P}{R_P}\left(\tau_s + \tilde{\tau}_{A'}\right) \equiv \frac{V_P}{R_P}\tilde{\tau}_A = 2\pi - 2|s_1| \tag{6.100}$$

The $x(\tau')$, $y(\tau')$ state solutions subject to the boundary conditions of Eqs (6.89) - (6.96) are

$$\frac{x(\tau')}{R_P} = -\cos\left(\theta_{ps} + \frac{V_P}{R_P}\tau'\right) + \left(\frac{\ell}{R_P} - \frac{V_E}{V_P}\theta_{ps}\right)\sin\left(s_1 + \theta_{ps} + \frac{V_P}{R_P}\tau'\right) +$$
$$+ \frac{R_E}{R_P}\cos\left(s_1 + \theta_{ps} + \frac{V_P}{R_P}\tau'\right) + 1 - \frac{R_E}{R_P}\cos\theta(\tau') \tag{6.101}$$

$$\frac{y(\tau')}{R_P} = \left(\frac{\ell}{R_P} - \frac{V_E}{V_P}\theta_{ps}\right)\cos\left(s_1 + \theta_{ps} + \frac{V_P}{R_P}\tau'\right) + \sin\left(\theta_{ps} + \frac{V_P}{R_P}\tau'\right) +$$
$$- \frac{R_E}{R_P}\sin\left(s_1 + \theta_{ps} + \frac{V_P}{R_P}\tau'\right) + \frac{R_E}{R_P}\sin\theta(\tau') \tag{6.102}$$

Eqs (6.99), (6.101) and (6.102) are the equations for the C type Barrier trajectories in terms of θ_{ps}, τ', and the parameters of the problem. The equations are only valid provided P switching does not occur i.e. Eq (6.100).

Again it is noted that for $\dot{\theta}_E > \dot{\theta}_P$, that $\Theta(T')$ (Eq (6.99)) will decrease towards the x--y plane where $\Theta = 0$. Likewise, the mirror image of the C trajectory off the left BUP will increase toward the plane of $\Theta = 2\pi$. As with the B trajectories, if these C trajectories meet the $\Theta = O(2\pi)$ planes at $x = O$, this will be a case of Barrier trajectory closure.

The importance of the B Barrier trajectory closure and the C Barrier trajectory closure is seen when it is realized that the closure is taking place on the totally singular surface i.e. the y -axis. Since a majority of the trajectories from the state space come down this totally singular surface, partial Barrier closure on the y -axis provides an E escape route for a majority of the state space.

The parameters of the problem determine the y position at which the Barrier partially closes on the y -axis. Assuming that the combat has started from a state that has led to the totally singular y -axis (see Fig 20) and assuming that E has not passed the y point of Barrier closure, as that point is reached E pulls max gs and P pulls max gs . Depending on the parameter magnitudes of the problem (see Figure 26), E may or may not switch to the singular non-turning trajectory. P always maintains max gs . The result is that E escapes. To better visualized the shape of the Barrier in the region of interest (i.e. the B and C type trajectories which occur when $-\cos^{-1}\frac{V_E}{V_P} \leq S_2 \leq \cos^{-1}\frac{V_E}{V_P}$) and the interesting case of Barrier trajectory closure with the y- singular

axis, cross sections of the Barrier perpendicular to the $\Theta(S_2)$ axis in Figure 23 were calculated.

Figure 24 shows cross sections of the Barrier for $0 \leq S_2 \leq \cos^{-1}\frac{V_E}{V_P} = \cos^{-1}(.9) = 25.84°$ for a specific case of vehicle parameters that result in Barrier trajectory closure with the y-singular axis. For $-\cos^{-1}\frac{V_E}{V_P} \leq S_2 \leq 0$, the mirror image of Figure 24 about the y - axis applies. Cross sections of the Barrier are presented for $S_2 = 0$ and $S_2 = 25°$. The cross sections for any S_2 between 0° and 25° are curves of smooth transition (not shown so as not to clutter Figure 24) between the two shown. Note that each cross section represents those $x-y$ positions that lead to escape for E provided E's velocity angle off is initially the S_2 value of the cross section. Note also how the $S_2 = 0$ cross section closes with its mirror image on the y - singular axis at $\frac{y}{R_P} = .490$. For the given system parameters, this $\frac{y}{R_P}$ position is the closest distance that E can be from P in a direct tail chase and still effect an escape. The importance of this $\frac{y}{R_P}$ position is pointed out later.

Note that by increasing $\frac{\rho}{R_P}$ to .250, closure of the Barrier with itself and the y singular axis is not possible (see dashed line in Figure 24).

Figure 25 presents cross sections of the Barrier for $0 \leq S_2 \leq \cos^{-1}\frac{V_E}{V_P} = \cos^{-1}(.9) = 25.84°$, however, in the region of the left BUP and Dispersal surface where the roles are ill defined. As can be seen, the cross sections are inside of $\mathcal{C}$ and terminate very close

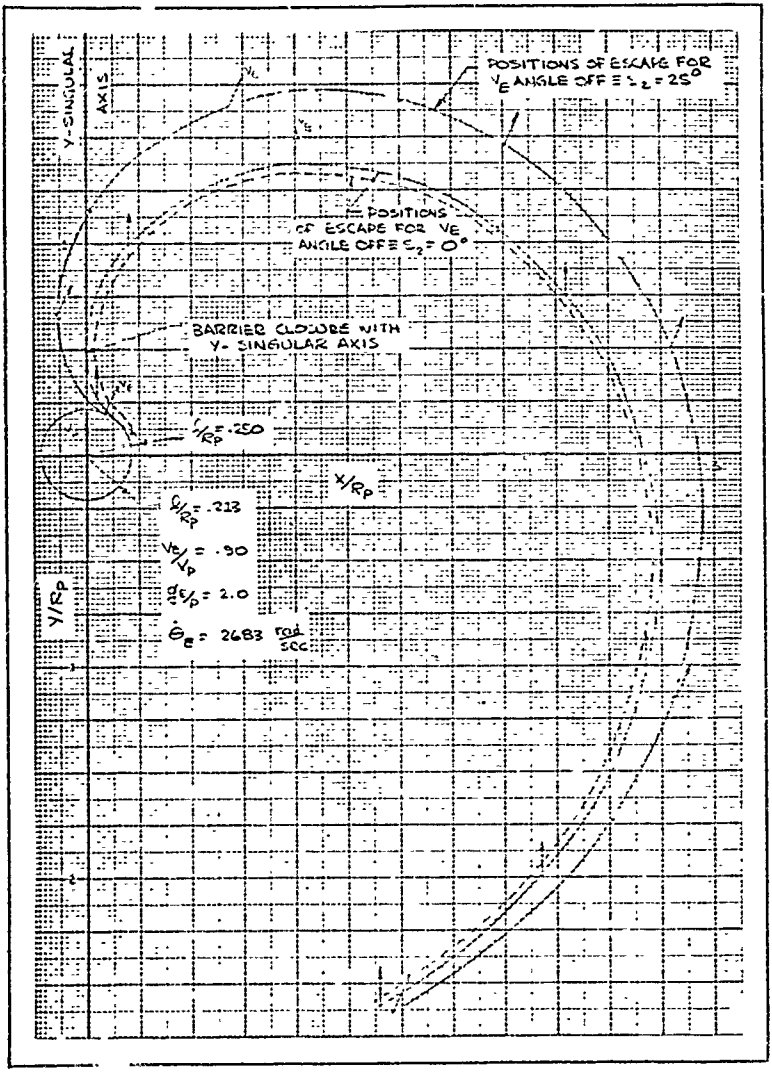

Figure 24: Barrier Σ_2 Cross Sections Right BUP

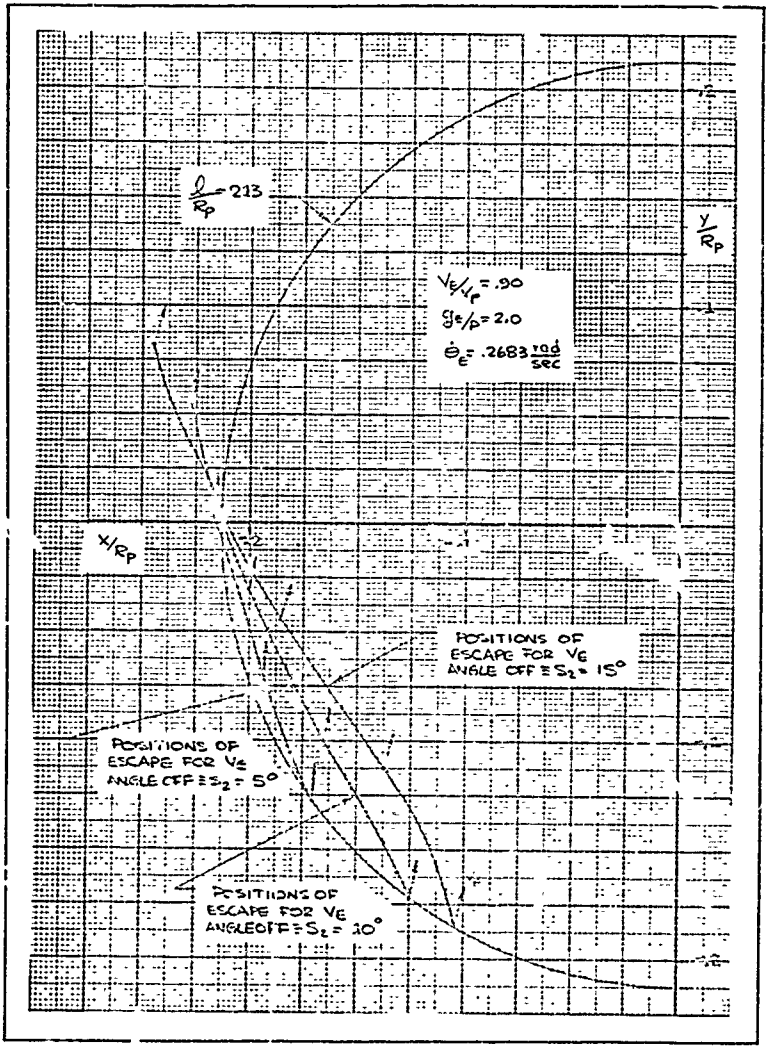

Figure 25: Barrier S_2 Cross Sections Left BUP

to $\mathcal{C}$. Isaacs [7: 217] treats this condition as an anomaly in the Barrier since the Barrier is only defined physically external to $\mathcal{C}$. As can be seen by Figures 21 and 25, E is considerably behind and left of P with $\underline{V}_E$ pointing towards P. Both P and E are doing hard left turns since P is pursuing and E evading. It is very obvious that E has the wrong role i.e. he should be turning right to attack, not left to evade. The fixed role situation happens to be poorly defined for this region of the Barrier and is causing the above anomaly. For this reason, extensive analysis of the Barrier in this region is not done. The role problem is discussed later in Chapter IX.

A computer program was written, using the equations defining the B and C trajecto y types, to calculate the parameter conditions that result in the interesting Barrier trajectory closure on the y singular axis. The results of these computations are shown in Figures 26 and 27.

Figure 26 shows the maximum value of $\frac{\ell}{R_P}$ for closure, versus the combat velocity ratio $\frac{V_E}{V_P}$ for fixed turning radius ratio $\frac{R_P}{R_E}$. The results are based on $\dot{\Theta}_E > \dot{\Theta}_P$. The significance of "max" is the following: for a given $\frac{V_E}{V_P}$ and $\frac{R_P}{R_E}$ (i.e. $\frac{\dot{\Theta}_E}{\dot{\Theta}_P} = \frac{V_E}{V_P}\frac{R_P}{R_E}$), if the actual $\frac{\ell}{R_P}$ is larger than the max $\frac{\ell}{R_P}$, then closure is not possible (see Figure 24 for example). Superimposed on the data are lines of constant g ratio, $g_{E/P} = a_{\perp E}/a_{\perp P} = \left(\frac{V_E}{V_P}\right)^2 \frac{R_P}{R_E}$. Below the dashed line, the escape trajectories are non-singular i.e. type B. Above the dashed line the escape trajectories are partially

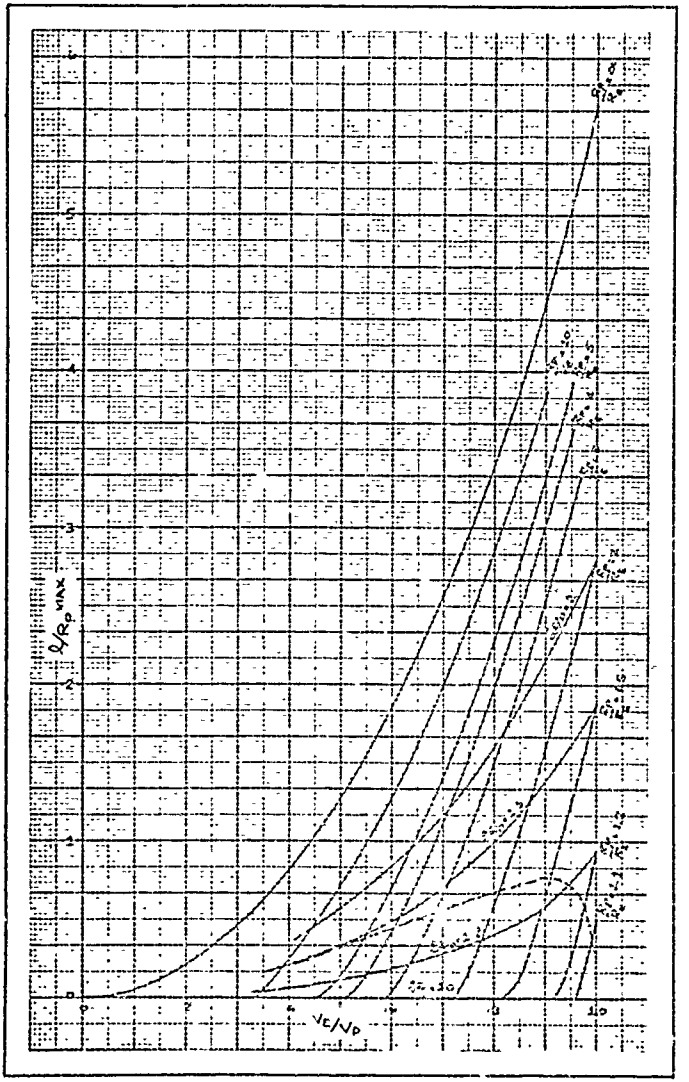

Figure 26: Closure Conditions in θ=o plane, $\dot{\theta}_t > \dot{\theta}_p$

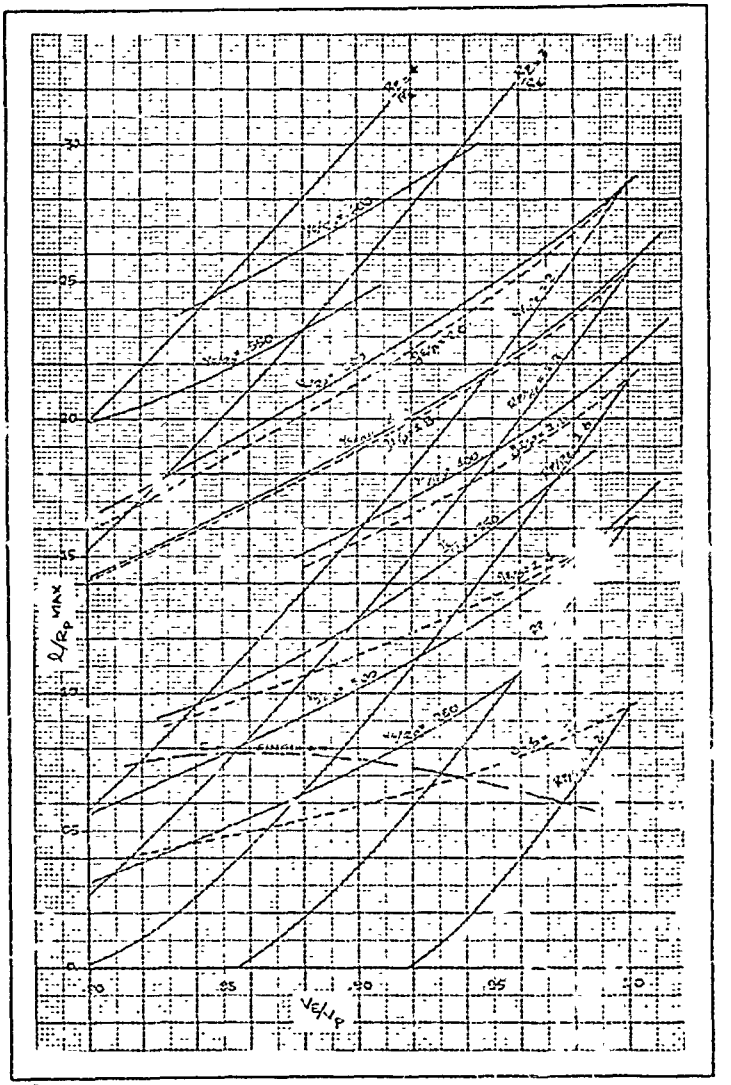

Figure 27: Y_c/R_p Dependence

singular for E, i.e. type C. Computer results showed that the switching of E to the non-turning singular control always occurred at the point where E made a quarter turn in real space. Knowledge of the dependence of the closure point on the state of the game (i.e. Figure 27) together with the above optimal control information yields the following closed loop control Barrier escape laws:

(1) At the γ Barrier closure point, both P and E pull max gs .

(2) Provided E has not already grazed ζ (i.e. B type trajectory), E switches to the non-turning singular control at the 90° point in his turn.

Figure 27 shows the closure $\frac{\gamma}{R_P}$ dependence for the lower right region of Figure 26 - a region of practical interest.

Some general comments can be made about both Figures 26 and 27:

1) As $\frac{R_P}{R_E}$ goes to infinity (i.e. $R_E = 0$ and E can turn instantaneously), the closure conditions are the same as for the Limited Pursuer model.

2) For points above the dashed line, E is not pulling gs terminally.

3) $g_{E/P}$ is greater than one (1).

4) Note the parallel tendencies of the $\frac{\gamma}{R_P}$ and $g_{E/P}$ curves.

The effects on the closure conditions of making E more realistic, can be seen from Figure 26. Note that the $\frac{\ell}{R_P}$ max value is always less than that value for the Limited Pursuer model i.e. the decreased

capability of E requires less capability of P to insure capture. A specific case helps to point this out. Take the case where $V_p = 800$ ft/sec, $a_{\perp_p} = 5g$s (i.e. $R_p = 4000$ ft) and let $\frac{V_E}{V_p} = .9$ Figure 7 or Figure 26 ($\frac{R_p}{R_E} = \infty$) shows that ℓ/R_p max equals .445 in the Limited Pursuer model. Assume that in an escape maneuver that $a_{\perp E} = 7g$s (i.e. a structural limit) implying that $\frac{a_{\perp E}}{a_{\perp p}} = \frac{7}{5} =$ = 1.4. Figure 27 then shows that ℓ/R_p max = .114 - a considerable reduction in the required capability of P's weapons system to insure capture.

Having examined the basic Barrier shape and the closing conditions of interest, we now examine the sensitivity of the closing conditions in an attempt to learn more about the parameters most influencing the combat outcome. We begin by constructing a "realistic" combat situation similar to that used in Chapter V.

Consider a combat engagement where P is a Mach # = .8 at 30000 ft altitude (i.e. V_p = 800 ft/sec). It is assumed that P's tracking ability limits him to a 3g maneuver (i.e. R_p = 6600 ft). It is further assumed that in an evasive situation, E can sustain 6gs (i.e. $g_{E/p} = 2.$). It is further assumed that the gun capability of P is effective at ℓ = 1400 ft. (i.e. $\frac{\ell}{R_p} = .212$). To guarantee that the Barrier does not close, Figure 27 shows that P must have sufficient velocity advantage to have $\frac{V_E}{V_p} < .9$.

Figure 27 also shows that at $\frac{V_E}{V_P} = .9$, $\left.\frac{Y}{R_P}\right|_c = .490$ implying that $Y_c = 3230$ ft. Note that this Y_c is within pilot visibility, yet not so far away from P that E could be inside this point under a surprise engagement.

Considering this, or any other specific engagement condition, we are interested in the best ways that P and E can improve their combat capabilities. These combat capabilities are given analytical measure through the distance Y_c : a decrease in Y_c indicates a more capable evader in that E is closer to P and yet escapes; a larger Y_c indicates a more capable pursuer in that E must be farther away from P to escape. The parameters under P's control are ℓ, V_P and $a_{\perp P}$. The parameters under E's control are V_E and $a_{\perp E}$. Improvements in E are examined first. As an example, we begin with the "realistic" combat engagement just discussed.

Since $\frac{\ell}{R_P} = .212$, E does not want to change the parameters to bring the combat condition below the .212 line i.e. escape is not possible if E does this. Since $V_E/V_P = .9$, then $Y_c = 3230$ ft (i.e. $Y_c/R_P = .490$). Two cases arise here: actual $Y > Y_c$ or actual $Y < Y_c$. In the $Y > Y_c$ case, Figure 27 indicates several possibilities for E to escape:

1) Since $Y > Y_c$, E can remain on the totally singular y - axis until P closes to where $Y = Y_c = 3230$ ft. At this point E initiates the required 6 gs (i.e. $g_{E/P} = 2.0$ required for escape) turn and P does a

3g turn. The result is that E escapes.

2) Since $\gamma > \gamma_c$ (i.e. assume $\frac{\gamma}{R_p} = .550 > \frac{\gamma_c}{R_p} = .490$ where .490 is that $\frac{\gamma_c}{R_p}$ for $g_{E/P} = 2.0$), Figure 27 indicates that E need not wait until $\gamma/R_p = .490$ to escape, but could escape at $\gamma/R_p = .550$ provided $g_{E/P} \simeq 2.27$ i.e. $g_E \simeq 6.8$ gs. E could also reduce V_E (i.e. V_{E/V_p}) on the γ - singular axis while P is closing (i.e. while γ/R_p is reducing below .550). This will reduce the required $g_{E/P}$ for escape below 2.27 yet not as low as 2.0. In essence E is trading his velocity for a lesser value of $g_{E/P}$ to escape. The net result is that if E chooses to escape at a $\gamma/R_p > .490$, by either option, it will require $g_{E/P} > 2.0$.

3) The final option is that if E has the ΔP_s advantage, he can increase V_{E/V_p} while P is closing. For example, if $\frac{V_E}{V_p}$ can be increased on the γ -singular axis to .91, then at $\ell/R_p = .212$ the required conditions for escape are $\frac{\gamma_c}{R_p} = .480$, $g_{E_p} = 1.95$. Note this allows E to be closer to P, use less than 6 gs, and still escape. If we continue to assume that a smaller γ_c indicates a better evader, then in the $\gamma > \gamma_c$ case, 3) is the most attractive improvement for E. Note here the increased emphasis on velocity and reduced gs. In the $\gamma < \gamma_c$ case, E must reduce γ_c. Figure 27 indicates only one option:

1) Increase V_E (i.e. $\frac{V_E}{V_p}$). This will decrease γ_c and the gs required.

Note again the increased emphasis on larger velocity and reduced gs. Improvements in P are examined next.

The same "realistic" combat engagement is assumed. We now examine the effects of increases in ℓ, V_p and $a_{\perp_p}$ on escape. Since ℓ/R_p max = .212 (R_p = 6600 ft), Figure 27 shows that any increase of ℓ makes $\frac{\ell}{R_p} > \frac{\ell}{R_p}$ max and escape by E impossible unless E increases $\gamma_{E/p}$ (at V_E/V_p = .9) or increases $\frac{V_E}{V_p}$ (at $\gamma_{E/p}$ = 2). This is advantageous from P's design standpoint since it forces E to higher $\frac{V_E}{V_p}$ and $\gamma_{E/p}$ to escape. Note also that it can increase Y_c/R_p. For example, consider a 100 ft increase of ℓ to 1500 ft (i.e. $\ell/R_p = \frac{1500}{6600}$ = .227). If E increases $a_{\perp_E}$ to escape, Figure 27 shows that $\frac{Y_c}{R_p}$ equals .520 yielding Y_c = 3430 ft - a 200 ft increase in Y_c.

Now consider an increase in V_p of 25 ft/sec. The new $\frac{V_E}{V_p}$ is $\frac{720}{825}$ = .873 and at the same $\gamma_{E/p}$ Figure 27 yields ℓ/R_p max = .197. Now R_p equals $825^2/3(32.2)$ = 7050 ft and the actual ℓ/R_p is $\frac{1400}{7050}$ = .198. Therefore $\frac{Y_c}{R_p}$ is approximately unchanged at .49 yielding Y_c = 3450 ft - a 220 ft increase in Y_c.

Finally consider an increase of $a_{\perp_p}$ by 10 ft/sec^2 i.e. $a_{\perp_p}$ = 3(32.2)+ 10 = 106.6 ft/sec^2. Then $\gamma_{E/p}$ equals 6(32.2)/106.6 = 1.81 and Figure 27 shows ℓ/R_p max = .190. Since R_p equals $800^2/106.6$ = 6000 ft, the actual ℓ/R_p is 1400/6000 = .233. Under these conditions Figure 27 shows that escape is impossible unless E increases $a_{\perp_E}$ or V_E. If E increases $a_{\perp_E}$

enough to escape then $\frac{Y_c}{R_p}$ = .535 and Y_c = 3210 – a decrease of 20 ft in Y_c . If E increases V_E enough to escape then $\frac{Y_c}{R_p}$ = .49 and Y_c = 2940 ft – a decrease of 290 ft in Y_c .

Summarizing these cases we find:

1) For a 1 ft increase of ℓ , Y_c increases 2 ft

2) For a 1 ft/sec increase of V_p , Y_c increases 8.8 ft

3) For a 1 ft/sec^2 increase of $a_{\perp_p}$, Y_c decreases 2 ft.

Note that in each case of an improvement to P, that E is captured unless he improves $a_{\perp_E}$, etc. Assuming that this increase in $a_{\perp_E}$ is within E's capability, the results indicate that an increase of V_p is the best improvement to make to P. Since E's strategy for improvement is clearly to increase V_E , this also suggests that P should consider increasing V_p . Apparently, the aircraft with the greater P_s will have the advantage in improving the combat condition in its favor.

7. Model and Barrier Conclusions:

1) In this model, E's dynamics was made more realistic by limiting his turning rate. As with the Limited Pursuer model, this decrease capability of E was reflected in the parametric conditions causing Barrier trajectory closure. Again it is pointed out that the Barrier is a tool that does analytically reflect the combat capabilities of the players.

2) In this model the control laws are more refined, but still reflect the combatants attempts to align their velocity vectors along the line of sight P to E. Closed form control laws for the important cases of Barrier trajectory closure were found.

3) Sensitivity analysis of the Barrier continues to show that $\frac{V_E}{V_P}$ is the most important parameter. Figures 26 and 27 optimally reveal how turning g_s, velocity, P's gun capability, and relative position affect the outcome of a given terminal combat engagement. Its application to relative evaluation of fighter aircraft is discussed in Chapter VII.

3D Limited Pursuer-Evader

In the 3D Limited Pursuer model, the out-of-plane optimal maneuver for the case of a highly maneuverable evader was examined. The optimal maneuver was shown to be the "slice maneuver". The intent of the present model is to examine the out-of-plane maneuver for a more realistic evader, who like the pursuer is also limited in turning rate and must control by g_s and bank angle. Williamson-Noble [15] partially examines this problem in the realistic ten (10) dimensional space ξ. The 10-D ξ makes characterization of the 3D maneuvers and associated controls extremely difficult. Williamson-Noble also alludes to a problem with the model near a tail chase situation. He attributes this to the singular surfaces near this position.

The model development that follows is original in that the ten (10) dimension problem is reduced to four (4) dimensions. Also, the four dimensions are chosen in such a way as to be physically meaningful to the combatants involved and to take advantage of the previous two dimensional model work. As will be seen, this choice of coordinate system does much to aid the characterization of the controls associated with the 3D maneuvers.

1. State Equation Formulation:

The coordinate system for this model is shown in Figure 28. The reduced space ξ is used. The details of the state equation derivation can be found in Appendix B.

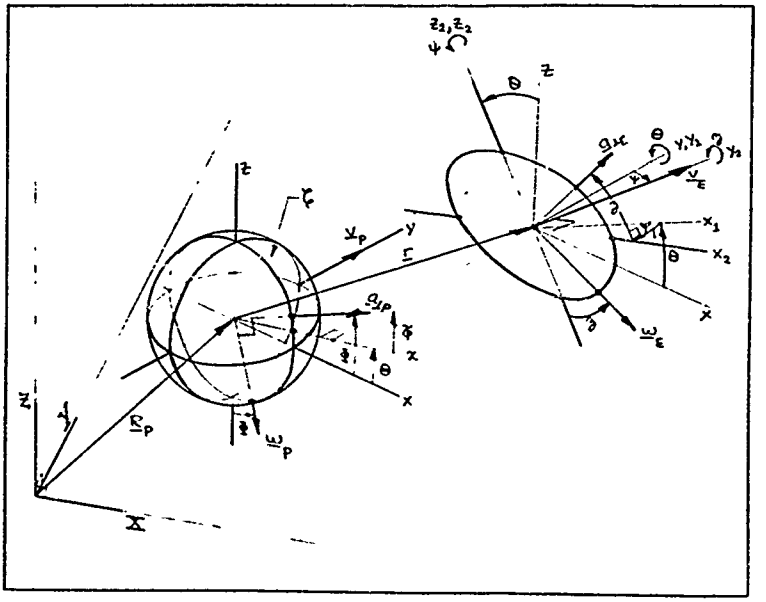

Figure 28: 3D Coordinate System

The state equations are

$$\dot{\underline{x}} = \begin{bmatrix} \dot{x} \\ \dot{y} \\ \dot{\psi} \\ \dot{\zeta}_1 \end{bmatrix} = \begin{bmatrix} V_E \sin\psi \cos\zeta_1 - \alpha \frac{V_P}{R_P} y \cos\tilde{\phi} \\ V_E \cos\psi - V_P + \alpha \frac{V_P}{R_P} x \cos\tilde{\phi} \\ \beta \frac{V_E}{R_E} \cos\gamma - \alpha \frac{V_P}{R_P} \cos(\zeta_1 - \tilde{\phi}) \\ \beta \frac{V_E}{R_E} \sin\gamma \sin\psi + \frac{1}{x}\left[-V_E \sin\psi \sin\zeta_1 + \alpha \frac{V_P}{R_P} y \sin\tilde{\phi}\right] \end{bmatrix} \quad (6.103)$$

Note the physical meaning of the states and controls:

x - distance from y -axis to E in the plane of $\underline{v}_P$ and $\underline{r}$

y - distance along y -axis to E in the plane of $\underline{v}_P$ and $\underline{r}$

ψ - angle between $\underline{v}_P$ and $\underline{v}_E$

$\zeta_1 = \Theta - \bar{\Theta}$ - angle from x -axis to projection of $\underline{v}_E$ onto the z-x plane

$\tilde{\phi}$ - P's bank angle from x -axis to position of $\underline{a}_{\perp_P}$

γ - E's bank angle from x_2 -axis to position of $\underline{a}_{\perp_E}$

Three Euler angle rotations are involved in defining the above angles: first a counter clockwise rotation, Θ , about the y -axis; second a counter clockwise rotation, ψ , about the z_1 -axis; third a counter clockwise rotation, γ , about the y_2 -axis. These Euler angles are defined more explicitly in Appendix B.

It is instructive to note that for $\zeta_4 = 0$, the first three state equations of Eq (6.103) reduce to the state equations for the 2D Limited Pursuer-Evader model. By comparison to the 2D Limited Pursuer-Evader model, the added fourth dimension for the 3D problem is therefore seen to be ζ_4 .

2. Problem Setup:

In the reduced space ξ , the terminal surface is three dimensional. It can be thought of as a set of circles of radius ℓ - one circle for each of the velocity angles ψ and ζ_4 . Its usual description with Eq (2.3) is

$$\psi[\underline{x}(t_f)] = x^2(t_f) + y^2(t_f) - \ell^2 = 0 \qquad (6.104)$$

where $\psi(t_f)$ and $\zeta_4(t_f)$ are free. ζ_ℓ can also be described with Eq (2.19) as

$$\begin{aligned} x(t_f) &= h_1(\underline{s}) = \ell \sin s_1 \\ y(t_f) &= h_2(\underline{s}) = \ell \cos s_1 \\ \psi(t_f) &= h_3(\underline{s}) = s_2 \\ \zeta_4(t_f) &= h_4(\underline{s}) = s_3 \end{aligned} \qquad (6.105)$$

where

$$\underline{s} = \begin{bmatrix} s_1 \\ s_2 \\ s_3 \end{bmatrix} \qquad (6.106)$$

The controls for the players are

$$\underline{u} = \begin{bmatrix} \alpha \\ \tilde{\phi} \end{bmatrix} \quad , \quad \underline{v} = \begin{bmatrix} \beta \\ \zeta \end{bmatrix} \tag{6.107}$$

and the costate vector $\underline{\lambda}$ is

$$\underline{\lambda} = \begin{bmatrix} \lambda_x \\ \lambda_y \\ \lambda_\psi \\ \lambda_z \end{bmatrix} . \tag{6.108}$$

As with the other models, the roles of the players are preselected by choosing $\phi = 0$, $L = 1$ with P minimizing and E maximizing.

3. Application of Necessary Conditions:

ME1 becomes

$$0 = \min_{(\tilde{\phi},\alpha)} \max_{(\zeta,\beta)} \left\{ \lambda_x \left[V_E \sin\psi \cos\zeta - \alpha \frac{V_P}{R_P} y \cos\tilde{\phi} \right] + \right.$$

$$+ \lambda_y \left[V_E \cos\psi - V_P + \alpha \frac{V_P}{R_P} x \cos\tilde{\phi} \right] +$$

$$+ \lambda_\psi \left[\beta \frac{V_E}{R_E} \cos\zeta - \alpha \frac{V_P}{R_P} \cos(\zeta - \tilde{\phi}) \right] +$$

$$\left. + \lambda_z \left[\beta \frac{V_E}{R_E} \sin\zeta \sin\psi + \frac{1}{x} \left(\alpha \frac{V_P}{R_P} y \sin\tilde{\phi} - V_E \sin\psi \sin\zeta \right) \right] + 1 \right\} =$$

$$= \min_{(\tilde{\phi},\alpha)} H_P + \max_{(\zeta,\beta)} H_E + H_0 \tag{6.109}$$

where

$$H_P = \alpha \frac{V_P}{R_P} \left[A \cos\tilde{\phi} + B \sin\tilde{\phi} \right] \tag{6.110}$$

$$A = x\lambda_y - y\lambda_x - \lambda_\psi \cos\zeta \tag{6.111}$$

$$B = \frac{y}{x} \lambda_z - \lambda_\psi \sin\zeta \tag{6.112}$$

$$H_E = \beta \frac{V_E}{R_E} \left[\lambda_z \sin\zeta \sin\psi + \lambda_y \cos\zeta \right] \tag{6.113}$$

$$H_o = 1 - v_p\lambda_y + v_E\left[\lambda_x \sin\psi\cos\xi + \lambda_y\cos\psi - \frac{\lambda_\xi}{\chi}\sin\psi\sin\xi\right] \quad (6.114)$$

The max H_E conditions subject to the constraints, Eqs (B.86) and (B.88), are

$$\beta^* = h\left(\lambda_\xi \sin\zeta\sin\psi + \lambda_\psi\cos\zeta\right) \quad (6.115)$$

where h is the Heavyside step function. Notice the singular possibility if $\lambda_\xi\sin\zeta\sin\psi + \lambda_\psi\cos\zeta = 0$ for a finite time.

It is also necessary that

$$\frac{\partial H_E}{\partial\zeta} = \beta^*\frac{v_E}{R_E}\left[\lambda_\xi\sin\psi\cos\zeta^* - \lambda_\psi\sin\zeta^*\right] = 0 \quad (6.116)$$

implying that

$$\tan\zeta^* = \frac{\lambda_\xi\sin\psi}{\lambda_\psi} \quad (6.117)$$

or

$$\sin\zeta^* = \frac{\pm\lambda_\xi\sin\psi}{\sqrt{\lambda_\psi^2 + \lambda_\xi^2\sin^2\psi}}, \quad \cos\zeta^* = \frac{\pm\lambda_\psi}{\sqrt{\lambda_\psi^2 + \lambda_\xi^2\sin^2\psi}}. \quad (6.118)$$

Substituting Eq (6.117) for $\lambda_\xi\sin\psi$ into Eq (6.115) yields

$$\beta^* = h\left(\lambda_\psi\tan\zeta^*\sin\zeta^* + \lambda_\psi\cos\zeta^*\right) = h\left(\frac{\lambda_\psi}{\cos\zeta^*}\right) \quad (6.119)$$

It is further necessary that

$$0 \geq \frac{\partial^2 H_E}{\partial\zeta^2} = \beta^*\frac{v_E}{R_E}\left[-\lambda_\xi\sin\psi\sin\zeta^* - \lambda_\psi\cos\zeta^*\right] \equiv -H_E^* \quad (6.120)$$

implying that $H_E^* \geq 0$. The plus (+) sign in Eq (6.118) must be chosen to make Eqs (6.119) and (6.120) compatible. In this case the controls are

$$\beta^* = +1$$

$$\sin\zeta^* = \frac{\lambda_\xi \sin\psi}{\sqrt{\lambda_\psi^2 + \lambda_\xi^2 \sin^2\psi}}, \quad \cos\zeta^* = \frac{\lambda_\psi}{\sqrt{\lambda_\psi^2 + \lambda_\xi^2 \sin^2\psi}} \tag{6.121}$$

with a singular possibility if $\lambda_\xi \sin\zeta \sin\psi + \lambda_\psi \cos\zeta = 0$ for a finite time.

The min H_P conditions are similar to the max H_E conditions yielding

$$\alpha^* = h\left[-(A\cos\tilde{\phi} + B\sin\tilde{\phi})\right] \tag{6.122}$$

with a singular possibility if $A\cos\tilde{\phi} + B\sin\tilde{\phi} = 0$ for a finite time. Now $\frac{\partial H_P}{\partial \tilde{\phi}} = 0$ implies

$$\tan\tilde{\phi}^* = \frac{B}{A} \tag{6.123}$$

or

$$\sin\tilde{\phi} = \frac{\pm B}{\sqrt{A^2 + B^2}}, \quad \cos\tilde{\phi} = \frac{\pm A}{\sqrt{A^2 + B^2}} \tag{6.124}$$

Substituting Eq (6.123) into Eq (6.122) yields

$$\alpha^* = h\left[-\left(\frac{A}{\cos\tilde{\phi}^*}\right)\right] \quad . \tag{6.125}$$

It is also necessary that

$$0 \le \frac{\partial^2 H_p}{\partial \tilde{\phi}^2} \equiv -H_p \quad . \tag{6.126}$$

The minus (- sign in Eq (6.124) makes Eqs (6.125) and (6.126) compatible yielding

$$\alpha^* = +1$$

$$\sin\tilde{\phi}^* = \frac{-B}{\sqrt{A^2+B^2}} \quad , \quad \cos\tilde{\phi}^* = \frac{-A}{\sqrt{A^2+B^2}} \tag{6.127}$$

with a singular possibility if $A\cos\tilde{\phi} + B\sin\tilde{\phi} = 0$ for a finite time.

Appendix B shows that the singular controls are the same as in the 2D model.

Substituting the optimal controls into ME1 yields ME2.

$$-\frac{V_p}{R_p}\sqrt{A^2+B^2} + \frac{V_E}{R_E}\sqrt{\lambda_\psi^2 + \lambda_{\xi_1}^2 \sin^2\psi} + H_o = 0 \tag{6.128}$$

The costate equations are

$$\dot{\underline{\lambda}} = \begin{bmatrix} \dot{\lambda}_\chi \\ \dot{\lambda}_\gamma \\ \dot{\lambda}_\psi \\ \dot{\lambda}_{\xi_1} \end{bmatrix} = \begin{bmatrix} \frac{\lambda_{\xi_1}}{\chi^2}\left(\alpha\frac{V_p}{R_p}\gamma\sin\tilde{\phi} - V_E\sin\psi\sin\xi_1\right) - \alpha\frac{V_p}{R_p}\lambda_\gamma\cos\tilde{\phi} \\ \alpha\frac{V_p}{R_p}\left(\lambda_\chi\cos\tilde{\phi} - \frac{\lambda_{\xi_1}}{\chi}\sin\tilde{\phi}\right) \\ V_E\left(\lambda_\gamma\sin\psi + \frac{\lambda_{\xi_1}}{\chi}\cos\psi\cos\xi_1 - \lambda_\chi\cos\psi\cos\xi_1\right) - \delta\frac{V_E}{R_E}\lambda_{\xi_1}\sin\xi_1\cos\psi \\ V_E\left(\lambda_\chi\sin\psi\sin\xi_1 + \frac{\lambda_{\xi_1}}{\chi}\sin\psi\cos\xi_1\right) - \alpha\frac{V_p}{R_p}\lambda_\psi\sin(\xi_1 - \tilde{\phi}) \end{bmatrix} .$$

The transversality conditions $\sum_{i=1}^{4} \lambda_i \frac{\partial h_i(\xi)}{\partial s_j} = \frac{\partial \phi(\xi)}{\partial s_j} = 0$ yield (6.129)

$$j = 1 \Rightarrow \lambda_x(t_f)\ell\cos s_1 - \lambda_y(t_f)\ell\sin s_1 = 0 \qquad (6.130)$$

$$\text{or} \quad \left.\frac{\lambda_x}{\lambda_y}\right|_{t_f} = \tan s_1$$

$$j = 2 \Rightarrow \lambda_\psi(t_f) = 0 \qquad (6.131)$$

$$j = 3 \Rightarrow \lambda_{z_1}(t_f) = 0 \qquad (6.132)$$

4. Problem Backward Solution From $\mathcal{C}$:

Appendix B contains a major portion of the analysis of the backward solution from $\mathcal{C}$ of which the following is a summary. On the terminal surface $\mathcal{C}$ the controls are

$$\tan\zeta^*(t_f) = \left.\frac{\sin\psi\tan s_1\tan\psi\sin z_1}{\tan\psi - \tan s_1\cos z_1}\right|_{t_f} \qquad (6.133)$$

$$\operatorname{sgn}[\cos\zeta^*(t_f)] = \left.\frac{-\operatorname{sgn}(\cos s_1)\operatorname{sgn}(\sin\psi - \tan s_1\cos\psi\cos z_1)}{\operatorname{sgn}[v_p\cos s_1 - v_E(\cos s_1\cos\psi + \sin s_1\sin\psi\cos z_1)]}\right|_{t_f} \qquad (6.134)$$

$$\tan\tilde{\phi}^*(t_f) = \left.\frac{\cos\psi\cos z_1\sin z_1}{\frac{v_p}{v_E} - \cos\psi\sin^2 z_1}\right|_{t_f} \qquad (6.135)$$

$$\operatorname{sgn}[\cos\tilde{\phi}^*(t_f)] = \left.\frac{\operatorname{sgn}(\sin s_1)\operatorname{sgn}\left(\frac{v_p}{v_E} - \cos\psi\sin^2 z_1\right)}{\operatorname{sgn}[v_p\cos s_1 - v_E(\cos s_1\cos\psi + \sin s_1\sin\psi\cos z_1)]}\right|_{t_f} \qquad (6.136)$$

The singular controls of the present 3D model are the same as the singular cases in the 2D Limited Pursuer-Evader model.

Before proceeding with the backward solution and mapping the controls $\alpha = \phi$, the following two theorems are proved.

Theorem 1: If in the backward solution $z(\tau') = 0$ and $\lambda_z(\tau') = 0$ for some $\tau = \tau'$, then z and λ_z remain zero for $\tau \geq \tau'$ and the problem is planar for $\tau \geq \tau'$.

Proof: $z(\tau') = \lambda_z(\tau') = 0$ and Eq(6.112) $\Rightarrow B(\tau') = 0$ and Eq(6.127) $\Rightarrow$

$\sin\tilde{\phi}(\tau') = 0$, $\cos\tilde{\phi}(\tau') = -\text{sgn}A$. Also Eq (6.121) $\Rightarrow \sin\tilde{\gamma}(\tau') = 0$, $\cos\tilde{\gamma}(\tau') = \text{sgn}\lambda_\psi(\tau')$.

The state Equations (6.103) therefore become

$$\dot{x}(\tau') = V_E \sin\psi + \frac{V_P}{R_P} y \, \text{sgn}A(\tau')$$

$$\dot{y}(\tau') = V_E \cos\psi - V_P - \frac{V_P}{R_P} x \, \text{sgn}A(\tau')$$

$$\dot{\psi}(\tau') = \frac{V_E}{R_E} \text{sgn}\lambda_\psi(\tau') + \frac{V_P}{R_P} \text{sgn}A(\tau')$$

$$\dot{z}(\tau') \equiv 0 \quad .$$

The costate Equations (6.129) become

$$\dot{\lambda}_x(\tau') = \frac{V_P}{R_P} \lambda_y \, \text{sgn}A(\tau')$$

$$\dot{\lambda}_y(\tau') = -\frac{V_P}{R_P} \lambda_x \, \text{sgn}A(\tau')$$

$$\dot{\lambda}_\psi(\tau') = V_E(\lambda_y \sin\psi - \lambda_x \cos\psi)$$

$$\dot{\lambda}_z(\tau') \equiv 0 \quad .$$

Since $\dot{z}(\tau') = \dot{\lambda}_z(\tau') = 0 \Rightarrow z(\tau) = \lambda_z(\tau) = 0$ for $\tau \geq \tau'$ and $\sin\tilde{\phi}^*(\tau) = 0$, $\cos\tilde{\phi}^*(\tau) = -\operatorname{sgn} A(\tau)$, $\sin\zeta^*(\tau) = 0$, $\cos\zeta^*(\tau) = \operatorname{sgn}\lambda_\psi(\tau)$ for $\tau \geq \tau'$.

As such, the above state and costate equations are identical in form to the state and costate equations (i.e. Eqs (6.1) and (6.22) of the 2D Limited Pursuer-Evader model. ∎

Theorem 2: Let $z^+|_{t_f} = |z|$ and let $x^+(\tau)$, $y^+(\tau)$, $\psi^+(\tau)$, $z^+(\tau)$, $\tilde{\phi}^+(\tau)$, $\zeta^+(\tau)$ represent the backward solution for $z^+|_{t_f}$. Furthermore let $z^-|_{t_f} = -|z|$ and let $x^-(\tau)$, $y^-(\tau)$, $\psi^-(\tau)$, $z^-(\tau)$, $\tilde{\phi}^-(\tau)$, $\zeta^-(\tau)$ represent the backward solution for $z^-|_{t_f}$. Then $x^-(\tau) = x^+(\tau)$, $y^-(\tau) = y^+(\tau)$, $\psi^-(\tau) = \psi^+(\tau)$, $z^-(\tau) = -z^+(\tau)$, $\tilde{\phi}^-(\tau) = -\tilde{\phi}^+(\tau)$ and $\zeta^-(\tau) = -\zeta^+(\tau)$.

Proof: Eq (6.103) shows that $\dot{x}$, $\dot{y}$ and $\dot{\psi}$ remain unchanged provided $\cos\tilde{\phi}$, $\cos z$, $\cos\zeta$ and $\cos(z - \tilde{\phi})$ remain unchanged. Eq (6.103) shows that $\dot{z}$ will change sign if $\sin\zeta$, $\sin z$, and $\sin\tilde{\phi}$ change sign. Eq (6.121) shows that the above conditions on $\sin\zeta$ and $\cos\zeta$ will hold provided λ_ψ is unchanged and λ_z changes sign. Eqs (6.111), (6.112) and (6.127) show that the above conditions on $\sin\tilde{\phi}$ and $\cos\tilde{\phi}$ will hold provided λ_y, and λ_ψ remain unchanged and λ_z changes sign. Eq (6.129) shows that under the above conditions $\dot{\lambda}_x$, $\dot{\lambda}_y$ and $\dot{\lambda}_\psi$ remain unchanged and $\dot{\lambda}_z$ changes sign. As such, all the above conditions are met and the backward trajectory z symmetry as stated, is proved. ∎ We now continue with the backward solution and map the controls on ζ.

Eqs (6.133), (6.134), (6.135) and (6.136) define the optimal controls $\tilde{\phi}^*$ and $\tilde{\gamma}^*$ on $\mathcal{C}$. In the denominator of Eqs (6.134) and (6.136) the term

$$\dot{r}|_{t_f} \equiv V_p \cos s_1 - V_E (\cos s_1 \cos\psi + \sin s_1 \sin\psi \cos\chi_1)\Big|_{t_f} \tag{6.137}$$

appears. It will be shown later that $\dot{r}|_{t_f} > 0$ defines the UP of $\mathcal{C}$, $\dot{r}|_{t_f} < 0$ defines the NUP of $\mathcal{C}$, and $\dot{r}|_{t_f} = 0$ defines the BUP on $\mathcal{C}$. Therefore, on the UP of $\mathcal{C}$ Eqs (6.133), (6.134), (6.135) and (6.136) become (note that for $\frac{V_p}{V_E} > 1$, $\frac{V_p}{V_E} > \cos\psi \sin^2\chi_1$)

$$\tan\tilde{\phi}^*(t_f) = \frac{\cos\psi \cos\chi_1 \sin\chi}{\frac{V_p}{V_E} - \cos\psi \sin^2\chi_1}\Bigg|_{t_f} \tag{6.138}$$

$$\operatorname{sgn}[\cos\tilde{\phi}^*(t_f)] = \operatorname{sgn}(\sin s_1) \tag{6.139}$$

$$\tan\gamma^*(t_f) = \frac{\tan s_1 \sin^2\psi \sin\chi}{\sin\psi - \tan s_1 \cos\psi \cos\chi}\Bigg|_{t_f} \tag{6.140}$$

$$\operatorname{sgn}[\cos\gamma^*(t_f)] = -\operatorname{sgn}(\cos s_1)\operatorname{sgn}(\sin\psi - \tan s_1 \cos\psi \cos\chi)\Big|_{t_f} . \tag{6.141}$$

Another expression for $\tan\tilde{\phi}^*(t_f)$ can be obtained by subtracting $\tan\chi_1$ from both sides of Eq (6.138) i.e.

$$\tan\tilde{\phi}^*(t_f) = \tan\chi_1 \left(1 - \frac{\frac{V_p}{V_E} - \cos\psi}{\frac{V_p}{V_E} - \cos\psi \sin^2\chi_1}\right)\Bigg|_{t_f} . \tag{6.142}$$

Eq (6.142) shows that on ζ , $\tilde{\phi}$ lags ζ_1 . For small ζ_1 Eq (6.142) can be approximated by

$$\tan\tilde{\phi}^*(t_f) \simeq \tan\zeta_1\left[\frac{V_E}{V_P}\cos\psi\right]\Big|_{t_f} \qquad (6.143)$$

or even more crudely by

$$\tilde{\phi}^*(t_f) \simeq \zeta_1\frac{V_E}{V_P}\cos\psi\Big|_{t_f} . \qquad (6.144)$$

For small ζ_1 (i.e. 0 - 10°), $\frac{V_E}{V_P} \simeq .9$

and $|\psi| < 25°$, Eq (6.144) implies $\tilde{\phi}^*(t_f) \simeq .8\,\zeta_1(t_f)$.

For a given $\frac{V_P}{V_E}$, S_1 , and ζ_1 , Eq (6.137) equated to zero defines the BUP and is quadratic in $\sin\psi$ yielding

$$\sin\psi_{1,2} = \frac{\frac{V_P}{V_E}\tan s_1\cos\zeta_1 \pm \sqrt{\tan^2 s_1\cos^2\zeta_1 - \left[\left(\frac{V_P}{V_E}\right)^2 - 1\right]}}{1 + \tan^2 s_1\cos^2\zeta_1} \qquad (6.145)$$

The two ψ_1 , ψ_2 solutions on the BUP exist provided the radical is real i.e.

$$\tan^2 s_1 < \frac{\left(\frac{V_P}{V_E}\right)^2 - 1}{\cos^2\zeta_1} . \qquad (6.146)$$

It will be shown later that the controls on the BUP have the same form as Eqs (6.138) - (6.141); however, because Eq (6.137) equated to zero holds on the BUP, $\frac{V_p}{V_e}$ can be eliminated from Eq (6.138) yielding

$$\tan \tilde{\phi}(t_f)\Big|_{BUP} = \frac{\sin \chi}{\tan s_1 \tan \psi + \cos \chi}\Bigg|_{BUP} \quad (6.147)$$

An expression for $\tan(\tilde{\phi}-\chi)\big|_{BUP}$ can also be derived and is

$$\tan(\tilde{\phi}-\chi)\Big|_{BUP} = \frac{-\sin\chi \tan s_1 \tan\psi}{1+\cos\chi \tan s_1 \tan\psi}\Bigg|_{BUP} \quad (6.148)$$

Note again that $\tilde{\phi}$ lags χ and for small χ that $\tilde{\phi}\big|_{BUP} \simeq \chi\big|_{\zeta}$.

A computer program was written to compute the BUP and map the UP of ζ and the BUP with the optimal controls. Results of a typical computation are shown in Figures 29 and 30.

Figure 29 is a plot of the BUP (in the area of ζ of practical interest) for $\frac{V_e}{V_p}$=.9 and χ = 30°. The dashed line is the BUP for χ = 0°. Note that the χ effect is to increase the area of the UP of ζ ; however, even for a χ of 30 degrees the effect is small.

Figure 30 is an enlarged portion of an area of Figure 29 of practical interest. On the ψ axis is plotted $\tilde{\phi}^*(t_f)$ and $\tilde{\phi}^*-\chi\big|_{t_f}$ As can be seen from Eq (6.138), for a given χ and $\frac{V_p}{V_e}$, $\tilde{\phi}^*(t_f)$ is only a function of $\psi(t_f)$. Note that, as suggested by Eqs (6.142) - (6.144), $\tilde{\phi}^*(t_f)$ slightly lags χ. There are two numbers plotted at each (s_1 , ψ) coordinate in the UP of ζ. The uncircled number is $\chi^*(t_f)$ which is measured from the χ plane. Note that $\chi^*(t_f)$ very slightly

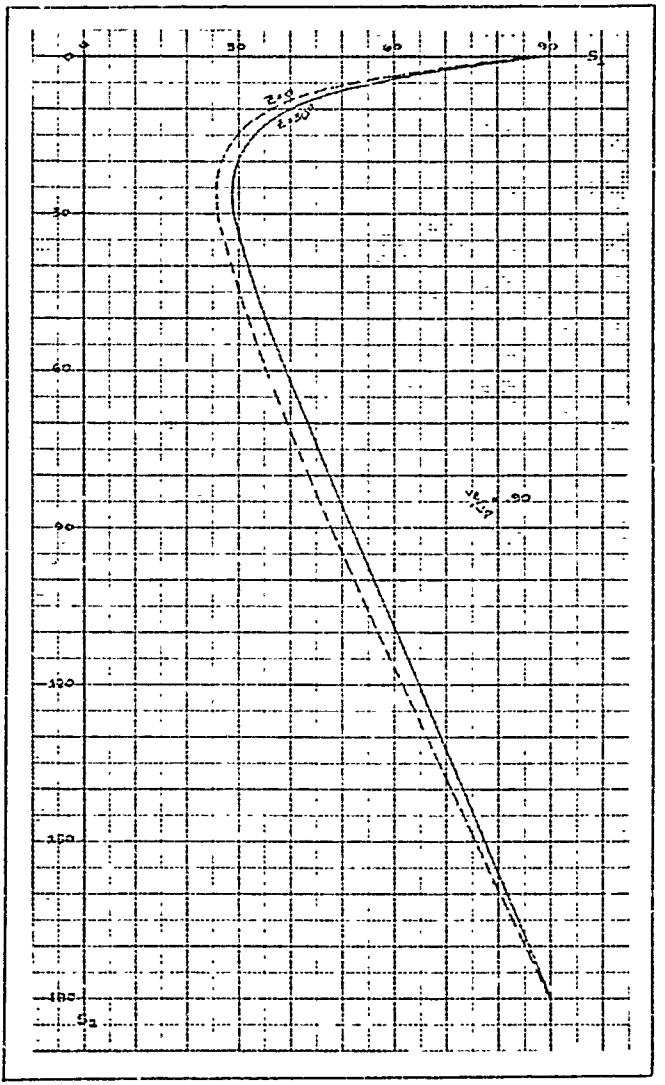

Figure 29: Z Effects on BUP

lags ζ_1 . The circled number is $\zeta^*(t_f) - [\tilde{\Phi}^*(t_f) - \zeta_1]$.

This latter number is small, implying that P and E are banking and pulling gs in approximately the same direction i.e. a direction that slightly lags ζ_1 . These results are suggesting the following approximate 3D control logic at termination:

1) P should bank towards E slightly lagging the relative clock angle direction in which E is going.

2) E should bank very slightly lagging the plane defined by the coincident velocity vectors.

Note if both P and E play this pseudo optimal terminal strategy, their wings will be approximately parallel i.e. P will be banked just slightly to the right of E.

To see if the above approximate 3D control logic applies, not only at termination, but also along the backward trajectories, the highly coupled, non-linear state and costate equations must be numerically integrated backwards. Since it will be necessary to do this also for the BUP, the Barrier necessary conditions are developed first.

5. Barrier Necessary Conditions:

As was done with the other models, we first examine ζ and determine the UP, NUP, and BUP.

Define $\underline{v}|_{\zeta}$ as

$$\underline{v}|_{\zeta} = \begin{bmatrix} v_x \\ v_y \\ v_\psi \\ v_{z_1} \end{bmatrix} \equiv \begin{bmatrix} v_1 \\ v_2 \\ v_3 \\ v_4 \end{bmatrix} \tag{6.149}$$

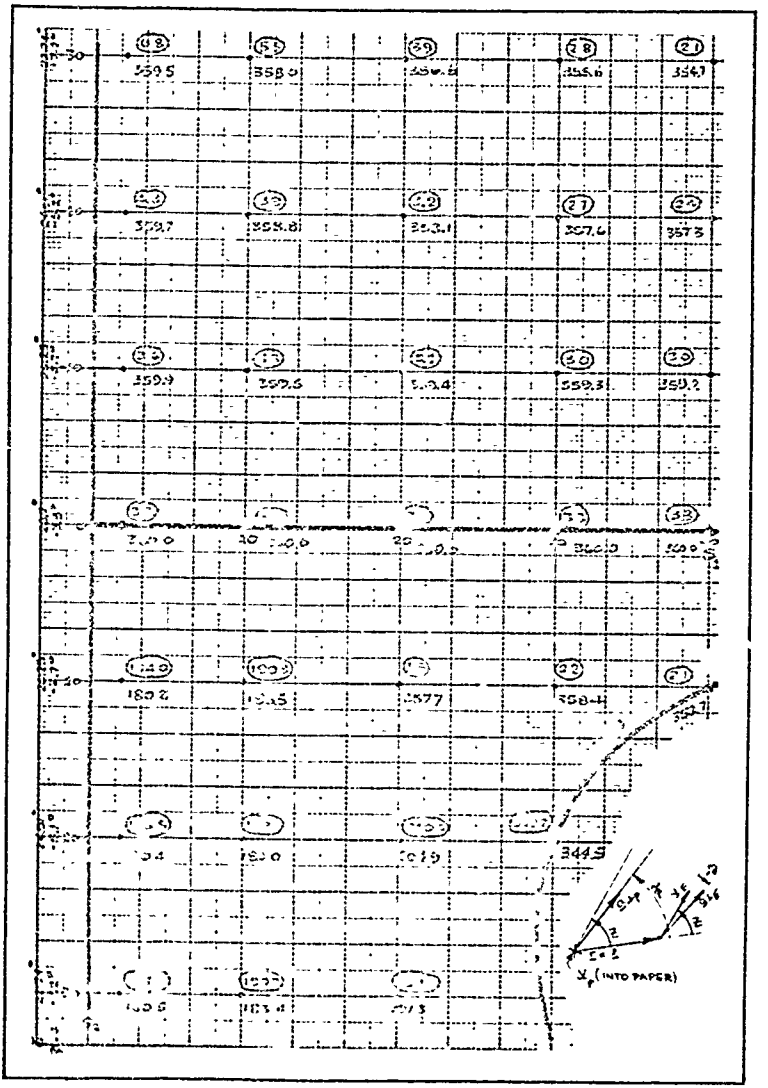

Figure 30: ζ Controls, $\frac{V_E}{V_p} = .9$, $\Sigma = 30°$

The normality conditions of $\underline{\upsilon}$ on $\mathcal{C}$, $\sum_{i=1}^{4} \upsilon_i \frac{\partial h_i(\underline{s})}{\partial s_j} = 0$, $j = 1,2,3$ yield for

$$j = 1 \Rightarrow \upsilon_x(t_f)\cos s_1 - \upsilon_y(t_f)\sin s_1 = 0 \tag{6.150}$$

$$j = 2 \Rightarrow \upsilon_\psi(t_f) = 0 \tag{6.151}$$

$$j = 3 \Rightarrow \upsilon_z(t_f) = 0 \tag{6.152}$$

The unit vector condition implies

$$\left(\upsilon_x^2 + \upsilon_y^2 + \upsilon_\psi^2 + \upsilon_z^2\right)\Big|_{t_f} = 1 \tag{6.153}$$

Substituting Eqs (6.151), (6.152) and Eq (6.150) for $\upsilon_x(t_f)$ into Eq (6.153) yields

$$\upsilon_y(t_f) = \cos s_1 \tag{6.154}$$

Substituting Eq (6.154) into Eq (6.150) yields

$$\upsilon_x(t_f) = \sin s_1 \tag{6.155}$$

Expression (2.28) becomes

$$\min_{\underline{\upsilon}} \max_{\underline{\nu}} \underline{\upsilon}^T \underline{f}\Big|_{\mathcal{C}} = \min_{(\tilde{\Phi},\alpha)} \max_{(\beta,\beta)} \Big\{ \upsilon_x \Big[V_E \sin\psi\cos\chi_1 - \alpha \frac{V_p}{R_p} Y \cos\tilde{\Phi} \Big] +$$

$$+ \upsilon_y \Big[V_E \cos\psi - V_p + \alpha \frac{V_p}{R_p} X \cos\tilde{\Phi} \Big] +$$

$$+ \upsilon_\psi \Big[\beta \frac{V_E}{R_E} \cos\beta - \alpha \frac{V_p}{R_p} \cos(\chi_1 - \tilde{\Phi}) \Big] +$$

$$+v_z\left[\beta\frac{V_E}{R_E}\sin\zeta\sin\psi+\frac{1}{\chi}\left(\alpha\frac{V_P}{R_P}\gamma\sin\tilde{\phi}-V_E\sin\psi\sin\tilde{\zeta}\right)\right]\Bigg\}\equiv$$

$$\equiv \min_{(\tilde{\phi},\alpha)}\tilde{H}_P+\max_{(\tilde{\zeta},\beta)}\tilde{H}_E+H_o \qquad (6.156)$$

where

$$\tilde{H}_P=\alpha\frac{V_P}{R_P}\left[\tilde{A}\cos\tilde{\phi}+\tilde{B}\sin\tilde{\phi}\right] \qquad (6.157)$$

$$\tilde{A}=\chi v_y-\gamma v_x-v_\psi\cos\tilde{\zeta} \qquad (6.158)$$

$$\tilde{B}=\frac{\gamma}{\chi}v_z-v_\psi\sin\tilde{\zeta} \qquad (6.159)$$

$$\tilde{H}_E=\beta\frac{V_E}{R_E}\left[v_z\sin\zeta\sin\psi+v_\psi\cos\zeta\right] \qquad (6.160)$$

$$\tilde{H}_o=-V_P v_y+V_E\left[v_x\sin\psi\cos\tilde{\zeta}+v_y\cos\psi-\frac{v_z}{\chi}\sin\psi\sin\tilde{\zeta}\right] \qquad (6.161)$$

The similarity of Eqs (6.156) - (6.161) with those of Eqs (6.109) - (6.114) is readily apparent. Therefore, using the results of section 3, it is seen that the Barrier controls are

$$\tilde{\alpha}^*=+1 \qquad (6.162)$$

$$\sin\tilde{\phi}^*=\frac{-\tilde{B}}{\sqrt{\tilde{A}^2+\tilde{B}^2}}\quad,\quad \cos\tilde{\phi}^*=\frac{-\tilde{A}}{\sqrt{\tilde{A}^2+\tilde{B}^2}}$$

with a singular possibility if $\tilde{A}\cos\tilde{\phi}+\tilde{B}\sin\tilde{\phi}=0$ and

$$\tilde{\beta}^*=+1 \qquad (6.163)$$

$$\sin\tilde{\zeta}^*=\frac{v_z\sin\psi}{\sqrt{v_\psi^2+v_z^2\sin^2\psi}}\quad,\quad \cos\tilde{\zeta}^*=\frac{v_\psi}{\sqrt{v_\psi^2+v_z^2\sin^2\psi}}$$

with a singular possibility if $v_z\sin\zeta\sin\psi+v_\psi\cos\zeta=0$.

Substituting Eqs (6.162) and (6.163) into Eq (6.156) and evaluating Eq (6.156) on $\mathcal{C}_\ell$ yields

$$\min_{\underline{u}}\max_{\underline{v}}\underline{v}^T\underline{\dot{x}}\Big|_{\mathcal{C}_\ell}=\tilde{H}_o\Big|_{\mathcal{C}_\ell}=\Big[-V_P\cos s_1+ \qquad (6.164)$$

$$+V_E\left(\sin s_1\sin\psi\cos\tilde{\zeta}+\cos s_1\cos\psi\right)\Big]\Big|_{\mathcal{C}_\ell}.$$

Eq (6.164) implies that if

$$\begin{aligned}
&1)\ \tilde{H}_o\big|_{\zeta_e} < 0 \text{ then } \{s_1, \psi, z\}\big|_{\zeta_e} \in \text{UP of } \zeta_e \\
&2)\ \tilde{H}_o\big|_{\zeta_e} = 0 \text{ then } \{s_1, \psi, z\}\big|_{\zeta_e} \in \text{BUP of } \zeta_e \qquad (6.165) \\
&3)\ \tilde{H}_o\big|_{\zeta_e} > 0 \text{ then } \{s_1, \psi, z\}\big|_{\zeta_e} \in \text{NUP of } \zeta_e \ .
\end{aligned}$$

Note that Eq (6.165) is in agreement with the previously assumed Eq (6.137).

The costate equations for the Barrier are

$$\underline{\dot{v}} = \begin{bmatrix} \dot{v}_x \\ \dot{v}_y \\ \dot{v}_\psi \\ \dot{v}_z \end{bmatrix} = \begin{bmatrix} \frac{v_z}{\chi^2}\left(\tilde{\alpha}\frac{v_p}{R_p}\gamma \sin\tilde{\tilde{\phi}} - V_E \sin\psi \sin\zeta\right) - \tilde{\alpha}\frac{v_p}{R_p} v_y \cos\tilde{\tilde{\phi}} \\ \tilde{\alpha}\frac{v_p}{R_p}\left(v_x \cos\tilde{\tilde{\phi}} - \frac{v_z}{\chi}\sin\tilde{\tilde{\phi}}\right) \\ V_E\left(v_y \sin\psi + \frac{v_z}{\chi}\cos\psi\sin\zeta - v_x \cos\psi\cos\zeta\right) - \tilde{\beta}\frac{v_E}{R_e} v_z \sin\tilde{\gamma}\cos\psi \\ V_E\left(v_x \sin\psi\sin\zeta + \frac{v_z}{\chi}\sin\psi\cos\zeta\right) - \tilde{\alpha}\frac{v_p}{R_p} v_\psi \sin(\zeta - \tilde{\tilde{\phi}}) \end{bmatrix} . \qquad (6.166)$$

As was pointed out in the other models, there is a direct similarity between the form of the necessary conditons for the UP of ζ_e and the form of the necessary condition for the Barrier - the only real difference being the initial values of the state and costate variables in each case. With this similarity of the necessary conditions recognized, we now return to the numerical integration of the state and costate necessary conditions backward from the UP and BUP of ζ_e .

6. Backward Trajectories from $\mathcal{C}$:

To exhibit the ratios $\frac{V_E}{V_P}$, $\frac{\dot{\theta}_E}{\dot{\theta}_P}$, $\frac{x}{R_P}$, $\frac{y}{R_P}$ etc., the state and costate equations were rearranged into a new form. The new states and costates are $\frac{x}{V_P}$, $\frac{y}{V_P}$, $\frac{\psi}{\dot{\theta}_P}$, $\frac{z_1}{\dot{\theta}_P}$, λ_x , λ_y , $\frac{\lambda_\psi}{R_P}$ and $\frac{\lambda_{z_1}}{R_P}$. Note that the new states have dimensions, seconds, and the new costates have dimension, ft/second. Also note that

$$\frac{x}{R_P} = \frac{x}{V_P}\dot{\theta}_P \quad , \quad \psi = \frac{\psi}{\dot{\theta}_P}\dot{\theta}_P \qquad (6.167)$$

$$\frac{y}{R_P} = \frac{y}{V_P}\dot{\theta}_P \quad , \quad z_1 = \frac{z_1}{\dot{\theta}_P}\dot{\theta}_P \; .$$

The new state equations become

$$\left(\frac{\dot{x}}{V_P}\right) = \frac{V_E}{V_P}\sin\psi\cos z_1 - \alpha\,\dot{\theta}_P\left(\frac{y}{V_P}\right)\cos\tilde{\phi}$$

$$\left(\frac{\dot{y}}{V_P}\right) = \frac{V_E}{V_P}\cos\psi - 1 + \alpha\,\dot{\theta}_P\left(\frac{x}{V_P}\right)\cos\tilde{\phi}$$

$$\left(\frac{\dot{\psi}}{\dot{\theta}_P}\right) = \beta\frac{\dot{\theta}_E}{\dot{\theta}_P}\cos\gamma - \alpha\cos(\tilde{\phi} - z_1)$$

$$\left(\frac{\dot{z}_1}{\dot{\theta}_P}\right) = \beta\frac{\dot{\theta}_E}{\dot{\theta}_P}\sin\gamma\sin\psi + \alpha\frac{\left(\frac{V}{V_P}\right)}{\left(\frac{x}{V_P}\right)}\sin\tilde{\phi} + \qquad (6.168)$$

$$- \frac{\left(\frac{V_E}{V_P}\right)}{\dot{\theta}_P\left(\frac{x}{V_P}\right)}\sin\psi\sin z_1 \; .$$

The boundary conditions for the new state equations are

$$\left.\frac{x}{V_p}\right|_{t_f} = \frac{1}{\dot{\theta}_p}\left(\frac{l}{R_p}\right)\sin s_1$$

$$\left.\frac{y}{V_p}\right|_{t_f} = \frac{1}{\dot{\theta}_p}\left(\frac{l}{R_p}\right)\cos s_1$$

$$\left.\frac{\psi}{\dot{\theta}_p}\right|_{t_f} = \frac{\psi(t_f)}{\dot{\theta}_p} = \frac{s_2}{\dot{\theta}_p}$$

$$\left.\frac{z_1}{\dot{\theta}_p}\right|_{t_f} = \frac{z(t_f)}{\dot{\theta}_p} = \frac{s_3}{\dot{\theta}_p} \qquad (6.169)$$

In the case of the Barrier, the state equations are the same as Eq (6.168) and the boundary conditions are the same as Eq (6.169) except that s_1, s_2 and s_3 are on the BUP.

The new costate equations become

$$\dot{\lambda}_x = \frac{\left(\frac{\lambda_{z_1}}{R_p}\right)}{\left(\frac{x}{V_p}\right)^2}\left[\alpha\left(\frac{y}{V_p}\right)\sin\tilde{\phi} - \frac{V_E/V_p}{\dot{\theta}_p}\sin\psi\sin z_1\right] - \alpha\dot{\theta}_p\lambda_y\cos\tilde{\phi}$$

$$\dot{\lambda}_y = \alpha\left[\dot{\theta}_p\lambda_x\cos\tilde{\phi} - \frac{\left(\lambda_{z_1}/R_p\right)}{\left(x/V_p\right)}\sin\tilde{\phi}\right]$$

$$\left(\frac{\dot{\lambda}_\psi}{R_p}\right) = \frac{V_E}{V_p}\left[\dot{\theta}_p\left(\lambda_y\sin\psi - \lambda_x\cos\psi\cos z_1\right) + \frac{\left(\frac{\lambda_{z_1}}{R_p}\right)}{\left(x/V_p\right)}\cos\psi\sin z_1\right] +$$
$$- \beta\dot{\theta}_E\left(\frac{\lambda_{z_1}}{R_p}\right)\sin z_2\cos\psi$$

$$\left(\frac{\dot{\lambda}_{z_1}}{R_f}\right) = \frac{V_E}{V_p}\left[\dot{\theta}_p\lambda_x\sin\psi\sin z_1 + \frac{\left(\frac{\lambda_{z_1}}{R_p}\right)}{\left(\frac{x}{V_p}\right)}\sin\psi\cos z_1\right] + \qquad (6.170)$$
$$+ \alpha\dot{\theta}_p\left(\frac{\lambda_\psi}{R_p}\right)\sin(\tilde{\phi} - z_1)$$

In the case of the Barrier, the λ_i in Eq (6.170) simply become the σ_i. The boundary conditions on the new costate variables are

$$\lambda_x(t_f) = \frac{\sin S_1}{V_P\left(\frac{\dot{r}}{V_P}\right)\Big|_{t_f}}$$

$$\lambda_y(t_f) = \frac{\cos S_1}{V_P\left(\frac{\dot{r}}{V_P}\right)\Big|_{t_f}}$$

$$\left(\frac{\lambda_\psi}{R_P}\right)\Big|_{t_f} = \left(\frac{\lambda_z}{R_P}\right)\Big|_{t_f} = 0 \qquad (6.171)$$

where

$$\frac{\dot{r}}{V_P}\Big|_{t_f} = \cos S_1 - \frac{V_E}{V_P}\left(\cos S_1 \cos\psi + \sin S_1 \sin\psi \cos\xi\right)\Big|_{t_f}.$$

The boundary conditions on the Barrier costate variables are

$$\sigma_x(t_f) = \sin S_1$$

$$\sigma_y(t_f) = \cos S_1$$

$$\frac{\sigma_\psi(t_f)}{R_P} = 0 \qquad (6.172)$$

$$\frac{\sigma_z(t_f)}{R_P} = 0$$

where S_1 is on the BUP.

The optimal controls take the form

$$\sin\zeta^* = \frac{(\lambda_\zeta/R_p)\sin\psi}{\sqrt{\left(\frac{\lambda_\psi}{R_p}\right)^2+\left(\frac{\lambda_\zeta}{R_p}\right)^2\sin^2\psi}}$$

$$\cos\zeta^* = \frac{(\lambda_\psi/R_p)}{\sqrt{\left(\frac{\lambda_\psi}{R_p}\right)^2+\left(\frac{\lambda_\zeta}{R_p}\right)^2\sin^2\psi}}$$

$$\sin\tilde{\phi}^* = \frac{-B/R_p}{\sqrt{(A/R_p)^2+(B/R_p)^2}}$$

$$\cos\tilde{\phi}^* = \frac{-A/R_p}{\sqrt{(A/R_p)^2+(B/R_p)^2}}$$

where

$$\frac{A}{R_p} = \dot{\epsilon}_p\left[\left(\frac{x}{V_p}\right)\lambda_y - \left(\frac{y}{V_p}\right)\lambda_x\right] - \left(\frac{\lambda_\psi}{R_p}\right)\cos\zeta,$$

$$\frac{B}{R_p} = \frac{(y/V_p)}{(x/V_p)}\left(\frac{\lambda_\zeta}{R_p}\right) - \left(\frac{\lambda_\psi}{R_p}\right)\sin\zeta \quad . \qquad (6.173)$$

In the case of the Barrier, the optimal controls have the same form as Eq (6.173) except the λ_i are replaced with the σ_i .

To check the optimality of the backward numerical integration, the numerical value of ME2 and pseudo ME2 can be computed and checked against the zero optimal value i.e.

$$\left.\frac{H}{R_P}\right|_{ME2} = -\dot{\Theta}_P\left(\frac{A}{R_P}\right)^2+\left(\frac{B}{R_P}\right)^2 + \dot{\Theta}_E\left(\frac{\lambda_\psi}{R_P}\right)^2+\left(\frac{\lambda_\zeta}{R_P}\right)^2\sin^2\psi - \dot{\Theta}_P\lambda_\gamma +$$
$$+\frac{V_E}{V_P}\dot{\Theta}_P\left[\lambda_x\sin\psi\cos\zeta+\lambda_y\cos\psi\right]-\frac{V_E}{V_P}\frac{\left(\frac{\lambda_\zeta}{R_P}\right)}{\left(\frac{\chi}{V_P}\right)}\sin\psi\sin\zeta + \frac{1}{R_P} \quad (6/174)$$

The value for $\left.\frac{H}{R_P}\right|_{\substack{\text{pseudo}\\ME2}}$ has the same form as Eq (6.174) except the $\frac{1}{R_P}$ term is dropped.

The player parameters required to define the new state and costate equation are $\frac{V_E}{V_P}$, $\dot{\Theta}_P$ and $\frac{\dot{\Theta}_E}{\dot{\Theta}_P}$. The player parameter required for the new state boundary conditions is $\frac{\ell}{R_P}$. Note that it does not take a player parameter to define the costate boundary conditions, Eq (6.172), for the Barrier. Therefore, in the five dimensional vector space $\left\{V_E, V_P, \dot{\Theta}_P, \dot{\Theta}_E, \ell\right\}$ the parameters $\frac{V_E}{V_P}$, $\dot{\epsilon}_P$, $\frac{\dot{\Theta}_E}{\dot{\Theta}_P}$, $\frac{\ell}{R_P}$ form a vector subspace of one (1) dimension i.e. a given Barrier trajectory in the new state-costate system will correspond to a family of Barrier trajectories in the original state-costate system. However, the costate boundary conditions for the UP of ζ_ℓ, Eq (6.171), requires the added player parameter V_P which makes each trajectory from the UP in the new state-costate system, corresponds to only one (1) trajectory in the original state-costate system.

A computer program was written to solve the new state-costate equations backward from the UP and BUP of $\mathcal{C}$. A fixed step Runge-Kutta integration technique was used to numerically integrate the differential equations.

To demonstrate the results of Theorem 1 and to provide a check on the program, a Barrier computation for $\zeta_1 = 0$ was done for which the closed form solution is known i.e. a Limited Pursuer-Evader model case. The specific parameters used were $V_E/V_P = .95$, $\dot{\Theta}_P = .2$ rad/sec, $\dot{\Theta}_E/\dot{\Theta}_P = 1.25$ and $\ell/R_P = .25$.

A fixed step of .1 second was used in the numerical integration. ζ_1 remained on the order of 10^{-4}deg and $\frac{U_{\zeta_1}}{R_P}$ remained on the order of 5. x 10^{-6} sec. $\tilde{\Phi}$ and $\tilde{\zeta}$ were on the order of 1. x 10^{-4}degrees. Had the numerical integration been performed exactly, these variables would have been exactly zero. These results demonstrate Theorem 1 and provide a check on the computer program. Non-zero ζ_1 trajectories were then examined.

Figure 31 shows sample control history results for trajectories backward from the BUP. Three specific cases are shown: $z_1(t_f) = 1°$, $z_1(t_f) = 15°$, $z_1(t_f) = 30°$. The parameters for the problem are the same as in the $z_1(t_f) = 0$ case previously discussed. In each case $z_1(\tau)$, $\tilde{\phi}(\tau)$ and $z_1(\tau) + \tilde{\gamma}(\tau)$ are plotted. All these trajectories exhibited the trend to graze ζ and go to the right and back of ζ. The trajectories were terminated around T=10 seconds as $\frac{V}{R_p}$ is negative (i.e. for large negative $\frac{V}{R_p}$ the present fixed evader roll probably does not apply). In each case the following trends are noted:

1) $z_1(\tau)$ is reducing to zero and appears to be doing so asymptotically.

2) $\tilde{\phi}(\tau)$ slightly lags $z_1(\tau)$

3) $\tilde{\gamma}(\tau)$ very slightly lags $z_1(\tau)$

It is important to note that the approximate 3D control logic that exists on ζ continues for the backward trajectory. Here it can be seen how the reduced space concept has greatly helped the characterization of the 3D controls that would otherwise be extremely difficult in the 10D realistic space.

Because these trajectories (including the $z_1(t_f) = 0$ case) exhibited the trend to immediately go to the right and behind ζ, an attempt was made at changing the system parameters to make the $z_1 \neq 0$ Barrier trajectories go in a direction more forward of ζ into an area of ξ having more practical interest. These attempts were not very successful. The 2D Limited Pursuer-Evader model also exhibited this characteristic

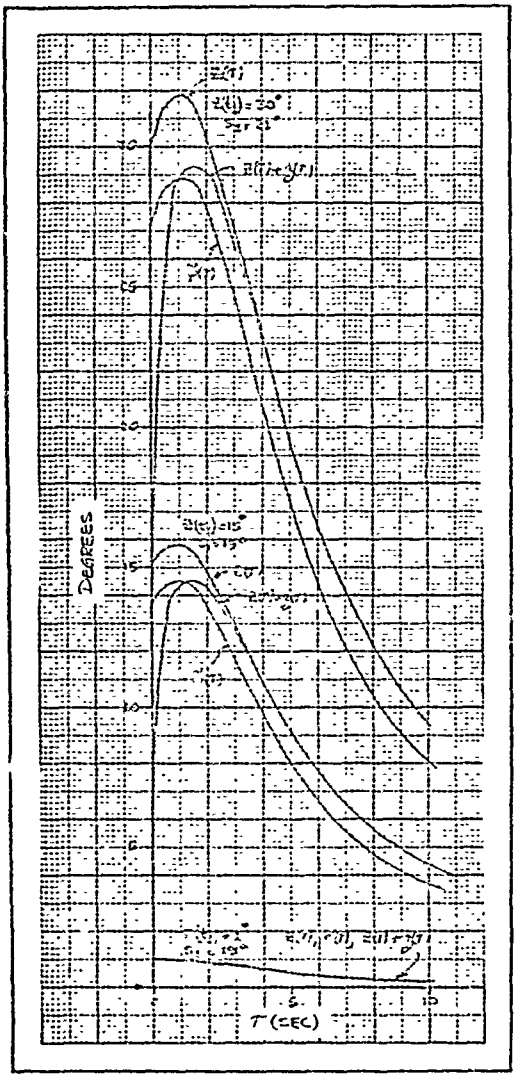

Figure 31: Control Histories

for non-singular trajectories. Figures 26 and 27 show that below the dashed line (i.e. non-singular cases) the $\frac{V}{R_p}$ values are small. Those Barrier trajectories in the 2D model that go forward of ζ into an area of interest, branch off the E-singular surface. It was therefore concluded that, as with the 2D model, to get the Barrier trajectories to go in a forward direction of ζ for the 3D model, the singular surfaces in the 3D model had to be used immediately from ζ followed by a possible branching off the singular surface later on. Note, however, that the singular surfaces in the 3D model are the singular surfaces in the 2D model. Since the singular surfaces are the same, it can be seen that the parametric relationships of real importance in the 3D model (i.e. that determine the interesting conditions of escape and that should be used for sensitivity studies) are already those parametric relationships found for the 2D model. We are, however, still interested in how the non-zero $\frac{h}{z}$ trajectories branch off the planar singular cases for two reasons: to see how a non-zero $\frac{h}{z}$ case migrates to the planar case of real parametric interest; to see what 3D control logic is used in migrating to the planar case. An impasse was met at this point; for based on Theorem 1, it is impossible to branch off the planar singular case to a non-planar (i.e. $\zeta \neq 0$) case. The reason for this problem is in part associated with the following theorem:

Theorem 3: If λ_ζ and ζ are approaching zero simultaneously to meet the conditions of Theorem 1, then they approach zero asymptotically.

Proof: Since $\lambda_{z_1} \to 0$ and $z_1 \to 0$, Eq (6.112) $\Rightarrow B \to 0$. Together with Eqs (6.121) and (6.127) this implies $\sin\gamma^* \to 0$ and $\sin\Phi^* \to 0$. Based on this, Eq (6.103) and (6.129) show $\dot{z}_1 \to 0$ and $\dot{\lambda}_{z_1} \to 0$. ∎

Isaacs [7, 133] alludes to the possible existence of a singular surface made up by the limit of parallel trajectories. He calls this kind of singular surface a (P, U, P) singular surface. Based on Theorem 3, the planar singular case in the present 3D model appears to be a specific case of a (P, U, P) singular surface. The problem of investigating these parallel trajectories close to the planar singular case (note Williamson-Nobel [15] also alluded to problems in this area) is left to other investigators as they are not the main intent of this dissertation and appear to require considerable examination.

7. Model and Barrier Conclusions

1) In the 3D model, the parametric relationships of real importance that determine the escape conditions are those found in the 2D model.

2) For those terminal conditions having non-zero $z_1(t_f)$, an approximate 3D closed form control logic has been found.

VII. Application of the Limited Pursuer-Evader Model

This chapter discusses the practical application of the Barrier results of Chapter VI to the same problem addressed in Chapter V i.e. the relative evaluation of fighter A/C capability. This method is the original work of the author and represents a more "realistic" (to that of Chapter V) practical application of differential game theory to the above problem. The method is more "realistic" in the sense that the Evader is no longer highly maneuverable and that the parameter relationships for escape involve another important variable - the turning gs of the Evader. The method is being developed into a computer program by the Air Force Flight Dynamics Laboratory as an analysis tool to evaluate the relative combat capability of fighter aircraft. The purpose of this chapter is to outline the method and the computational procedures.

Results of the Limited Pursuer-Evader Model

Results of the 3D Limited Pursuer-Evader showed that parametric relationships of real importance in the 3D model (i.e. that determine the interesting conditions of escape and that should be used for sensitivity studies) were those found in the 2D Limited Pursuer-Evader. These 2D results are contained in Figures 26 and 27. These figures, under the assumptions of the Limited Pursuer-Evader model, optimally reveal how the turning gs , velocities, and relative positions of the two aircraft and the gun capability of the Pursuer affect the outcome of a given terminal combat engagement. Sensitivity analysis of these

results continued to show that the ratio of combat velocities, V_E/V_P, was the most important parameter. The sensitivity analysis, along with Figures 26 and 27, yielded logics for improving both aircraft systems - the logic with the most payoff was to increase V_E and V_P.

Methods and Computational Procedure

The method compares each aircraft in the evaluation against a standard Pursuer. The Pursuer is standardized by selecting fixed values for the weapons capability, ℓ, tracking gs, $a_{\perp p}$, and specific power map $P_s(M^*, h)$. A realistic ratio of combat velocities V_E/V_P (i.e. like .9 etc) is picked for the method. For a grid of points in the altitude - Mach (velocity) diagram, the following computations are made: $R_P = \frac{V_P^2}{a_{\perp p}}$, $\frac{\ell}{R_P}$, $g_{E/P}$, $\frac{Y_c}{R_P}$, $g_E = \frac{g_{E/P}}{P} a_{\perp p}$, and $Y_c = \frac{Y_c}{R_P} R_P$. The ratios $g_{E/P}$ and $\frac{Y_c}{R_P}$ are obtained by the escape conditions in Figures 26 and 27. Lines of constant g_E and constant Y_c are drawn on the altitude - Mach diagram. These lines represent the required distance that E must be in front of P and the associated gs E must pull to effect an escape. This map of the altitude - Mach diagram with the escape requirements is a function only of the standard Pursuer and the ratio V_c/V_p.

The following series of computations is then done for each aircraft in the evaluation:

1) The specific power, P_s (for one (1) g flight) and turning g lines in the h-Mach diagram are computed.

2) The g requirements for escape are overlayed on the g capabilities of the aircraft computed in 1).

3) The combat arena (call it Area 0) is defined - much like that done in Chapter V.

4) The area of the combat arena where the g capability of the aircraft is greater or equal to that required for escape is established (call it Area 1) and the average γ_c , $\bar{\gamma}_c$, in this area is computed.

The results in line 4) show the portion of Area 0 where E has sufficient g capability to escape and the $\bar{\gamma}_c$ to effect the escape. A large Area 1 and small $\bar{\gamma}_c$ in that area is indicative of a good aircraft.

The area of the combat arena outside the escape area in line 4), i.e. Area 0 $\sim$ Area 1, represents an area where E does not have sufficient g capability to escape. However, E may have a P_s advantage in a portion of Area 0 $\sim$ Area 1 (call this portion of Area 0 $\sim$ Area 1, Area 0 $\sim$ 1/E). Based on the Barrier results, E should employ his P_s advantage in Area 0 $\sim 1/_E$ and render a portion of it an escape region (call this area Area 0 $\sim 1/_{E^*}$). Likewise there may be a portion of Area 1 where P has the P_s advantage (call it Area $1/P$) and P may render a portion of Area 1 a capture region (call this Area $1/\overset{*}{P}$). Figure 32 is a Boolean algebra diagram of the sets (i.e. areas) involved.

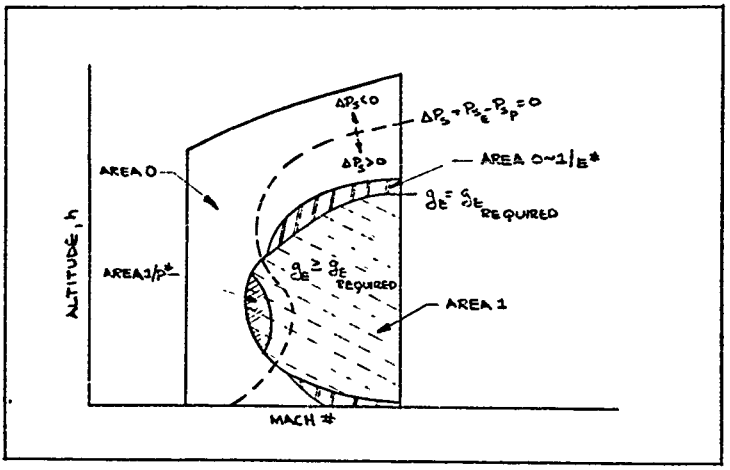

Figure 32: Boolean Sets

The sum

$$\text{Area/E} = [\text{Area } 1 \sim \text{Area } 1/p^*] \cup \text{Area } 0 \sim 1/_{E^*}$$

represents the escape region of the combat arena. The ratio, Area/E/Area 0, is a good measure of the combat capability of a given aircraft against the standard Pursuer.

To compute Area $0 \sim 1/_{E^*}$, the following computations must be done for a grid of points in Area $0 \sim 1/_{E}$ beginning at the $g_E = g_{E_{REQUIRED}}$ line:

1) At a given point in Area $0 \sim 1/_{E}$ (i.e. a given h, V_E, P_{S_E}, $V_P = V_E / \frac{V_E}{V_P}$, P_{S_P}) apply P_{S_E} and P_{S_P} and compute $V_E(t)$, $V_P(t)$,

$\frac{V_E}{V_P}(t)$ (will increase), $\gamma(t)$, $R_p(t)$ (will increase) versus time.

2) As computation 1) is done, compute $\frac{\ell}{R_p(t)}$ (will decrease) and using $\frac{V_E}{V_P}(t)$ compute ϑ_{E_P} and $\frac{\gamma_c}{R_P}$ required for escape from Figure 27 (note ϑ_{E_P} and $\frac{\gamma_c}{R_P}$ will decrease).

3) One of three (3) events will occur which will determine if the grid point is an Escape or a Capture point:

a) The required ϑ_{E_P} for escape reduces to the δ capability of E. At this point compute $\gamma_c(t) = \frac{\gamma_c}{R_P} R_p(t)$. If $\gamma_c(t) \leq \gamma(t)$ then the grid point is an Escape point. If $\gamma_c(t) > \gamma(t)$ then the grid point is a Capture point.

b) E crosses ζ, i.e. $\gamma(t) \leq \ell$, and the grid point is a Capture point.

c) $\frac{V_E}{V_P}(t) \geq 1$ and the grid point is an Escape point.

To compute Area 1/p*, the following computations must be done for a grid of points in Area 1/p beginning at the $\vartheta_E = \vartheta_E$ required line:

1) At a given point in Area 1/p, apply P_{SE} and P_{SP} and compute $V_E(t)$, $V_P(t)$, $V_E/V_P(t)$ (will decrease), $\gamma(t)$, $R_p(t)$ (will increase) versus time.

2) As computation 1) is done, compute $\frac{\ell}{R_p(t)}$ (will decrease) and using $\frac{V_E}{V_P}(t)$ compute ϑ_{E_P} and $\frac{\gamma_c}{R_P}$ for escape from Figure 27. Note that ϑ_{E_P} and $\frac{\gamma_c}{R_P}$ tend to remain unchanged (γ_c will increase because of larger $R_p(t)$) but will depend on the specific instance.

3) One of two (2) events will occur which will determine the Capture or Escape nature of the grid point:

a) $g_{E/P}$ required for escape will exceed the g capability of E in which case the grid point is a Capture point.

b) $g_{E/P}$ required for escape will be less than the capability of E in which case the grid point is an Escape point.

In this manner the areas in the altitude - Mach diagram are established for each aircraft in the relative evaluation, and Eq (7.1) is computed. The relative measure of combat capability is embodied in the numbers $\bar{Y}_c$ and Area E/Area O for each aircraft.

VIII Variable Velocity Models

The models of the previous chapters assumed constant velocity magnitudes. The models were applied to the terminal phase of the air-to-air combat where constant speed appeared to be a good first order assumption. The main purpose of this chapter is to examine the first order effects of variable velocity magnitudes on the problem. A secondary purpose is to relate the constant velocity models of the previous chapters to a more realistic aircraft model.

Aircraft Model

The following vertical plane model is the standard point mass model found in most texts on aircraft performance, for example [12, 7]. Figure 33 shows the aircraft coordinate system and the main variables. The model assumes

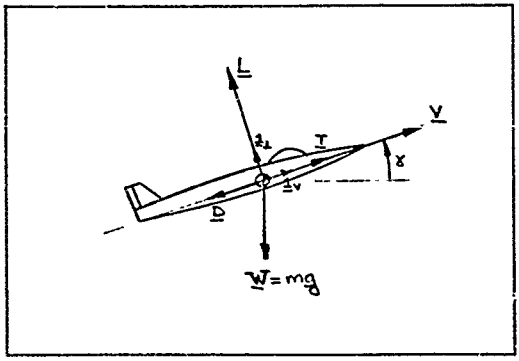

Figure 33: Aircraft Coordinate System

that the angle of attack is small and that the thrust vector $\underline{T}$ is essentially longitudinal. The aircraft maneuvers with the thrust and lift vectors ($\underline{T}$, $\underline{L}$).

The kinematic acceleration of the aircraft, $\dot{\underline{V}}$, can be written

$$\dot{\underline{V}} = \dot{V}\,\underline{1}_V + \dot{\gamma}V\,\underline{1}_\perp \quad . \tag{8.1}$$

The net vector force, $\underline{F}$, on the aircraft can be written

$$\underline{F} = (T - D - mg\sin\gamma)\,\underline{1}_V + (L - mg\cos\gamma)\,\underline{1}_\perp \quad . \tag{8.2}$$

Applying $\underline{F} = m\dot{\underline{V}}$, the equations of motion become

$$\dot{V} = \frac{T-D}{m} - g\sin\gamma \tag{8.3}$$

$$\dot{\gamma}V = \frac{L}{m} - g\cos\gamma \quad . \tag{8.4}$$

The aerodynamic forces are modelled by

$$L = QSC_L \tag{8.5}$$

$$D = QSC_D \tag{8.6}$$

where

Q = dynamic pressure

S = reference area

C_L = lift coefficient

C_D = drag coefficient

and

$$C_D = C_{DO} + kC_L^2 \quad . \tag{8.7}$$

k is obtained by the best parabolic fit of Eq (8.7) to the actual drag polar of the aircraft or approximately by

$$k \simeq \frac{1}{\pi e \mathcal{R}} \tag{8.8}$$

where

e = effectiveness ratio

$\mathcal{R}$ = aspect ratio = $(\text{wing span})^2/S$

Substituting Eqs (8.5), (8.6) and (8.7) into Eqs (8.3) and (8.4) yields

$$a_v \equiv \dot{V} = \frac{T - \bar{q}S(C_{D_0} + kC_L^2)}{m} - g\sin\gamma \tag{8.9}$$

$$a_\perp \equiv \dot{\gamma}V = \frac{\bar{q}SC_L}{m} - g\cos\gamma \tag{8.10}$$

Figure 34 is a plot of Eqs (8.9) and (8.10) (i.e. acceleration vectogram) with varying γ, for a typical F4 aircraft at 35000 ft, M # = .8, W = 38600 lbs, S = 530 ft^2, C_{D_0} = .019, k = .116 and max thrust = 11000 lbs. The vector from the origin to the 1g circle represents vector subtraction of the 1g vector. As can be seen, $a_\perp$ greatly exceeds a_v ten to one (10:1) which in part substantiates the first order approximation of constant velocity magnitude. Note that a_v and $a_\perp$ are the maneuvering accelerations and not the acceleration forces felt by the pilot.

If we assume $|\gamma| < 20°$ then $g\cos\gamma < .94g \simeq g$ and Eq (8.10) is approximated by

$$\dot{\gamma}V \equiv a_\perp \simeq \frac{\bar{q}SC_L}{m} - g \tag{8.11}$$

C_L is then related to $a_\perp$ by

$$C_L \simeq \frac{m}{\bar{q}S}(a_\perp + g) \tag{8.12}$$

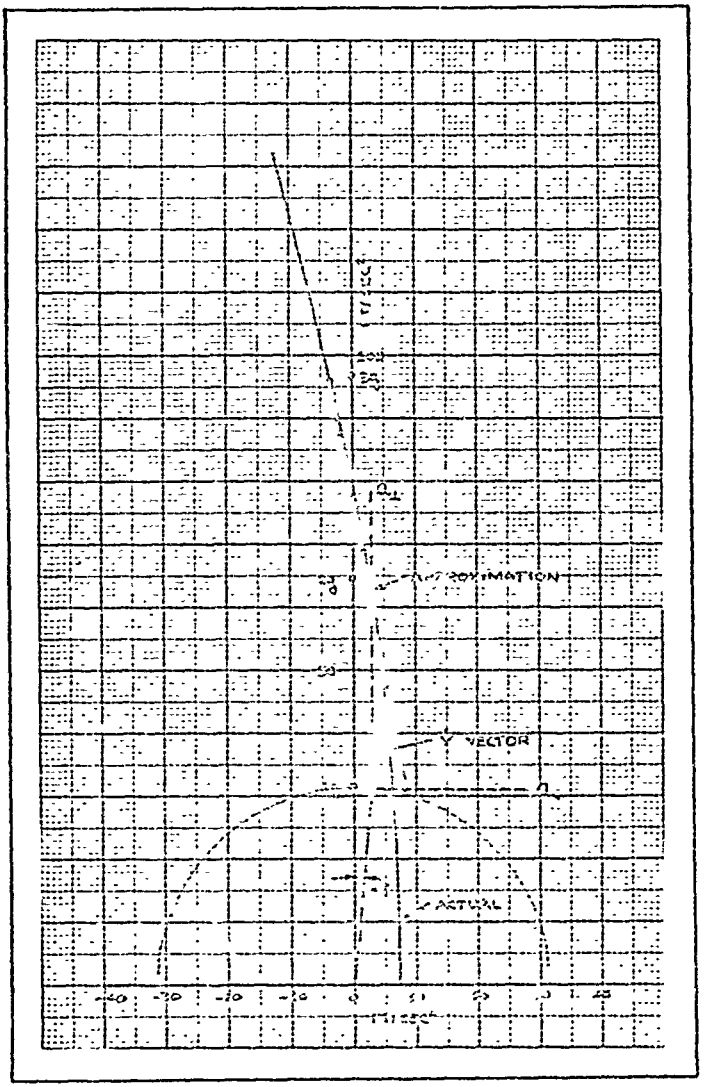

Figure 34: Acceleration Vectogram

Substituting Eq (8.12) into Eq (8.9) and rearranging yields

$$\dot{V} = g\left[\frac{T - \bar{q}S\left(C_{D_0} + \frac{kW^2}{(\bar{q}S)^2}\right)}{W}\right] - \frac{kW}{g\bar{q}S}\left(2ga_\perp + a_\perp^2\right) \quad (8.13)$$

where we have assumed γ small and neglected the $g\sin\gamma$ term. Note that $\frac{kW^2}{(\bar{q}S)^2}$ is the added drag coefficient for straight level flight.

Define C_T as

$$C_T = g\left[\frac{T}{W} - \frac{\bar{q}S}{W}\left(C_{D_0} + \frac{kW^2}{(\bar{q}S)^2}\right)\right] \quad (8.14)$$

Under a given flight condition, C_T will be bounded by

$$C_{T_L} \leq C_T \leq C_{T_U} \quad (8.15)$$

where C_{T_L} and C_{T_U} are the lower and upper bounds respectively and are determined by the bounds on thrust. The bounds on $a_\perp$ are determined by the V-N diagram in Figure 35.

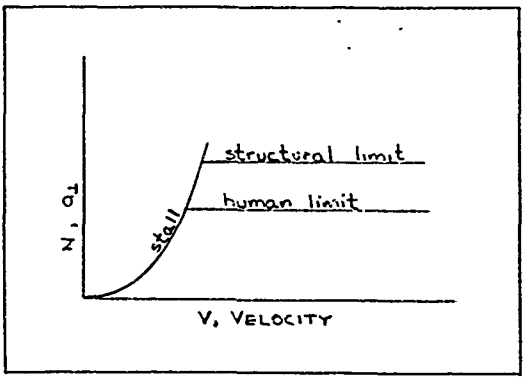

Figure 35: V-N Diagram

For $|\gamma| < 20^\circ$, a good approximation to the equations of motion are therefore

$$\dot{V} = C_T - \frac{kW}{gQS}\left(2g a_\perp + a_\perp^2\right) \tag{8.16}$$

$$\dot{\gamma} V = a_\perp \tag{8.17}$$

where C_T and $a_\perp$ are bounded as just described. As mentioned previously, note that the $\dot{V}$ capability of the aircraft will be small in comparison to the $\dot{\gamma}V$ capability. Note also that $\frac{kW}{gQS} \equiv \frac{W}{g\pi e b^2 Q}$ (b=wingspan) determines the drag acceleration penalty for pulling transverse gs (i.e. $a_\perp$). Since $a_\perp \propto \frac{QS}{W} C_L$, it is seen that a highly maneuverable aircraft (i.e. large $\dot{V}$ and $\dot{\gamma}V$) is characterized by an aircraft with large $\frac{SC_L}{W}$, $\frac{T}{W}$, and small $\frac{W}{b^2}$ implying high T, SC_L, b, and low W. A high maneuverable aircraft is therefore characterized by high thrust, large wing and low weight.

The constant velocity model dynamics of the previous chapters were of the form

$$\dot{V} = 0 \tag{8.18}$$

$$\dot{\gamma} = \frac{a_\perp}{V} \tag{8.19}$$

Eqs (8.17) and (8.19) are the same. On comparing Eq (8.16) with Eq (8.18), it is seen that to model the first order effects of variable velocity magnitude, that $\dot{V}$ should be represented by a small bounded acceleration, C_T, followed by a drag penalty term for transverse acceleration, $a_\perp$.

The main purpose of this chapter is to examine the first order effects of varying velocity. Therefore, since Figure 34 shows the dominance of $a_\perp$ as compared to $\frac{kW}{g\rho S}(2ga_\perp+u_\perp^2)$, the following approximation to Eq (8.16) results

$$\dot{v} = c_T - K|a_\perp| \tag{8.20}$$

where

$$K = \frac{kW}{g\rho S}(2g + a_{\perp_{max}}) \quad . \tag{8.21}$$

The heaving dashed line in Figure 34 shows the degree of approximation (for $a_{\perp_{max}} = 3g$) by using Eq (8.20) and (8.21). As can be seen, the approximation is very good. This approximate aircraft model is the same as Othling's [11, 48] Linearized Drag Polar Model.

Linearized Drag Polar Model

Othling [11] examined this model in the realistic space ξ from the standpoint of control logic; the following analysis is done in the reduced space, ξ, and includes the Barrier analysis.

1. State Equation Formulation:

The coordinate system for this model is the same as Figure 18 viewed from the side. The Θ_p and Θ_E are equivalent to γ in Figure 33. The kinematic equations for this model are the same as Eqs (6.1) except that a $\frac{V}{R}=\dot{\Theta}$ term in Eq (6.1) is replaced with the $\dot{\gamma} = \frac{a_\perp}{V}$ term in Eq (8.17) i.e.

$$\dot{x} = V_E \sin\theta - y\frac{a_{\perp P}}{V_P} \tag{8.22}$$

$$\dot{y} = V_E \cos\theta - V_P + x\frac{a_{\perp P}}{V_P} \tag{8.23}$$

$$\dot{\theta} \equiv \dot{\gamma}_E - \dot{\gamma}_P = \frac{a_{\perp E}}{V_E} - \frac{a_{\perp P}}{V_P} \tag{8.24}$$

and

$$\dot{V}_P = C_{TP} - K_P|a_{\perp P}| \tag{8.25}$$

$$\dot{V}_E = C_{TE} - K_E|a_{\perp E}| \tag{8.26}$$

where Eqs (8.25) and (8.26) come from Eq (8.20). Note that

$$\theta \equiv \gamma_E - \gamma_P \tag{8.27}$$

and that the bounds on the controls are

$$-a_{\perp E_{max}} \leq a_{\perp E} \leq a_{\perp E_{max}}$$

$$-a_{\perp P_{max}} \leq a_{\perp P} \leq a_{\perp P_{max}}$$

$$C_{TP_L} \leq C_{TP} \leq C_{TP_U}$$

$$C_{TE_L} \leq C_{TE} \leq C_{TE_U} \tag{8.28}$$

and are determined as previously discussed. Note that the state Eqs (8.22)-(8.26) are the same as the state Eqs (6.1) for the 2D Limited Pursuer-Evader model with the exception that V_P and V_E are now state variables instead of fixed model parameters.

2. Problem Setup:

The terminal surface, $\mathcal{C}$, can be visualized as in Figure 19 except V_E and V_P are also variables. Its usual description with Eq (2.3) is

$$\psi\left[\underline{x}(t_f)\right] = x^2(t_f) + y^2(t_f) - \ell^2 = 0 \tag{8.29}$$

where $\Theta(t_f)$, $V_p(t_f)$, and $V_E(t_f)$ are free. $\mathcal{C}$ can also be described with Eq (2.19) as

$$\begin{aligned} x(t_f) &= h_1(\underline{s}) = \ell \sin s_1 \\ y(t_f) &= h_2(\underline{s}) = \ell \cos s_1 \\ \Theta(t_f) &= h_3(\underline{s}) = s_2 \\ V_p(t_f) &= h_4(\underline{s}) = s_3 \\ V_E(t_f) &= h_5(\underline{s}) = s_4 \end{aligned} \tag{8.30}$$

where

$$\underline{s} = \begin{bmatrix} s_1 \\ s_2 \\ s_3 \\ s_4 \end{bmatrix} \tag{8.31}$$

The controls for the players are

$$\underline{u} = \begin{bmatrix} C_{TP} \\ a_{\perp P} \end{bmatrix} \quad , \quad \underline{v} = \begin{bmatrix} C_{TE} \\ a_{\perp E} \end{bmatrix} \tag{8.32}$$

and the costate vector $\underline{\lambda}$ is

$$\underline{\lambda} = \begin{bmatrix} \lambda_x \\ \lambda_y \\ \lambda_\Theta \\ \lambda_{V_P} \\ \lambda_{V_E} \end{bmatrix} \tag{8.33}$$

As done previously, the roles of the players are preselected by choosing $\phi=0$, $L=1$ with P minimizing and E maximizing.

3. Application of Necessary Conditions:

MEl becomes

$$0=\min_{C_{TP},a_{\perp P}}\max_{C_{TE},a_{\perp E}}\Big[\lambda_x\Big(V_E\sin\theta-\gamma\frac{a_{\perp P}}{V_P}\Big)+\lambda_y\Big(V_E\cos\theta-V_P+x\frac{a_{\perp P}}{V_P}\Big)+$$

$$+\lambda_\theta\Big(\frac{a_{\perp E}}{V_E}-\frac{a_{\perp P}}{V_P}\Big)+\lambda_{V_P}\Big(C_{TP}-K_P|a_{\perp P}|\Big)+\lambda_{V_E}\Big(C_{TE}-K_E|a_{\perp E}|\Big)\Big]+1\equiv$$

$$\equiv\min_{C_{TP},a_{\perp P}}\Big[\frac{(x\lambda_y-y\lambda_x-\lambda_\theta)}{V_P}a_{\perp P}-K_P\lambda_{V_P}|a_{\perp P}|+\lambda_{V_P}C_{TP}\Big]+$$

$$+\max_{C_{TE},a_{\perp E}}\Big[\frac{\lambda_\theta}{V_E}a_{\perp E}-K_E\lambda_{V_E}|a_{\perp E}|+\lambda_{V_E}C_{TE}\Big]+$$

$$+V_E(\lambda_x\sin\theta+\lambda_y\cos\theta)-V_P\lambda_y+1\equiv$$

$$\equiv\min_{C_{TP},a_{\perp P}}H_P+\max_{C_{TE},a_{\perp E}}H_E+H_O \qquad (8.34)$$

where

$$H_P=\frac{A}{V_P}a_{\perp P}-K_P\lambda_{V_P}|a_{\perp P}|+\lambda_{V_P}C_{TP}$$

$$H_E=\frac{\lambda_\theta}{V_E}a_{\perp E}-K_E\lambda_{V_E}|a_{\perp E}|+\lambda_{V_E}C_{TE}$$

$$H_O=V_E(\lambda_x\sin\theta+\lambda_y\cos\theta)-V_P\lambda_y+1 \qquad (8.35)$$

and

$$A=x\lambda_y-y\lambda_x-\lambda_\theta \qquad (8.36)$$

The min H_P conditions yield

$$C_{TP} = \begin{cases} C_{PL} & \lambda_{V_P} > 0 \\ C_{PU} & \lambda_{V_P} < 0 \end{cases} \tag{8.37}$$

$$A \neq 0 \Rightarrow a_{\perp P} = -a_{\perp P_{max}} \operatorname{sgn}(A)\, h\left[K_P \lambda_{V_P} + \frac{|A|}{V_P}\right]$$

$$A = 0 \Rightarrow a_{\perp P} = a_{\perp P_{max}} h\left[\lambda_{V_P}\right] . \tag{8.38}$$

with a totally singular possibility if both $\lambda_{V_P} = A \equiv 0$ for a finite time. The max H_E conditions yield

$$C_{TE} = \begin{cases} C_{EL} & \lambda_{V_E} < 0 \\ C_{EU} & \lambda_{V_E} > 0 \end{cases} \tag{8.39}$$

$$\lambda_\theta \neq 0 \Rightarrow a_{\perp E} = a_{\perp E_{max}} \operatorname{sgn}(\lambda_\theta)\, h\left[\frac{|\lambda_\theta|}{V_E} - K_E \lambda_{V_E}\right]$$

$$\lambda_\theta = 0 \Rightarrow a_{\perp E} = a_{\perp E_{max}} h\left[-\lambda_{V_E}\right] \tag{8.40}$$

with a totally singular possibility if both $\lambda_\theta = \lambda_{V_E} \equiv 0$ for a finite time. Othling [11, 99] shows that the singular cases are not possible. The costate equations are

$$\dot{\underline{\lambda}} = -\nabla H^T = -\begin{bmatrix} \frac{\partial H}{\partial x} \\ \frac{\partial H}{\partial y} \\ \frac{\partial H}{\partial \theta} \\ \frac{\partial H}{\partial V_P} \\ \frac{\partial H}{\partial V_E} \end{bmatrix} = \begin{bmatrix} -\lambda_y \frac{a_{\perp P}}{V_P} \\ \lambda_x \frac{a_{\perp P}}{V_P} \\ V_E(\lambda_y \sin\theta - \lambda_x \cos\theta) \\ \lambda_y + A\, a_{\perp P}/V_P^2 \\ \lambda_\theta a_{\perp E}/V_E^2 - (\lambda_x \sin\theta + \lambda_y \cos\theta) \end{bmatrix} . \tag{8.41}$$

Note that the first three (3) costate equations are the same as the costate Eq (6.22) for the 2D Limited Pursuer-Evader model. The transversality conditions yield

$$\lambda_x(t_f) = \left.\frac{\sin s_1}{V_p \cos s_1 - V_E \cos(s_1-\theta)}\right|_{t_f}$$

$$\lambda_y(t_f) = \left.\frac{\cos s_1}{V_p \cos s_1 - V_E \cos(s_1-\theta)}\right|_{t_f} \qquad (8.42)$$

$$\lambda_\theta(t_f) = \lambda_{V_p}(t_f) = \lambda_{V_E}(t_f) = 0$$

4. Problem Backward Solution From $\mathcal{C}_e$:

From the transversality conditions, Eq (8.42), and the equations for $\mathcal{C}_e$, Eq (8.30), it can be shown that on $\mathcal{C}_e$ $A = \lambda_\theta = \lambda_{V_p} = \lambda_{V_E} = 0$ and Eqs (8.37)-(8.40) for the controls are undefined. Evaluating the backward derivatives of the arguements in Eqs (8.37)-(8.40), it can be shown that the controls an infinitesimal distance away from the UP of $\mathcal{C}_e$ are

$$\begin{aligned} c_{TP}\big|_{\mathcal{C}_e} &= c_{PU} \\ a_{\perp_P}\big|_{\mathcal{C}_e} &= a_{\perp_{P_{max}}} h\left[|\sin s_1| - K_p \cos s_1\right] \\ c_{TE}\big|_{\mathcal{C}_e} &= c_{EU} \\ a_{\perp_E}\big|_{\mathcal{C}_e} &= a_{\perp_{E_{max}}} \operatorname{sgn}\left[\sin(s_1-s_2)\right] h\left[|\sin(s_1-s_2)| - K_E \cos(s_1-s_2)\right] \end{aligned} \qquad (8.43)$$

Figure 36 is a plot of $\mathcal{C}$ (similar to Figure 21) and the terminal controls, Eq (8.43) for the parameters of the F4 aircraft previously mentioned. The BUP, which for a given terminal velocity ratio is the same as for the 2D Limited Pursuer-Evader model, is shown for the ratio $\frac{V_E}{V_P}\Big|_{t_f} = .9$. Note how the P and E singular surfaces of the Limited Pursuer-Evader model do not appear in the present model. There are however, switching surfaces in the present model. Note also that the switching surfaces retain the basic $\mathcal{C}$ control characteristics of those singular surfaces.

The parallogram shaped area around the origin in Figure 36 is a region of $\mathcal{C}$ where both P and E are non-turning terminally. This can be likened to the totally singular surface (i.e. the y axis with $\Theta = 0$) of the Limited Pursuer-Evader model. Because both P and E are non-turning off of $\mathcal{C}$ in this region, the backward solution from this region back to the first control switching can be done closed form i.e.

$$\lambda_x(T) = \lambda_x(t_f) = \sin s_1 / [V_p \cos s_1 - V_E \cos(s_1 - s_2)] \quad (8.44)$$

$$\lambda_y(T) = \lambda_y(t_f) = \cos s_1 / [V_p \cos s_1 - V_E \cos(s_1 - s_2)] \quad (8.45)$$

$$\Theta(T) = \Theta(t_f) = s_2 \quad (8.46)$$

$$V_E(T) = V_E(t_f) - C_{EU} T \quad (8.47)$$

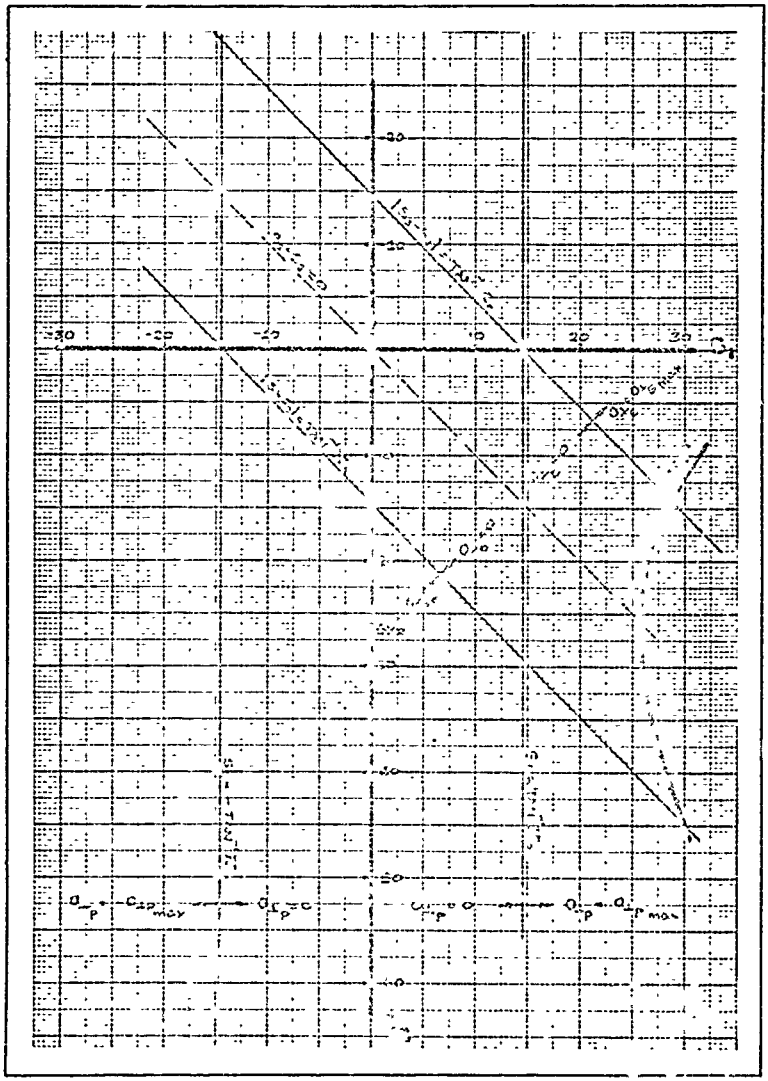

Figure 36: ζ Controls

$$\lambda_\theta(\tau) = \frac{\sin(s_1 - s_2)}{V_p \cos s_1 - V_E \cos(s_1 - s_2)} \left[V_E(t_f)\tau - C_{EU}\tau^2/2 \right] \quad (8.48)$$

$$\lambda_{V_E}(\tau) = \frac{\cos(s_1 - s_2)}{V_p \cos s_1 - V_E \cos(s_1 - s_2)} \tau \quad (8.49)$$

$$V_p(\tau) = V_p(t_f) - C_{PU}\tau \quad (8.50)$$

$$A(\tau) = \frac{-\sin s_1}{V_p \cos s_1 - V_E \cos(s_1 - s_2)} \left[V_p(t_f)\tau - C_{PU}\tau^2/2 \right] \quad (8.51)$$

$$\lambda_{V_p}(\tau) = \frac{-\cos s_1}{V_p \cos s_1 - V_E \cos(s_1 - s_2)} \tau \quad (8.52)$$

The control switching times, τ_E and τ_p, are obtained from the following expressions

$$\frac{|\lambda_\theta| - K_E \lambda_{V_E} V_E}{\left[\frac{K_E \cos(s_1 - s_2)}{V_p \cos s_1 - V_E \cos(s_1 - s_2)} \right]} = \frac{|\sin(s_1 - s_2)|}{K_E \cos(s_1 - s_2)} \left(s_4\tau - C_{EU}\frac{\tau^2}{2} \right) - \left(s_4\tau - C_{EU}\tau^2 \right) \equiv$$

$$\equiv \tau \left[-s_4(1 - K_E') + C_{EU}\tau(1 - K_E'/2) \right] \quad (8.53)$$

$$\frac{K_p \lambda_{V_p} V_p + |A|}{\left[\frac{K_p \cos s_1}{V_p \cos s_1 - V_E \cos(s_1 - s_2)} \right]} = \frac{|\sin s_1|}{K_p \cos s_1} \left(s_3\tau - C_{PU}\frac{\tau^2}{2} \right) - \left(s_3\tau - C_{PU}\tau^2 \right) \equiv$$

$$\equiv \tau \left[-s_3(1 - K_p') + C_{PU}\tau(1 - K_p'/2) \right] \quad (8.54)$$

where

$$K_E' \equiv \frac{|\sin(s_1 - s_2)|}{K_E \cos(s_1 - s_2)} \tag{8.55}$$

$$K_P' \equiv \frac{|\sin s_2|}{K_P \cos s_1} \tag{8.56}$$

Note that the denominators of Eqs (8.53) and (8.54) are ≥ 0 in the UP of $\mathcal{C}$ and that K_E' and K_P' are ≤ 1 in the non-turning region of $\mathcal{C}$. The switching times, T_E and T_P, are therefore determined from Eqs (8.53) and (8.54) respectively i.e.

$$T_E = \frac{s_4}{C_{EU}}\left[\frac{1 - K_E'}{1 - K_E'/2}\right] \tag{8.57}$$

$$T_P = \frac{s_2}{C_{PU}}\left[\frac{1 - K_P'}{1 - K_P'/2}\right] \tag{8.58}$$

The X(T) and Y(T) solutions from the non-turning region of $\mathcal{C}$ are

$$x(T) = \ell \sin s_1 - \sin s_2 \left(s_4 T - C_{EU} T^2/2\right) \tag{8.59}$$

$$y(T) = \ell \cos s_1 + (s_3 - s_4 \cos s_2) T - (C_{PU} - C_{EU} \cos s_2) T^2/2 \tag{8.60}$$

and are valid up to the smaller of T_E or T_P.

A computer program was written using Eqs (8.44)-(8.60) to solve for the shape of the switching surface emanating from the non-turning region on $\mathcal{C}$. This switching surface forms a closed region in ξ whose base is the non-turning region on $\mathcal{C}$. Figure 37 is a two dimensional representation of the switching surface for a particular $V_E(t_f)$

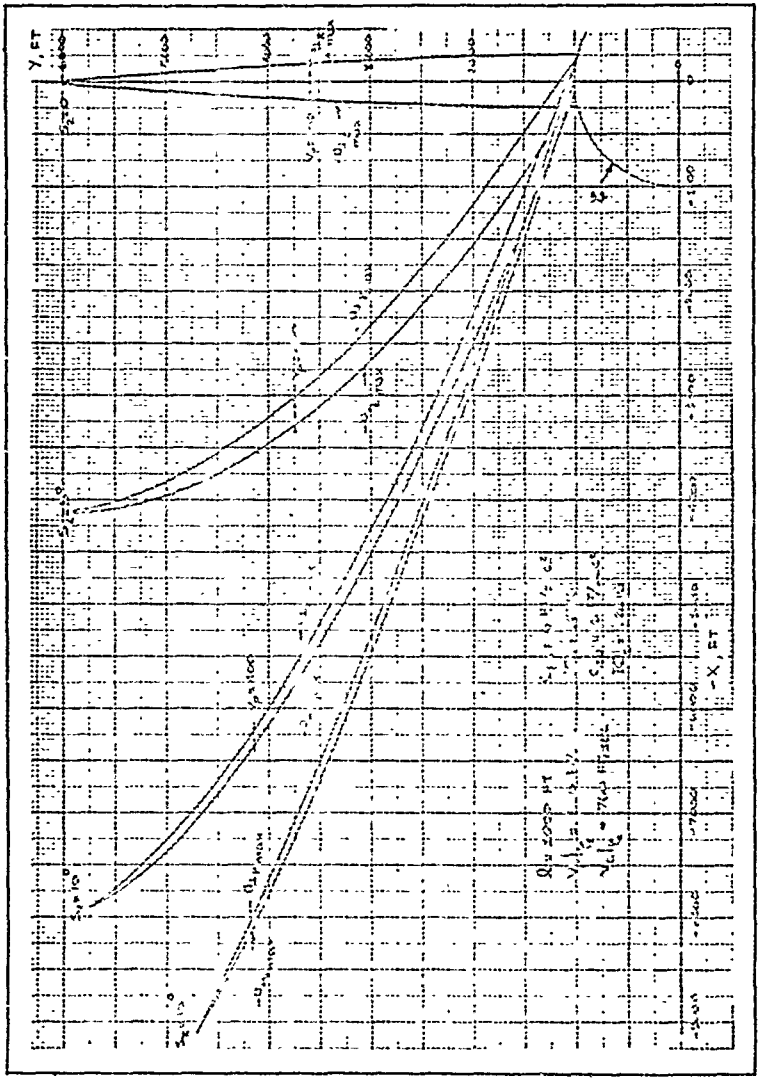

Figure 37: Non-turning "Fingers"

and $V_p(t_f)$ and system parameters. The S_2, i.e. Θ, axis can be thought of as positive out of the paper. Only the positive values (the negative S_2 have a mirror image about y-axis) of $S_2 = \Theta(t_f)$ are shown. For a particular value of S_2, the x-y region inside the switching surface resemble "fingers" emanating from the non-turning region of $\mathcal{C}$. As the S_2 values get larger, the "fingers" fan out to the left (would be to the right for increasing negative S_2) and get narrower. The surfaces of the "fingers" are labeled with the particular control switching that occurs first. The "fingers" represent regions of the state space where it is best for both players to accelerate and not turn. The trajectories backward off the finger surfaces will be the turning portion of the trajectories. The tips of the "fingers" are associated with zero velocities and are therefore not very physically meaningful. Lines of constant velocity in the "fingers" are shown. Note that the $S_2=0$ "finger" is the variable velocity model counterpart of the totally singular surface in the Limited Pursuer-Evader model. Note also that the trajectories coming into the "fingers" are of real interest since they lead to position angles off (i.e. S_1) and velocity angles off (i.e. S_2) where the Pursuer and Evader roles, as selected, are well defined. If the Barrier can be made to cut through a given "finger", then this will represent an interesting and physically applicable means of Evader

escape. As will be shown, Barrier closure and Evader escape in the Limited Pursuer model is associated with escape from a non-zero S_2 "finger" in the present model; the interesting Barrier closure and Evader escape condition of the Limited Pursuer-Evader model is associated with escape from the $S_2=0$ "finger" of the present model.

5. Barrier Necessary Conditions :

In each of the previous models, the similarity between the necessary conditions for the UP of $\mathcal{C}$ and the necessary conditions for the Barrier has been pointed out. The following necessary conditions for the Barrier can be obtained directly by applying the results of Chapter II; however, taking advantage of the above similarity they are simply stated. The BUP is defined by those states on $\mathcal{C}$ for which

$$V_P \cos S_1 - V_E \cos(S_1 - S_2) = 0 \quad . \tag{8.61}$$

The normality conditions of $\underline{\nu}$ on $\mathcal{C}$ yield

$$\begin{aligned} \nu_x(t_f) &= \sin S_1 \\ \nu_y(t_f) &= \cos S_1 \\ \nu_\theta(t_f) &= \nu_{V_P}(t_f) = \nu_{V_E}(t_f) = 0 \end{aligned} \quad . \tag{8.62}$$

The control equations on the Barrier have the same form as Eqs (8.37), (8.38), (8.39), (8.40) and (8.43) except that $\underline{\lambda}$ is replaced with $\underline{\nu}$. The costate equations on the Barrier have the same form as Eq (8.41) except that $\underline{\lambda}$ is replaced with $\underline{\nu}$.

6. Barrier Solution/Evaluation Constant Velocity Barrier Results:

The main purpose of this chapter is to examine the variable

velocity effects on the results of the constant velocity models. The main results of the Limited Pursuer model are contained in the Barrier closure conditions of Figure 7. The main results of the Limited Pursuer-Evader model are contained in the Barrier trajectory closure conditions of Figures 26 and 27. We examine the variable velocity effects on Figure 7 first.

As discussed in the 2D Limited Pursuer-Evader model paragraph 6, the closed Barrier trajectory in the Limited Pursuer model is also a specific Barrier trajectory of the Limited Pursuer-Evader model, however, it does not represent a closed Barrier trajectory in the Limited Pursuer-Evader model. Except for the variable velocity effects, the same is true for the present model i.e. the closed Barrier trajectory of the Limited Pursuer model is also closely resembled by a non-closed Barrier trajectory in the present variable velocity model.

To see the variable velocity effects on Figure 7, the following specific Barrier computation was done for the Linearized Drag Polar model: $\ell = 1400$ ft, $C_{P_U} = 6 \frac{ft}{sec^2}$, $K_P = .2615$, $a_{L_{P_{max}}} = 3gs$, $V_P(t_f) = 800 \frac{ft}{sec}$, $V_E(t_f) = 720 \frac{ft}{sec}$, $C_{E_U} = 6 \frac{ft}{sec^2}$ $K_E = .2615$, $a_{L_{E_{max}}} = 6gs$. This is the data previously used for a specific flight condition of the F4 aircraft. The above data shows that $V_E(t_f)/V_P(t_f) = .90$, $R_P(t_f) = 6622$ ft and $\frac{\ell}{R_P(t_f)} = .212$.

Figure 7 shows that escape is possible for the constant velocity, highly maneuverable Evader of the Limited Pursuer model if the Evader is at the tip of the Barrier located at $\frac{Y}{R_P} = .257$ (i.e. $Y_c = 1702$ ft) with a velocity angle off $\Theta_c = 43.7$ degrees. The highly maneuverable Evader pulls no gs to effect the escape and the constant velocity Pursuer pulls the maximum 3gs. The results of the Linearized Drag Polar Barrier computation showed the following:

1) Both players use maximum forward thrust. E pulls no gs and P pulls the maximum 3gs .

2) The tip of the Barrier was located at 1792 ft and the required velocity angle off was 43.6 degrees.

3) V_E at the tip had reduced to 704 $\frac{ft}{sec}$ and V_P at the tip had increased to 850 $\frac{ft}{sec}$.

Even though the velocities vary, the required escape conditions and control laws to effect the escape for the Linearized Drag Polar model, agree closely to those of the constant velocity model. Note that the constant velocity model slightly underestimates the required Y_c for escape. Note also that each player is using maximum forward thrust in the variable velocity model in an attempt to increase the velocity advantage; this was also suggested by the Barrier sensitivity analysis of the Limited Pursuer model. Next we examine the variable velocity effects on Figures 26 and 27.

As previously mentioned, the escape conditions of Figures 26 and 27 for the constant velocity Limited Pursuer-Evader model, should be similar to the necessary escape conditions from the $S_z = 0$ "finger"

of the present variable velocity Linearized Drag Polar model. To examine the variable velocity effects on Figures 26 and 27, the following flight conditions were used: ℓ = 1400 ft.,

$V_P(t_f)$ = 800 ft/sec, $a_{L_{P\,max}}$ = 3 gs , $V_E(t_f)$ = 720 ft/sec, $a_{L_{E\,max}}$ = 6 gs.

Figure 26 and 27 show that for E to effect the escape, $\frac{Y_c}{R_p}$ = .490 implying Y_c = 3244 ft. The controls for the constant velocity players are maximum gs with E non-turning after a ninety (90) degree rotation in real space. Two specific computations of Linearized Drag Polar Barrier closure with the S_2=0 "finger" were done. Each is discussed in turn.

The first computation was done using the aforementioned flight conditions and the following aircraft parameter values;

C_{P_U} = 1. ft/sec^2 , K_P = .09 , C_{E_U} = 1. ft/sec^2 , K_E = .09 .

The aircraft parameter values are indicative of an aircraft with small longitudinal acceleration capability and about one third (1/3) the drag penalty of the F4. The results of this computation showed the following:

1) Both players use maximum forward thrust. P pulls the maximum 3 gs . E pulls the maximum 6 gs initially and switches to 0 gs after an 87 degree turn in real space.

2) The Barrier closed with the S_2 = 0 finger at Y_c = 3382 ft.

3) The velocities at the closure point were V_P = 876 ft/sec, V_E = 814 ft/sec.

4) The minimax time to $\mathcal{C}$ via the $S_2 = 0$ "finger" was 31.9 sec; the time for escape along the Barrier was 9.95 sec. Even though the velocities vary, the required escape conditions and control laws to effect the escape for the Linearized Drag Polar model, agree closely to those of the constant velocity model. Note how the time for escape is very different from the minimax time to via the optimal $S_2 = 0$ "finger". This discontinuity in the time payoff is another characteristic of the Barrier.

The second specific computation of the Linearized Drag Polar model Barrier used the same flight conditions of the first computation, but used the following more realistic aircraft parameter values:

$C_{PU} = 6 \frac{ft}{sec^2}$, $K_P = .2615$, $C_{PE} = 6 \frac{ft}{sec^2}$, $K_E = .2615$.

These are the values for the F4 aircraft. The results of the computation showed the following:

1) Both players use maximum forward thrust. P pulls the maximum 3 gs . E pulls the maximum 6gs initially and switches to 0 gs after a 83.5 degree turn in real space.

2) The Barrier closed with the $S_2 = 0$ "finger" at $Y_C = 3629$ ft.

3) The velocities at the closure point were $V_P = 1009$ ft/sec, $V_E = 960$ ft/sec.

4) The minimax time to $\mathcal{C}$ via the $S_2 = 0$ finger was 45.3 sec; the time for escape along the Barrier was 10.83 sec.

Even though the velocities vary considerably in this more realistic case, the error in the Y_C closure point is only around 10%. The escape

control logic agree very well with only a 6.5 degree error in the E control switch point.

7. Model Conclusions

The escape conditions of Figures 7, 26, and 27 appear to be a very good first estimate of the requirements for escape. The escape control logics appear to be very good. Note that the major effect of variable velocity is to cause the γ_c closure point to be under estimated; however, the error is not large. The main reason for the good agreement between the constant velocity and variable models is, as reasoned earlier, that in the terminal phase of combat the velocities do not have time to vary enough to appreciably effect the problem. From a practical point of view, it should also be realized that in a real combat engagement there will probably only be a rough estimate of the opponent's velocity magnitude, which would tend to justify using the escape requirements of the simpler constant velocity model in real combat.

IX The Barrier and Its Use in Air-to-Air Combat Role Decision

The analysis of the previous chapters always a priori assumed the roles of the combatants. To make P pursue and E evade with the payoff Eq (2.4), ϕ was made zero (0) and L was made one (1) with P minimizing and E maximizing. Chapter I mentioned the role selection problem (major factor 3) and payoff problem (major factor 2). Chapter II pointed out the importance and physical interpretation of the Barrier as regards escape and capture. The problem of fixed roles and payoff function form was demonstrated in the Limited Pursuer-Evader model in Figure 22 where state positions in the UP of $\mathcal{C}$ obviously did not correspond to the assigned fixed roles. Consequently, only the portion of the UP of $\mathcal{C}$ where the fixed roles made sense, was used for analysis. As discussed in Chapter I, "the ideal model of the air-to-air combat problem would have an analytical structure which would couple these seven (7) major factors together".

The research and ideas in this chapter are the original work of the author, and are first attempts at building the analytical structure into Zero-Sum Differential Games to additionally couple the major factors of payoff function form and role decision. As will be shown, the problem of role decision, payoff function form, and the Barrier are all interrelated. The results of this research lead to a broader concept of zero-sum differential games than that found in Isaacs [7] or elsewhere in the literature.

The General Purpose Payoff

The following general zero sum, air-to-air combat payoff was deduced

to eliminate the role - payoff problems encountered in the Limited Pursuer-Evader model. Refer to Figure 28 and consider the following payoff function with P minimizing and E maximizing

$$J = a\sin^2\left(\frac{\theta_P}{2}\right) + b\sin^2\left(\frac{\theta_E}{2}\right) + c\cos\theta_P \int dt \qquad (9.1)$$

where

θ_P = angle between $\underline{v}_P(t_f)$ and $\underline{r}(t_f)$

θ_E = angle between $\underline{v}_E(t_f)$ and $\underline{r}(t_f)$.

Note that

$$\sin^2(\theta/2) \equiv \frac{1-\cos\theta}{2} \qquad (9.2)$$

and that

$$\cos\theta_P = \frac{\underline{v}_P^T(t_f)\,\underline{r}(t_f)}{|\underline{v}_P(t_f)||\underline{r}(t_f)|} \qquad (9.3)$$

$$\cos\theta_E = \frac{\underline{v}_E^T(t_f)\,\underline{r}(t_f)}{|\underline{v}_E(t_f)||\underline{r}(t_f)|} \qquad (9.4)$$

Substituting Eq (9.2) into Eq (9.1) yields another form of the payoff

$$J = \frac{a+b}{2} - \frac{1}{2}\left[a\cos\theta_P + b\cos\theta_E\right] + c\cos\theta_P \int dt \qquad (9.5)$$

The effect of the three terms in Eq (9.1), will be to cause P (near ζ) to force E to cross ζ at small $|\theta_P|$ and small $|\theta_E|$ as quickly as possible for $|\theta_P| \leq \pi/2$. Note also that the three terms will cause E (near ζ) to force P to a $|\theta_P|$ near π and $|\theta_E|$ near π as quickly as possible for $\pi/2 \leq |\theta_P| \leq \pi$. Figure 38 shows the best possible position that P and E can hope to achieve at ζ .

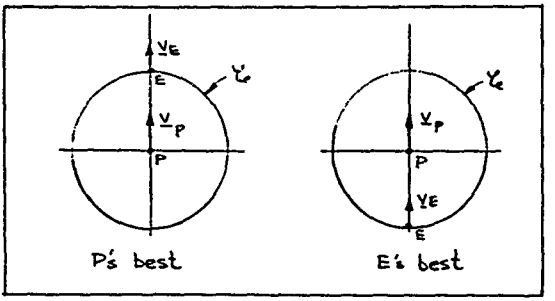

Figure 38: Best Conditions at $\mathcal{C}_c$

As can be seen, the single minimax, zero-sum payoff in Eqs (9.1) or (9.5) allows the roles of the combatants near $\mathcal{C}_c$ to be automatically structured in the payoff form. In each case, the combatants are attempting to achieve a direct tail chase firing position as quickly as possible. Note also that if P finds himself in a poor position near $\mathcal{C}_c$ (i.e. $|\theta_P| \simeq \pi$, $|\theta_E| \simeq \pi$), the payoff function form is structured to cause P to evade logically i.e. maximize time to $\mathcal{C}_c$ while decreasing $|\theta_P|$ and $|\theta_E|$ (note this increases P's position and velocity angle off relative to E). The same is true when E finds himself in a poor position near $\mathcal{C}_c$.

Zero-Sum Differential Games and Roll Determination

To solve the roll determination problem, the general purpose payoff, Eq (9.1), is used in the following three (3) ways:

1) $a = b = 0$, $c = 1$

2) $a = b = 0$, $c = -1$

3) $a > 0$, $b > 0$, $c > 0$

In problem 1), the minimizing player is a definite pursuer and the maximizing player is a definite evader. The problem is solved backward from the UP of $\mathcal{C}$ and the Barrier is established. This is the same as was done for the model of the previous chapters.

In problem 2), the minimizing player is a definite evader and the maximizing player is a definite pursuer i.e. the roles are switched. The problem is solved backward from the UP of $\mathcal{C}$ and the Barrier is established.

In problem 3), the UP of $\mathcal{C}$ is determined and based on terminal state is divided into four (4) regions: Region 1 represents terminal states of clear advantage for the minimizing player; Region 2 represents terminal states of clear advantage for the maximizing player; Region 3 represents terminal states resulting in a mutual kill; Region 4 is the remainder of the UP where no clear outcome is indicated or may be thought of as a "draw". An example of a Region 1 has already been given by the area of $\mathcal{C}$ inside the heavy dashed lines of Figure 21. Regions 1-4 are disjoint and their union is the UP of $\mathcal{C}$. The problem is solved backward from the UP of $\mathcal{C}$. Problem 3) can be thought of as a case where the game is inherently structured so that both players assume the proper roles based on terminal state.

The backward trajectories from the three (3) distinct uses of the general purpose payoff, go into regions of the state space and in general the regions will intersect. Based on the desires of the combatants, a role logic then developes for the state space.

Some Illustrative Examples

The following simple examples are intended solely to illustrate the basic concepts for role determination with zero-sum differential games; the examples are not intended as ends in themselves.

1. The Simplest Model:

For problem 1) (i.e. $a=b=0$, $c=1$) the results of Chapter III show that if

1) $V_P > V_E$ then all of $\mathcal{C}$ is the UP and line of sight pursuit and evasion is used with E always captured.

2) $V_P < V_E$ then all of $\mathcal{C}$ is the NUP and the maximizing player E always escapes with line of sight evasion.

For problem 2) (i.e. $a=b=0$, $c=-1$), the results of Chapter III apply again and show that if

1) $V_P > V_E$ then all of $\mathcal{C}$ is the NUP and P always escapes by using line of sight evasion.

2) $V_P < V_E$ then all of $\mathcal{C}$ is the UP and P is always captured provided E uses line of sight pursuit.

For problem 3) (i.e. $a>0, b>0, c>0$), the general purpose payoff is not applied since the controls appear in the Mayer payoff; however, it is clear that if both highly maneuverable players are aggressive, the result is always a mutual kill.

Assuming that both combatants prefer the outcomes in the order kill opponent, draw, mutual kill, then regardless of whether $V_P > V_E$ or $V_E > V_P$ the role logic is always a draw. If one of the combatants

is aggressive (i.e. has a kill at all cost objective) and has the velocity advantage, then the role logic is always a mutual kill.

2. Limited Pursuer-Model:

For problem 1) (i.e. $a=b=0$, $c=1$) the results of Chapter IV apply and are contained in the Barrier closure conditions of Figure 7.

For problem 2) (i.e. $a=b=0$, $c=-1$), the necessary conditions of Chapter II are straight forward to apply and solve the problem. A summary of the main results follows.

The coordinate system is shown in Figure 39.

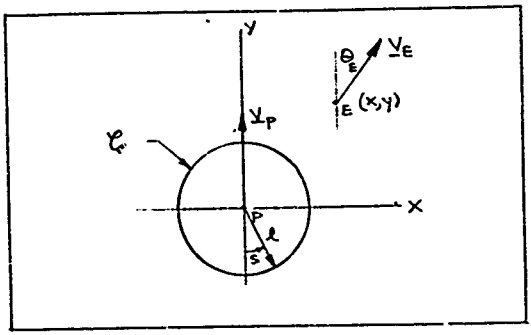

Figure 39: Limited Evader Coordinate System

The state equations are the same as Eq (4.1). The terminal surface is described with Eq (2.19) as

$$x(t_f) = h_1(\xi) = \ell \sin s \qquad (9.6)$$
$$y(t_f) = h_2(\xi) = -\ell \cos s$$

Application of ME1 yields

$$\min_{\alpha} \max_{\theta_E} \left[\underline{\lambda}^T \underline{f} - 1 \right] = V_E \min_{\theta_E} H_E + \frac{V_P}{R_P} \max_{\alpha} H_P + H_0 = 0 \qquad (9.7)$$

where

$$\begin{aligned} H_P &= (x\lambda_y - y\lambda_x)\alpha \equiv A\alpha \\ H_E &= \lambda_x \sin\theta_E + \lambda_y \cos\theta_E \\ H_0 &= -V_P\lambda_y + 1 \end{aligned} \qquad (9.8)$$

The controls are

$$\alpha^* = \operatorname{sgn} A \qquad (9.9)$$

with a singular possibility if A = 0 for a finite time and

$$\tan\theta_E^* = \lambda_x/\lambda_y \qquad (9.10)$$

or

$$\sin\theta_E^* = \frac{-\lambda_x}{\sqrt{\lambda_x^2 + \lambda_y^2}} \quad , \quad \cos\theta_E^* = \frac{-\lambda_y}{\sqrt{\lambda_x^2 + \lambda_y^2}} \qquad (9.11)$$

ME2 becomes

$$-V_E\sqrt{\lambda_x^2 + \lambda_y^2} + \frac{V_P}{R_P}|A| - V_P\lambda_y + 1 = 0 \qquad (9.12)$$

The costate equations are the same as Eq (4.18). The transversality conditions yield

$$\tan s = \left.\frac{-\lambda_x}{\lambda_y}\right|_{t_f} \qquad (9.13)$$

implying

$$\left.\theta_E^*\right|_{t_f} = -s \qquad (9.14)$$

and

$$\begin{aligned} \lambda_x(t_f) &= \frac{\sin s}{V_E - V_P\cos s} \\ \lambda_y(t_f) &= \frac{-\cos s}{V_E - V_P\cos s} \end{aligned} \qquad (9.15)$$

Note that at termination, E orients his velocity vector directly at P. Note also that E will close on P at ζ_c provided $V_E - V_p \cos S > 0$ i.e. $\cos S \leq \frac{V_E}{V_p}$ or

$$S > \cos^{-1}\frac{V_E}{V_p} \equiv S_o \quad . \tag{9.16}$$

Since $\dot{A} = V_p \lambda_x$ and $\mathring{A} = -V_p \lambda_x$, P's terminal control is for $S > S_o$

$$\alpha^*\Big|_{\zeta_c} = \operatorname{sgn} A\Big|_{\zeta_c} = \operatorname{sgn} \mathring{A}\Big|_{\zeta_c} = \operatorname{sgn}\left[\frac{-V_p \sin S}{V_E - V_p \cos S}\right] = -\operatorname{sgn} S \quad . \tag{9.17}$$

At ζ_c it can be seen that P is turning away from E.

Investigating P's singular control we find the following:

$$A = 0 \Rightarrow \tan \theta_E^* = \frac{\lambda_x}{\lambda_y} = \frac{x}{y}$$

$$\dot{A} = 0 \Rightarrow \lambda_x = 0 \Rightarrow \dot{\lambda}_x = 0 \text{ and } S = 0, \pi \Rightarrow$$

$$\alpha_S = 0 \Rightarrow x = 0 \ , \ \theta_E^* = 0 \text{ and } \lambda_y = \lambda_y(t_f) \quad .$$

The last requirement of Eq (2.16) requires $\lambda_y(t_f) \leq 0$.

For $S = 0$

$$\lambda_y(t_f) = \frac{-1}{V_E - V_p} \quad . \tag{9.18}$$

For $S = \pi$

$$\lambda_y(t_f) = \frac{1}{V_E + V_p} \quad . \tag{9.19}$$

Therefore, a P singular case only exists at $S = 0$ in the uninteresting case where $V_E > V_p$ and all of ζ_c is the UP. For the case $V_E < V_p$, no E singular control exists; however, it will be seen later that the portion of the y-axis inside the closed Barrier is a Dispersal surface.

For $s_o < s < \pi$ (note as with the Limited Pursuer model, the problem is symmetric in S), the costate solutions are

$$\lambda_x(\tau) = \sin\left(s+\frac{V_p}{R_p}\tau\right)\Big/\left[V_E - V_p\cos s\right] \tag{9.20}$$

$$\lambda_y(\tau) = -\cos\left(s+\frac{V_p}{R_p}\tau\right)\Big/\left[V_E - V_p\cos s\right] \tag{9.21}$$

and

$$\theta_E^*(\tau) = -\left(s+\frac{V_p}{R_p}\tau\right) . \tag{9.22}$$

Since P is turning left at the rate $\frac{V_p}{R_p}$, Eq (9.22) shows that E is in straight line motion in real space. The state equation solution is

$$x(\tau) = (\ell+V_E\tau)\sin\left(s+\frac{V_p}{R_p}\tau\right) - R_p\left(1-\cos\frac{V_p}{R_p}\tau\right) \tag{9.23}$$

$$y(\tau) = -(\ell+V_E\tau)\cos\left(s+\frac{V_p}{R_p}\tau\right) + R_p\sin\frac{V_p}{R_p}\tau \tag{9.24}$$

and $A(\tau)$ is

$$A(\tau) = \frac{R_p}{V_E - V_p\cos s}\left[-\cos s + \cos\left(s+\frac{V_p}{R_p}\tau\right)\right] . \tag{9.25}$$

Note that $A(\tau)$ initially goes negative off of ζ and switching occurs when

$$\frac{V_p}{R_p}\tau_s = 2(\pi - s) . \tag{9.26}$$

At switching $x(\tau)$ is

$$x(\tau)\Big|_{\tau_s} = -\left[\ell + 2R_p\frac{V_E}{V_p}(\pi-s)\right]\sin s - R_p(1-\cos 2s) < 0$$

i.e. $x(\tau_s)$ is always negative. Switching in reality never occurs since the Dispersal surface at $x=0$, $y>0$ is intersected first.

The equations for the Barrier are simply a specialization of the equations for the UP of ζ to $S = S_o = \cos^{-1}\frac{V_E}{V_P}$ with the term $V_E - V_P \cos S$ missing i.e.

$$v_x(T) = \sin\left(S_o + \frac{V_P}{R_P}T\right) \tag{9.27}$$

$$v_y(T) = -\cos\left(S_o + \frac{V_P}{R_P}T\right) \tag{9.28}$$

$$\tilde{\Theta}_E^*(T) = -\left(S_o + \frac{V_P}{R_P}T\right) \tag{9.29}$$

$$\tilde{A}(T) = R_P\left[-\cos S_o + \cos\left(S_o + \frac{V_P}{R_P}T\right)\right] \tag{9.30}$$

$$x(T) = (\ell + V_E T)\sin\left(S_o + \frac{V_P}{R_P}T\right) - R_P\left(1 - \cos\frac{V_P}{R_P}T\right) \tag{9.31}$$

$$y(T) = -(\ell + V_E T)\cos\left(S_o + \frac{V_P}{R_P}T\right) + R_P \sin\frac{V_P}{R_P}T \tag{9.32}$$

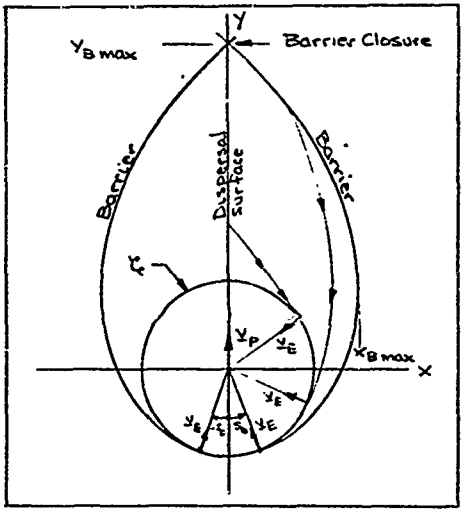

Figure 40: Limited Evader Barrier

Typical results are shown in Figure 40. As can be seen, the Barrier always exists for $\frac{V_E}{V_P} < 1$ and is always closed. The closure dimensions of the Barrier are shown in Figures 41 and 42. This finishes problem 2) for the Limited Evader model.

For problem 3) (i.e. $a>0, b>0, c>0$), the general purpose payoff is not applied since E's control appears in the Mayer payoff; however, it is clear that on ℓ_c E has the capability to always effect at least a mutual kill if not a kill of P.

A specific example shows how the role logic can develope. Two specific cases are shown in Figure 43; one with the Limited Pursuer Barrier closed, the other with the Limited Pursuer Barrier open. As mentioned previously, the Limited Evader Barrier is always closed.

The role logic for the $V_E > V_P$ condition is not very interesting since E can effect any outcome he desires. However, for $V_E < V_P$, the role logic depends on the parameters of the problem which determine the specific cases in Figure 43.

Assume that $V_P = 800 \frac{ft}{sec}$, $V_E = 720 \frac{ft}{sec}$, $a_{\perp_P} = 5 g_s$ (i.e. $R_P = 4000$ ft) and $\ell = 1000$ ft. $S_o = 25.84°$, $\frac{\ell}{R_P} = .25$ and Figure 7 indicates that the Limited Pursuer Barrier is closed, i.e. case 1, at $\frac{Y_c}{R_P} = .315$ or $Y_c = 1260$ ft. Figures 41 and 42 indicate that the Limited Evader Barrier closes at $Y_c/R_P \simeq 2.41$ (i.e. $Y_c = 9640$ ft) with $\frac{X}{R_P}\Big|_{max} = .70$ (i.e. $X_{max} = 2800$ ft). Note how the Barrier of the Limited Evader is much larger and completely encloses the Barrier of the Limited Pursuer and reflects E's superiority in an aggressive role. Note also that if the actual Evader did have the high maneuverability modelled in the

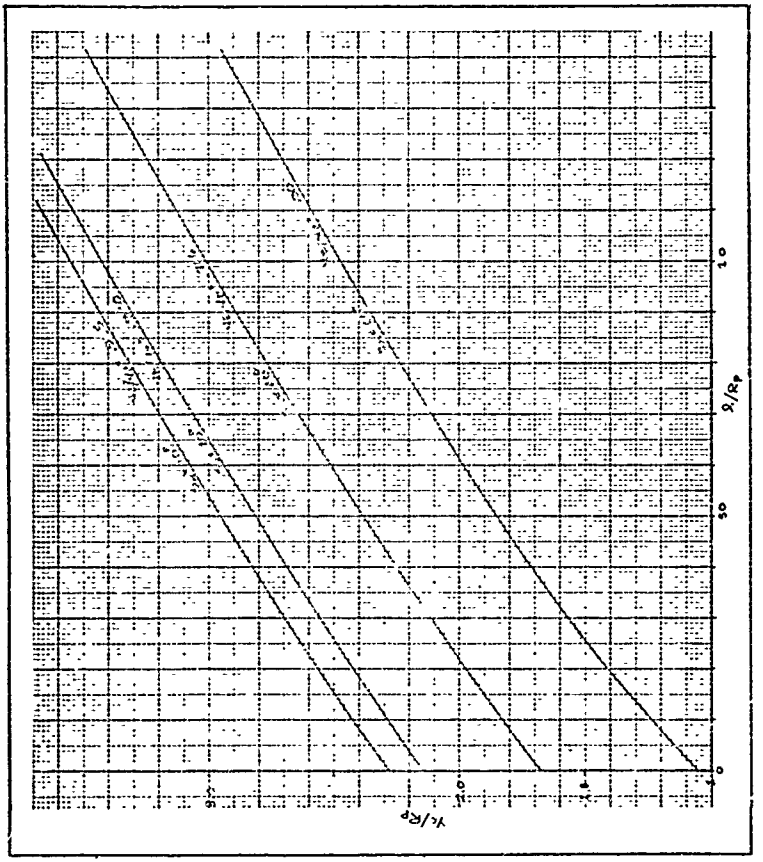

Figure 41: $\frac{\gamma_c}{R_p}$ Closure Conditions

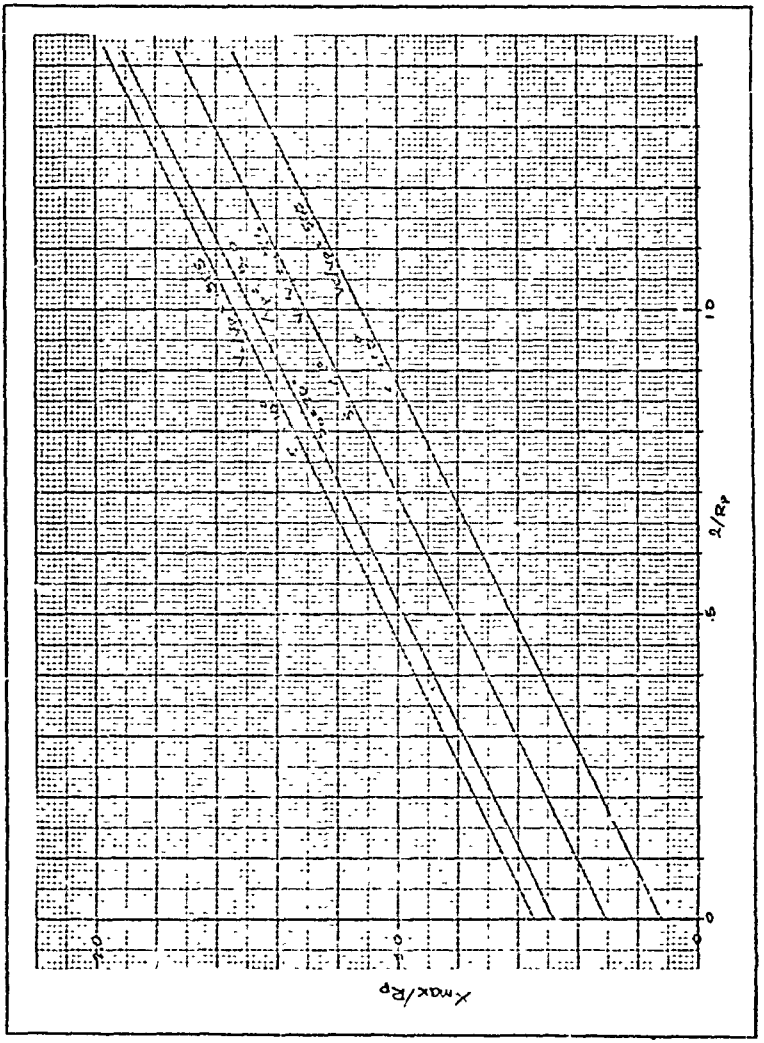

Figure 42: $\frac{X_{max}}{R_p}$ Conditions

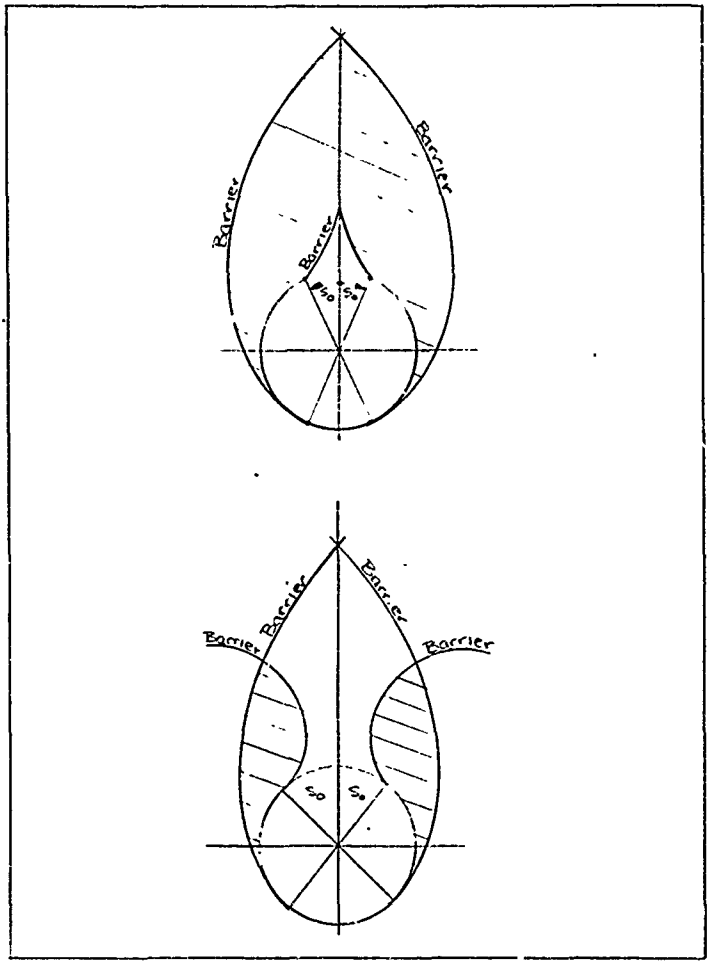

Figure 43: Limited Pursuer/Evader Role Logic

problem, how the results of the Limited Pursuer model alone would lead to an incomplete picture of his capability. However, with both analysis, it is clear that E should adopt an aggressive policy i.e. kill opponent, mutual kill, draw. The outcome of the combat is then largely dependent on the state of the game initially and P's mission. If P prefers a draw to a mutual kill, then outside the larger Barrier P should do a tight turn and use his velocity advantage in line of sight evasion to escape. If E is initially inside the larger Barrier (the larger Barrier is about a one mile wide and two miles in front of P), it is impossible for P to do better than possibly a mutual kill. If P decides to evade here, he is hopelessly captured. Finally, if P prefers a mutual kill to a draw, then the mutual kill will be the outcome regardless of E's initial position.

If P can improve his velocity to open the Limited Pursuer Barrier, the roll logic remains the same except now the cross-hatched area (where E has a definite advantage) is much smaller and a chance for a mutual kill is much larger for P.

3. 2D Limited Pursuer-Evader Model:

Because player controls appeared directly in the general purpose payoff (i.e. problem 3) where $a>0, b>0, c>0$), this problem was not solved in the previous two examples. The purpose here is to simply demonstrate that the general purpose payoff can be applied and that the automatic role determination near ℓ_e is structured inherently in the payoff function.

The state equations are the same as Eq (6.1) except that time,

t, is now made a state variable whose differential equation is

$$\dot{t} = 1 \quad . \tag{9.33}$$

The characterization of $\mathcal{C}$ is the same as Eq (6.3) except for the added state variable i.e.

$$t(t_f) = h_4(\underline{s}) = s_3 \quad . \tag{9.34}$$

The general purpose payoff is the Mayer form

$$J = \frac{a+b}{2} - \frac{1}{2}\left[a\cos s_1 + b\cos(s_2 - s_1)\right] + c s_3 \cos s_1 \tag{9.35}$$

ME1 is the same as Eq (6.6) except

$$H_o = V_E\left[\lambda_x \sin\theta + \lambda_y \cos\theta\right] - \lambda_y V_p + \lambda_t \tag{9.36}$$

where λ_t is the costate variable for the state t .

The form of the controls remains the same as Eqs (6.8) and (6.10).

ME2 is the same as Eq (6.21) except the 1 is replaced with λ_t i.e.

$$-\frac{V_p}{R_p}\left|A_\theta\right| + \frac{V_E}{R_E}\left|\lambda_\theta\right| + V_E\left[\lambda_x \sin\theta + \lambda_y \cos\theta\right] - \lambda_y V_p + \lambda_t = 0 \tag{9.37}$$

The costate equations are the same as Eq (6.22) except for the added costate equation

$$\dot{\lambda}_t = -\frac{\partial H}{\partial t} = 0 \quad \Rightarrow \quad \lambda_t = \text{constant} \quad . \tag{9.38}$$

The transversality conditions $\frac{\partial \phi(\underline{s})}{\partial s_j} \equiv \frac{\partial J(\underline{s})}{\partial s_j} = \sum_{i=1}^{4} \lambda_i \frac{\partial h_i(\underline{s})}{\partial s_j}$

yield

$$J=1 \Rightarrow \frac{\partial J}{\partial s_1} = \left(\frac{a}{2} - c s_3\right)\sin s_1 - \frac{b}{2}\sin(s_2 - s_1) = \tag{9.39}$$
$$= \ell\left[\lambda_x(t_f)\cos s_1 - \lambda_y(t_f)\sin s_1\right]$$

$$j=2 \Rightarrow \frac{\partial J}{\partial s_2} = \frac{b}{2}\sin(s_2-s_1) = \lambda_\theta(t_f) \qquad (9.40)$$

$$j=3 \Rightarrow \frac{\partial J}{\partial s_3} = c\cos s_1 = \lambda_t(t_f) \quad . \qquad (9.41)$$

Substituting Eq (6.3) into Eq (6.9) for $A_\theta(t_f)$ yields

$$A_\theta(t_f) = [x\lambda_y - y\lambda_x - \lambda_\theta]\Big|_{t_f} = [\ell\sin s_1\lambda_y - \ell\cos s_1\lambda_x - \lambda_\theta]\Big|_{t_f} \quad . \qquad (9.42)$$

Substituting Eq (9.40) for λ_θ and Eq (9.39) for $\ell\lambda_x(t_f)\cos s_1$, into Eq (9.42) yields

$$A_\theta(t_f) = -(a/2 - ct_f)\sin s_1 \quad . \qquad (9.43)$$

The controls on $\mathcal{C}_e$ are therefore

$$\alpha^*(t_f) = -\operatorname{sgn} A_\theta(t_f) = \operatorname{sgn}[(a/2 - ct_f)\sin s_1] \qquad (9.44)$$

$$\beta^*(t_f) = \operatorname{sgn}\lambda_\theta(t_f) = \operatorname{sgn}[\sin(s_2-s_1)] = -\operatorname{sgn}[\sin(s_1-s_2)] \quad . \qquad (9.45)$$

If it is assumed at termination that the combatants weight heavily a good firing position (i.e. advantageous s_1) then $a/2 \gg ct_f$ and Eq (9.44) becomes

$$\alpha^*(t_f) = \operatorname{sgn}[\sin s_1] \quad . \qquad (9.46)$$

Figure 44 is a map of Eqs (9.45) and (9.46) for the controls on the UP of $\mathcal{C}_e$. Note that P's controls in the UP of $\mathcal{C}_e$ are the same as in

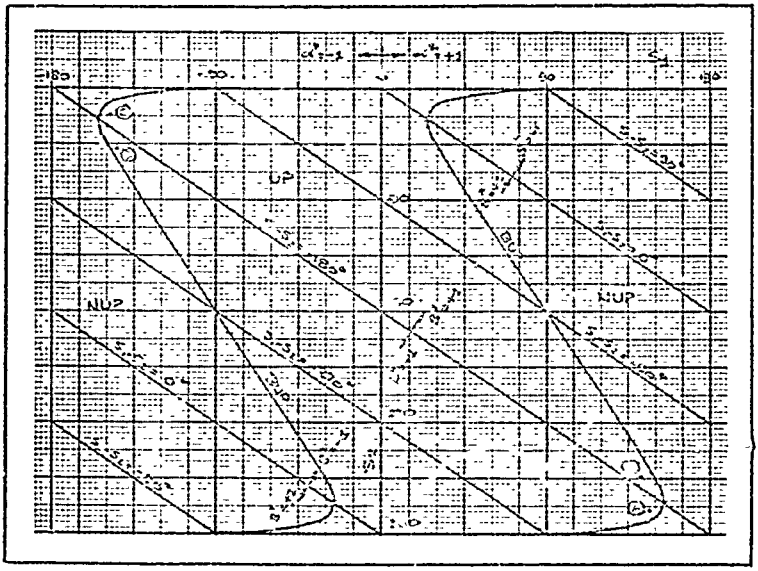

Figure 44: General Purpose Payoff χ Controls

Figure 21; however, E's controls in the UP of χ are the exact opposite of those in Figure 21. As such, P is turning into the line of sight P to E; likewise E is turning into the line of sight E to P. Note how for points such as A B C D, where E was evading in Figure 21, E is now turning into P to attack.

Results and Conclusions

The general purpose payoff and its use in the role decision logic of some illustrative models has been demonstrated. The work is far from complete and continued research in this area is suggested. What ever method is used to develope a role decision logic, the Barrier's under reversed role situations will have an important function in that role decision logic.

X Conclusions and Recommendations

The main conclusions of this dissertation are progressively contained in the last paragraphs of the main chapters. A summary of these conclusions shows the following:

1) "Dynamic Modelling" was most useful in learning the influence of added parameters on the game solution as the air-to-air combat model was made more complex and realistic. Had the simpler models not been solved first, the solution of the more complex models would have been much more difficult.

2) The differential game Barrier is a tool that analytically reflects the optimal combat capability of an aircraft. The Barrier shape and sensitivity to aircraft parameter changes is a useful tool to ferret out those aircraft design parameters that most affect air-to-air combat outcome. Results of Barrier sensitivity analysis in this dissertation show that the ability to longitudinally accelerate (i.e. better thrust to weight ratio) yields the best improvement in fighter aircraft combat capability. Since the turning g structural limits of most fighter aircraft are near or exceed sustained human capability, this also suggests that effort to enhance fighter combat capability might be best spent in another area - such as thrust to weight ratio.

3) For design purposes, results of the 3D models in this dissertation show that the important design tradeoffs are revealed in the 2D models.

4) Variable velocity magnitude did not significantly affect the Barrier closure conditions of the simpler constant velocity magnitude models.

5) As demonstrated in Chapters V and VII, differential game results for simplified models can be properly applied to give useful and meaningful results for real Air Force problems. The techniques of Chapters V and VII represent the first known practical applications of differential game results to a real Air Force air-to-air combat problem.

6) The 3D Limited Pursuer model is the only completely solved 3D air-to-air combat model that includes a closed form control bank schedule. This maneuver has been called the "slice maneuver" by tacticians.

Based on the research in this dissertation, the following recommendations are made:

1) The relative aircraft evaluation of Chapter VII should be designed into a computer program whose output is the map of Figure 32. The Air Force Flight Dynamics Laboratory presently plans to do this.

2) The coordinate system used in the 3D Limited Pursuer-Evader model is a physically appealing coordinate system for characterizing approximate 3D control laws. Based on the way the singular surfaces of the 2D Limited Pursuer-Evader model disappeared in the 2D Linearized

Drag Polar model, it is postulated that the "impasse" encountered with the singular controls in the 3D Limited Pursuer-Evader model will not exist for a 3D Linearized Drag Polar model using the same 3D relative coordinate system. This latter 3D problem should be analyzed to characterize the approximate 3D control laws.

3) The general purpose payoff for problem 3, i.e. $a>0$, $b>0$, $c>0$ started in Chapter IX should be examined in detail. When forward solving differential game numerical techniques are developed into useful computer programs, the programs should be capable of handling the general purpose payoff.

Bibliography

[1] Anderson, Gerald M., "Necessary Conditions for Singular Solutions in Differential Games with Controls Appearing Linearly", Proceedings of the First International Conference on the Theory and Application of Differential Games, University of Massachusetts, Amherst, Massachusetts, September 29 to October 1, 1969.

[2] Baron, S., "Differential Games and Optimal-Pursuit-Evasion Strategies", Ph.D Dissertation, Engineering and Applied Physics, Harvard University, 1966.

[3] Berkovitz, L.D., "A Variational Approach to Differential Games", Advances in Game Theory, Annals of Math. Study 52, Princeton University Press, 1964, pp 127-174.

[4] Bryson, A.E., and Y.C. Ho, Applied Optimal Control. Waltham, Massachusetts: Blaisdell Publishing Company, 1969.

[5] Cootz, T.A., "The Calculation of a Barrier for a Pursuit-Evasion Game", McDonnell Douglas Astronautics Company, Rept # DAC-63260, May 1969.

[6] Ho, Y.C., A.E. Bryson and S. Baron, "Differential Games and Optimal Pursuit-Evasion Strategies", IEEE Transactions on Automatic Control, Vol. AC-10, No.-4, 1965, pp 385-389.

[7] Isaacs, R., Differential Games, New York: John Wiley & Sons, 1965.

[8] Leatham, A.L., "Some Theoretical Aspects of Nonzero Sum Differential Games and Applications to Combat Problems", Ph.D Dissertation, DS/MC/71-3, Air Force Institute of Technology, School of Engineering, WPAFB, Ohio, June 1971.

[9] Leitmann, G., "An Introduction to Optimal Control, New York: McGraw-Hill Book Company, 1966

[10] Miller, E.L., "Tactics Optimization Study: Constant Speed Case", ASBES WP68-8, Aeronautical Systems Division, Wright Patterson AFB, Ohio, 1968.

[11] Othling, W.L., "Application of Differential Game Theory to Pursuit-Evasion Problems of Two Aircraft", Ph.D Dissertation, DS/MC/67-1, Air Force Institute of Technology, School of Engineering, WPAFB, Ohio June 1970.

[12] Perkins, C.D. and R.E. Hage, Airplane Performance Stability and Control, New York: John Wiley & Sons, 1963.

[13] Roberts, D.A. and R.C. Montgomery, "Development and Application of a Gradient Method for Solving Differential Games", NASA TN D-6502, Langley Research Center, Hampton, Virginia, Nov 1971.

[14] Starr, A.W. and Y.C. Ho, "Nonzero-Sum Differential Games", Journal of Optimization Theory and Application, Vol 3, No. 3 March, 1969, pp 184-206.

[15] Williamson-Nobel, S.M.D., "Toward a Differential Game Solution to a Practical Two-Aircraft Pursuit-Evasion Problem in Three Dimensional Space", MS Thesis, GA/MC/71-5, Air Force Institute of Technology, School of Engineering, WPAFB, Ohio, June 1971.

Appendix A

Analysis Details of the Limited Pursuer Model

1. State Equation Formulation of 2D Model:

Refer to Figure 3. The position of E as observed by P is $\underline{X}$.

$$\underline{X} = x\underline{1}_x + y\underline{1}_y \tag{A.1}$$

The rotation rate of $\underline{1}_y$ and $\underline{1}_x$ is

$$\underline{\omega} = \dot{\theta}_P \underline{1}_z = \frac{a_{\perp P}}{V_P}\underline{1}_z = \frac{V_P}{R_P}\alpha\underline{1}_z \tag{A.2}$$

where

$a_{\perp P} = V_P^2/R_P$ = acceleration of P perpendicular to $\underline{V}_P$

R_P = turning radius of P

and

$$-1 \leq \alpha \leq +1 \tag{A.3}$$

The scalar, α , is P's control i.e. $\alpha = +1$ is a hard turn to the right and $\alpha = -1$ is a hard turn to the left. Now $\underline{X}_E$ can be written

$$\underline{X}_E = \underline{X}_P + \underline{X} \tag{A.4}$$

and

$$\dot{\underline{X}}_E = \dot{\underline{X}}_P + \dot{\underline{X}}\Big|_r + \underline{\omega} \times \underline{X} \tag{A.5}$$

where

$\dot{\underline{X}}\Big|_r$ = velocity of X as observed in the rotating coordinate frame.

and

$$\underline{\omega} \times \underline{X} = \begin{vmatrix} \underline{1}_v & \underline{1}_\perp & \underline{1}_z \\ 0 & 0 & \frac{V_p}{R_p}\alpha \\ y & x & 0 \end{vmatrix} = -x\frac{V_p}{R_p}\alpha\,\underline{1}_v + y\frac{V_p}{R_p}\alpha\,\underline{1}_\perp \quad . \tag{A.6}$$

Solving Eq (A.5) for $\dot{\underline{x}}|_r$ yields

$$\dot{\underline{x}}|_r = \dot{\underline{x}}_E - \dot{\underline{x}}_p - \underline{\omega} \times \underline{x} \tag{A.7}$$

and since

$$\dot{\underline{x}}_p = \underline{V}_p = V_p \underline{1}_v \tag{A.8}$$

$$\dot{\underline{x}}_E = \underline{V}_E = V_E \sin\theta_E \underline{1}_\perp + V_E \cos\theta_E \underline{1}_v \tag{A.9}$$

then Eq (A.7) becomes

$$\dot{\underline{x}}|_r = \left(V_E \sin\theta_E - y\frac{V_p}{R_p}\alpha\right)\underline{1}_\perp + \left(V_E \cos\theta_E - V_p + x\frac{V_p}{R_p}\alpha\right)\underline{1}_v \quad . \tag{A.10}$$

From Eq (A.1) $\dot{\underline{x}}|_r$ is

$$\dot{\underline{x}}|_r = \dot{x}\,\underline{1}_\perp + \dot{y}\,\underline{1}_v \quad . \tag{A.11}$$

Eqs (A.10) and (A.11) yield the state equation

$$\dot{\underline{x}}|_r = \begin{bmatrix} \dot{x} \\ \dot{y} \end{bmatrix} = \begin{bmatrix} V_E \sin\theta_E - y\frac{V_p}{R_p}\alpha \\ V_E \cos\theta_E - V_p + x\frac{V_p}{R_p}\alpha \end{bmatrix} \quad . \tag{A.12}$$

2. Problem Backward Solution From $\mathcal{C}$ for 2D Model:

We begin by determining the controls on $\mathcal{C}$. Eqs (4.19) and (4.10) indicate that

$$\tan\theta_E^*(t_f) = \left.\frac{\lambda_x}{\lambda_y}\right|_{t_f} = \tan s \qquad \text{(A.13)}$$

so that

$$\theta_E^*(t_f) = s \quad . \qquad \text{(A.14)}$$

Since $A|_{t_f} = \ell \sin s\, \lambda_y(t_f) - \ell \cos s\, \lambda_x(t_f)$, this and Eq (4.19) shows that

$$A|_{t_f} = 0 \quad . \qquad \text{(A.15)}$$

Substituting Eq (A.15), and Eq (4.19) for $\lambda_x(t_f)$ into Eq (4.17) yields ME2 on $\mathcal{C}$ as

$$V_E\, \lambda_y(t_f)\sqrt{1+\tan^2 s} - V_p \lambda_y(t_f) + 1 = 0 \quad . \qquad \text{(A.16)}$$

Eqs (A.16) and (4.19) show that

$$\lambda_y(t_f) = \frac{\cos s}{V_p \cos s - V_E} \quad .$$

$$\lambda_x(t_f) = \frac{\sin s}{V_p \cos s - V_E} \qquad \text{(A.17)}$$

Note that $V_p \cos s - V_E$ is the rate at which P is closing on E at termination.

Since $A|_{t_f} = 0$ on $\mathcal{C}$, we must examine $-\dot{A}|_{\mathcal{C}}$ to determine $\alpha^*|_{\mathcal{C}}$.

$$\dot{A} = \dot{x}\lambda_y + x\dot{\lambda}_y - \dot{y}\lambda_x - y\dot{\lambda}_x \qquad \text{(A.18)}$$

Substituting the state and costate equations into Eq (A.18) yields

$$\dot{A} = V_p \lambda_x \quad . \tag{A.19}$$

Therefore, an infinitesinal distance away from ζ , α^* is

$$\alpha^*|_{\zeta} = -\operatorname{sgn} A|_{\zeta} = -\operatorname{sgn}(\dot{A}|_{\zeta}) = \operatorname{sgn} \dot{A}|_{\zeta} =$$

$$= \operatorname{sgn} \lambda_x|_{\zeta} = \operatorname{sgn}\left(\frac{\sin s}{V_p \cos s - V_E}\right) = \operatorname{sgn}(\sin s) \quad . \tag{A.20}$$

The last equality in Eq (A.20) will be justified later by showing that on the UP of ζ the closing rate $V_p \cos s - V_E > 0$. Note that $\dot{A}|_{\zeta} = 0$ for $s = 0$ (i.e. a direct tail chase termination) and the possibility of a singular control here. Now we examine the singular control necessary conditions.

First it is necessary that

$$A = x\lambda_y - y\lambda_x \equiv 0 \quad . \tag{A.21}$$

Eqs (4.10) and (A.21) yield

$$\tan \theta_E^* = \frac{\lambda_x}{\lambda_y} = \frac{x}{y} \tag{A.22}$$

implying the closed form control for E, while P is possibly singular, is line of sight evasion. Now the second necessary condition is

$$\dot{A} = V_p \lambda_x \equiv 0 \tag{A.23}$$

implying that

$$\lambda_x \equiv 0 \quad . \tag{A.24}$$

Eqs (A.22) and (A.21) show that,

$$X \equiv 0 \qquad \text{and} \qquad \Theta_E^* = 0 \tag{A.25}$$

since $\lambda_Y \equiv 0$ is a trivial problem with $\underline{\lambda} = 0$. The third necessary condition is

$$\ddot{A} = V_P \dot{\lambda}_X = -\frac{V_P^2}{R_P} \lambda_Y \alpha \equiv 0 \tag{A.26}$$

implying that

$$\alpha_s = 0 \tag{A.27}$$

is the candidate singular control in α. Since α_s is P's control, the last necessary condition is Eq (2.16), i.e.

$$(-1)^q \frac{\partial}{\partial \alpha}\left[\frac{d^{2q} H_P}{dt^{2q}}\right] \equiv (-1)^1 \frac{\partial}{\partial \alpha}\left[\frac{d^2 A}{dt^2}\right] \geq 0 \tag{A.28}$$

or

$$-\frac{\partial}{\partial \alpha}\left[-\frac{V_P^2}{R_P} \lambda_Y \alpha\right] \geq 0 \tag{A.29}$$

or finally

$$\lambda_Y \geq 0 \tag{A.30}$$

Since $\alpha_s = 0$, Eq (4.18) shows that $\dot{\underline{\lambda}} = 0$ implying $\underline{\lambda}$ = constant vector. Because of Eqs (A.24) and (A.17), the P singular surface meets $\mathcal{C}_E$ at $S = 0$ and

$$\underline{\lambda} = \text{constant vector} = \begin{bmatrix} 0 \\ \dfrac{1}{V_P - V_E} \end{bmatrix} \tag{A.31}$$

All the necessary conditions of the singular control are met provided $\lambda_y \geq 0$ i.e. $V_p \geq V_E$. The singular surface in the reduced ξ is simply the y - axis and represents a non-turning direct tail chase. We now continue with the backward solution and examine the optimal trajectories backward from ξ_f for $S>0$ (note $S<0$ is symmetric about y-axis).

Solution of the costate Eq (4.18) backward from ξ_f with the boundary conditions of Eq (A.17) yields

$$\lambda_x(T) = \frac{\sin\left(S+\frac{V_p}{R_p}T\right)}{V_p\cos S - V_E}$$

$$\lambda_y(T) = \frac{\cos\left(S+\frac{V_p}{R_p}T\right)}{V_p\cos S - V_E} \qquad \text{(A.32)}$$

where

$T = t_f - t$ time backwards from ξ_f.

By Eqs (4.10) and (A.32) it is seen that

$$\tan\theta_E^* = \frac{\lambda_x}{\lambda_y} = \tan\left(S+\frac{V_p}{R_p}T\right) \qquad \text{(A.33)}$$

implying

$$\theta_E^*(T) = S+\frac{V_p}{R_p}T \quad . \qquad \text{(A.34)}$$

Since $\frac{d\theta_E}{dt} = -\frac{d\theta_E}{dT} = -\frac{V_p}{R_p}$ and since we know P is turning into E at the rate $\frac{V_p}{R_p}$, this shows that in the realistic ξ, E is in straight line motion. We now solve for A to check switching of α from +1.

Eqs (A.19) and (A.32) show

$$\frac{dA}{dT} = -V_p\lambda_x(T) = \frac{-V_p\sin\left(S+\frac{V_p}{R_p}T\right)}{V_p\cos S - V_E} \qquad \text{(A.35)}$$

Integrating Eq (A.35) with the boundary condition of Eq (A.15) yields

$$A(\tau) = \frac{-R_P}{V_P \cos S - V_E}\left[\cos S - \cos\left(S + \frac{V_P}{R_P}\tau\right)\right] \quad . \qquad (A.36)$$

Eq (A.36) shows that A initially goes negative (as suggest by $-\dot{A}\big|_{\zeta} < 0$) and then positive when

$$\frac{V_P}{R_P}\tau = 2(\pi - S) \quad . \qquad (A.37)$$

The angle $2(\pi-S)$ can physically be shown to be the circular angle P must turn through going backwards to recross E's straight line path. As will be shown later, the Barrier is closed for realistic system parameters and the $S>0$ trajectories intersect the Barrier before the switching condition of Eq (A.37).

If we examine the trajectories branching off the y-axis singular surface for $\alpha^* = +1$, we find the costate solutions have the same form as Eq (A.32) only with $S \equiv 0$, i.e.

$$\lambda_x(\tau_s) = \frac{\sin\left(\frac{V_P}{R_P}\tau_s\right)}{V_P - V_E} \quad . \qquad (A.38)$$

$$\lambda_y(\tau_s) = \frac{\cos\left(\frac{V_P}{R_P}\tau_s\right)}{V_P - V_E}$$

where

τ_s = backwards time off singular surface. Likewise, $A(\tau_s)$ is the specialization of Eq (A.36) to $S \equiv 0$ i.e.

$$A(\tau_s) = \frac{-R_P}{V_P - V_E}\left[1 - \cos\left(\frac{V_P}{R_P}\tau_s\right)\right] \quad . \qquad (A.39)$$

Note that $A(\tau_s)$ initially goes negative off the y-axis singular surface, goes to zero when $\frac{V_p}{R_p}\tau_s = 2\pi$ but does not switch. Like the $S>0$ trajectories, these trajectories off the portion of the y-axis inside the closed Barrier, intersect the Barrier and terminate.

For the $S>0$ case, and assuming A does not switch, $\alpha^* = +1$ and $\theta_E^* = S + \frac{V_p}{R_p}\tau$. Substituting these controls into the state Eq (A.12) and solving backwards from τ_f with the boundary conditions of Eq (4.3) yields

$$x(\tau) = (\ell - V_E\tau)\sin(S + \frac{V_p}{R_p}\tau) + R_p(1 - \cos\frac{V_p}{R_p}\tau) \quad \text{(A.40)}$$

$$y(\tau) = (\ell - V_E\tau)\cos(S + \frac{V_p}{R_p}\tau) + R_p\sin\frac{V_p}{R_p}\tau \quad \text{(A.41)}$$

3. State Equation Formulation of 3D Model:

The position of E as observed by P is $\underline{X}$.

$$\underline{x} = x\,\underline{1}_x + y\,\underline{1}_y + z\,\underline{1}_z \quad \text{(A.42)}$$

The instantaneous rotation rate of the $\underline{1}_x, \underline{1}_y, \underline{1}_z$ axes system is

$$\underline{\omega} = \frac{V_p}{R_p}(\sin\phi\,\underline{1}_x - \cos\phi\,\underline{1}_z)\,\alpha \quad \text{(A.43)}$$

where

$$0 \le \phi \le 2\pi$$
$$0 \le \alpha \le 1 \quad \text{(A.44)}$$

Eq (A.7) applies in this case with

$$\dot{\underline{x}}_P = \underline{V}_P = V_P\,\underline{1}_y \quad \text{(A.45)}$$

$$\dot{\underline{x}}_E = \underline{V}_E = V_E(\bar{\ell}\,\underline{1}_x + \bar{m}\,\underline{1}_y + \bar{n}\,\underline{1}_z) \quad \text{(A.46)}$$

where

$$\bar{\ell}^2 + \bar{m}^2 + \bar{n}^2 = 1 \quad . \tag{A.47}$$

Since

$$\underline{\omega} \times \underline{x} = \frac{V_p}{R_p} \alpha \begin{vmatrix} \underline{1}_x & \underline{1}_y & \underline{1}_z \\ \sin\phi & 0 & -\cos\phi \\ x & y & z \end{vmatrix} = \tag{A.48}$$

$$= \frac{V_p}{R_p} \alpha \left[y\cos\phi\, \underline{1}_x - (x\cos\phi + z\sin\phi)\, \underline{1}_y + y\sin\phi\, \underline{1}_z \right]$$

then Eq (A.7) becomes

$$\dot{\underline{x}}\Big|_r = \left[V_E \bar{\ell} - \frac{V_p}{R_p} \alpha\, y\cos\phi \right] \underline{1}_x + \tag{A.49}$$

$$+ \left[V_E \bar{m} - V_p + \frac{V_p}{R_p} \alpha\, (x\cos\phi + z\sin\phi) \right] \underline{1}_y +$$

$$+ \left[V_E \bar{n} - \frac{V_p}{R_p} \alpha\, y\sin\phi \right] \underline{1}_z \quad .$$

Since

$$\dot{\underline{x}}\Big|_r = \dot{x}\,\underline{1}_x + \dot{y}\,\underline{1}_y + \dot{z}\,\underline{1}_z \tag{A.50}$$

the state equations are

$$\dot{\underline{x}}\Big|_r = \begin{bmatrix} \dot{x} \\ \dot{y} \\ \dot{z} \end{bmatrix} = \begin{bmatrix} V_E \bar{\ell} - \frac{V_p}{R_p} \alpha\, y\cos\phi \\ V_E \bar{m} - V_p + \frac{V_p}{R_p} \alpha\, (x\cos\phi + z\sin\phi) \\ V_E \bar{n} - \frac{V_p}{R_p} \alpha\, y\sin\phi \end{bmatrix} \tag{A.51}$$

Appendix B

Analysis Details of the Limited Pursuer-Evader Model

1. State Equation Formulation:

The position of E as observed by P is $\underline{X}$.

$$\underline{X} = X\underline{1}_{\perp} + Y\underline{1}_{V} \tag{B.1}$$

The rotation rate of $\underline{1}_{V}$ and $\underline{1}_{\perp}$ is

$$\underline{\omega}_P = \dot{\theta}_P \underline{1}_z = \frac{a_{\perp P}}{V_P}\underline{1}_z = \frac{V_P}{R_P}\alpha\underline{1}_z \tag{B.2}$$

where

$a_{\perp P} = V_P^2/R_P$ = acceleration of P perpendicular to $\underline{V}_P$

R_P = turning radius of P

and $$-1 \leq \alpha \leq +1 \tag{B.3}$$

The scalar, α, is P's control.

The vector $\underline{X}_E$ can be written

$$\underline{X}_E = \underline{X}_P + \underline{X} \tag{B.4}$$

and

$$\dot{\underline{X}}_E = \dot{\underline{X}}_P + \dot{\underline{X}}\big|_r + \underline{\omega}_P \times \underline{X} \tag{B.5}$$

where

$\dot{\underline{X}}\big|_r$ = velocity of E as observed in the rotating coordinate frame.

Since

$$\underline{\omega}'_P \times \underline{X} = -x \frac{V_P}{R_P} \alpha \underline{1}_v + y \frac{V_P}{R_P} \alpha \underline{1}_\perp \tag{B.6}$$

and $$\dot{\underline{X}}_P = \underline{V}_P = V_P \underline{1}_v \tag{B.7}$$

and $$\dot{\underline{X}}_E = \underline{V}_E = V_E \sin\theta \underline{1}_\perp + V_E \cos\theta \underline{1}_v \tag{B.8}$$

and $$\dot{\underline{X}}\Big|_r = \dot{x} \underline{1}_\perp + \dot{y} \underline{1}_v \tag{B.9}$$

then substituting Eqs (B.6), (B.7), (B.8), (B.9) into Eq (B.5) and solving for $\dot{\underline{X}}\Big|_r$ yields

$$\dot{\underline{X}}\Big|_r = \begin{bmatrix} \dot{x} \\ \dot{y} \end{bmatrix} = \begin{bmatrix} V_E \sin\theta - y \frac{V_P}{R_P} \alpha \\ V_E \cos\theta - V_P + x \frac{V_P}{R_P} \alpha \end{bmatrix} \tag{B.10}$$

From Figure 18 it is seen that

θ = Evader's velocity angle off = $\theta_E - \theta_P$ (B.11)

so $$\dot{\theta} \underline{1}_z = \underline{\omega}_E - \underline{\omega}_P \tag{B.12}$$

Similar to $\underline{\omega}_P$, $\underline{\omega}_E$ is

$$\underline{\omega}_E = \dot{\theta}_E \underline{1}_z = \frac{a_{\perp E}}{V_E} \underline{1}_z = \frac{V_E}{R_E} \beta \underline{1}_z \tag{B.13}$$

where

$a_{\perp E} = \frac{V_E^2}{R_E}$ = acceleration of E perpendicular to $\underline{V}_E$

R_E = turning radius of E

and

$$-1 \leq \beta \leq +1 \quad . \tag{B.14}$$

The scalar, β, is E's control. Substituting Eqs (B.2) and (B.13) into Eq (B.12) yields

$$\dot{\theta} = \frac{V_E}{R_E}\beta - \frac{V_P}{R_P}\alpha \quad . \tag{B.15}$$

The state equations for this model are therefore

$$\begin{bmatrix} \dot{x} \\ \dot{y} \\ \dot{\theta} \end{bmatrix} = \begin{bmatrix} V_E \sin\theta - y\frac{V_P}{R_P}\alpha \\ V_E \cos\theta - V_P + x\frac{V_P}{R_P}\alpha \\ \frac{V_E}{R_E}\beta - \frac{V_P}{R_P}\alpha \end{bmatrix} \quad . \tag{B.16}$$

2. Problem Backward Solution From ζ for 2D Model:

Equacions for the controls on the terminal surface ζ are found first. A rearrangement of Eq (6.24) yields

$$\tan s_1 = \lambda_x(t_f)/\lambda_y(t_f) \quad . \tag{B.17}$$

Note that both $A_\theta\big|_{t_f}$ and $\lambda_\theta\big|_{t_f} = 0$, so HE2 at t_f becomes

$$V_E\left[\lambda_x(t_f)\sin s_2 + \lambda_y(t_f)\cos s_2\right] - \lambda_y(t_f)V_P + 1 = 0 \quad . \tag{B.18}$$

Substituting Eq (B.17) for $\lambda_x(t_f)$ into Eq (B.18) and solving Eq (B.18) for $\lambda_y(t_f)$ yields

$$\lambda_y(t_f) = \frac{\cos s_1}{V_P\cos s_1 - V_E\cos(s_2 - s_1)} \quad . \tag{B.19}$$

Eq (B.19) substituted back into Eq (B.17) yields

$$\lambda_x(t_f) = \frac{\sin s_1}{V_P\cos s_1 - V_E\cos(s_2 - s_1)} \quad . \tag{B.20}$$

Note that $V_p\cos S_1 - V_E\cos(S_2 - S_1)$ is the rate at which P is closing on E at termination on $\mathcal{C}$. On the UP of $\mathcal{C}$, this term will be shown (see section on Barrier) to be positive.

Since both A_θ and λ_θ are zero on $\mathcal{C}$, $-\dot{A}_\theta$ and $-\dot{\lambda}_\theta$ must be examined to determine the controls an infinitesimal distance off $\mathcal{C}$. From Eq (6.22) we see that

$$-\dot{\lambda}_\theta\Big|_{\mathcal{C}} = V_E\left[\lambda_x(t_f)\cos S_2 - \lambda_y(t_f)\sin S_2\right] \quad . \quad \text{(B.21)}$$

Substituting Eqs (B.19) and (B.20) into Eq (B.21) yields

$$-\dot{\lambda}_\theta\Big|_{\mathcal{C}} = \frac{V_E(\sin S_1\cos S_2 - \cos S_1\sin S_2)}{V_p\cos S_1 - V_E\cos(S_2 - S_1)} = \frac{-V_E\sin(S_2 - S_1)}{V_p\cos S_1 - V_E\cos(S_2 - S_1)} \quad \text{(B.22)}$$

Assuming that the denominator of Eq (B.22) is positive, as previously indicated, the $\mathcal{B}^*$ control on $\mathcal{C}$ is

$$\mathcal{B}^*\Big|_{\mathcal{C}} = \operatorname{sgn}\left[\lambda_\theta(t_f)\right] = \operatorname{sgn}\left[-\dot{\lambda}_\theta(t_f)\right] = -\operatorname{sgn}\left[\sin(S_2 - S_1)\right] \quad \text{(B.23)}$$

Now from Eq (6.9) we get

$$\dot{A}_\theta = x\dot{\lambda}_y + \dot{x}\lambda_y - \dot{y}\lambda_x - y\dot{\lambda}_x - \dot{\lambda}_\theta \quad \text{(B.24)}$$

and substituting the state and costate equations yields

$$\dot{A}_\theta = V_p\lambda_x \quad \text{(B.25)}$$

Then

$$-\dot{A}_\theta\Big|_{\mathcal{C}} = -V_p\lambda_x(t_f) = \frac{-V_p\sin S_1}{V_p\cos S_1 - V_E\cos(S_2 - S_1)} \quad \text{(B.26)}$$

where Eq (B.20) has been substituted for $\lambda_x(t_f)$.

Therefore

$$\alpha^*\big|_{\ell} = -\mathrm{sgn}\left[A_\theta(t_f)\right] = -\mathrm{sgn}\left[-\dot{A}_\theta\big|_{\ell}\right] = \mathrm{sgn}\left[\sin s_1\right] \qquad \text{(B.27)}$$

where again it has been assumed that the denominator of Eq (B.26) is positive. Eqs (B.23) and (B.27) will be used later to determine the controls on the UP of ℓ.

To give more insight into the backward solution, the singular control necessary conditions are examined next. The E singular control conditions are examined first.

For E singular, it is first necessary that

$$\lambda_\theta = 0 \qquad \text{(B.28)}$$

Also it is necessary that

$$0 = \dot{\lambda}_\theta = v_E\left(\lambda_Y \sin\theta - \lambda_X \cos\theta\right) \qquad \text{(B.29)}$$

implying that

$$\tan\theta = \frac{\lambda_x}{\lambda_Y} \qquad \text{(B.30)}$$

It is also necessary that

$$0 = \ddot{\lambda}_\theta = v_E\left[\dot{\lambda}_Y \sin\theta + \lambda_Y \cos\theta\,\dot{\theta} - \dot{\lambda}_X \cos\theta + \lambda_X \sin\theta\,\dot{\theta}\right]. \qquad \text{(B.31)}$$

Substituting the state and costate equations into Eq (B.31) yields

$$0 = \ddot{\lambda}_\theta = \frac{v_E^2}{R_E}\beta\left[\lambda_X \sin\theta + \lambda_Y \cos\theta\right] . \qquad \text{(B.32)}$$

Eq (B.32) implied that either $\beta = 0$ or $\lambda_x \sin\theta + \lambda_y \cos\theta = 0$

for a finite time. If the latter case is true, then along with Eq (B.30) it implies that $\lambda_x = \lambda_y = 0$. Since $\lambda_\theta = 0$ already, the costate vector $\underline{\lambda} \equiv \underline{0}$ which is a trivial case. Therefore, the candidate singular E control, θ_s, is

$$\theta_s = 0 \tag{B.33}$$

implying that E is doing a non-turning straight line dash.

The last necessary condition to check is Eq (2.16), i.e.

$$(-1)^q \frac{\partial}{\partial \beta}\left[\frac{d^{2q}(H_{E\beta})}{dt^{2q}}\right] = (-1)^1 \frac{\partial}{\partial \beta}[\ddot{\lambda}_\theta] = -\frac{V_E^2}{R_E}[\lambda_x \sin\theta + \lambda_y \cos\theta] \leq 0. \tag{B.34}$$

Now Eq (B.30) implies

$$\sin\theta = \frac{\pm \lambda_x}{\sqrt{\lambda_x^2 + \lambda_y^2}} \quad , \quad \cos\theta = \frac{\pm \lambda_y}{\sqrt{\lambda_x^2 + \lambda_y^2}} \; . \tag{B.35}$$

The requirement of Eq (B.34) shows that the plus (+) signs in Eq (B.35) apply. The P singular control conditions are examined next.

For P singular it is first necessary that

$$A_\theta = x\lambda_y - y\lambda_x - \lambda_\theta = 0 \; . \tag{B.36}$$

Also it is necessary that (See Eq (B.25)

$$0 = \dot{A}_\theta = V_p \lambda_x \tag{B.37}$$

implying that

$$\lambda_x = 0 \tag{B.38}$$

Eq (B.38) implies that $\dot{\lambda}_y = 0$ (see Eq (6.22) i.e. λ_y is constant. Now it is also necessary that

$$\ddot{A}_\theta = V_p \dot{\lambda}_x = -\frac{V_p^2}{R_p} \lambda_y \alpha = 0 \tag{B.39}$$

implying either $\lambda_y = 0$ or $\alpha = 0$. Since $\lambda_y = 0$,

Eq (B.38) and Eq (B.36) imply $\underline{\lambda} \equiv \underline{0}$, this is a trivial case. Therefore, the candidate singular P control, α_s , is

$$\alpha_s = 0 \qquad (3.40)$$

Again it is seen that P is non-turning. The last necessary condition to check is Eq (2.16) i.e.

$$(-1)^q \frac{\partial}{\partial \alpha}\left[\frac{d^{2q}(H_{P_{\alpha}})}{dt^{2q}}\right] = (-1)^1 \frac{\partial}{\partial \alpha}\left[\ddot{A}_\Theta\right] = \frac{V_P^2}{R_P}\lambda_Y \geq 0 \qquad (B.41)$$

implying that

$$\lambda_Y \geq 0 \ . \qquad (B.42)$$

It is interesting to note that if P is singular then

$$\lambda_\Theta = x\lambda_Y \qquad (B.43)$$

and

$$\beta^* = \operatorname{sgn}\lambda_\Theta = \operatorname{sgn} x\lambda_Y = \operatorname{sgn} x \qquad (B.44)$$

the last equality coming from Eq (B.42). Eq (B.44) is a closed form control. If P is singular, then as x goes to zero λ_Θ goes to zero and E will switch to his singular arc provided

$$0 = \dot{\lambda}_\Theta = V_E(\lambda_Y \sin\Theta - \lambda_X \cos\Theta) = V_E\lambda_Y \sin\Theta \qquad (B.45)$$

i.e. as x goes to zero E will switch to his singular control if $\Theta = 0$. These two conditions, $x = 0$ and $\Theta = 0$, imply a direct tail chase. A direct tail chase therefore corresponds to the control case where both P and E are singular. The backward solution from the UP of ζ in the case where $\alpha^* \neq 0$ and $\beta^* \neq 0$ is done next.

Solution of the first two costate equations in Eq (6.22) backward using the boundary conditions of Eqs (B.19) and (B.20) yield

$$\lambda_x(T) = \sin\left(S_1+\alpha^*\frac{V_p}{R_p}T\right)\Big/\left[V_p\cos S_1 - V_E\cos(S_2-S_1)\right] \qquad (B.46)$$

$$\lambda_y(T) = \cos\left(S_1+\alpha^*\frac{V_p}{R_p}T\right)\Big/\left[V_p\cos S_1 - V_E\cos(S_2-S_1)\right] \qquad (B.47)$$

Solution of the $\dot{\Theta}$ equation backward in Eq (B.16) using the boundary conditions in Eq (6.3) yields

$$\Theta(T) = S_2 + \left(\frac{V_p}{R_p}\alpha^* - \frac{V_E}{R_E}\beta^*\right)T \qquad (B.48)$$

Substituting Eqs (B.46), (B.47) and (B.48) into the $\dot{\lambda}_\Theta$ (i.e. backward costate equation) in Eq (6.22) yields

$$\dot{\lambda}_\Theta(T) = \frac{V_E\sin\left(S_1-S_2+\frac{V_E}{R_E}\beta^*T\right)}{\left[V_p\cos S_1 - V_E\cos(S_2-S_1)\right]} \qquad (B.49)$$

Solving Eq (B.49) with the boundary condition of Eq (6.23) yields

$$\lambda_\Theta(T) = \frac{R_E\left[\cos(S_1-S_2)-\cos\left(S_1-S_2+\frac{V_E}{R_E}\beta^*T\right)\right]}{\beta^*\left[V_p\cos S_1 - V_E\cos(S_1-S_2)\right]} \qquad (B.50)$$

For $0 < S_1-S_2 < \pi/2$, Figure 21 shows that in the UP $\beta^* = +1$. For small T Eq (B.50) shows $\lambda_\Theta(T) > 0$ and switches when T equals T_Θ defined by

$$\frac{V_E}{R_E}T_\Theta = 2\pi - 2(S_1-S_2) \qquad (B.51)$$

For $-\pi/2 < S_1-S_2 < 0$, Figure 21 shows that in the UP $\beta^* = -1$. For small T Eq (B.50) shows $\lambda_\Theta(T) < 0$ and switches when T equals T_Θ defined by

$$-\frac{V_E}{R_E}T_\Theta = -2\pi - 2(S_1-S_2) \qquad (B.52)$$

In this latter case $S_1-S_2 < 0$, so the switching times in both Eq (B.51) and Eq (B.52) can be summarized by

$$\frac{V_E}{R_E}T_\Theta = 2\pi - 2|S_1-S_2| \qquad (B.53)$$

Eqs (B.52) and (B.53) must be applied in a coordinate system such that $|S_1 - S_2| < \pi$. Knowing that E is in a hard turn, the physical significance of E switching (i.e. Eq (B.53) can be shown to be that E recrosses the terminal line of sight in real space.

To examine P switching, Eq (B.46) is first substituted into Eq (B.25)

$$\dot{A}_\Theta = \frac{V_P \sin\left(S_1 + \alpha^* \frac{V_P}{R_P} T\right)}{\left[V_P \cos S_1 - V_E \cos(S_2 - S_1)\right]} \quad . \tag{B.54}$$

Using the boundary condition of Eq (6.24), Eq (B.54) is solved backward yielding

$$A_\Theta(T) = \frac{-R_P\left[\cos S_1 - \cos\left(S_1 + \alpha^* \frac{V_P}{R_P} T\right)\right]}{\alpha^*\left[V_P \cos S_1 - V_E \cos(S_2 - S_1)\right]} \quad . \tag{B.55}$$

For $S_1 > 0$, Figure 21 shows that in the UP $\alpha^* = 1$.

For small T Eq (B.55) shows $A_\Theta(T) < 0$ and switches when T equals T_A defined by

$$\frac{V_P}{R_P} T_A = 2\pi - 2S_1 \quad . \tag{B.56}$$

For $S_1 < 0$, Figure 21 shows that in the UP $\alpha^* = -1$.

For small T Eq (B.55) shows $A_\Theta(T) > 0$ and switches when T equals T_A defined by

$$-\frac{V_P}{R_P} T_A = -2\pi - 2S_1 \quad . \tag{B.57}$$

In this latter case $S_1 < 0$, and the switching times in both Eq (B.56) and (B.57) can be summarized by

$$\frac{V_P}{R_P} T_A = 2\pi - 2|S_1| \tag{B.58}$$

where $|S_1| \leq \pi$. Knowing that P is in a hard turn, the physical significance of P switching (i.e. Eq (B.58) can also be shown to be that P recrosses the terminal line of sight in real space. Because of switching, the solution presented so far is only valid up to the smaller of T_θ or T_A . As in the Limited Pursuer model, these trajectories will generally hit the Barrier prior to T_θ or T_A .

Eq (B.48) is now substituted into the $\dot{x}$ and $\dot{y}$ state equations of Eq (B.16) and set up for backward integration i.e.

$$\overset{\circ}{x} = -V_E \sin\left[S_2 + \left(\frac{V_p}{R_p}\alpha^* - \frac{V_E}{R_E}\beta^*\right)\tau\right] + \alpha^*\frac{V_p}{R_p}y \qquad \text{(B.59)}$$

$$\overset{\circ}{y} = -V_E \cos\left[S_2 + \left(\frac{V_p}{R_p}\alpha^* - \frac{V_E}{R_E}\beta^*\right)\tau\right] + V_p - \alpha^*\frac{V_p}{R_p}x \qquad \text{(B.60)}$$

Eqs (B.59) and (B.60) are solved simultaneously with the boundary conditions of Eq (5.3) yielding

$$x(T) = \alpha^* R_p\left(1-\cos\alpha^*\frac{V_p}{R_p}T\right) + \ell\sin\left(S_1+\alpha^*\frac{V_p}{R_p}T\right) + \frac{R_E}{\beta^*}\left[\cos\left(S_2+\alpha^*\frac{V_p}{R_p}T\right) - \cos\Theta(T)\right] \qquad \text{(B.61)}$$

$$y(T) = \alpha^* R_p \sin\alpha^*\frac{V_p}{R_p}T + \ell\cos\left(S_1+\alpha^*\frac{V_p}{R_p}T\right) - \frac{R_E}{\beta^*}\left[\sin\left(S_2+\alpha^*\frac{V_p}{R_p}T\right) - \sin\Theta(T)\right] \qquad \text{(B.62)}$$

where $\Theta(T)$ is defined in Eq (B.48).

3. C Trajectory Analysis

Solution of $\dot{\sigma}_x$ and $\dot{\sigma}_y$ in Eq (6.63) subject to the boundary conditions of Eqs (6.91) and (6.92) yields

$$\sigma_x(T') = \sin\left(S_1+\theta_{ps}+\frac{V_p}{R_p}T'\right) = \sin\left(S_1+\frac{V_p}{R_p}T\right) \qquad \text{(B.63)}$$

$$\sigma_y(T') = \cos\left(S_1+\theta_{ps}+\frac{V_p}{R_p}T'\right) = \cos\left(S_1+\frac{V_p}{R_p}T\right) \qquad \text{(B.64)}$$

where

$$\tau' = \tau - \tau_s \tag{B.65}$$

Note that the τ dependence of σ_x and σ_y is unaffected by E switching on the singular trajectory.

Solution of the $\dot{\theta}$ state equation subject to the boundary condition of Eq (6.94) yields (B.66)

$$\theta(\tau') = s_1 + \theta_{ps} + \left(\frac{V_p}{R_p} - \frac{V_E}{R_E}\right)\tau' = s_1 + \theta_{ps} - \frac{V_E}{R_E}\left(1 - \frac{V_p}{R_p}\frac{R_E}{V_E}\right)\tau' =$$

$$= s_1 + \theta_{ps} - \dot{\theta}_E\left(1 - \frac{\dot{\theta}_f}{\dot{\theta}_E}\right)\tau' \quad .$$

Solution of the $\dot{\sigma}_\theta$ equation subject to $\sigma_\theta(0)=0$ yields

$$\sigma_\theta(\tau') = R_E\left(1 - \cos\frac{V_E}{R_E}\tau'\right) . \tag{B.67}$$

Note that for small τ', $\sigma_\theta(\tau')>0$ which agrees with Eq (6.61) (i.e. $\tilde{\beta} = \operatorname{sgn}\sigma_\theta = +1$) and that $\sigma_\theta(\tau') \geq 0$ always.

Since $\dot{\tilde{A}}_\theta = -V_p\sigma_x$. and since $\sigma_x(\tau)$ is unaffected by E switching off the singular trajectory, the $\tilde{A}_\theta(\tau)$ solution remains unchanged (i.e. Eq (6.76)

$$\tilde{A}_\theta(\tau) = -R_p\left[\cos s_1 - \cos\left(s_1 + \frac{V_p}{R_p}\tau\right)\right] . \tag{B.68}$$

Therefore, the switching condition for P on the Barrier (i.e. Eq (6.77) remains unchanged i.e.

$$\theta_{ps} + \frac{V_p}{R_p}\tilde{\tau}_A' \equiv \frac{V_p}{R_p}\left(\tau_s + \tilde{\tau}_A'\right) \equiv \frac{V_p}{R_p}\bar{\tau}_A = 2\pi - 2|s_1| \tag{B.69}$$

where $\tilde{\tau}_A'$ is the time of P switching after E switches from the singular trajectory.

Simultaneous solution of the $\dot{x}$ and $\dot{y}$ state equations backward for $\tilde{\alpha} = +1$, $\tilde{\beta} = +1$ in terms of arbitrary constants "a" and "b" yields

$$x(T') = a \sin \frac{V_p}{R_p} T' + b \cos \frac{V_p}{R_p} T' + R_p - R_E \cos \theta(T') \quad \text{(B.70)}$$

$$y(T') = -b \sin \frac{V_p}{R_p} T' + a \cos \frac{V_p}{R_p} T' + R_E \sin \theta(T') \quad \text{(B.71)}$$

Applying the boundary conditions of Eqs (6.95) and (6.96) at $T' = 0$ yields

$$a = R_p \sin\theta_{ps} + R_p \left(\frac{\ell}{R_p} - \frac{V_E}{V_p} \theta_{ps} \right) \cos(s_1 + \theta_{ps}) - R_E \sin(s_1 + \theta_{ps}) \quad \text{(B.72)}$$

$$b = R_p \left(\frac{\ell}{R_p} - \frac{V_E}{V_p} \theta_{ps} \right) \sin(s_1 + \theta_{ps}) - R_p \cos\theta_{ps} + R_E \cos(s_1 + \theta_{ps}) \quad \text{(B.73)}$$

Substituting Eqs (B.72) and (B.73) into Eqs (B.70) and (B.71) and dividing by R_p yields

$$\frac{x(T')}{R_p} = -\cos\left(\theta_{ps} + \frac{V_p}{R_p} T'\right) + \left(\frac{\ell}{R_p} - \frac{V_E}{V_p} \theta_{ps} \right) \sin\left(s_1 + \theta_{ps} + \frac{V_p}{R_p} T'\right) + \quad \text{(B.74)}$$

$$+ \frac{R_E}{R_p} \cos\left(s_1 + \theta_{ps} + \frac{V_p}{R_p} T'\right) + 1 - \frac{R_E}{R_p} \cos\theta(T')$$

$$\frac{y(T')}{R_p} = \left(\frac{\ell}{R_p} - \frac{V_E}{V_p} \theta_{ps} \right) \cos\left(s_1 + \theta_{ps} + \frac{V_p}{R_p} T'\right) + \sin\left(\theta_{ps} + \frac{V_p}{R_p} T'\right) + \quad \text{(B.75)}$$

$$- \frac{R_E}{R_p} \sin\left(s_1 + \theta_{ps} + \frac{V_p}{R_p} T'\right) + \frac{R_E}{R_p} \sin\theta(T') \, .$$

4. State Equation Derivation for 3D Model:

Examine Figure 29 of the main text. $\underline{R}_p$ locates the coordinate system of the pursuer whose y axis is always along the velocity vector $\underline{V}_p$. The terminal surface, $\mathcal{C}$, is a sphere of radius, ℓ , about the

origin of P's coordinate system. The vector, $\underline{r}$, locates the evader's position relative to P. The projection of $\underline{r}$ onto the x-z plane (i.e. $\mathcal{X}$) has the angle Θ relative to the x-axis. The acceleration vector of P normal to $\underline{V}_p$, i.e. $\underline{a}_{\perp_p}$, lines in the X-Z (or $\mathcal{X}$-$\mathcal{Z}$) plane and has the angle Φ relative to the x-axis and the angle $\tilde{\Phi}$ relative to the $\mathcal{X}$-axis i.e.

$$\tilde{\Phi} = \Phi - \Theta \qquad (B.76)$$

P maneuvers by selecting the magnitude of $\underline{a}_{\perp_p}$, which is bounded, and the bank angle Φ (or $\tilde{\Phi}$).

Now

$$|\underline{a}_{\perp_p}| = \frac{V_p^2}{R_p}\alpha \qquad (B.77)$$

where

$$0 \le \alpha \le 1 \qquad (B.78)$$

and

$$\underline{\omega}_p = \alpha \frac{V_p}{R_p}\left(\sin\Phi\,\underline{i}_x - \cos\Phi\,\underline{i}_z\right) \qquad (B.79)$$

where

$$0 \le \Phi \le 2\pi \qquad (B.80)$$

The $\underline{V}_E$ orientation and acceleration, $\underline{a}_{\perp_E}$, are derived next.

A counterclockwise rotation, Θ , about the y-axis locates the x_1, y_1, z_1 axis system so that $\underline{V}_E$ lies in the x_1-y_1 plane. The rotation rate of the x_1, y_1, z_1 axis system, $\underline{\omega}_{E_1}$, relative to the x, y, z system and the coordinate system transformation after the Θ rotation are

$$\underline{1}_{y_1} = \underline{1}_y$$

$$\underline{1}_{x_1} = \cos\theta\,\underline{1}_x + \sin\theta\,\underline{1}_z$$

$$\underline{1}_{z_1} = -\sin\theta\,\underline{1}_x + \cos\theta\,\underline{1}_z \tag{B.81}$$

$$\underline{\omega}_{E_1} = -\dot{\theta}\,\underline{1}_{y_1} = -\dot{\theta}\,\underline{1}_y \tag{B.82}$$

Next a counterclockwise rotation ψ about the z_1-axis locates the vector $\underline{V}_E$ along the y_2- axis. The coordinate system transformation and total rotation rate of the x_2, y_2, z_2 axes system, $\underline{\omega}_{E2}$, relative to the x, y, z system are

$$\underline{1}_{z_2} = \underline{1}_{z_1}$$

$$\underline{1}_{x_2} = \cos\psi\,\underline{1}_{x_1} - \sin\psi\,\underline{1}_{y_1}$$

$$\underline{1}_{y_2} = \sin\psi\,\underline{1}_{x_1} + \cos\psi\,\underline{1}_{y_1} \tag{B.83}$$

$$\underline{\omega}_{E_2} = \underline{\omega}_{E_1} - \dot{\psi}\,\underline{1}_{z_2} \tag{B.84}$$

The x_2-z_2 plane is the plane of E's acceleration vector $\underline{a}_{1_E}$. $\underline{a}_{1_E}$ has the angle, ζ, relative to the x_2- axis. E maneuvers by selecting the magnitude of $\underline{a}_{1_E}$, which is bounded, and the bank angle ζ. Now

$$|\underline{a}_{1_E}| = \frac{V_E^2}{R_E}\beta \tag{B.85}$$

where

$$0 \le \beta \le 1 \tag{B.86}$$

and

$$\underline{\omega}_E = \beta\frac{V_E}{R_E}\left(\sin\zeta\,\underline{1}_{x_2} - \cos\zeta\,\underline{1}_{z_2}\right) \tag{B.87}$$

where

$$0 \le \zeta \le 2\pi \tag{B.88}$$

Substituting the Eqs (B.81) and (B.83) into Eqs (B.84) and (B.87) yields

$$\underline{\omega}_{E2} = \dot{\psi}\sin\theta\,\underline{1}_x - \dot{\theta}\,\underline{1}_y - \dot{\psi}\cos\theta\,\underline{1}_z \tag{B.89}$$

$$\underline{\omega}_E = \frac{V_E}{R_E} B\left[(\sin\gamma\cos\psi\cos\theta + \cos\gamma\sin\theta)\,\underline{1}_x + \right. \tag{B.90}$$
$$\left. -(\sin\gamma\sin\psi)\,\underline{1}_y + (\sin\gamma\cos\psi\sin\theta - \cos\gamma\cos\theta)\,\underline{1}_z\right] .$$

The formal derivation of the state equations is done next.

The position of E from P can be written

$$\underline{r} = x\,\underline{1}_x + y\,\underline{1}_y + z\,\underline{1}_z \equiv \chi\,\underline{1}_\chi + y\,\underline{1}_y \tag{B.91}$$

where

$$x = \chi\cos\theta \tag{B.92}$$
$$z = \chi\sin\theta \quad .$$

Eq (A.7) applies here so that

$$\dot{\underline{r}}\big|_r = \underline{V}_E - \underline{V}_P - \underline{\omega}_P \times \underline{r} \quad . \tag{B.93}$$

The vector $\underline{V}_E$ can be written

$$\underline{V}_E = V_E\,\underline{1}_{Y2} = V_E\left(\sin\psi\,\underline{1}_{X1} + \cos\psi\,\underline{1}_{Y1}\right) \tag{B.94}$$

where Eq (B.83) has been used for $\underline{1}_{Y2}$. Further substitution of Eq (B.81) into Eq (B.94) yields

$$\underline{V}_E = V_E\left[\sin\psi\cos\theta\,\underline{1}_x + \cos\psi\,\underline{1}_y + \sin\psi\sin\theta\,\underline{1}_z\right] . \tag{B.95}$$

The vector $\underline{V}_P$ can be written

$$\underline{V}_P = V_P\,\underline{1}_y \quad . \tag{B.96}$$

Substituting Eq (B.92) into Eq (B.91) and using Eq (B.79), the $\underline{\omega}_p \times \underline{r}$ term becomes

$$\underline{\omega}_p \times \underline{r} = \alpha \frac{V_p}{R_p} \begin{vmatrix} \underline{1}_x & \underline{1}_y & \underline{1}_z \\ \sin\Phi & 0 & -\cos\Phi \\ x\cos\Theta & y & x\sin\Theta \end{vmatrix} =$$

$$= \frac{V_p}{R_p} \alpha \left[y\cos\Phi \underline{1}_x - x\cos(\Theta-\Phi)\underline{1}_y + y\sin\Phi \underline{1}_z \right] . \quad (B.97)$$

Differentiating Eq (B.91) relative to the moving x,y,z system yields

$$\dot{\underline{r}}|_r = \dot{x}\underline{1}_x + \dot{y}\underline{1}_y + \dot{z}\underline{1}_z \equiv (\dot{x}\cos\Theta - x\sin\Theta\dot{\Theta})\underline{1}_x +$$
$$+ \dot{y}\underline{1}_y + (\dot{x}\sin\Theta + x\cos\Theta\dot{\Theta})\underline{1}_z . \quad (B.98)$$

Substituting Eqs (B.95) to (B.98) into Eq (B.93) and equating the scalar components yields

$$\dot{x} \equiv \dot{x}\cos\Theta - x\sin\Theta\dot{\Theta} = V_E \sin\psi\cos\Theta - \frac{V_p}{R_p}\alpha y\cos\Phi \quad (B.99)$$

$$\dot{y} \equiv V_E\cos\psi - V_p + \frac{V_p}{R_p}\alpha x\cos(\Theta-\Phi) \quad (B.100)$$

$$\dot{z} \equiv \dot{x}\sin\Theta + x\cos\Theta\dot{\Theta} = V_E\sin\psi\sin\Theta - \frac{V_p}{R_p}\alpha y\sin\Phi . \quad (B.101)$$

Multiplying Eq (B.99) by $\cos\Theta$ and Eq (B.101) by $\sin\Theta$, adding, and simplifying yields

$$\dot{x} = V_E\sin\psi\cos(\Theta-\Theta) - \frac{V_p}{R_p}\alpha y\cos(\Theta-\Phi) . \quad (B.102)$$

Multiplying Eq (B.99) by $\sin\Theta$ and substracting Eq (B.101) multiplied by $\cos\Theta$ yields

$$-x\dot{\Theta} = V_E\sin\psi\sin(\Theta-\Theta) - \frac{V_p}{R_p}\alpha y\sin(\Theta-\Phi) . \quad (B.103)$$

Since the total rotation rate of the x_t, y_t, z_t axes system, $\underline{\omega}_E$, equals the total rotation rate of P (i.e. $\underline{\omega}_P$) plus the rotation rate of E relative to P (i.e. $\underline{\omega}_{Et}$) it is seen that

$$\underline{\omega}_E = \underline{\omega}_P + \underline{\omega}_{Et} \quad . \tag{B.104}$$

Substituting Eqs (B.79) and (B.90) into Eq (B.104) yields

$$\underline{\omega}_{Et} = \underline{\omega}_E - \underline{\omega}_P = \left[\beta\frac{V_E}{R_E}\left(\sin\zeta\cos\psi\cos\theta + \cos\zeta\sin\theta\right) - \alpha\frac{V_P}{R_P}\sin\tilde{\Phi}\right]\underline{1}_x + \tag{B.105}$$

$$+\left[-\beta\frac{V_E}{R_E}\sin\zeta\sin\psi\right]\underline{1}_y + \left[\beta\frac{V_E}{R_E}\left(\sin\zeta\cos\psi\sin\theta - \cos\zeta\cos\theta\right) + \alpha\frac{V_P}{R_P}\cos\tilde{\Phi}\right]\underline{1}_z .$$

Equating scalar components in Eqs (B.89) and (B.105) yields

$$\dot{\psi}\sin\theta = \beta\frac{V_E}{R_E}\left(\sin\zeta\cos\psi\cos\theta + \cos\zeta\sin\theta\right) - \alpha\frac{V_P}{R_P}\sin\tilde{\Phi} \tag{B.106}$$

$$-\dot{\theta} = -\beta\frac{V_E}{R_E}\sin\zeta\sin\psi \tag{B.107}$$

$$-\dot{\psi}\cos\theta = \beta\frac{V_E}{R_E}\left(\sin\zeta\cos\psi\sin\theta - \cos\zeta\cos\theta\right) + \alpha\frac{V_P}{R_P}\cos\tilde{\Phi} \tag{B.108}$$

Multiplying Eq (B.106) by $\sin\theta$ and substracting Eq (B.108) multiplied by $\cos\theta$ yields

$$\dot{\psi} = \beta\frac{V_E}{R_E}\cos\zeta - \frac{V_P}{R_P}\alpha\cos(\theta - \tilde{\Phi}) \quad . \tag{B.109}$$

Now let

$$\zeta_1 \equiv \theta - \Theta \quad . \tag{B.110}$$

Substituting Eqs (B.76) and (B.110) into Eqs (B.102), (B.100), (B.103) and (B.109) yields

$$\dot{x} = V_E\sin\psi\cos\zeta_1 - \alpha\frac{V_P}{R_P}y\cos\tilde{\Phi} \tag{B.111}$$

$$\dot{y} = V_E\cos\psi - V_P + \alpha\frac{V_P}{R_P}x\cos\tilde{\Phi} \tag{B.112}$$

$$\dot{\Theta} = \frac{1}{\chi}\left[V_E \sin\psi \sin\xi - \alpha \frac{V_p}{R_p} \gamma \sin\tilde{\Phi}\right] \tag{B.113}$$

$$\dot{\psi} = \beta \frac{V_E}{R_E} \cos\zeta - \alpha \frac{V_p}{R_p} \cos(\xi - \tilde{\Phi}) \quad . \tag{B.114}$$

Differentiating Eq (B.110) and substituting Eqs (B.107) and (B.113) yields

$$\dot{\xi} = \dot{\Theta} - \dot{\tilde{\Theta}} = \beta \frac{V_E}{R_E} \sin\zeta \sin\psi + \frac{1}{\chi}\left[-V_E \sin\psi \sin\xi + \alpha \frac{V_p}{R_p} \gamma \sin\tilde{\Phi}\right] . \tag{B.115}$$

Therefore, the four (4) dimensional state vector $\underline{x}$ is

$$\underline{x} = \begin{bmatrix} \chi \\ \gamma \\ \psi \\ \xi \end{bmatrix} \tag{B.116}$$

and the state equations are Eqs (B.111), (B.112), (B.114) and (B.115).

5. Problem Backward Solution From ζ for 3D Model:

Equations for the controls on the terminal surface, ζ, are found first. Substituting Eqs (6.105), (6.130) and (6.131) into Eq (6.111) shows that $A(t_f) = 0$. Furthermore, Eqs (6.131) and (6.132) show that $B(t_f) = 0$ and $H_E(t_f) = 0$. Therefore at t_f main Eq (6.128) becomes

$$H_o(t_f) = 1 - V_p \lambda_\gamma(t_f) + V_E\left[\lambda_\chi(t_f)\sin\psi\cos\xi + \lambda_\gamma(t_f)\cos\psi\right]\Big|_{t_f} = 0 \tag{B.117}$$

Substituting Eq (6.130) for $\lambda_\chi(t_f)$ into Eq (B.117) yields

$$\lambda_\gamma(t_f) = \frac{-1}{V_E(\tan S_1 \sin\psi\cos\xi + \cos\psi)\big|_{t_f} - V_p} =$$

$$= \frac{\cos S_1}{V_p \cos S_1 - V_E(\cos S_1 \cos\psi + \sin S_1 \sin\psi \cos\xi)}\Big|_{t_f} . \tag{B.118}$$

Substituting Eq (B.118) back into Eq (6.130) yields

$$\lambda_\chi(t_f) = \frac{\sin S_1}{V_p \cos S_1 - V_E(\cos S_1 \cos\psi + \sin S_1 \sin\psi \cos\xi)}\Big|_{t_f} . \tag{B.119}$$

Since $A(t_f) = B(t_f) = \lambda_\psi(t_f) = \lambda_\zeta(t_f) = 0$, Eqs (6.127) and (6.121) show that $\dot{\phi}^*\big|_{t_f}$ and $\zeta^*\big|_{t_f}$ are undefined i.e. $\frac{0}{0}$. To evaluate the $\frac{0}{0}$ in $\zeta^*\big|_{t_f}$, Eqs (6.121) are first rearranged by dividing $\lambda_\psi(\lambda_\zeta)$ into the numerator and denominator of cos ζ^* (sin ζ^*) yielding

$$\cos\zeta^* = \frac{\operatorname{sgn}\lambda_\psi}{\sqrt{1+(\lambda_\zeta/\lambda_\psi)^2\sin^2\psi}} \quad , \quad \sin\zeta^* = \frac{\operatorname{sgn}(\lambda_\zeta)\sin\psi}{\sqrt{\left(\frac{\lambda_\psi}{\lambda_\zeta}\right)^2+\sin^2\psi}} \tag{B.120}$$

Therefore, an infinitesimal time away from t_f the ζ^* controls are

$$\cos\zeta^*(t_f) = \left.\frac{\operatorname{sgn}(\dot{\lambda}_\psi)}{\sqrt{1+\left(\lim_{t\to t_f}\frac{\dot{\lambda}_\zeta}{\dot{\lambda}_\psi}\right)^2\sin^2\psi}}\right|_{t_f}, \quad \sin\zeta^*(t_f) = \left.\frac{\operatorname{sgn}(\dot{\lambda}_\zeta)\sin\psi}{\sqrt{\left(\lim_{t\to t_f}\frac{\dot{\lambda}_\psi}{\dot{\lambda}_\zeta}\right)^2-\sin^2\psi}}\right|_{t_f} \tag{B.121}$$

Now

$$\lim_{t\to t_f}\frac{\dot{\lambda}_\zeta}{\dot{\lambda}_\psi} = \left.\frac{-V_E\lambda_x\sin\psi\sin\zeta}{-V_E(\lambda_y\sin\psi-\lambda_x\cos\psi\cos\zeta)}\right|_{t_f} = \tag{B.122}$$

$$= \left.\frac{\frac{\lambda_x}{\lambda_y}\sin\psi\sin\zeta}{\sin\psi-\frac{\lambda_x}{\lambda_y}\cos\psi\cos\zeta}\right|_{t_f} = \left.\frac{\tan s_1\sin\psi\sin\zeta}{\sin\psi-\tan s_1\cos\psi\cos\zeta}\right|_{t_f}$$

where Eqs (6.129) and (6.130) have been used. Since

$$\operatorname{sgn}[\cos\zeta^*(t_f)] = \operatorname{sgn}(\dot{\lambda}_\psi)\big|_{t_f} \tag{B.123}$$

then substituting

Eq (6.129) into Eq (B.123) yields

$$\operatorname{sgn}[\cos\zeta^*(t_f)] = \operatorname{sgn}\left[-V_E(\lambda_y\sin\psi - \lambda_x\cos\psi\cos\xi_1)\Big|_{t_f}\right] =$$

$$= -\operatorname{sgn}[\lambda_y(t_f)]\,\operatorname{sgn}\left(\sin\psi - \frac{\lambda_x}{\lambda_y}\cos\psi\cos\xi_1\right)\Big|_{t_f} =$$

$$= -\operatorname{sgn}[\lambda_y(t_f)]\,\operatorname{sgn}\left(\sin\psi - \tan s_1\cos\psi\cos\xi_1\right)\Big|_{t_f} \qquad \text{(B.124)}$$

Where Eq (6.130) has again been used. Substituting Eq (B.122) into Eq (6.117) yields

$$\tan\zeta^*(t_f) = \frac{\tan s_1\sin^2\psi\sin\xi_1}{\sin\psi - \tan s_1\cos\psi\cos\xi_1}\Bigg|_{t_f} = \qquad \text{(B.125)}$$

$$\equiv \frac{\sin\psi\tan s_1\tan\psi\sin\xi_1}{\tan\psi - \tan s_1\cos\xi_1}\Bigg|_{t_f}$$

and substituting Eq (B.118) into Eq (B.124) yields

$$\operatorname{sgn}[\cos\zeta^*(t_f)] =$$

$$= \frac{-\operatorname{sgn}(\cos s_1)\,\operatorname{sgn}(\sin\psi - \tan s_1\cos\psi\cos\xi_1)}{\operatorname{sgn}\left[V_p\cos s_1 - V_E(\cos s_1\cos\psi + \sin s_1\sin\psi\cos\xi_1)\right]}\Bigg|_{t_f} \qquad \text{(B.126)}$$

Eq (B.125) and (B.126) will be used later to determine $\zeta^*(t_f)$.

Note that for $\xi_1(t_f)=0$, Eqs (B.125) and (B.126) become

$$\tan\zeta^*(t_f) = 0 \qquad \text{(B.127)}$$

$$\operatorname{sgn}[\cos\zeta^*(t_f)] = \frac{-\operatorname{sgn}[\sin(\psi - s_1)]}{\operatorname{sgn}[V_p\cos s_1 - V_E\cos(\psi - s_1)]}$$

which give exactly the same result as in the 2D Limited Pursuer-Evader model.

To evaluate the $\frac{0}{0}$ in $\tilde{\phi}^*|_{t_f}$, Eq (6.123) is written as

$$\tan\tilde{\phi}^* = \frac{B}{A} = \frac{\frac{y}{x}\lambda_\xi - \lambda_\psi \sin\xi}{x\lambda_y - y\lambda_x - \lambda_\psi \cos\xi} \equiv \frac{\frac{y}{x}\frac{\lambda_\xi}{\lambda_\psi} - \sin\xi}{\frac{x\lambda_y - y\lambda_x}{\lambda_\psi} - \cos\xi} \quad \text{(B.128)}$$

Since $\frac{\lambda_\xi}{\lambda_\psi}\Big|_{t_f}$ is given by Eq (B.122), only $\frac{x\lambda_y - y\lambda_x}{\lambda_\psi}\Big|_{t_f}$ need be determined for Eq (B.128). And since $\frac{x\lambda_y - y\lambda_x}{\lambda_\psi}\Big|_{t_f} = \frac{0}{0}$, it too must be evaluated by L'Hopital's rule i.e.

$$\frac{x\lambda_y - y\lambda_x}{\lambda_\psi}\Big|_{t_f} = \frac{\lim_{t\to t_f} \frac{d}{dT}(x\lambda_y - y\lambda_x)}{\lim_{t\to t_f} \dot{\lambda}_\psi} \quad \text{(B.129)}$$

Now

$$\frac{d}{dT}(x\lambda_y - y\lambda_x)\Big|_{t_f} = (\dot{x}\lambda_y + x\dot{\lambda}_y - \dot{y}\lambda_x - y\dot{\lambda}_x)\Big|_{t_f} =$$

$$= V_E[\lambda_x\cos\psi - \lambda_y\sin\psi\cos\xi] - V_p\lambda_x\Big|_{t_f} \quad \text{(B.130)}$$

where the backward state and costate equations have been substituted and evaluated at t_f. Multiplying Eq (B.130) by $\frac{\lambda_y}{\lambda_y}$ and using Eq (6.130) yields

$$\frac{d}{dT}(x\lambda_y - y\lambda_x)\Big|_{t_f} = \lambda_y[V_E(\tan s_1\cos\psi - \sin\psi\cos\xi) - V_p\tan s_1]\Big|_{t_f} \quad \text{(B.131)}$$

Since $\dot{\lambda}_\psi(t_f)$ can be written,

$$\dot{\lambda}_\psi(t_f) = -\lambda_y V_E[\sin\psi - \tan s_1\cos\psi\cos\xi]\Big|_{t_f} \quad \text{(B.132)}$$

then substituting Eqs (B.131) and (B.132) into Eq (B.129) yields

$$\left.\frac{x\lambda_y - y\lambda_x}{\lambda_\psi}\right|_{t_f} = \left.\frac{V_E(\tan s_1 \cos\psi - \sin\psi\cos\xi) - V_p \tan s_1}{-V_E[\sin\psi - \tan s_1 \cos\psi\cos\xi]}\right|_{t_f} \quad \text{(B.133)}$$

Substituting Eq (B.133), (B.122) and (6.105) into Eq (B.128) yields

$$\tan\bar{\phi}^*(t_f) = \left.\frac{\cot s_1 \dfrac{\tan s_1 \sin\psi \sin\xi}{\sin\psi - \tan s_1 \cos\psi\cos\xi} - \sin\xi}{\dfrac{V_E(\tan s_1\cos\psi - \sin\psi\cos\xi) - V_p\tan s_1}{-V_E(\sin\psi - \tan s_1\cos\psi\cos\xi)} - \cos\xi}\right|_{t_f} \quad \text{(B.134)}$$

Simplifying Eq (B.134) yields

$$\tan\bar{\phi}^*(t_f) = \left.\frac{\cos\psi\cos\xi\sin\xi}{V_p/V_E - \cos\psi\sin^2\xi}\right|_{t_f} \quad \text{(B.135)}$$

From Eq (6.127) it is seen that

$$\text{sgn}[\cos\bar{\phi}^*(t_f)] = -\text{sgn}\,A(t_f) = -\text{sgn}\left[\left.\frac{d}{d\tau}(x\lambda_y - y\lambda_x) - \frac{d}{d\tau}(\lambda_\psi\cos\xi)\right|_{t_f}\right] \quad \text{(B.136)}$$

Also

$$\left.\frac{d}{d\tau}(\lambda_\psi\cos\xi)\right|_{t_f} = \left.\dot{\lambda}_\psi\cos\xi\right|_{t_f} \quad \text{(B.137)}$$

Substituting Eq (B.132) into Eq (B.137) and then substituting Eq (B.137) and (B.131) into Eq (B.136) yields

$$\text{sgn}[\cos\bar{\phi}^*(t_f)] = -\text{sgn}\left\{\left.\lambda_\gamma\left[V_E(\tan s_1\cos\psi - \sin\psi\cos\xi) - V_p\tan s_1\right] + V_E\lambda_\gamma(\sin\psi - \tan s_1\cos\psi\cos\xi)\cos\xi\right\}\right|_{t_f} \quad \text{(B.138)}$$

Simplifying Eq (B.138) yields

$$\operatorname{sgn}\left[\cos\tilde{\phi}^*(t_f)\right] = \operatorname{sgn}(\lambda_y)\operatorname{sgn}(\tan s_1)\operatorname{sgn}\left(\frac{V_p}{V_E} - \cos\psi \sin^2\xi_1\right)\Big|_{t_f} \quad (B.139)$$

Substituting Eq (B.118) for $\lambda_y(t_f)$ into Eq (B.139) yields

$$\operatorname{sgn}\left[\cos\tilde{\phi}^*(t_f)\right] = \frac{\operatorname{sgn}(\sin s_1)\operatorname{sgn}\left(\frac{V_p}{V_E} - \cos\psi \sin^2\xi_1\right)}{\operatorname{sgn}\left[V_p \cos s_1 - V_E(\cos s_1 \cos\psi + \sin s_1 \sin\psi \cos\xi_1)\right]}\Bigg|_{t_f} \quad (B.140)$$

Eqs (B.135) and (B.140) will be used later to determine $\tilde{\phi}^*(t_f)$.

Note that for $\xi_1(t_f) = 0$, Eqs (B.135) and (B.140) reduce to

$$\tan\tilde{\phi}^*(t_f) = 0 \quad (B.141)$$

$$\operatorname{sgn}\left[\cos\tilde{\phi}^*(t_f)\right] = \frac{\operatorname{sgn}(\sin s_1)}{\operatorname{sgn}\left[V_p \cos s_1 - V_E \cos(\psi - s_1)\right]}\Bigg|_{t_f}$$

which give exactly the same result as the 2D Limited Pursuer-Evader model.

To give more insight into the backward solution, the singular control necessary conditions are examined next. The E singular control conditions are examined first. For a singular control in β , it is necessary that

$$\lambda_\xi \sin\xi \sin\psi + \lambda_\psi \cos\xi = 0 \quad . \quad (B.142)$$

Substituting Eq (6.121) into Eq (B.142) yields

$$\sqrt{\lambda_\psi^2 + \lambda_\xi^2 \sin^2\psi} = 0 \quad . \quad (B.143)$$

Eq (B.143) implies that both

$$\lambda_\psi = 0 \quad (B.144)$$

$$\lambda_\xi \sin\psi = 0 \quad .$$

Eq (B.144) has two possible cases: 1) $\lambda_\psi = 0$ and $\lambda_\xi = 0$, 2) $\lambda_\psi \neq 0$ and $\sin\psi = 0$. In case 1), Eqs (6.111), (6.112) and (6.127) show that P's controls are

$$\begin{aligned} \alpha^* &= +1 \\ \sin\tilde{\phi}^* &= 0 \\ \cos\tilde{\phi}^* &= -\operatorname{sgn} A = -\operatorname{sgn}(x\lambda_y - y\lambda_x) \end{aligned} \tag{B.145}$$

which are the same as the P controls for the E singular case of the 2D Limited Pursuer-Evader model. Now, since $\lambda_\psi = \lambda_\xi = 0$, this implies that $\dot{\lambda}_\psi = \dot{\lambda}_\xi = 0$. Eq (6.129) shows therefore that both

$$\dot{\lambda}_\xi\Big|_{\lambda_\psi = \lambda_\xi = 0} = \lambda_x \sin\psi \sin\xi_1 = 0 \tag{B.146}$$

$$\dot{\lambda}_\psi\Big|_{\lambda_\xi = 0} = \lambda_y \sin\psi - \lambda_x \cos\psi \cos\xi_1 = 0 \tag{B.147}$$

are also necessary for β to be singular. Now Eq (B.146) implies three further possibilities for case 1): a) $\lambda_x = 0$, b) $\sin\psi = 0$, c) $\sin\xi_1 = 0$.

In case 1a), Eq (B.147) shows that $\lambda_y \sin\psi$ equals zero ($\lambda_y = 0$ yields the trivial case of $\underline{\lambda} = \underline{0}$) from which it is concluded

$$\sin\psi = 0 \,. \tag{B.148}$$

Now since $\lambda_x = \sin\psi = 0$, this implies that $\dot{\lambda}_x = \dot{\psi} = 0$. Therefore, Eq (6.129) shows that

$$0 = \dot{\lambda}_x\Big|_{\lambda_\xi = 0} = -\alpha \frac{V_p}{R_p} \lambda_y \cos\tilde{\phi} \tag{B.149}$$

from which it is concluded ($\lambda_y \neq 0$ since this will be the trivial case of $\underline{\lambda} = \underline{0}$) that

$$\alpha = 0 \,. \tag{B.150}$$

Eq (B.114) shows that

$$0 = \dot{\psi}\Big|_{\alpha=0} = \beta \frac{V_E}{R_E} \cos\zeta \qquad \text{(B.151)}$$

from which it is concluded that

$$\beta = 0 \quad .$$

Therefore, case 1a) shows the following $\lambda_\psi = \lambda_\xi = \lambda_\chi = \sin\psi = \alpha = \beta = 0$. Case 1a) is therefore the totally singular tail chase condition of the 2D Limited Pursuer-Evader model.

Turning to case 1b) it is seen that $\sin\psi = 0$ (i.e. $\cos\psi = \pm 1$) and Eq (B.147) implies

$$\dot{\lambda}_\psi\Big|_{\substack{\lambda_\xi = 0 \\ \sin\psi = 0}} = \pm \lambda_\chi \cos\xi = 0 \quad . \qquad \text{(B.152)}$$

In this case either $\lambda_\chi = 0$ or $\cos\xi = 0$. The former leads once again to case 1a). If $\sin\psi = \cos\xi = 0$, then $\dot{\psi} = \dot{\xi} = 0$. From Eqs (B.114) and (B.115) then

$$\dot{\psi} = \beta \frac{V_E}{R_E} \cos\zeta - \alpha \frac{V_P}{R_P} \cos(\xi - \tilde{\Phi}) = 0 \qquad \text{(B.153)}$$

$$\dot{\xi}\Big|_{\sin\psi=0} = \alpha \frac{V_P}{R_P} \frac{y}{\chi} \sin\tilde{\Phi} = 0 \qquad \text{(B.154)}$$

and it is concluded for case 1b) that $\alpha = \beta = 0$. Therefore, this latter case i.e. $\lambda_\psi = \lambda_\xi = \sin\psi = \cos\xi = \alpha = \beta = 0$, is also implying the non-turning totally singular tail chase of the 2D Limited Pursuer-Evader model.

Going to case 1c) with $\lambda_\psi = \lambda_{\xi_1} = \sin\xi_1 = 0$, the present state and costate equations become the same as the E singular case of the 2D Limited Pursuer-Evader model.

It can therefore be seen that the β singular conditions of case 1) are simply those already found in the 2D Limited Pursuer-Evader model.

Examining case 2) with $\lambda_\psi = \sin\psi = 0$ it is seen that $\dot{\lambda}_\psi = \dot{\psi} = 0$. Therefore, Eq (B.114) shows that

$$0 = \dot{\psi} = \beta \frac{V_E}{R_E} \cos\xi_3 - \alpha \frac{V_P}{R_P} \cos(\xi_3 - \phi) \qquad \text{(B.155)}$$

and Eq (6.129) shows that

$$0 = \dot{\lambda}_\psi \Big|_{\sin\psi = 0} = V_E \cos\psi \left(\frac{\lambda_{\xi_1}}{\chi} \sin\xi_1 - \lambda_\chi \cos\xi_1 - \beta \frac{\lambda_{\xi_3}}{R_E} \sin\xi_3 \right). \qquad \text{(B.156)}$$

It appears that the only possible way to satisfy Eq (B.155) is when $\alpha = \beta = 0$. This is partially substantiated when it is realized that ξ_1 and ξ_3 are really undefined for $\sin\psi = 0$. If $\beta = 0$, then Eq (B.156) shows that

$$\tan\xi_1 = \frac{\chi \lambda_\chi}{\lambda_{\xi_1}} \qquad \text{(B.157)}$$

But since ξ_1 is undefined then $\tan\xi_1$ must be of the form $\frac{0}{0}$ implying $\lambda_\chi = \lambda_{\xi_1} = 0$. Much of this in case 2) is very subjective, but once again is implying the totally singular tail chase situation.

In summary then, it appears that the singular control conditions for β are simply those already found in the 2D Limited Pursuer-Evader model. The singular control conditions for P are examined next.

For a singular control in α , it is necessary that

$$A\cos\bar{\phi} + B\sin\bar{\phi} = 0 \tag{B.158}$$

Substituting Eq (6.127) into Eq (B.158) yields

$$-\sqrt{A^2+B^2} = 0 \tag{B.159}$$

implying that both

$$0 = A \equiv x\lambda_y - y\lambda_x - \lambda_\psi \cos\xi \tag{B.160}$$

$$0 = B \equiv \frac{V}{\chi}\lambda_\xi - \lambda_\psi \sin\xi \quad .$$

Defining $B' \equiv \kappa B$, the requirements of Eqs (B.160) can also be written as

$$A = x\lambda_y - y\lambda_x - \lambda_\psi \cos\xi = 0 \tag{B.161}$$

$$B' = y\lambda_\xi - x\lambda_\psi \sin\xi = 0$$

Since $A = B' = 0$, it is also necessary that $\dot{A} = \dot{B}' = 0$.

Differentiating B' yields

$$\dot{B}' = \dot{y}\lambda_\xi + y\dot{\lambda}_\xi - (\dot{x}\lambda_\psi + x\dot{\lambda}_\psi)\sin\xi - x\lambda_\psi\cos\xi\dot{\xi} = 0 . \tag{B.162}$$

Substituting the state and costate operations into Eq (B.162) and simplifying the resulting expression with Eq (B.161) yields

$$\dot{B}' = \lambda_\xi\left[\alpha\frac{V_P}{R_P}x\cos\bar{\phi} + g\frac{V_E}{R_E}\sin\gamma(x\sin\xi\cos\psi - y\cot\xi\sin\psi) + \right.$$

$$\left. -V_P + V_E\frac{\lambda_\gamma}{\lambda_\psi}x\cos\psi\cos\xi\right] = 0 \quad . \tag{B.163}$$

Differentiating A yields

$$\dot{A} = \dot{x}\lambda_y + x\dot{\lambda}_y - \dot{y}\lambda_x - y\dot{\lambda}_x - \dot{\lambda}_\psi\cos\xi + \lambda_\psi\sin\xi\dot{\xi} = 0. \tag{B.164}$$

Substituting the state and costate equations into Eq (B.164) and simplifying the resulting expression with Eq (B.161) yields

$$\dot{A} = \lambda_{\xi}\left[-\alpha\frac{V_P}{R_P}\sin\tilde{\phi} + \beta\frac{V_E}{R_E}\sin\zeta\left(\cos\xi\cos\psi + \frac{\gamma}{\chi}\sin\psi\right) + \right. \tag{B.165}$$
$$\left. + V_P\left(\frac{\lambda_\gamma}{\lambda_\psi\sin\xi} - \cot\xi\right) - V_E\frac{\lambda_\gamma}{\lambda_\psi}\cos\psi\sin\xi\right] = 0.$$

Eqs (B.163) and (B.165) both indicate that

$$\lambda_{\xi} = 0 \tag{B.166}$$

is another necessary condition for a singular control in α .

Since $\lambda_\xi = 0$, it is also necessary that

$$0 = \dot{\lambda}_\xi\Big|_{\lambda_\xi=0} = V_E\lambda_\chi\sin\psi\sin\xi - \alpha\frac{\dot{V}_P}{R_P}\lambda_\psi\sin(\xi-\tilde{\phi}) \tag{B.167}$$

With $\lambda_\xi = 0$, Eq (B.160) shows that $\lambda_\psi\sin\xi$ equals zero which yields two possibilities: 1) $\lambda_\psi = 0$ or 2) $\sin\xi = 0$.

Case 1) is examined first.

In case 1) $\lambda_\psi = 0$ also implies $\dot{\lambda}_\psi = 0$ i.e.

$$0 = \dot{\lambda}_\psi\Big|_{\lambda_\xi=0} = V_E(\lambda_\gamma\sin\psi - \lambda_\chi\cos\psi\cos\xi) . \tag{B.168}$$

From Eq (B.167) with $\lambda_\psi = 0$, there are three distinct possibilities for case 1): a) $\lambda_\chi = 0$, b) $\sin\psi = 0$, c) $\sin\xi = 0$.

In case 1a), Eq (B.168) implies

$$\sin\psi = 0 \tag{B.169}$$

since $\lambda_\gamma = 0$ is the trivial case of $\underline{\lambda} = \underline{0}$. Eq (B.169) further implies that $\dot{\psi} = 0$ i.e.

$$0 = \dot{\psi} = \beta\frac{V_E}{R_E}\cos\zeta - \alpha\frac{V_P}{R_P}\cos(\xi-\tilde{\phi}) . \tag{B.170}$$

A summary of case 1a) shows $A = B = \lambda_\xi = \lambda_\psi = \lambda_\chi = \sin\psi = 0$. Since Eqs (6.121) and (6.127) show that ζ and $\tilde{\phi}$ are undefined under the conditions of case 1a), α and β must be zero to satisfy Eq (B.170). Note once again that this is the totally singular tail chase situation of the 2D Limited Pursuer-Evader model.

In case 1b) (i.e. $\sin\psi=0$, $\cos\psi=\pm1$), Eq (B.168) shows that $\pm\lambda_\chi \cos\xi$ equals zero implying either $\lambda_\chi = 0$ or $\cos\xi=0$. If $\lambda_\chi=0$, the present case is the same as case 1a (i.e. $A=B=\lambda_\xi=\lambda_\psi=\sin\psi=\lambda_\chi=0$, etc). If $\cos\xi=0$, this implies $\dot{\xi} = 0$ i.e.

$$\dot{\xi}\Big|_{\sin\psi=0} = \alpha \frac{V_p}{R_p} \frac{V}{\chi} \sin\tilde{\phi} = 0 \qquad \text{(B.171)}$$

which also implies $\alpha=0$. Since $\dot{\psi}\neq0$ also, Eq (B.170) implies $\beta=0$. A summary of this latter case shows $A=B=\lambda_\xi=\lambda_\psi=\sin\psi=\cos\xi=\alpha=\beta=0$ which is also indicating the totally singular tail chase condition.

In case 1c) (i.e. $A=B=\lambda_\xi=\lambda_\psi=\sin\xi=0$), it can be seen that with $\lambda_\xi=\sin\xi=0$ (i.e. $B=0$) ζ^* (Eq (6.121)) and $\tilde{\phi}^*$ (Eq (6.127)) become

$$\sin\zeta^* = 0 \quad , \quad \cos\zeta^* = \operatorname{sgn}\lambda_\psi \qquad \text{(B.172)}$$

$$\sin\tilde{\phi}^* = 0 \quad , \quad \cos\dot{\tilde{\phi}}^* = -\operatorname{sgn} A \quad . \qquad \text{(B.173)}$$

As such, the $\dot{x}$, $\dot{y}$ and $\dot{\psi}$ state equations reduce to the state equations for the 2D Limited Pursuer-Evader model. The $\dot{z}_1$ state equation is identically zero. Likewise the costate equations $\dot{\lambda}_x$, $\dot{\lambda}_y$ and $\dot{\lambda}_\psi$ reduce to the costate equations for the 2D Limited Pursuer-Evader model. The $\dot{\lambda}_{z_1}$ costate equation is also identically zero. Case 1c) is therefore the same as the 2D model. In particular, since $A = \lambda_\psi = 0$, it is seen that case 1c), as well as cases 1a) and 1b), corresponds to the totally singular tail chase of the 2D Limited Pursuer-Evader model.

Examining case 2) (i.e. $A = B = \lambda_{z_1} = \sin z_1 = 0$) it is again seen, as with case 1c), that the 3D model reduces identically to the 2D Limited Pursuer-Evader model. As such, the α singular conditions for case 2) are the same as the α singular conditions for the 2D Limited Pursuer-Evader model.

In summary then, it is seen that the α singular control conditions, as it was found with the β singular control conditions, are simply those already found in the 2D Limited Pursuer-Evader model. This concludes the singular control necessary conditions.

Vita

Urban H.D. Lynch was born 30 Nov 1938 in Baltimore, Maryland. He graduated from High School in BelAir, Maryland in 1956. He attended the University of Maryland and in 1961 graduated with a Bachelor of Science degree in Mechanical Engineering and a commission in the United States Air Force. He attended the Air Force Institute of Technology at Wright Patterson AFB and in 1963 received a Master of Science degree (with distinction) in Aeronautical Engineering. He was admitted to candidacy for the Ph.D degree in August 1971 and assigned as an Aerospace Engineer in the High Speed Aero Performance Branch, Flight Mechanics Division, Air Force Flight Dynamics Laboratory, Wright-Patterson AFB, Ohio.

This dissertation was typed by Miss Marcia Tanner